de Jongh, Marli Elizabeth (2022) *The role of clay minerals in the decay and durability of Scotland's vulnerable sandstone heritage.* PhD thesis, University of Glasgow.

The role of clay minerals in the decay and durability of Scotland's vulnerable sandstone heritage.

Marli Elizabeth de Jongh

BSC HONS, UNIVERSITY OF GLASGOW

SUBMITTED IN FULFILMENT OF THE REQUIREMENTS FOR THE DEGREE OF

Doctor of Philosophy

SCHOOL OF GEOGRAPHICAL AND EARTH SCIENCES

COLLEGE OF SCIENCE AND ENGINEERING

UNIVERSITY OF GLASGOW

MAY 2022

Abstract

Sandstone is an integral part of Scotland's built heritage, dating back to settlements in Orkney ~ 3700 BC. As well as preserving Scotland's history throughout the ages, the built heritage is a valuable economic asset through employment and tourism. According to Historic Environment Scotland (HES), some sandstone-built sites are extremely vulnerable to weathering and decay. Many of these sandstones have been sourced locally and are perhaps of a poor-quality. Sandstone is a porous rock type, and it's weathering in the built heritage is driven by the interaction between intrinsic stone properties and climate. Many sandstone types found in the built heritage of Scotland lack a thorough physical and mineralogical characterisation, limiting our understanding of stone decay and durability associated with specific sites. This is particularly true regarding the type and nature of clay minerals present in sandstones, and the impact they have on sandstone durability.

The aims of this research are to: refine analytical procedures for the analysis of clay minerals using pXRD (Ch. 2), improve understanding of sandstone durability through detailed characterisation of physical and mineralogical properties (Ch. 3), investigate the use of hydrophobic treatments as a means of protecting poor-quality sandstones at Arbroath Abbey (Ch. 4), and finally, provide recommendations to Historic Environment Scotland (HES) regarding topics such as understanding sandstone durability, preservation of vulnerable sandstone, and future research (Ch. 6). The aims of this research have been met using a broad range of destructive and non-destructive techniques.

Results show that there is a diverse range of clay minerals present in studied sandstones including mixed layer and expansive type clays. Clay minerals can impact durability both directly and indirectly. Indirect impacts on durability include how clay minerals alter textural properties, including pore size distribution, of sandstones, potentially heightening their vulnerability to certain weathering processes. Many studied sandstones were heterogenous meaning their mineralogy and physical properties vary considerably giving rise to analytical challenges and making stone durability and decay more difficult to define and understand. For example, the use of hydrophobic treatments at Arbroath is risky mainly because of the heterogenous nature of the stone, and so the efficiency of the treatment, as shown by experiments, is extremely variable.

The project findings offer a better understanding of sandstone durability in Scotland, and a thorough characterisation of the clay mineralogy of studied sandstones. Moving forward, the impact of climate change on durability of these poor-quality stones, such as the impact of increased precipitation, should be assessed through both long-term field monitoring and lab-based experiments.

Table of Contents

List of Tables

List of Figures

Acknowledgements

This research would not have been possible without the continuous support of supervisors, mentors, family, and friends. I would also like to acknowledge the University of Glasgow and Historic Environment Scotland (HES) for funding this project in the first place. Although there are too many people to name, I would like to thank certain individuals for the positive impact they have made during my time as a researcher at Glasgow.

Firstly, Prof. Martin Lee, who has supervised and guided me through both my BSc Hons and Ph.D. research projects. I am thankful for the opportunities you have helped me realise and the freedom you offered me when designing and working on my own projects. Thank you to the rest of my supervisory team, Dr. Maureen Young and Dr. Amanda Owen, who were always there to answer questions and provide support. I would also like to thank Dr. Callum Graham at HES – who offered up countless hours assisting me with XRD analysis at the Engine Shed.

I would like to express gratitude to Dr. David Benavente at the University of Alicante, who dedicated their time and expertise towards helping me become a better researcher. Thank you for your patience and kindness, and for making me feel at home in Alicante.

I have made some fantastic memories in the Molema building over the course of my undergraduate and postgraduate studies and will forever consider the place a second home. I am grateful for the friends I have made while studying here and the many walks, cakes, coffees, and alcoholic beverages, we have enjoyed together. A special thanks to all the technicians I have worked with at the Molema and elsewhere, who helped set up experiments, prepare samples, and run analysis. The cogs of research would not turn without you all.

Finally, I would like to acknowledge the support of my family, and in particular my husband, David, who has supported and encouraged me throughout my entire time at university. He has been my biggest fan on both my best and worst days and helped me to become more confident in myself and have trust in my own abilities. He is also the best dad to our two-year-old son Alasdair, born during the COVID-19 pandemic. Returning to my Ph.D. after becoming a mother would have been impossible without David, and an army of grandparents of course.

I dedicate this piece of work to my son, Ally, who makes me smile and laugh every day. This thesis will not make you smile or laugh, but I hope it encourages you to do something for yourself one day.

Author’s Declaration

I, Marli de Jongh, declare that, except where explicit reference is made to the contribution of others, this dissertation is the result of my own work and has not been submitted for any other degree at the University of Glasgow or any other institution. Any published or unpublished work by other authors has been given full acknowledgement in the text.

Signature:

Date: 30.05.2022_______________________

1.0 Introduction

1.1 Scotland’s sandstone-built heritage

During 2019-2020 (pre-Covid) Historic Environment Scotland welcomed over 5.2 million visitors to properties in their care, and over 206, 000 new members to their organisation (HES, 2020). The economic growth associated with heritage tourism was in the region of £1.1 billion (HES, 2020). Sandstone is the most common stone used in Scotland’s built heritage (HES, 2020). Sandstones use as a building material in Scotland dates back to settlements in Orkney ~ 3700 BC, making sandstone the material of the oldest standing stone building in northwest Europe. Scotland’s culture and history are preserved through these historic sandstone buildings and monuments which continue to be an invaluable asset for the country through tourism, employment, and economic growth.

HES have noticed that certain sandstone-derived heritage sites, over the last few decades, are experiencing rapid decay and are becoming increasingly vulnerable to ruin. Although the petrography of many original and replacement stones in Scotland has been characterised in detail previously, in many cases there is still a lack of understanding regarding the nature and causes of stone decay in monuments and buildings. This may be partly due to an absence of data characterising properties other than petrography, including physical properties of stone such as pore size distribution, stone strength, and resistance to weathering. Despite being common throughout recent literature (Calia et al., 2000; Warke & Smith., 2007; Benavente et al., 2008; Eslami et al., 2018; Scrivano & Gaggero., 2020), this holistic approach of characterising all stone properties seems to be lacking in relation to sandstones found in the built heritage of Scotland, and the UK more generally. Moreover, decay of sandstone can be a complex process to understand due to the porous nature of the stone, and the variability in mineralogy and physical properties which influence decay (Figure 1.1).

Sandstones often contain reactive minerals including clay minerals which are prone to weathering and alteration. The prevalence of clay minerals in Scottish sandstones and the impact they have on sandstone durability and decay is currently unknown. As well as being vulnerable to weathering and alteration, clay minerals have complex and variable chemical structures, crystal defects, and a very fine grain size, properties which make their study and understanding them in the context of stone durability and decay a considerable challenge.

1.2 Research aims

The sandstone heritage of Scotland is becoming increasingly vulnerable to weathering and decay. The properties of sandstones, in particular the petrophysical properties, have not been characterised in detail previously, and so the mechanisms and causes of weathering and decay are poorly understood. This poor understanding limits potential preservation efforts aimed at protecting vulnerable sandstone buildings made by conservation bodies such as HES. This research aims to elucidate the nature of these poor-quality sandstone through extensive characterisation of both mineralogical and physical properties to provide new insights into sandstone durability and decay in Scotland. The primary objectives of this research are listed below with reference to relevant chapter numbers:

I. Critical evaluation of the preparatory and analytical procedures for clay minerals using pXRD. (Chapter 2)

II. Improve understanding of the durability of selected sandstones used in the built heritage of Scotland through detailed characterisation of their physical and mineralogical properties. (Chapter 3)

III. Investigate the use of hydrophobic treatments as a means of protecting vulnerable sandstone from accelerated weathering and decay. (Chapter 4)

IV. Provide recommendations for Historic Environment Scotland around topics including: sandstone durability, preservation of vulnerable sandstone sites, and future research. (Chapter 6)

V.

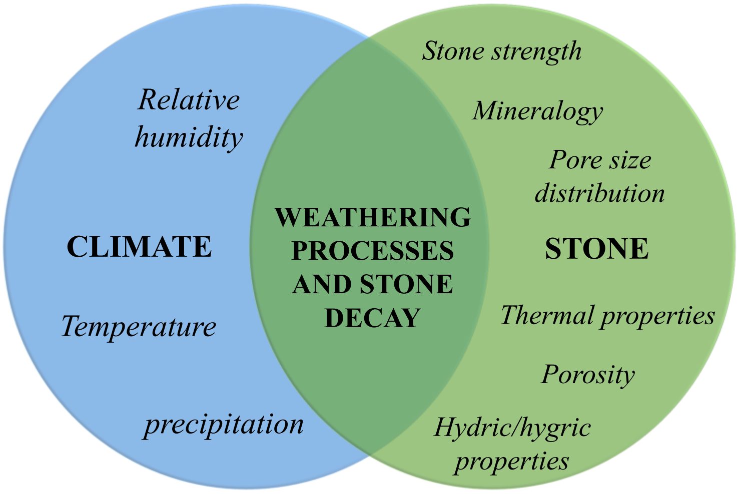

Figure 1.1: The interaction between stone properties and climate – the driving forces of weathering and decay in the built heritage. There are many stone properties, both mineralogical and physical, which impact stone durability.

1.3 Sandstone distribution in Scotland

Most of the sandstone bedrock in Scotland is part of the Old Red Sandstone (ORS), which was deposited as sediment during the Devonian (Hillier et al., 2006). In addition to ORS, Carboniferous sandstone deposits and coal measures are found in the Midland Valley, an ancient basin where most of Scotland's sandstone is concentrated. The Midland Valley is bound to the North by the Highland Boundary Fault (HBF) and to the South by the Southern Uplands Fault (SUF). These deposits of the Midland Valley have been quarried extensively through history (Figure 1.2). ORS can be found North and South of the Midland Valley including areas such as: Borders, Inverness, Elgin, Thurso, Orkney, and Shetland. The NE of Scotland and Orkney have been quarried extensively in the past for flagstone. The sandstone deposits in the Borders region (SE) haven't been quarried as much as other sandstone deposits in Scotland. New Red Sandstone (NRS) is less common in Scotland, most outcrops of which are found near Dumfriesshire and Ayrshire (south of the Midland Valley), Elgin (North of the Midland Valley), and the Isle of Arran. ORS, including the building sandstone Locharbriggs, which is disproportionately represented in historic and present-day architecture of Scotland due to the sandstones attractive red appearance and generally good physical properties and durability.

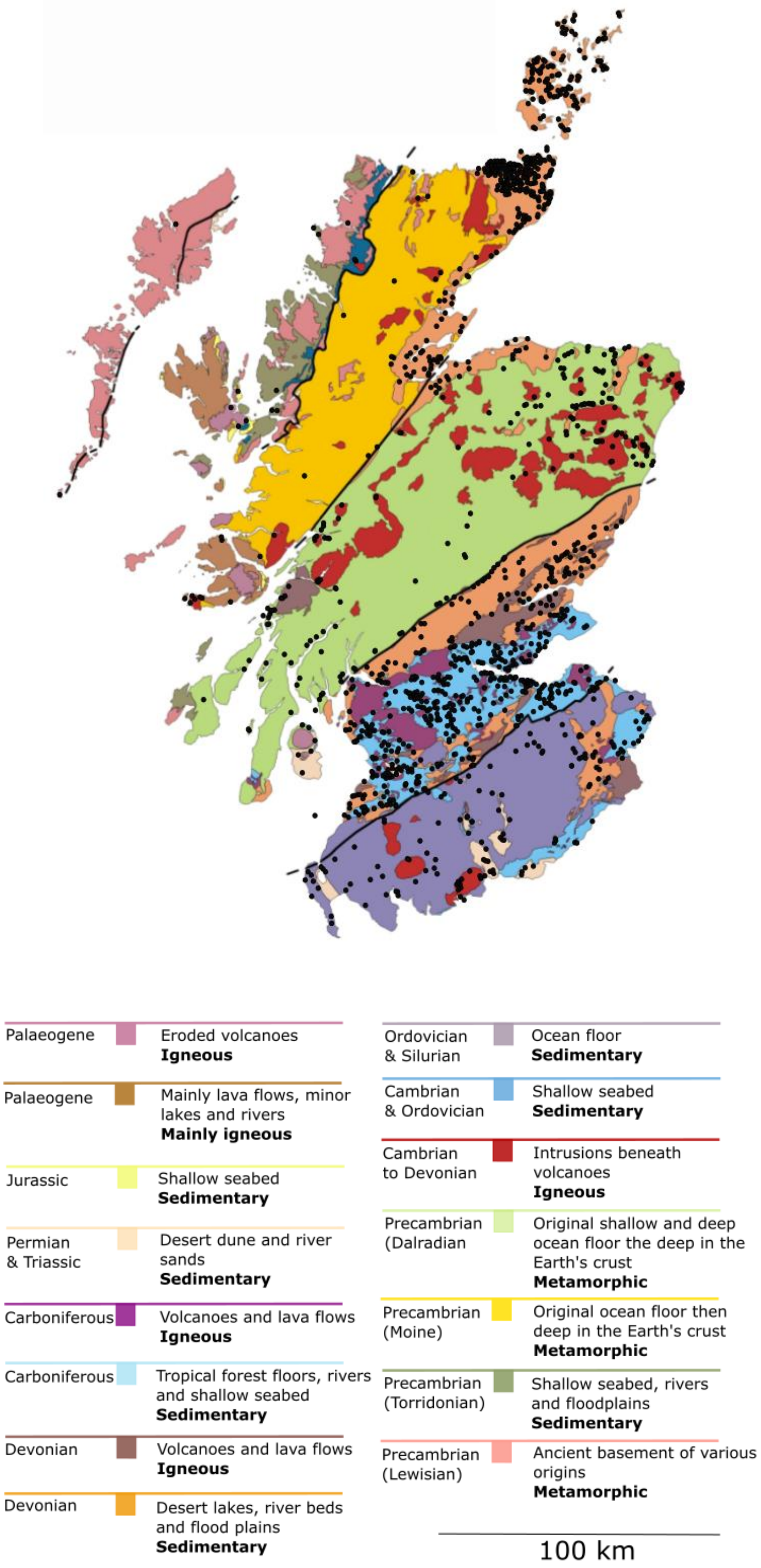

Figure 1.2: Locations of historic and present quarries in relation to the environmental conditions operating during sediment deposition. Quarry data source: BGS Interactive Scotland Stone Database. Map source: Scottish Geology Trust, www.scottishgeology.com/geology-of-scotland-map/

1.4 Sandstones

Sandstones are rocks made of sediment accumulations which have been compacted and lithified and subject to diagenetic processes (Pettijohn., 2019). The sediment comprises varying amounts of quartz, feldspars, lithic fragments, and clay minerals, as well as other trace minerals including oxides. Minerals found in sandstone can be either detrital or authigenic in origin. Detrital material is pre-existing material eroded at the Earth’s surface which is then incorporated into the sediment and lithified rock. Authigenic material originates during diagenesis and is associated with the breakdown of other minerals, facilitated often by temperature and the presence of fluids (Pettijohn., 2019).

There are several schemes available to use when classifying sandstones. In most cases, sandstone classification depends on the relative amounts of major components: quartz, feldspars and lithic (rock) fragments (Garzanti., 2019). The three major sandstone types featured in most classification schemes are: quartz arenites, feldspathic arenites, and litharenites, as seen from the Folk (1974) model (Figure 1.3). As mentioned above, clay minerals are typically a minor component of sandstone consisting of a few wt % (Sebástian et al., 2008), existing as clasts, cement and/or matrix material, and can either be detrital or authigenic in origin (Figure 1.4). In addition to arenites, wackes are composed of 15-75% clay matrix however, as less commonly used as building stone relative to sandstone.

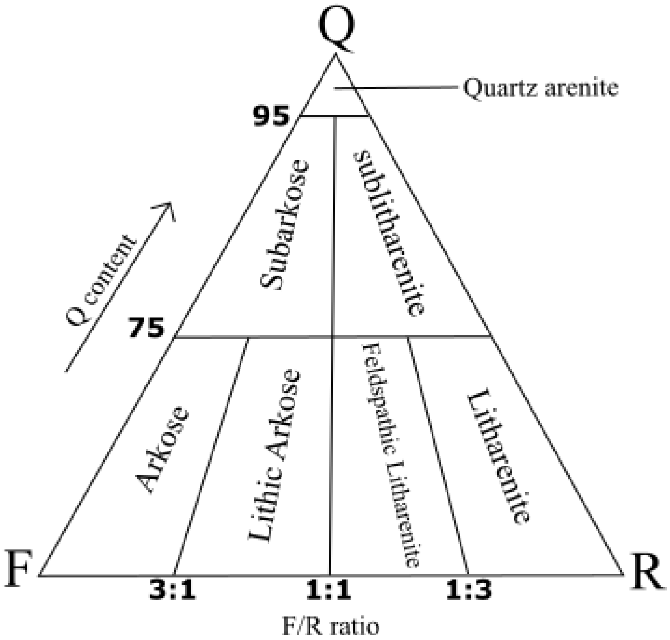

Figure 1.3: Sandstone classification based on relative proportions of quartz, feldspars, and rock fragments (lithics). The primary mineral for all sandstones is quartz (Folk, 1974).

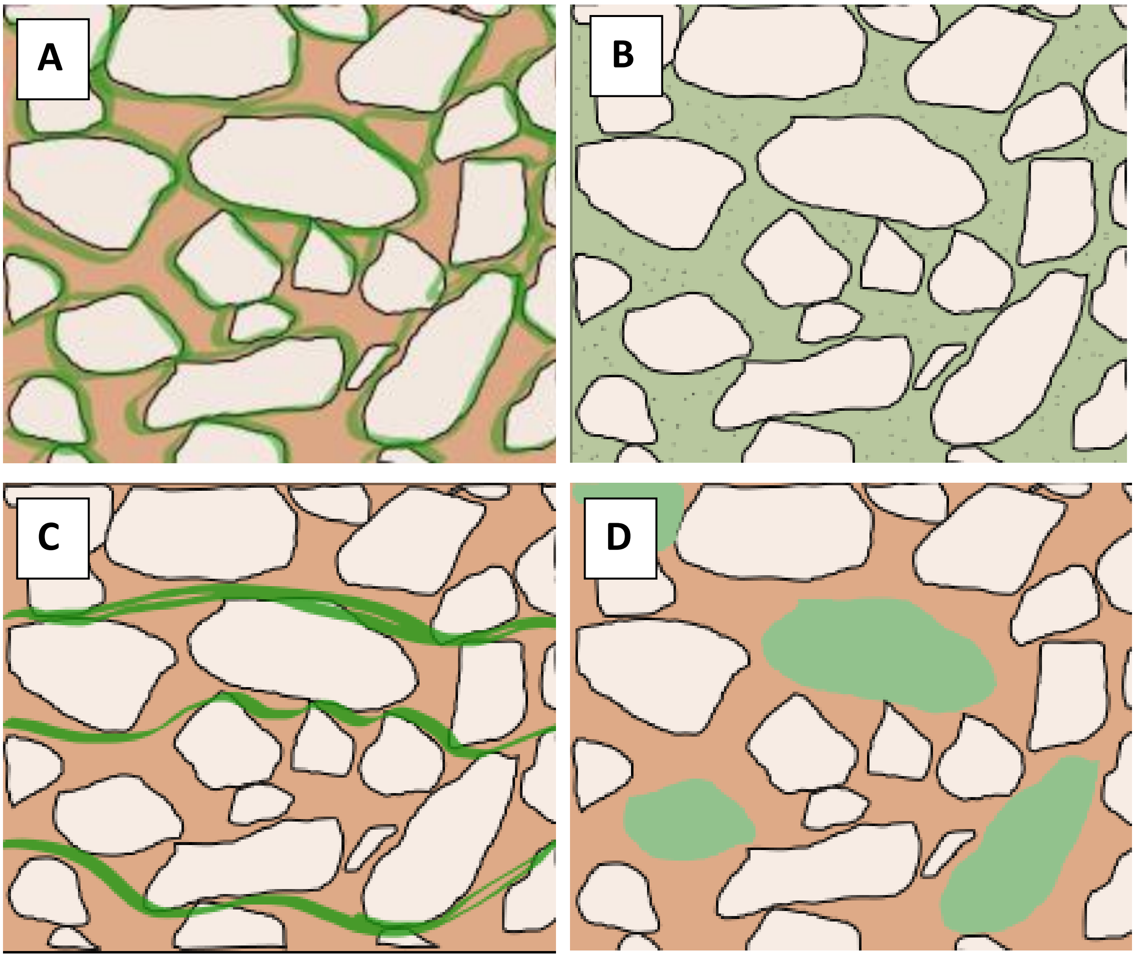

Figure 1.4: Distribution of clay minerals in sandstone. Clay minerals are represented in the colour green. Clay minerals can be detrital or authigenic and distributed in a variety of ways. They can exist as: detrital or authigenic clay mineral coatings (A); detrital or authigenic clay matrix (B); detrital clays found in layers/concentrated on bedding planes (C); and detrital clasts (D).

The mineralogy and petrography of sandstone is controlled by the environment and climate during the time of sediment deposition. The depositional environment and climate influence the maturity and composition of the sand deposited prior to burial and diagenesis (Worden & Morad., 2003; McKinley et al., 2003). Clays are more likely to be deposited in environments which are closer to the sediment source; limiting time for chemical weathering. Furthermore, the deposition of clay- and sand-sized particles in the same location requires fluctuation in energy levels associated with the depositional environment. The depositional environments more commonly associated with preservation of clays and clay-rich sandstones are primarily fluvial environments. In these environments sediment of varying grain size and composition can be transported by water and deposited as immature sands. Clays are also more likely to be preserved in an arid climate, where chemical weathering is limited. An aeolian input also aids in clay mineral preservation as it facilitates faster transport of material. An arid desert climate with fluvial environments is characteristic of the

Devonian period of Scotland. As seen from Figure 1.2, ORS deposits of Devonian age can be found across Scotland in the Borders region, Midland Valley, Orcadian Basin (including Orkney), and Shetland (Hillier et al., 2006). Some of the sandstones were deposited closer to the end of the Devonian into the early carboniferous, including the sandstones of the Stratheden and Inverclyde Formation in the Borders, meaning the climate may have been progressing to a more humid environment by this point, and accelerating chemical weathering of reactive minerals. However, generally speaking these Devonian sandstones may have a relatively higher potential in comparison to other sandstones for preserving clay-rich sediment deposits due to the environmental and climatological conditions during the Devonian.

Another factor contributing to prevalence of clays in sandstones, is source of sediment. Incorporation of less stable minerals and rock fragments can facilitate weathering and transformation of minerals during diagenesis. This is particularly relevant in the case of igneous rocks which often contain unstable, reactive minerals which often contain the elements (Ca, Mg, Na) desirable for clay mineral formation during diagenesis through mineral weathering and alteration. Therefore, immature sediments which contain reactive minerals increase the likelihood of clay mineral formation during diagenesis. ORS deposits located in and around Dundee City, form part of the Dundee Flagstone Formation, in which sandstones consist mostly of litharenites where many of the lithic fragments have an igneous origin. For example, the Kingoodie sandstone is a purplish sandstone with lithic fragments of mainly andesite, likely originating from nearby lava deposits. The Kingoodie sandstone, and other nearby sandstones are commonly found in Dundee’s built heritage.

Clay minerals in sandstone can also form and transform during diagenesis. The occurrence of authigenic clay minerals is controlled by factors related to diagenesis (changes in temperature, pressure, availability of fluid) and composition of the sediment, which is influenced by sediment source. For example, authigenic clay minerals are most likely to form in immature sediments as they contain reactive minerals which are more likely to weather and provide the necessary ions for clay mineral formation (Worden & Morad., 2003; McKinley et al., 2003). Furthermore, different stages of diagenesis are associated with different compositions of clay minerals. For example, dioctahedral and trioctahedral smectites are common during the early stages of diagenesis (eogenesis) when temperatures and pressures are relatively low (McKinley et al., 2003). With increasing burial and temperature, smectite loses its structural H_2O and with it its ability to expand and contract.

Eventually smectite transforms to kaolinite, illite, or chlorite through the processes of kaolitization, illitization and chloritization, respectively.

Table 1.1 summarises the building sandstones in Scotland which are relatively more likely to be clay-rich based primarily on climate and depositional environment. As noted previously other factors including sediment source and diagenetic processes impact the amount and types of clays present in any sandstone, and so Table 1.1 acts only as a guide to getting started.

Table 1.1: the potential for clay-rich sandstone based on depositional environmental and climate. As discussed in the introduction, an arid climates with fluvial depositional environments are considered places where clay minerals are more likely to be preserved.

Potential for preservation of detrital clay minerals	Sandstone	Geologic Age	Depositional environment	Depositional climate
High potential	Swanshaw	Late Silurian – Early Devonian	Fluvial, aeolian	Arid
	Cromlix, Teith, Scone	Early Devonian	Fluvial, aeolian	Arid
	Gardenstown, Raddery	Mid Devonian	Fluvial, aeolian	Arid
	Berriedale	Mid Devonian	Lake floor	Arid
	John O’ Groats	Mid Devonian	Fluvial, aeolian	Arid
Moderate-high potential	Dunnet Head, Glenvale, Alves, Scaat Craig,	Late Devonian	Fluvial	Transitioning from arid to sub-tropical and tropical
	Stratheden and Inverclyde, Kinnesswood	Late Devonian – Early Carboniferous	Fluvial	Sub-tropical to tropical
	Isle of Skye*	Jurassic	Shallow seabed	Tropical

1.5 Clay minerals in sandstone

Clay minerals are a large and diverse group of phyllosilicate minerals consisting of four main sub-groups: illite, kaolin, smectite, and chlorite (Table 1.2) (Elert & Rodriguez-Navarro., 2022). The crystallographic structure of clay minerals consists of octahedral and tetrahedral sheets. Depending on the crystallographic arrangement, clay minerals can be described as having a 2:1 or a 1:1 structure (Dyar et al., 2008). Clay minerals can be further subdivided based on how many octahedral sites are occupied by ions. Table 1.2 also illustrates the different sheet assemblages associated with each clay mineral group.

Smectite is a chemically variable sub-group of clay minerals known for their physically expansive properties. Smectites have a 2:1 layered silicate structure comprising two tetrahedral sheets which are weakly bonded to an octahedral sheet. The tetrahedral sheets are primarily composed of Si and Al, while the octahedral sheet is composed of metal hydroxides (e.g. $Fe_3(OH)$, $Al_2(OH)_6$). Smectites can be further sub-divided into dioctahedral and trioctahedral depending on how many of the three octahedral units are occupied (Dyar et al., 2008). Two of three octahedral units are occupied in the case of dioctahedral smectite, usually with trivalent cations including Al^{3+} or Fe^{3+}. All three octahedral units are occupied in trioctahedral smectite, where occupants are usually divalent cations including Mg^{2+} and Fe^{2+}. The cations occupying both tetrahedral and octahedral units in smectite are exchangeable, meaning other ions, ideally with the same charge, can act as substitutions and occupy the units. If the charge of the sheet is not balanced by substituting ions, due to limited availability, an overall negative charge is produced (e.g. Fe^{2+} substituting Fe^{3+} in an octahedral sheet). The net negative surface charge of a clay mineral attracts the cation of H_2O, allowing smectite to absorb water and physically expand (Figure 1.5) (Madsen & Müller-Vonmoos., 1989). It is this ability to absorb water into its chemical crystal structure, as well as the presence of exchangeable cations, which distinguishes the smectite group from other clay groups. It is this characteristic of smectite which negatively impacts the durability of some clay-rich sandstones by enhancing physical weathering through cycles of expansion and contraction (Sebastián et al., 2008).

Table 1.2: Main clay mineral groups, their layer structure, and example minerals with chemical composition.

Clay group	Layer structure	Example minerals
Kaolin	1:1	kaolinite; dickite; halloysite; nacrite $[Al_2Si_2O_5(OH)_4]$
Smectite	2:1	montmorillonite $[(Na,Ca)_{0.33}(Al,Mg)_2(Si_4O_{10})(OH)_2 \cdot nH_2O]$; nontronite $[Na_{0.3}Fe_2((Si,Al)_4O_{10})(OH)_2 \cdot nH_2O]$; saponite $[Ca_{0.25}(Mg,Fe)_3((Si,Al)_4O_{10})(OH)_2 \cdot nH_2O]$
Illite (and other clay-micas)	2:1	illite $[K_{0.65}Al_{2.0}[Al_{0.65}Si_{3.35}O_{10}](OH)_2]$; glauconite $[(K,Na)(Fe^{3+},Al,Mg)_2(Si,Al)_4O_{10}(OH)_2]$; phengite $[KAl_{1.5}(Mg,Fe)_{0.5}(Al_{0.5}Si_{3.5}O_{10})(OH)_2]$; muscovite $[KAl_2(AlSi_3O_{10})(OH)_2]$
Chlorite	2:1:1	clinochlore $[Mg_5Al(AlSi_3O_{10})(OH)_8]$; chamosite $[(Fe^{2+},Mg,Al,Fe^{3+})_6(Si,Al)_4O_{10}(OH,O)_8]$; pennantite $[Mn^{2+}{}_5Al(AlSi_3O_{10})(OH)_8]$

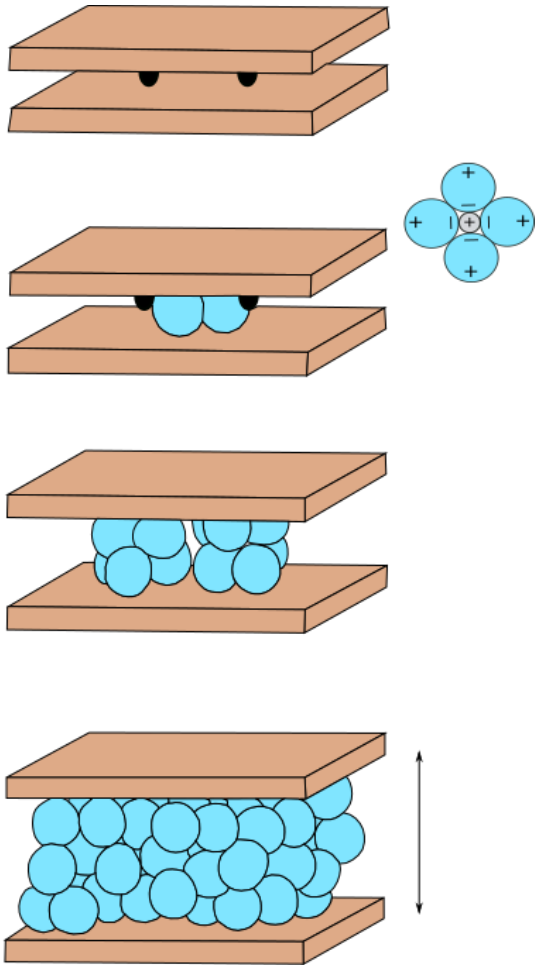

Exchangeable cations are located between layers of expansive clay minerals such as montmorillonite. In the case of montmorillonite, cations are usually Ca^+ or Na^+.

During interaction with water, the positive charge of these ions attracts the negative dipole of the water molecules. As the cations hydrate, the space between layers becomes larger (i.e. there is an increase in d-spacing of the 001 plane).

Different expansive clays have different swelling potentials. Montmorillonite can experience a volume increase of up to 100%

Figure 1.5: Intracrystalline swelling mechanism associated with expansive clay minerals. The example in the figure is montmorillonite. Blue spheres represent H_2O while the smaller black spheres represent cations. Figure adapted from Madsen & Müller-Vonmoos (1989).

1.6 Climate change in Scotland

The vulnerability of clay minerals to physical expansion and contraction will ultimately be influenced by climate change. During the most recent decade (2008-2017) Scotland’s annual average rainfall has increased by 11% in comparison to 1961-1990 (Met Office., 2018) This trend looks to continue as the UKCP18 forecast that UK will see increases in average annual precipitation of up to 35% (RCP8.5) and increases in the intensity of rain events (UKCP18). These changes in precipitation are most noticeable in Scotland and will be part of wetter and colder winters (Figure 1.6). More precipitation may lead to periods of prolonged stone wetness and accelerate weathering and decay. Moreover, different weathering processes, such as chemical weathering, may become more dominant as the climate becomes wetter and warmer. Finally prolonged periods of stone wetness may soften clay minerals which may have detrimental impacts on the physico-mechanical properties of some stones (Jiménez González & Scherer., 2004; Jiménez González et al., 2008). It is therefore important to consider the outcomes of the following research chapters in relation to climate change with the overall goal focussed towards adapting the built heritage where possible to protect it from the effects of climate change. As well the effects of climate and climate change, stone weathering and decay is also influenced by the intrinsic properties of the stone, both mineralogical and petrophysical. These intrinsic properties in the context of weathering and decay are discussed in the following section.

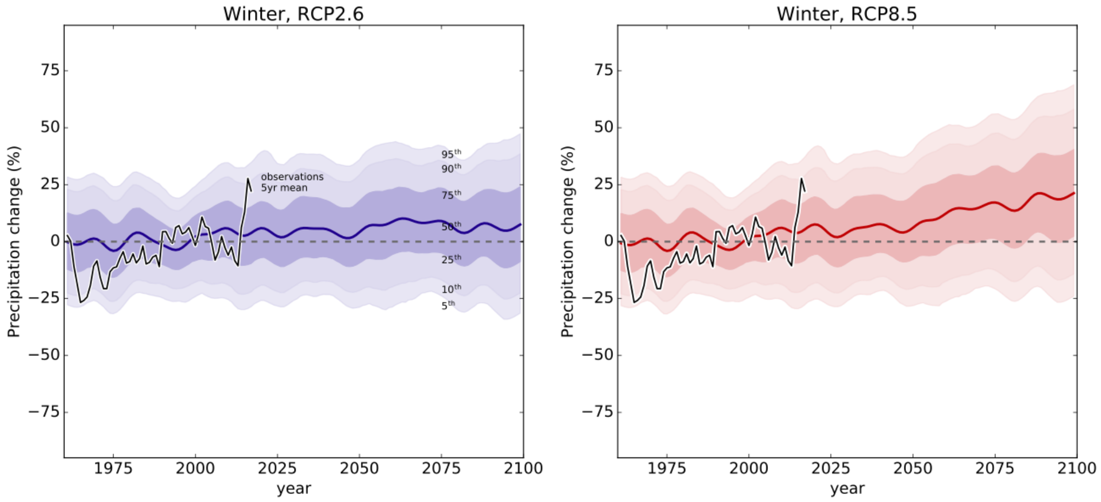

Figure 1.6: Precipitation change for UK for low emission (RCP2.6) and high emission (RCP8.5) scenarios. Increasing precipitation change is consistent across all emission scenarios.

1.7 The role of clay minerals in the decay and durability of sandstone

1.7.1 Defining decay and durability

Decay patterns are diverse in both appearance and scale, and the type of patterns that manifest depend on the weathering mechanisms responsible for decay, which are themselves determined by stone properties and climate. Decay patterns are usually described through visual assessment of a site during the earlier stages of a specific conservation project. The ICOMOS-ISCS illustrative glossary on stone deterioration patterns is a global reference guide used in the identification of decay patterns. The glossary aids in a consistent approach to identifying and describing decay, reducing potential ambiguity of decay-related terminology.

According to the ICOMOS-ISCS glossary, stone deterioration can be subdivided into five categories: crack and deformation, detachment, featured induced by material loss, discolouration and deposits, and biological colonisation. Some examples of decay of sandstone are shown in Figure 1.7.

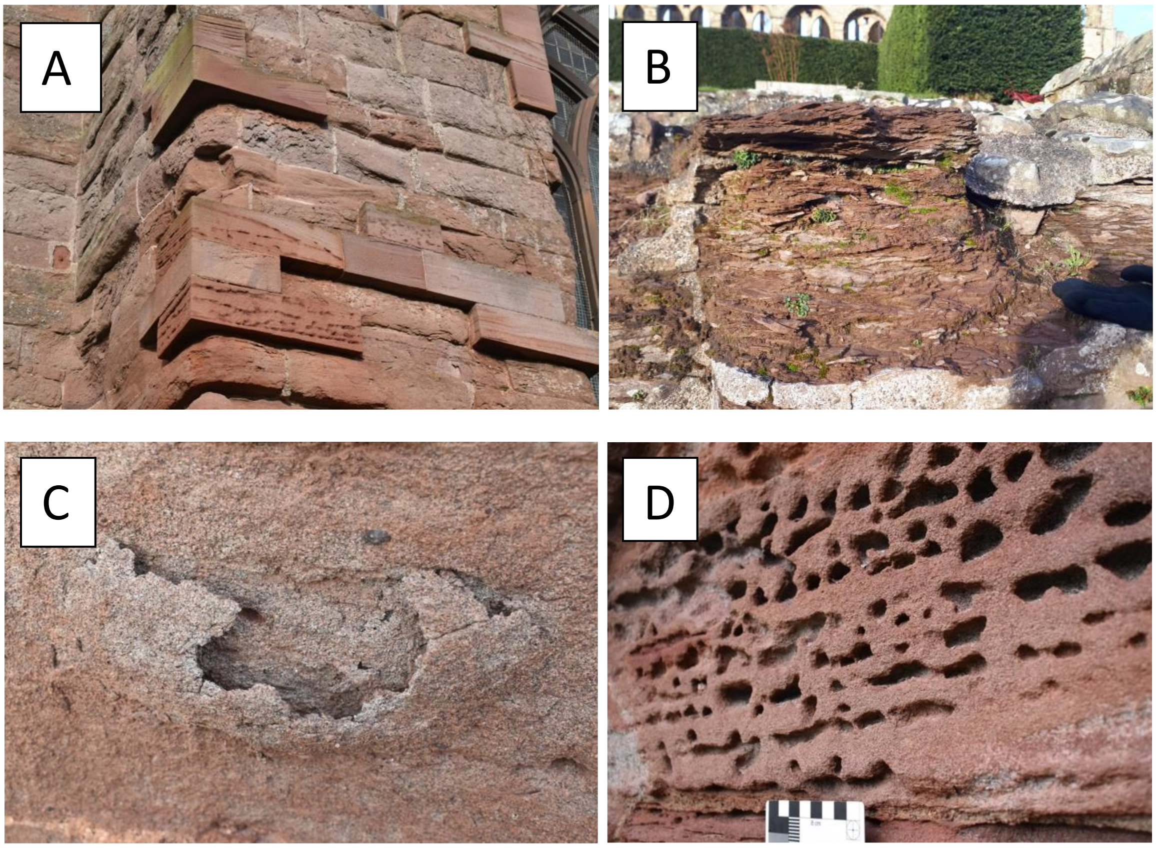

Figure 1.7: Different types of decay manifesting at historic sandstone buildings around Scotland: A) Spalling and flaking of sandstone. Replacement stones visible show extent of weathering; B) Spalling and granular disintegration of bedded sandstone; C) Blistering of sandstone; D) Aveolization weathering, a common pattern produced through salt weathering.

The glossary also defines general terms which are often, incorrectly, used interchangeably. Table 1.3 provides the definition for several terms which are often used interchangeably in the study of stone decay despite having slightly different meanings. Weathering refers to processes leading to modification and/or deterioration while decay is associated with loss in value or impairment of use and is therefore used commonly in the context of ornamental stone (Table 1.3).

Table 1.3: Definitions for general terms often used in the study of stone decay according to ICOMOS-ISCS glossary. Most commonly used words throughout this thesis marked by * where ** = very common, * = common.

Word	Definition
Alteration*	*Modification of the material that does not necessarily imply a worsening of its characteristics from a conservational point of view. For example, a reversible coating applied on a stone may be considered as an alteration.*
Damage	*Human perception of the loss of value due to decay*
Decay**	*Any chemical or physical modification of the intrinsic stone properties leading to a loss of value or to impairment of use.*
Degradation	*Decline in condition, quality, or functional capacity.*
Deterioration*	*Process of making or becoming worse or lower in quality, value, character, etc.*
Weathering**	*Any chemical or mechanical process by which stones exposed to the weather undergo changes in character and deteriorates.*

Stone durability can be defined as a stones resistance to weathering, and is influenced by intrinsic stone properties, both mineralogical and physical, and the external environment (climate) (Přikryl., 2013). There is considerable variation in literature regarding the type and number of intrinsic properties which have the greatest influence on stone durability. Some previous studies have defined durability indices using selected stone properties (Winkler 1986; Richardson 1991; Ordonez et al., 1997; Benavente et al., 2004; Yu & Oguchi., 2010). Some studies have used as few as two properties to estimate stone durability, as in the case with Winkler (1986), who suggested durability could be estimated by comparing wet and dry compressive strength of stone. Similarly, Delgado Rodrigues (1988) used two key properties, porosity and swelling strain, to estimate durability of carbonate rocks. However, it is generally considered that the more intrinsic stone properties characterised, the most accurately stone durability can be understood (Benavente et al., 2008). Intrinsic stone properties interact with the external environment (climate) to influence weathering processes and decay (Figure 1.1).

1.7.2 Stone properties

Intrinsic stone properties can be subdivided into mineralogical and physical properties. Mineralogy of sandstone is often assessed using a combination of both Scanning Electron Microscopy (SEM) and X-ray Diffraction (XRD) to determine the ratio of major sandstone components (quartz, feldspar, and lithics) and characterise the clay fraction and other minor components such as micas (Vázquez et al., 2013; Scrivano 2017; Scrivano et al., 2018). Moreover, the petrography of the stone including grain size, shape, sorting, cements, bedding, distribution of minerals, etc can be obtained through optical and SEM imaging.

Physical properties of sandstone which have been previously studied in the context of sandstone durability in literature include, but are not limited to: density, porosity and pore size distribution, water transport properties, hydric/hygric expansion properties, thermal properties, stone strength, and durability (resistance to weathering) (Benavente et al., 2008; Přikryl., 2013; Viles., 2013). Pore characterisation is considered one of the most important physical properties in the study of sandstone durability (Benavente., 2004). The pore network determines how and to what extent water will percolate through the stone, which in turn will facilitate weathering processes. Porosity and pore size distribution are typically measured using Mercury Intrusion Porosimeter (MIP), and microporosity using nitrogen absorption (Çelik & Ergül., 2018; Germinario & Török., 2020; Benavente et al., 2021).

Furthermore, additional information on pore shape, connectivity of pores ect can be obtained through SEM imaging. Water transport properties including capillary absorption and vapour diffusion. Water transport properties define how moisture interacts with stone in different states (liquid vs vapour). Capillary water absorption refers to the absorption of water via capillary processes and is closely related to the pore structure and porosity of stone where stones with larger pores and higher porosity usually exhibit higher rates of capillary absorption (Benavente et al., 2007; Ruedrich et al., 2011). Water vapour diffusion resistance is also a common water transport property and is commonly characterised before and after treatment with consolidants and water repellents. Characterising this property helps to determine the 'breathability' of the stone; defined by the rate at which water vapour can still move freely (Elhaddad et al., 2018; Aslanidou et al., 2018).

Hygric and hydric expansion properties characterises deformation of stone when in contact with water. Hydric dilatation refers to expansion of stone with increasing moisture content related to intrusion of liquid water (Ruedrich et al., 2011; Aguilar et al., 2018); while hygric dilatation refers to expansion of stone with increasing moisture content related to changes in RH between 0% and 95% RH (Ruedrich et al., 2011; Ferrer et al., 2021). Dilatation can be measured using several methods which all aim to quantify deformation on a mm-scale using some kind of strain gauge or dilatometer. Thermal properties characterise how a stone responds to exposure to different temperatures. For example, thermal expansion is a commonly studied property in understanding stone durability (López-Doncel et al., 2018; Vigroux et al., 2021). The thermal expansion coefficient of a stone is closely related to mineralogy (Siegesmund and Dürrast., 2011). Sandstones typically have higher values (in the range of 10 x 10-6 K-1) compared to other rock types as they contain mostly quartz, with thermal expansion coefficient typically between 9 x 10^{-6} K^{-1} and 14 x 10^{-6} K^{-1}. Similar to hydric and hygric expansion, thermal expansion can be quantified using a dilatometer which measures deformation on a mm-scale. Stone strength is considered a crucial property influencing sandstone durability (Benavente et al., 2004). Uniaxial Compressive Strength (UCS) is the most commonly studied rock strength in the study of durability however, other types, including tensile and flexural, have been studied in stone conservation studies (Zhou et al., 2018; Noor-E-Khuda et al., 2019; Vigroux et al., 2021).

Finally, weathering experiments are used to define the durability of a stone. Whereas all the aforementioned properties influence the durability of stone, resistance to weathering defines the durability of stone. Both accelerated lab-based and natural outdoor weathering experiments are used as a means of characterising a stones resistance to weathering (durability) and typically occur over several week periods (in a lab setting), although some natural outdoor experiments have occurred on a much longer time scale (Behzadtabar et al., 2019; Dias Filho et al., 2020). Lab-based accelerated weathering experiments are often conducted in a controlled environment, most commonly a climate chamber where temperature and RH can be maintained at desired conditions. These experiments often induce weathering through means of either crystallisation-dissolution of salts, freeze-thaw, wet-dry cycles, thermal cycles, or exposure to UV (Zhou et al., 2017; Sbardella et al., 2018).

As seen from the number of stone properties described above, characterising stone durability and identifying causes of decay isn't a simple problem. This is further complicated by the various weathering processes which may be operating at any given site. Below is a description of major weathering processes which can act upon clay-rich sandstone with varying intensity depending on the durability of stone, with reference to contributing intrinsic stone properties where relevant.

1.7.3 Major weathering processes of sandstone

Sandstones are porous and permeable rocks which makes them susceptible to moisture ingress (Sun & Jia., 2019). Water acts as a catalyst for physical, chemical and biological weathering processes. The following section describes common physical, chemical and biological weathering processes associated with sandstone with related case studies from literature focussed on understanding the decay and durability of clay-rich sandstones.

1.7.3.1 Physical weathering

Physical weathering processes commonly exert pressure internal to the stone leading to decay. Salt weathering is considered the most damaging type of weathering process and is common in porous stones such as sandstone (Charola., 2000). The damage associated with salt weathering is caused by cyclic crystallisation and dissolution of salts which exerts internal pressure on pore walls and over time leads to decay (Charola & Bläuer., 2015). Moreover, the presence of clay minerals in texturally and mineralogically immature sandstones, in particular the affect they have on porosity, has been shown to increase sandstone's vulnerability to decay caused by salt weathering (McGreevy & Smith., 1984; Warke and Smith., 2000; Warke et al., 2006). The interaction of clay minerals and salts can also enhance decay as described by Sebastián et al (2008) who noted the presence of NaCl in the Tarifa building sandstone, and its ability to enhance osmotic-type expansion of clay minerals by acting as an effective electrolyte in solution.

Hydric and hygric expansion of sandstone when in contact with moisture is commonly associated with the presence of clay minerals, especially the intracrystalline swelling of expansive smectites (Madsen & Müller-Vonmoos, 1989; Ruedrich et al., 2011). Swelling strains of > 1.5 mm/m are considered significant in the context of tensile stone strength, while some sandstones have reported values as high as 6.7 mm/m (Esbert et al., 1997; Jiménez-González et al., 2008). Outwith the intracrystalline expansion of smectites, Ruedrich et al (2011) highlighted that porosity and pore size distribution were contributing factors influencing observed swelling strains due to the internal pressures generated inside micropores during cyclic wetting and drying. Micropores play an important role in determining moisture transport and vapour flow through stone. The Macigno sandstone is a common building stone throughout Tuscany which is commonly studied in relation to its expansive properties and pore size distribution (Franzini et al., 2007; Scrivano et al 2017; Scrivano et al 2018). The sandstone has a clay -rich matrix which comprises ~15 wt % of the bulk rock and so the stone classification borders feldspathic litharenite and greywacke. The sandstone contains expansive interlayer clay sequences consisting of chlorite-smectite, and corrensite. As well as containing expansive smectite, the sandstone has a high abundance of micropores which contribute to its sensitivity to expansion, especially in the presence of water (Scrivano et al 2017; Scrivano et al 2018). Moreover, the microporous texture of the Macigno sandstone makes it more susceptible to salt weathering as greater crystallisation pressures are generated in smaller pores (Scrivano et al., 2018).

As well as leading to cyclic expansion and contraction, the absorption of water and increase in saturation degree has been shown to affect the strength of sandstone, particularly stone containing clay minerals (Hawkins & McConnell., 1992). The Pennant sandstone is commonly studied in the context of understanding how clay minerals impact overall rock strength under different degrees of saturation. Forest of Dean, a common building stone in the UK and studied in this project, is also part of the Pennant Formation (Vásárhelyi & Ván., 2006; Shi et al., 2016; Li & Wang., 2019). The clay-rich sandstone shows remarkable decreases in Uniaxial Compressive Strength (UCS) reducing by 40-55% when saturated (Hadizadeh & Law., 1991; Hawkins & McConnell., 1992). Furthermore, this weakening occurs when water saturation is as low as 1%, showing the strength of clay-rich sandstone is particularly sensitive to the presence of moisture (Shi et al., 2016). Hawkins & McConnel (1992) attribute this sensitivity to the presence of clay minerals found in the matrix and coating rigid quartz grains which soften when wet creating internal stress and overall weakening of stone. Other physical properties including porosity, pore size distribution, grain size and shape also influence the sensitivity of stone strength to water saturation (Cai et al., 2019).

Sandstone can also physically expand and contract with temperature; a weathering process known as thermal cycling. Sandstone expands when subject to relatively higher temperatures and contracts when exposed to relatively cooler temperatures. Over time exposure to cyclic heating and cooling will contribute to decay and lead to an accumulation of residual strain (Steiger & Charola., 2011). Clay-bearing stones can have a negative residual strain upon heating due to their contraction caused by dehydration. When subject to high temperatures (600-1000oC) clay-bearing stones are some of the most negatively impacted stone types, where Sirdesai et al (2019) calculated the porosity of claystone to being x6 higher after exposure to 1000oC – the second worse affected stone type in their study before carbonate-rich sandstone. However, it is important to note that clay minerals commonly exist in sandstones as minor components, so the thermal-related decay effects listed above are typically not as severe.

1.7.3.2 Chemical weathering

Sandstones often contain minerals including feldspars and clay minerals that are unstable and readily react in the presence of water (Turkington & Paradise., 2005). Minerals can alter or dissolve completely through chemical weathering processes which over time leads to decay and potential precipitation of new minerals (i.e. the weathering of feldspar to produce kaolinite or smectite) (Figure 1.8). The H+ ion of water is responsible for the onset of dissolution and mineral alteration eventually leading to pore waters enriched in ions released from reacting minerals. The nature and rate of mineral dissolution depends on: availability of liquid water, mineral solubility, and acidity. Minerals with the highest solubility, and most prone to weathering, are carbonates (calcite and dolomite), feldspars, and clay minerals. When subject to wet-dry cycles, An et al (2020) identified chemical weathering processes associated with clay-bearing arkosic sandstone including the hydrolysis of K-Na feldspar and formation of kaolinite, and the dissolution of feldspar and kaolinite. Both processes lead to changes in porosity and pore size distribution, and formation of microcracks. Other studies have shown similar chemical weathering effects on physical stone properties (Scrivano et al., 2018; Zhang et al., 2018). Studies like these highlight the important controls chemical weathering can have on the physical properties of stone and decay.

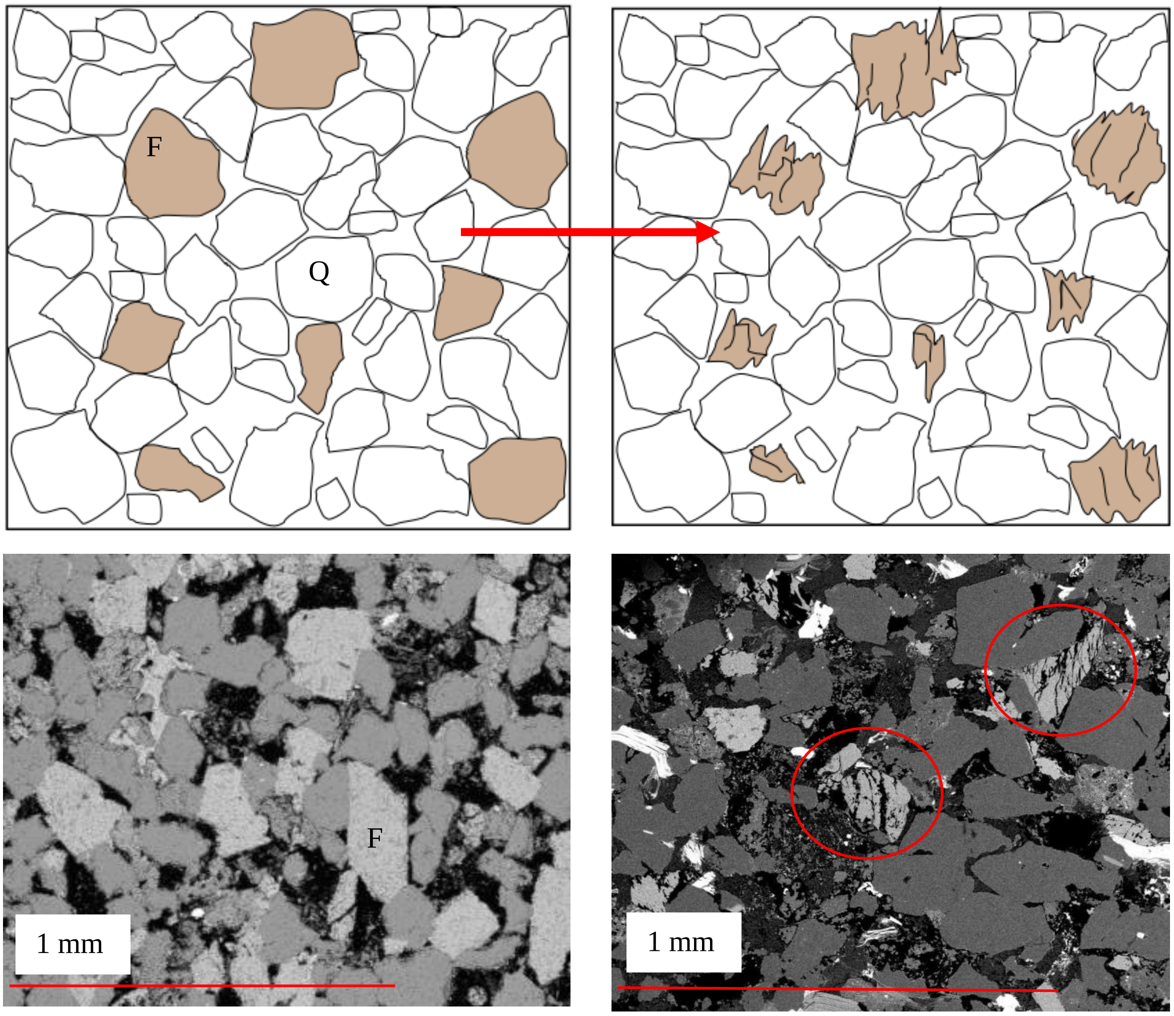

Figure 1.8: Secondary Electron (SE)SEM images polished thin sections showing a relatively fresh and weathered sandstone. Chemical weathering and alteration of relatively less stable minerals (e.g. feldspars, clays) and clay-rich cements in sandstone can lead an increase in porosity and decrease in grain cohesion making the stone more susceptible to further weathering.

1.7.3.3 Biological weathering

Finally, microorganisms (bacteria, archaea, algae, fungi and lichens) can colonise building stone, especially in instances where stone is damp or wet. Biofilms can lead to a blockage of pores at the surface, affecting properties including porosity and vapour diffusion rate (Sterflinger., 2011). Biofilms also attract more water and can enhance chemical weathering. In other instances, microorganisms can create a dark brown/black crusts which amplify thermal decay by absorbing more incoming UV radiation (Sterflinger, 2011; Lui et al., 2020). Biodeterioration may become more common in Scotland according to Smith et al (2011) who suggest a link between enhanced precipitation in the UK associated with climate change, and increased risk of biodeterioration and chemical weathering due to periods of prolonged stone wetness.

1.8 Rock anisotropy and weathering

Rock anisotropy refers to local (mm to cm scale) differences in rock properties (porosity, mineralogy, bedding etc) which result in a directional dependency of certain measured properties. For example, when measuring the capillary absorption of bedded sandstone, absorption rates are typically faster parallel to bedding (where parallel or perpendicular refers to the direction of water flow relative to the direction of bedding) (Sebastián et al., 2008; Benavente et al., 2008; Fořt., 2015). This directional dependency is the result of petrophysical variations along bedding planes which promote faster uptake of water. Sandstones commonly display a degree of anisotropy due to their geological origins involving deposition of sand in layers. Directional dependencies can be observed when characterising properties including hydric expansion, capillary absorption, stone strength, s- and p- wave velocities, and thermal expansion (Fort et al., 2011; Molina et al., 2015). Anisotropy can have important impacts on stone decay and durability. Stones with strong anisotropy may display preferential decay along bedding planes which are more prone to moisture ingress and potential weathering (Fort et al., 2011; Molina et al., 2015).

1.9 Preservation of Scotland’s built heritage

As discussed in the previous section, the petrophysical properties of sandstone, mainly its porous and permeable nature, make it more vulnerable to moisture ingress, weathering, and decay in comparison to other stone types, and similarly make it more sensitive to climate change.

Hydrophobic treatments have been previously applied to sandstone and monitored at several locations around Scotland since the early 1970s. These locations include Elgin Cathedral, Huntly Castle, Arbroath Abbey, Dunkeld Cathedral, and Tantallon Castle (Young et al., 2003). These treatments aim to limit moisture ingress through capillary absorption and in some cases also strengthen stone (consolidants). The composition of the treatments applied in Scotland vary however, most are silane-based materials, and are either resins which consolidate the stone material, liquid agents which provide a hydrophobic coating once dried, or a combination of the two. The suitability of hydrophobic treatments in protecting in Scotland and further afield reveal variable results with regards to the effectiveness and suitability of hydrophobic treatments in protecting porous sandstone (Young et al., 2003; Cnudde et al., 2004; Stefanidou et al., 2013; Vicini & Princi., 2013; Kunz et al., 2022).

In some instances, hydrophobic treatments are shown to alter the porosity and pore size distribution of sandstone. Mercury Intrusion Porosimetry (MIP) showed that treated stone at Arbroath Abbey showed an overall decrease in total porosity in comparison to untreated stone, although this decrease was very slight (1.2%). The other test sites showed almost no difference in pore size distribution (PSD) and total porosity between treated and untreated stone. Changes in porosity can impact sandstone durability and increase the stone's vulnerability to processes such as freeze-thaw and salt weathering. Moreover, changes in porosity can also affect the drying behaviour of stone. Cnudde et al (2004; 2008) showed using XCT that in some instances hydrophobic treatments completely infilled pores, as opposed to lining them; increasing the water vapour diffusion resistance, which in turn prohibits evaporation of water and drying out of stone. Both changes in petrophysical properties and drying properties of stone can lead to a variety of problems including: enhanced chemical weathering, accumulation of soluble salts behind the treated surface, and increased sensitivity of surface layer to processes such as hydric expansion. All of the above problems can lead to accelerated weathering and decay of surface stone.

Penetration depth of hydrophobic treatment is considered an important parameter in selecting a suitable treatment and assessing its efficiency (Charola., 2003; Young et al., 2003). The depth of penetration varied between ~ 18-65 mm when comparing different test sites around Scotland. (Young et al., 2003). The variability in penetration depth across and within sites is partly due to the variation in sandstone porosity, where lower porosity sandstones lead to lower penetration depth. The nature of the substrate (i.e. porosity of stone, hydric properties) should be considered when selecting an appropriate treatment. For example, hydrophobic creams, as opposed to liquids, can be used to increase application time allowing deeper penetration of treatment in lower porosity substrates (Charola., 2003; Snethlage and Sterflinger., 2011). The method of application can also influence the penetration depth of a given treatment (Charola., 2003). There are many application methods including, but not limited to: brushing, spraying, capillary absorption, total immersion, and vacuum impregnation (Young et al., 2003). The type of application method selected depends on several factors including the porosity and permeability of the substrate as well as the condition of the substrate and desired penetration depth.

Finally, there is uncertainty surrounding the long-term behaviour of hydrophobic treatments and how changes in such may affect the condition of the stone (Young et al., 2003; Charola., 2003; Elhaddad et al., 2018). Young et al (2003) noted that at some sites including Arbroath Abbey, treated areas were showing signs of hydrophobicity more than 20 years after initial application. However, Young et al (2003) also acknowledge the difficulty of determining the durability and performance of such treatments which is often limited by sampling restrictions and the long-term nature of the investigations. In a large-scale study, Wendler (1995) investigated changes in water repellency of treated buildings over time, by measuring water absorption rates in-situ using the Karsten tube method. A linear relationship was observed between water absorption rates and time, where water absorption rates became higher with increased time since application of hydrophobic treatment, indicating that hydrophobicity becomes less effective over time. Wendler (1995) noted that some sites of cultural significance still showed hydrophobicity after 15 years, which was attributed to the careful application by trained professionals, emphasising the importance of the application process.

In summary, Scotland provides several unique opportunities to study the long-term behaviour and effects of hydrophobic treatments in the preservation of sandstone. Such treatments may be essential in Scotland's future climate which will subject the built heritage to more severe weather particularly regarding amount of annual rainfall and intensity of rainfall events.

1.10 References

Aguilar, J. G., Fandos, O. B., Lázaro, B. B., Peddis, F., & Cuccuru, F. (2018). Deterioration caused by dimensional change in stone (EBD pathology): the role of the organic matter—pore network—salt combination. Journal of Cultural Heritage, 34, 198-207.

An, W., Wang, L., & Chen, H. (2020). Mechanical Properties of Weathered Feldspar Sandstone after Experiencing Dry-Wet Cycles. Advances In Materials Science And Engineering, 2020, 1-15. doi: 10.1155/2020/6268945

Aslanidou, D., Karapanagiotis, I., & Lampakis, D. (2018). Waterborne superhydrophobic and superoleophobic coatings for the protection of marble and sandstone. Materials, 11(4), 585.

Behzadtabar, P., Ghobadi, M., Fereidooni, D., & Sepahi, A. A. (2019). Comparison between Salt crystallization weathering test and natural weathering in Mesozoic's anisotropic rocks, a case study: Arak᾿s Calcareous slates, Iran. Geopersia, 9(2), 265-277.

Benavente, D., Cueto, N., Martínez-Martínez, J., Del Cura, M. G., & Cañaveras, J. C. (2007). The influence of petrophysical properties on the salt weathering of porous building rocks. *Environmental Geology*, *52*(2), 215-224.

Benavente, D., Cultron, G. & Gomez-Heras, M. 2008. The combined influence of mineralogical, hygric and thermal properties on the durability of porous building stone. European Journal of Mineralogy, 20, 673–685.

Benavente, D., Garcia Del Cura, M.A., Fort, R. & Ordonez, S. 2004. Durability estimation of porous building stones from pore structure and strength. Engineering Geology, 74, 113–127.

Benavente, D., Such-Basañez, I., Fernandez-Cortes, A., Pla, C., Cazorla-Amorós, D., Cañaveras, J. C., & Sanchez-Moral, S. (2021). Comparative analysis of water condensate porosity using mercury intrusion porosimetry and nitrogen and water adsorption techniques in porous building stones. Construction and Building Materials, 288, 123131.

Cai, X., Zhou, Z., Liu, K., Du, X., & Zang, H. (2019). Water-weakening effects on the mechanical behavior of different rock types: phenomena and mechanisms. Applied Sciences, 9(20), 4450.

Calia, A., Mecchi, A. M., & Quarta, G. (2000, January). A research into intrinsic parameters material to the durability of highly porous building stones. In Proceedings of the 9th International Congress on Deterioration and Conservation of Stone (pp. 49-57). Elsevier Science BV.

Carmona-Quiroga, P. M., Martínez-Ramírez, S., & Viles, H. A. (2018). Efficiency and durability of a self-cleaning coating on concrete and stones under both natural and artificial ageing trials. Applied surface science, 433, 312-320.

Çelik, M. Y., & Ergül, A. (2018). Pore characterization of volcanic tuffs used as building stone in Afyonkarahisar (Turkey). Politeknik Dergisi, 21(1), 101-112.

Charola, A. E. (2003). Water Repellents and Other" Protective" Treatments: A Critical Review/Hydrophobieren und andere" schützende" Maßnahmen: Ein kritischer Überblick. Restoration of Buildings and Monuments, 9(1), 3-22.

Charola, A.E.; Bläuer, C. (2015) Salts in Masonry: An overview of the problem. Restor. Build. Monum, 21, 119–135.

Cnudde, V., Cnudde, J. P., Dupuis, C., & Jacobs, P. J. S. (2004). X-ray micro-CT used for the localization of water repellents and consolidants inside natural building stones. Materials characterization, 53(2-4), 259-271.

Delgado Rodrigues, J. 1988 - "Proposed geotechnical classification of carbonate rocks based on Portuguese and Algerian examples". Engineering Geology, 25,(1), pp. 33-43

Dias Filho, J. L. E., Xavier, G. D. C., & Maia, P. C. D. A. (2020). Durability of ornamental gneiss stones from Pádua, Rio de Janeiro, Brazil. Journal of Materials in Civil Engineering, 32(7), 04020176.

Elert, K., & Rodriguez-Navarro, C. (2022). Degradation and conservation of clay-containing stone: A review. Construction and Building Materials, 330, 127226.

Elhaddad, F., Carrascosa, L. A., & Mosquera, M. J. (2018). Long-term effectiveness, under a coastal environment, of a novel conservation nanomaterial applied on sandstone from a Roman archaeological site. Journal of Cultural Heritage, 34, 208-217.

Eslami, J., Walbert, C., Beaucour, A. L., Bourges, A., & Noumowe, A. (2018). Influence of physical and mechanical properties on the durability of limestone subjected to freeze-thaw cycles. Construction and Building Materials, 162, 420-429.

Ferrer, B., Tomás, M. B., & Mas, D. (2021). Use of image correlation to measure macroscopic strains by hygric swelling in sandstone rocks. Applied Sciences, 11(6), 2495.

Fořt, J. (2015). Effect of Sandstone Anisotropy on its Heat and Moisture Transport Properties. Materials Science, 21(3), 455-459.

Garzanti, E. (2019). Petrographic classification of sand and sandstone. Earth-Science Reviews, 192, 545-563.

Germinario, L., & Török, Á. (2020). Surface weathering of tuffs: compositional and microstructural changes in the building stones of the Medieval Castles of Hungary. Minerals, 10(4), 376.

Hawkins, A. B., & McConnell, B. J. (1992). Sensitivity of sandstone strength and deformability to changes in moisture content. Quarterly Journal of Engineering Geology and Hydrogeology, 25(2), 115-130.

Hillier, S., Wilson, M. J., & Merriman, R. J. (2006). Clay mineralogy of the Old Red Sandstone and Devonian sedimentary rocks of Wales, Scotland and England. Clay Minerals, 41(1), 433-471.

Huang, S., He, Y., Liu, X., & Xin, Z. (2021). Experimental investigation of the influence of dry-wet, freeze-thaw and water immersion treatments on the mechanical strength of the clay-bearing green sandstone. International Journal Of Rock Mechanics And Mining Sciences, 138, 104613. doi: 10.1016/j.ijrmms.2021.104613

Jiménez-González, I., Rodríguez-Navarro, C., & Scherer, G. (2008). Role of clay minerals in the physicomechanical deterioration of sandstone. Journal Of Geophysical Research, 113(F2). doi: 10.1029/2007jf000845

Kunz, A., Groh, M., Braun, F., Brüggerhoff, S., & Orlowsky, J. (2022). Durability assessment of differently orientated surfaces of treated long-term weathered natural stones. Journal of Cultural Heritage, 53, 176-183.

Li, D., & Wang, W. (2019). Quantitative analysis of the influence of saturation on rock strength reduction considering the distribution of water. Geomechanics and Geophysics for Geo-Energy and Geo-Resources, 5(2), 197-207.

Li, D., & Wang, W. (2019). Quantitative analysis of the influence of saturation on rock strength reduction considering the distribution of water. Geomechanics and Geophysics for Geo-Energy and Ge

Liu, X., Koestler, R.J., Warscheid, T. et al. Microbial deterioration and sustainable conservation of stone monuments and buildings. Nat Sustain 3, 991–1004 (2020). https://doi.org/10.1038/s41893-020-00602-5

López-Doncel, R., Wedekind, W., Aguillón-Robles, A., Dohrmann, R., Molina-Maldonado, S., & Leiser, T. et al. (2018). Thermal expansion on volcanic tuff rocks used as building stones: examples from Mexico. Environmental Earth Sciences, 77(9). doi: 10.1007/s12665-018-7533-0

Madsen, F.T., & Müller-Vonmoos, M. (1989). The swelling behaviour of clays, Applied Clay Science, 4(2), 143-156, doi.org/10.1016/0169-1317(89)90005-7.

McGreevy, J., & Smith, B. (1984). The possible role of clay minerals in salt weathering. CATENA, 11(1), 169-175. doi: 10.1016/s0341-8162(84)80016-8

McKinley, J.M., Worden, R.H., Ruffell, A.H. (2003) Smectite in sandstones: a review of the controls on occurrence and behaviour during diagenesis, clay mineral cements in sandstone, Int. Assoc. Sedimentol. Spec. Publ., 34, 109-128, ISBN: 978-1-405-10587-3

Noor-E-Khuda, S., & Albermani, F. (2019). Flexural strength of weathered granites under wetting-drying cycles: implications to steel structures. Adv Steel Constr, 15(3), 225-231.

Ordonez, S., Fort, R. & Garcia Del Cura, M.A. 1997. Pore size distribution and the durability of a porous limestone. Quarterly Journal of Engineering Geology, 30, 221–230.

Pettijohn, F. J., Potter, P. E., & Siever, R. (2012). Sand and sandstone. Springer Science & Business Media.

Přikryl, R. (2013). Durability assessment of natural stone. Quarterly Journal Of Engineering Geology And Hydrogeology, 46(4), 377-390. doi: 10.1144/qjegh2012-052

Richardson, B.A. 1991. The durability of porous stones. Stone Industries, 26, 22–25.

Ruedrich, J., Bartelsen, T., Dohrmann, R., & Siegesmund, S. (2011). Moisture expansion as a deterioration factor for sandstone used in buildings. Environmental Earth Sciences, 63(7-8), 1545-1564. doi: 10.1007/s12665-010-0767-0

Sbardella, F., Pronti, L., Santarelli, M. L., Asua Gonzàlez, J. M., & Bracciale, M. P. (2018). Waterborne acrylate-based hybrid coatings with enhanced resistance properties on stone surfaces. Coatings, 8(8), 283.

Scrivano, S., Gaggero, L., & Gisbert Aguilar, J. (2018). Micro-porosity and minero-petrographic features influences on decay: Experimental data from four dimension stones. Construction And Building Materials, 173, 342-349. doi: 10.1016/j.conbuildmat.2018.04.041

Scrivano, S., Gaggero, L., Aguilar, J. G., De Kock, T., Derluyn, H., & Cnudde, V. (2017). Texture and mineralogy influence on durability: the Macigno sandstone. Quarterly Journal of Engineering Geology and Hydrogeology, 50(4), 393-401.

Scrivano, S., & Gaggero, L. (2020). An experimental investigation into the salt-weathering susceptibility of building limestones. Rock Mechanics and Rock Engineering, 53(12), 5329-5343.

Sebastián, E., Cultrone, G., Benavente, D., Fernandez, L. L., Elert, K., & Rodriguez-Navarro, C. (2008). Swelling damage in clay-rich sandstones used in the church of San Mateo in Tarifa (Spain). Journal of cultural heritage, 9(1), 66-76.

Shi, X., Cai, W., Meng, Y., Li, G., Wen, K., & Zhang, Y. (2016). Weakening laws of rock uniaxial compressive strength with consideration of water content and rock porosity. Arabian Journal of Geosciences, 9(5), 369.

Siegesmund, S., Snethlage, R., Török, Á., Dürrast, H., Steiger, M., & Charola, A. et al. (2011). Stone in Architecture. Heidelberg: Springer.

Sirdesai, N., Mahanta, B., Ranjith, P., & Singh, T. (2017). Effects of thermal treatment on physico-morphological properties of Indian fine-grained sandstone. Bulletin Of Engineering Geology And The Environment, 78(2), 883-897. doi: 10.1007/s10064-017-1149-6

Smith, B. J., McCabe, S., McAllister, D., Adamson, C., Viles, H. A., & Curran, J. M. (2011). A commentary on climate change, stone decay dynamics and the ‘greening’of natural stone buildings: new perspectives on ‘deep wetting’. Environmental Earth Sciences, 63(7), 1691-1700.

Stefanidou, M., Matziaris, K., & Karagiannis, G. (2013). Hydrophobization by means of nanotechnology on Greek sandstones used as building facades. Geosciences, 3(1), 30-45.

Sun, Q., Dong, Z., & Jia, H. (2019). Decay of sandstone subjected to a combined action of repeated freezing–thawing and salt crystallization. Bulletin of Engineering Geology and the Environment, 78(8), 5951-5964.

Turkington, A. V., & Paradise, T. R. (2005). Sandstone weathering: a century of research and innovation. Geomorphology, 67(1-2), 229-253.

Vásárhelyi, B., & Ván, P. J. E. G. (2006). Influence of water content on the strength of rock. Engineering Geology, 84(1-2), 70-74.

Vázquez, P., Alonso, F. J., Carrizo, L., Molina, E., Cultrone, G., Blanco, M., & Zamora, I. (2013). Evaluation of the petrophysical properties of sedimentary building stones in order to establish quality criteria. Construction and Building Materials, 41, 868-878.

Vicini, S., Gaggero, L., & Princi, E. (2013). Characterization, weathering, and protection of sandstones: The case of 'Agro d'Ardesia'. Studies in conservation, 58(1), 50-57.

Vigroux, M., Eslami, J., Beaucour, A. L., Bourges, A., & Noumowe, A. (2021). High temperature behaviour of various natural building stones. Construction and Building Materials, 272, 121629.

Viles, H. A. (2013). Durability and conservation of stone: coping with complexity. Quarterly Journal of Engineering Geology and Hydrogeology, 46(4), 367-375.

Warke, P., & Smith, B. (2000). Salt distribution in clay-rich weathered sandstone. Earth Surface Processes And Landforms, 25(12), 1333-1342. doi: 10.1002/1096-9837(200011)25:12<1333::aid-esp141>3.0.co;2-6

Warke, P. A., & Smith, B. J. (2007). Complex weathering effects on durability characteristics of building stone. Geological Society, London, Special Publications, 271(1), 211-224.

Warke, P., McKinley, J., & Smith, B. (2006). Variable weathering response in sandstone: factors controlling decay sequences. Earth Surface Processes And Landforms, 31(6), 715-735. doi: 10.1002/esp.1284

Winkler, E.M. (1986) A durability index for stone. Association of Engineering Geologists Bulletin, Vol. 23,1986, pp. 344-347

Worden, R.H., & Morad, S. (2003) Clay minerals in sandstones: controls on formation, distribution and evolution, clay mineral cements in sandstone, Int. Assoc. Sedimentol. Spec. Publ., 34, 3-41, ISBN: 978-1-405-10587-3

Yu, S. & Oguchi, C.T. 2010. Role of pore size distribution in salt uptake, damage and predicting salt susceptibility of eight types of Japanese building stones. Engineering Geology, 115, 226–236.

Zhang, J., Deng, H., Taheri, A., Ke, B., Liu, C., & Yang, X. (2018). Degradation of physical and mechanical properties of sandstone subjected to freeze-thaw cycles and chemical erosion. Cold Regions Science And Technology, 155, 37-46. doi: 10.1016/j.coldregions.2018.07.007

Zhou, Z., Cai, X., Ma, D., Chen, L., Wang, S., & Tan, L. (2018). Dynamic tensile properties of sandstone subjected to wetting and drying cycles. Construction and Building Materials, 182, 215-232.

2.0 Critical evaluation of the preparatory and analytical procedures for clay minerals using pXRD.

2.1 Introduction

Clay minerals can be characterised using a variety of microscopy techniques including optical microscopy, Scanning Electron, and Transmission Electron. These techniques provide information on the distribution, morphology, chemistry and crystallographic structure of clay minerals. Powdered X-ray Diffraction (pXRD) is a unique tool in the sense that it characterises the crystallographic structure of clay minerals and offers a ‘fingerprint’ (diffractogram pattern) which can be used to identify different species of clays. Furthermore, samples can be exposed to different treatment between successive pXRD analyses to further define their crystallographic structure. Analysis of clay minerals using pXRD is a common technique used in the study of sandstone decay and durability (Wangler & Scherer., 2008; Benavente et al., 2008; Pötzl & Siegesmund., 2018; Tiennot et al., 2019; Shekofteh et al., 2019). Clay minerals can make sandstones more vulnerable to weathering and decay (Delgado Rodrigues., 2001; Sebástian et al., 2008; Scrivano et al., 2017). This is particularly true for expansive clay minerals which physically expand in the presence of water and contract upon drying leading to accelerated weathering of stone in some instances (Jiménez-González et al., 2008). Clay minerals are typically present in small quantities in sandstones (a few wt%) but previous research has shown that even in such small quantities clay can impact sandstone durability (Sebástian et al., 2008).

Prior to pXRD analysis, clay minerals must be extracted from a bulk sandstone powder mixture and prepared onto a glass slide. Clay mineral peaks in the pXRD diffractogram can be small due to the limited quantities of clay that typically exist in sandstones, and their poor crystallographic structure. Thus, the extraction process removes minerals which are not necessary when assessing the clay fraction (quartz, feldspars, etc). This ultimately increases the relative clay content of the sample and often leads to more intense clay peaks which are easier to observe and study. There is a lack of literature detailing the most appropriate methods for clay mineral extraction and preparation for pXRD in the context of building sandstone and sandstone conservation. Moreover, due to the platy crystal structure and complex chemistry of clay minerals, it can be difficult to gauge the amount of clay minerals present in a sandstone based on diffractogram patterns obtained using pXRD. The aim of this research chapter is to establish that expansive clay (saponite) in various quantities can be easily detected using pXRD and to assess the efficiency of the method used for clay mineral extraction from bulk sandstone.

In this study, two sandstones were doped with varying amounts of expansive saponite to determine: (i) whether or not all of the added amounts could be detected and how specific quantities correlate to the resulting diffractogram, and (ii) the efficiency of the process used to extract clays from sandstones prior to analysis. In addition to this work, a second study incorporated into this chapter compares two different methods for preparing extracted clay minerals on to glass slides for pXRD analysis.

2.2 Samples

2.2.1 Doping experiment

Two sandstones were selected for the doping experiment based on their contrasting petrographies (Figure 2.1). Cullalo is a Carboniferous quartz arenite building stone quarried in Fife, Scotland, containing a negligible clay fraction (Dassow et al., 2020). In contrast Forest of Dean, a Carboniferous sandstone quarried in Gloucestershire, is a litharenite with a considerable clay fraction comprised of illite, chlorite, and kaolinite (HES., 2018). The saponite used as an internal standard (the dopant), referred to herein as saponite X, is a mixture consisting of 58 wt % saponite C, and 42 wt % saponite D (details on saponite samples A-D below). The mixing of two saponites was required to create enough sample for this study.

2.2.2 Preparing orientated samples for pXRD

Samples used for this part of the study include four expansive saponites (A-D), and a weathered building sandstone (Dcath). Saponites are part of the smectite group with a general formula $Ca_{0.25}(Mg,Fe)_3((Si,Al)_4O_{10})(OH)_2 \cdot nH_2O$. The expansive saponite samples consist of two saponites (referred to as saponite A and B) and two weathered saponites (formerly known as bowlingite) (referred to as saponite C and D) loaned from the Hunterian Museum, Glasgow. Saponite A is a very soft powdery clay, which is white in colour and has a very greasy texture. It is sourced from the Isle of Skye, Scotland. Saponite B is a very hard clay that is dark brown in colour. B appears to have the finest grain size of all saponite samples giving it a smooth, glassy appearance with concavo-convex fracture surfaces. Saponite C is an amorphous, hard clay which is grey-green colour sourced from a quarry near Bowling, West Dunbartonshire, Scotland. Saponite D is a soft clay which is dark-grey-black in colour. D has a bladed habit and metallic lustre, and was sourced near the Kilpatrick Hills, Scotland. Dcath is a weathered clay-rich, litharenite building sandstone from Dunkeld Cathedral – a 13th century historic building located in the county of Perthshire, Scotland. This building stone from Dunkeld Cathedral provides the opportunity to first extract clay from a bulk sandstone and then analyse clay minerals from a building sandstone which has experienced prolonged weathering, which may affect the types of clay minerals present and their crystallinity.

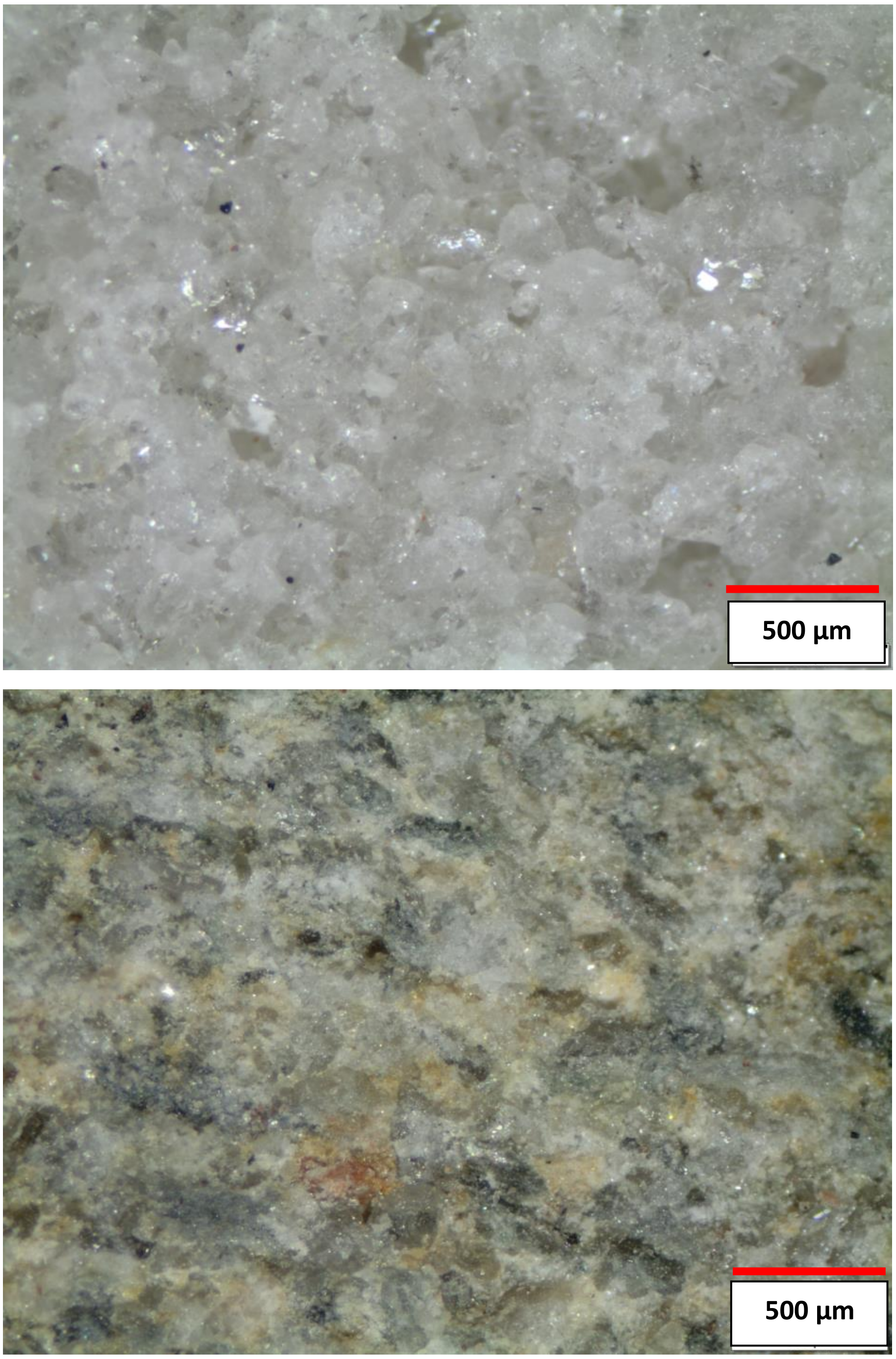

Figure 2.1: Macroscopic images showing appearance of two sandstones used in the doping study: Cullalo, C (top), and Forest of Dean, F (bottom).

2.3 Methods

2.3.1 Doping experiment

X-ray Diffraction (XRD) analyses was carried out using a Thermo Electron ARL X'TRA XRD at the Engine Shed (HES) in Stirling. The settings were as follows: CuKα radiation, running at 45mA and 44kV, step size of 0.02 degrees, and a scan rate of 1^o per minute. Results from XRD are displayed as diffractograms reflecting the crystallographic structure of the minerals present in the sample.

Cullalo (C), Forest of Dean (F), and Saponite X were gently crushed in a mortar and pestle, with the saponite sample subsequently passed through a 63-micron sieve. Crushed sandstone fractions were divided into three subsamples and doped with saponite amounts corresponding to 5 wt % saponite (referred to as C/F-5), 10 wt % (C/F-10) and 40 wt % (C/F-40) to create six samples in total. Two further subsamples were run containing 0 wt % (C/F-0) added saponite to characterise original sandstone mineralogy (including original clay fraction) prior to doping. The bulk mixtures were then weighed before being packed into a holder and analysed using XRD to determine the detection limits of clay minerals in crushed bulk sandstone mixtures.

2.3.2 Clay extraction method

In addition to understanding how different clay mineral abundances are reflected in the obtained diffractograms, the doping study gives the opportunity to assess the efficiency of the clay extraction process in removing the total amount of clay present in the sandstone. After preparing and analysing bulk samples, an attempt was made to separate and extract clay minerals from the bulk mixtures. Ideally all of the saponite that was added to the sandstones should be extracted along with any clay that was originally present in the sandstone. The crushed bulk mixture was placed in a centrifuge tube (~2.5g bulk mixture per tube) with deionised water and gently shaken before being placed in an ultrasonic bath for 10 minutes allowing for deflocculation of clay minerals. The centrifuge tube was then dried off and placed in the centrifuge chamber. The settings for the centrifuge chamber (which are specific to the type of centrifuge tube used, and model of centrifuge) leaves the 2-μm grain size fraction suspended in deionised water, which was then pipetted into glass jars. These settings are calculated using the cvort program developed by U.S Geological

Survey (USGS) for the calculation of centrifugal velocity and times for settling out particles of a given medium. Prior to pipetting, the glass jars were weighed so that the weight of clay minerals after water evaporation can be calculated. These jars were then left on a hotplate or inside an oven no hotter than 50 ^{o}C to allow for evaporation of water. After thorough drying over approximately sixteen hours, the glass jars and extracted clay were weighed again. The clay minerals were then retrieved from the bottom of the glass jars and gently crushed again in a mortar and pestle before being mounted onto a glass-slide for pXRD analysis.

The extracted clay mineral samples were then analysed by XRD in four ways according the USGS standard for analysis and identification of clay minerals: (i) prior to any treatment, (ii) after 48hr treatment with ethylene glycol (EG) in an oven at 60 °C for 48 hours, (iii) after treatment in a furnace at 400 °C, (iv) and after treatment in a furnace at 550 °C. These treatments are used to identify (via EG) and further characterise (via heat treatment) expansive clay minerals present. The resulting diffractograms of both bulk and separated clay fractions for varying saponite amounts (0-40 wt %) are compared in the Discussion.

2.3.3 Preparing orientated samples for pXRD

In a separate study, two mounting techniques were compared using the saponite samples (A-D) and a weathered sandstone from Dunkeld (Dcath): (i) the filter peel method, and (ii) the acetone slurry method. Both methods aim to achieve an orientated sample – i.e., where clay mineral particles lie in a common crystallographic orientation. Orientated samples are prepared when identifying and characterising expansive clay minerals (smectite), as expansion predominantly occurs perpendicular to the 001 plane. An extensive review of different mounting techniques is given by Gibbs (1965).

According to the acetone slurry method, the separated clay fraction (see section 3.1.1 for details of clay mineral extraction from sandstone) is mixed with a small amount of acetone in a mortar and pestle to create a fast-drying slurry. The slurry is applied to a zero-background glass slide using a pipette. As the acetone evaporates the clay minerals preferentially align onto the slide.

The filter peel method uses a vacuum system to draw water through filter paper while allowing clay minerals to deposit on the paper's surface in a similar orientation (Drever, 1973; USGS). In this study, the vacuum system consists of a conical flask connected to a vacuum oven, where the pressure of the vacuum is kept at ~ 400-450 mbar. The separated clay minerals are combined with ~ 2 ml of deionised water and gently mixed. The outlet for the vacuum is then opened and the clay-water mixture is pipetted onto the 2.7 µm filter paper. After water has been drawn through the filter paper, and while the deposited clay minerals still appear ‘wet’ (shiny surface), the filter paper is wrapped round a small beaker which is then gently pressed and rolled onto a glass slide transferring the aligned clay minerals in the process.

Two slides were prepared for each saponite sample: one using the acetone method, and one using the filter peel method. In addition to saponite samples, a weathered building stone (Dcath) was also compared. All samples were then analysed using XRD before being treated with EG over a 48-hour period in an oven at ~ 60 °C before being analysed again. Samples were also analysed after exposure to 400 °C, and 550 °C in a furnace. The diffractograms of clay fractions mounted using different methods are compared in the Discussion.

2.3.4 Scanning Electron Microscopy (SEM)

Scanning Electron Microscopy (SEM) was carried out using a FEI Quanta 200F Environmental SEM with EDAX Microanalysis. SEM was used to evaluate textural properties and morphology of clay minerals. Small gold-coated chips of samples were analysed under high vacuum conditions, at 20 kV using backscattered and secondary electron imaging.

2.4 Results and Discussion

2.4.1 Doping experiment: characterisation of Saponite X

Saponite X was used as an internal standard in this study. Saponite X was prepared for analysis using the filter peel method. The main diffractogram characteristics of this sample, including the behaviour of the clay when subject to treatment using EG and heat, can be seen in Figure 2.2. The largest and most prominent peak at ~ 6° 2ϴ is referred to throughout this chapter as the primary clay peak. This peak represents the 001 plane of the clay minerals. The intensity of this peak can be at least partially affected by the alignment of platy clay minerals (Zhou et al., 2018). This clay peak is the most important when identifying expansive clay minerals as expansion occurs normal to the 001 plane. There is a noticeable shift of the primary clay peak to a lower angle after treatment with EG confirming the expansive nature of the internal standard (Figure 2.2). Further heat treatment leads to the total collapse of this clay mineral peak as well as several others. Identifying the exact type of expansive clay mineral based solely on diffractogram patterns can be difficult as clay minerals are well known for their chemical diversity and complex structures. In addition to the primary clay peak shift after EG treatment, the small 060 peak (~ 60 2ϴ), confirms that the internal standard is a trioctahedral smectite – smectite where all three octahedral units are occupied by ions. This subdivision of smectite includes minerals saponite, stevensite, and hectorite (Christidis & Koutsopoulou., 2013).

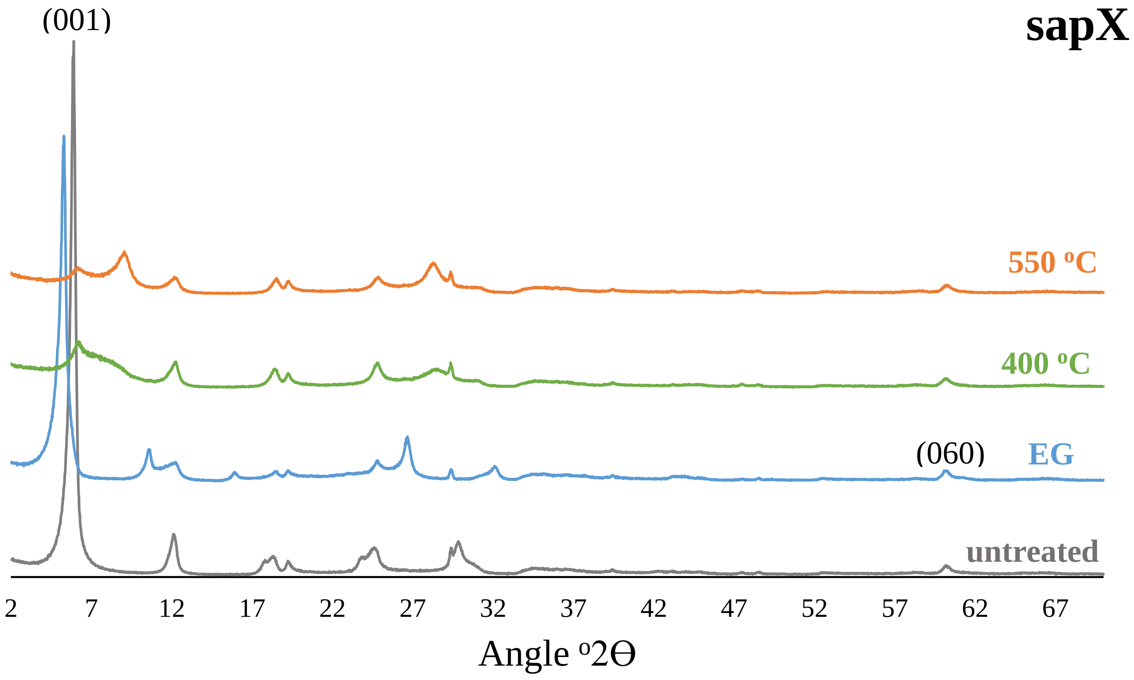

Figure 2.2: Diffractograms of saponite X, which has been used as an internal standard. Four samples were analysed: prior to any treatment, after treatment with EG, and after heating to 400ºC and 550ºC.

2.4.2 Doping experiment: Bulk sandstone samples

2.4.2.1 Original bulk mineralogy (F-0, C-0)

F-0 and C-0 are bulk sandstone mixtures prior to any doping. Figure 2.3 shows the diffractograms of each bulk sandstone, annotated with mineralogical composition. The main differences between F and C are the greater abundance of feldspars in F, and its greater diversity of platy minerals including clays and micas. Moreover, there is a primary clay peak at ~ 6° 2Ѳ (14.7 Å) in F which is absent in C, suggesting a relatively higher proportion of naturally present clay minerals. Chlorite, illite and kaolinite are also identified in F, confirming its mineralogical immaturity (Figure 2.3). The diffractogram of C shows that it is a very mineralogically mature sandstone. The main quartz peak in C-0 is considerably higher than the rest of the mineral peaks in C-0, in comparison to F-0, reflecting the higher quartz content and overall better crystallinity of C-0.

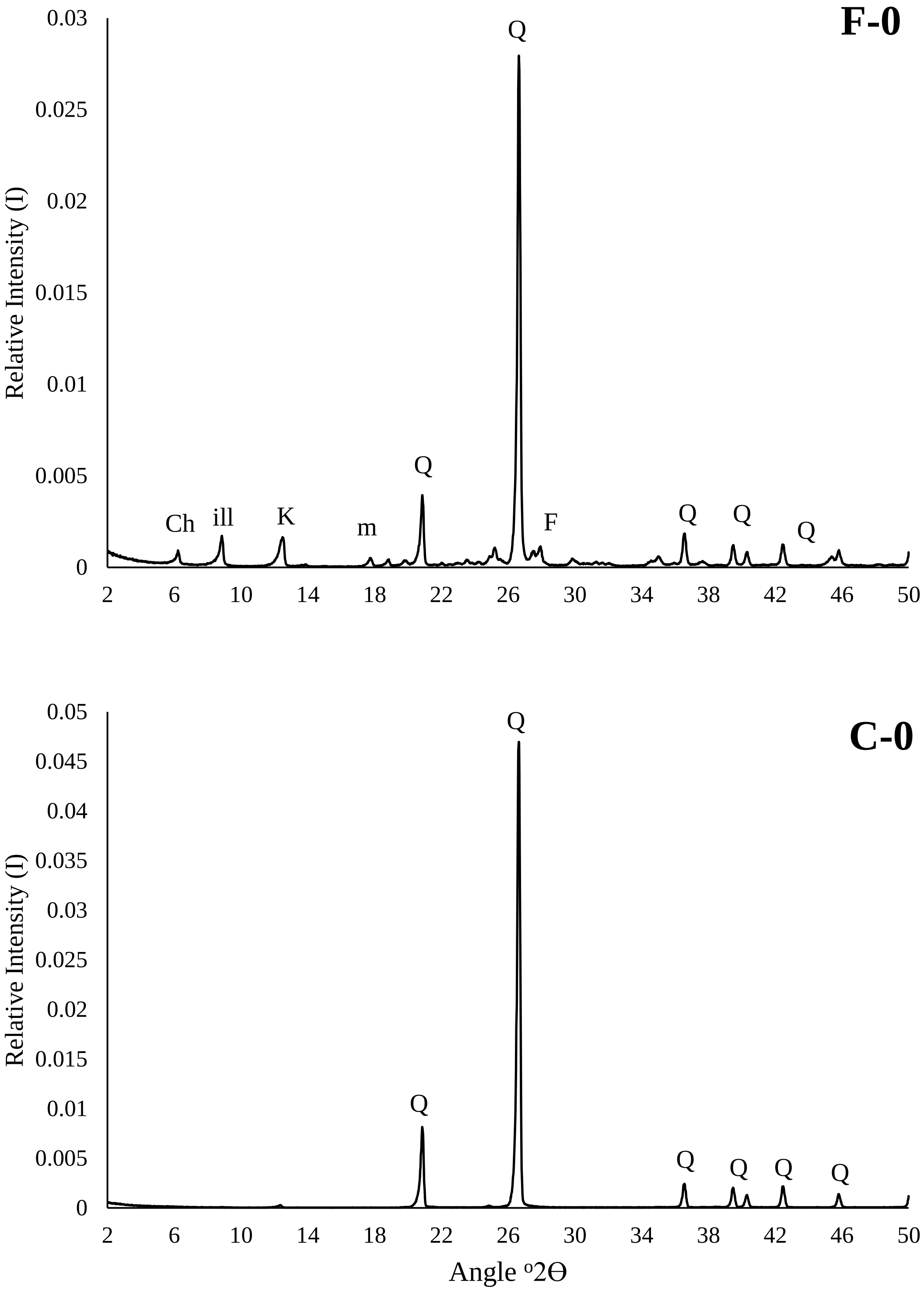

Figure 2.3: Diffractograms of bulk samples of F-0 and C-0. Analysis reveals the presence of minerals including quartz, feldspars, micas, and some clays. C-0 is more mineralogically mature than F-0 as the diffractogram shows that most peaks represent quartz. Q = quartz; K = kaolinite; ill = illite; F = feldspar; Ch = chlorite.

2.4.2.2 Doped bulk sandstone samples

Doped samples (both bulk and extracted clays) are discussed in relation to changes in the primary clay peak at ~6° 2Θ, and the primary quartz peak at ~ 26° 2Θ. Figure 2.4 shows the effects of increasing saponite content on overall diffractogram pattern of sandstone samples C and F. Additionally, Table 2.1 shows the changes in relative intensity (I) of the primary clay and quartz peaks, and the *p*C/*p*Q peak ratio. Relative intensity is calculated by dividing each diffractogram point (in CPS) by the total sum of CPS for that diffractogram. Calculating relative intensity helps to normalise the data allowing for more accurate comparison between diffractograms. The *p*C/*p*Q ratio is calculated by dividing the relative intensity of the clay peak by the height of the quartz peak. Across both sandstones, there is an increase in relative intensity with increasing clay content of the primary clay peak at ~6° 2ϴ. This coincides with a decrease in relative intensity with increasing clay content of the primary quartz peak. This likely reflects the decrease in crystallinity of the overall sample as clay minerals become more dominant. However, there is an initial increase in relative intensity of the primary quartz peak between 0 wt % and 5 wt % saponite. In both sandstones, 5 wt% saponite can be clearly detected, which is particularly noticeable in the Cullalo sandstone, where a new clay peak appears at ~6° 2ϴ after doping with 5 wt %. Moreover, the primary clay peak also gradually becomes larger relative to the quartz peak, as seen by the increase in *p*C/*p*Q ratio. In sample F-40, the relative intensity of the primary clay peak is actually greater than the primary quartz peak. The increase in relative intensity of the main clay peak relative to other peaks reflects the increasing amount of clay minerals relative to other minerals in the bulk mixture, and their preferential alignment on the glass slide. As seen from Figure 2.4, the *p*C/*p*Q ratio of bulk samples becomes higher with increasing clay content across both samples reflecting the relatively greater amount of saponite to quartz present in the sample.

There is a difference in *p*C/*p*Q ratios between the two sandstone types despite both types containing the same relative abundances of saponite and crushed sandstone (Figure 2.5). Cullalo is a mineralogically mature sandstone containing mostly well crystalline quartz with very little evidence of mineral weathering and/or alteration. In comparison, Forest of Dean is a mineralogically immature sandstone with a higher proportion of less crystalline minerals that are also more susceptible to weathering and alteration including feldspars, micas and clay. So for example, with regards to sandstones doped with 5 wt % saponite: the remaining 95% of the crushed Cullalo sandstone is almost entirely crystalline quartz, while the remaining 95% of the Forest of Dean sandstone is a mixture of quartz, with relatively higher proportions of feldspars, micas, and clays. Therefore, the quartz peak is relatively higher in C than F reflecting the mineralogical maturity and higher proportion of quartz associated with the sandstone (Table 2.1). These differences in ratios seem to become more pronounced with increasing clay content, reflecting the progressive decrease in crystallinity of Forest of Dean relative to Cullalo (Figure 2.5).

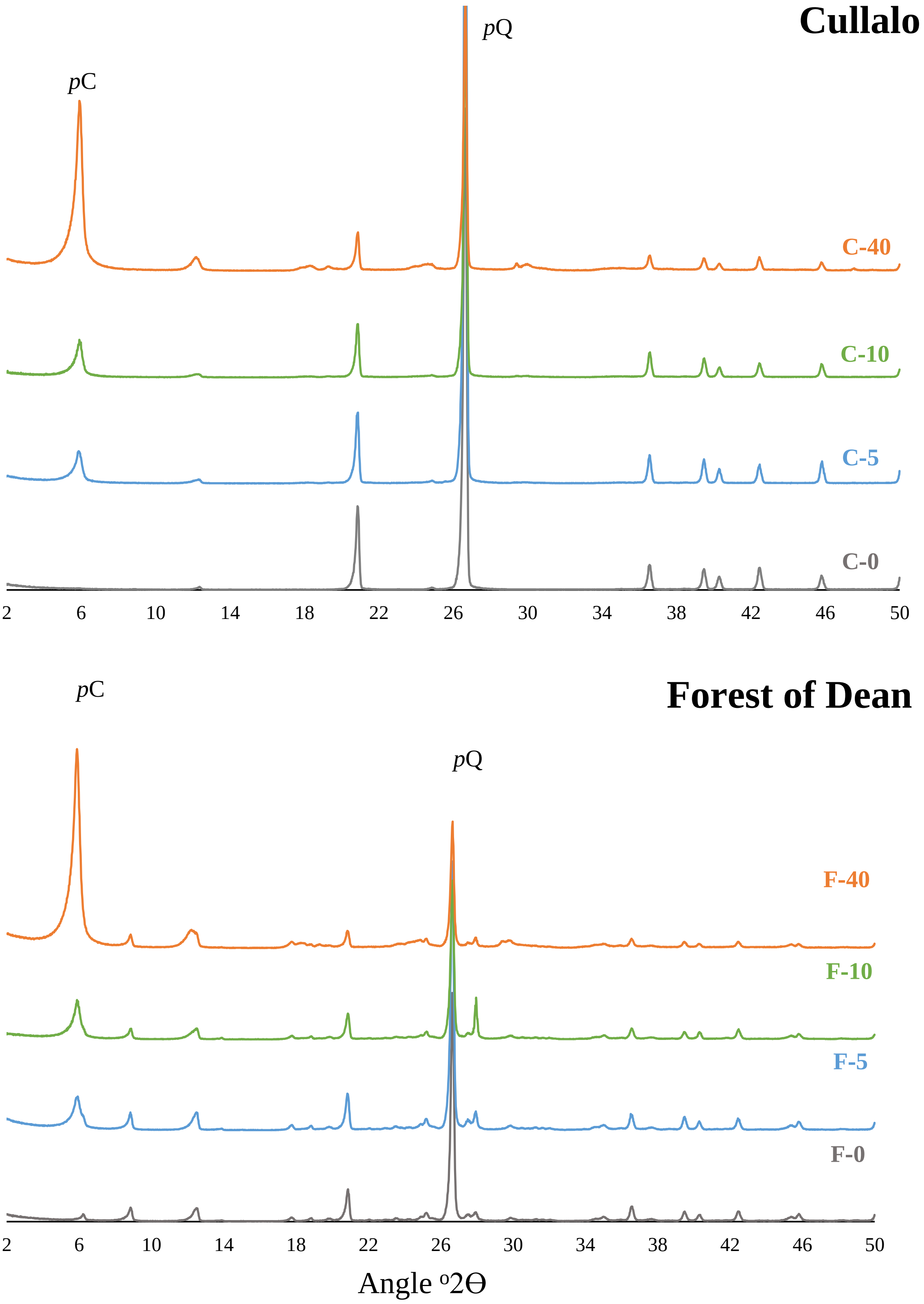

Figure 2.4: Diffractograms of bulk Cullalo (C, top) and Forest of Dean (F, bottom) sandstones that have been doped with different amounts of saponite X (0-40 wt %). ***p*****Q = primary quartz peak;** ***p*****C = primary clay peak (saponite).**

Table 2.1: Relative Intensity of primary peaks and *p*C/*p*Q ratio (ratio between peak heights of the primary clay peak and primary quartz peak), for both bulk and clay fraction samples. *no natural clay peak present in bulk sample C-0.

	sample	Relative Intensity		
		Quartz peak (*p*Q)	Clay peak (*p*C)	*p*C/*p*Q ratio
Bulk	C-0	0.047	-	-
	C-5	0.041	0.002	0.06
	C-10	0.042	0.004	0.09
	C-40	0.017	0.011	0.62
	F-0	0.028	0.0009	0.03
	F-5	0.023	0.003	0.13
	F-10	0.018	0.005	0.25
	F-40	0.008	0.012	1.57
Extracted clay	C-0	0.022	0.0005	0.02
	C-5	0.013	0.006	0.50
	C-10	0.006	0.012	1.91
	C-40	0.00095	0.018	19.41
	F-0	0.006	0.001	0.22
	F-5	0.005	0.004	0.84
	F-10	0.004	0.006	1.62
	F-40	0.001	0.015	10.84

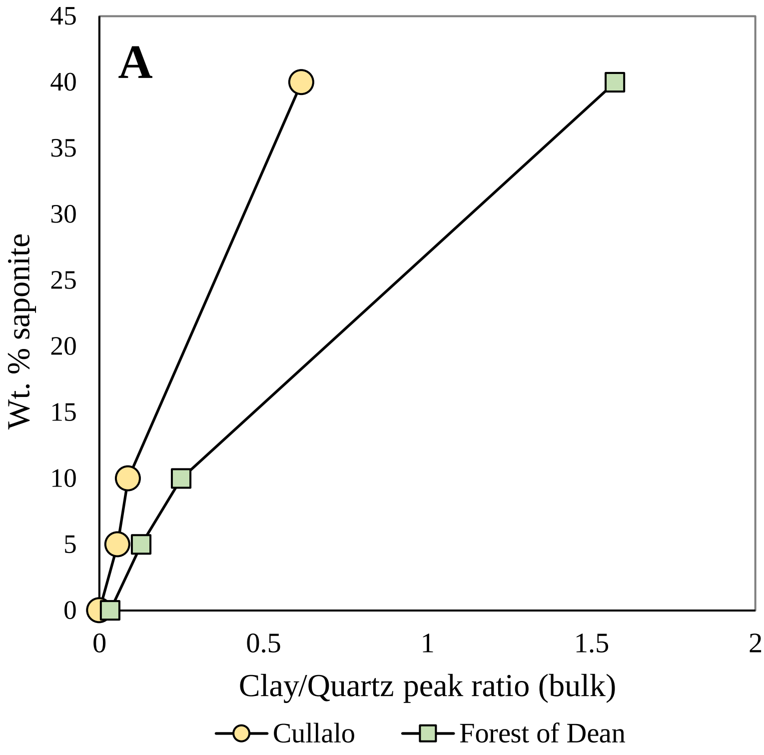

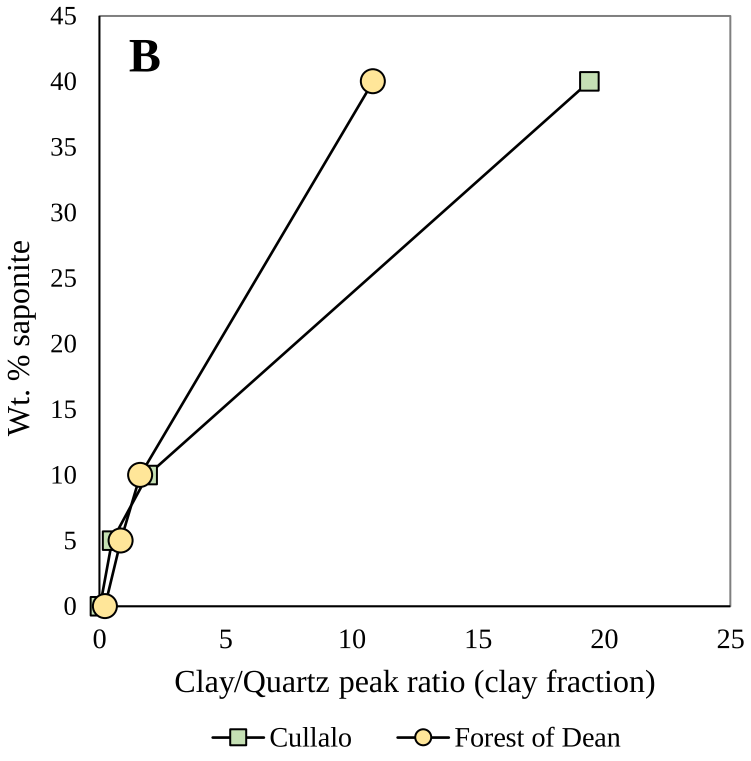

Figure 2.5: correlation between the clay/quartz ratio and amount of added saponite (wt %) for both bulk (A) and clay fractions (B).

2.4.3 Doping experiment: Extracted clay fraction

2.4.3.1 Original clay mineralogy (F-0, C-0)

Figure 2.6 shows the clay fraction naturally present in both C-0 and F-0 after it has been separated from the rest of the sandstone. There is more clay present in the clay fraction of F-0 as the sandstone is more mineralogically immature than C-0. F-0 contains mainly chlorite and illite with minor amounts of kaolinite while C-0 contains mostly kaolinite with some traces of illite and possibly chlorite. Upon first appearance, the diffractograms of extracted clay fractions are very similar to the diffractograms of the bulk sandstone. However, the relative intensity and C/Q ratios of the primary clay peak are generally higher now that there is a greater proportion of clay minerals relative to feldspars and quartz, etc. Extraction of the clay fraction allows for a more accurate identification and description of clay peaks due to removal or partial removal of other minerals. Neither of the sandstones contained expansive clay minerals prior to doping. C-0 shows a chlorite (?) peak around ~6° 2ϴ, and two kaolinite peaks, which were not observable in bulk analysis (Figure 2.6) highlighting the importance of analysing the separated clay fraction in addition to the bulk sandstone. Note that even in the extracted clay fraction, non-clay minerals, especially quartz, can still be identified. This is due to minerals (quartz, feldspars, etc) being unintentionally ground into the less than 2-µm fraction and therefore suspended in the water after centrifugation.

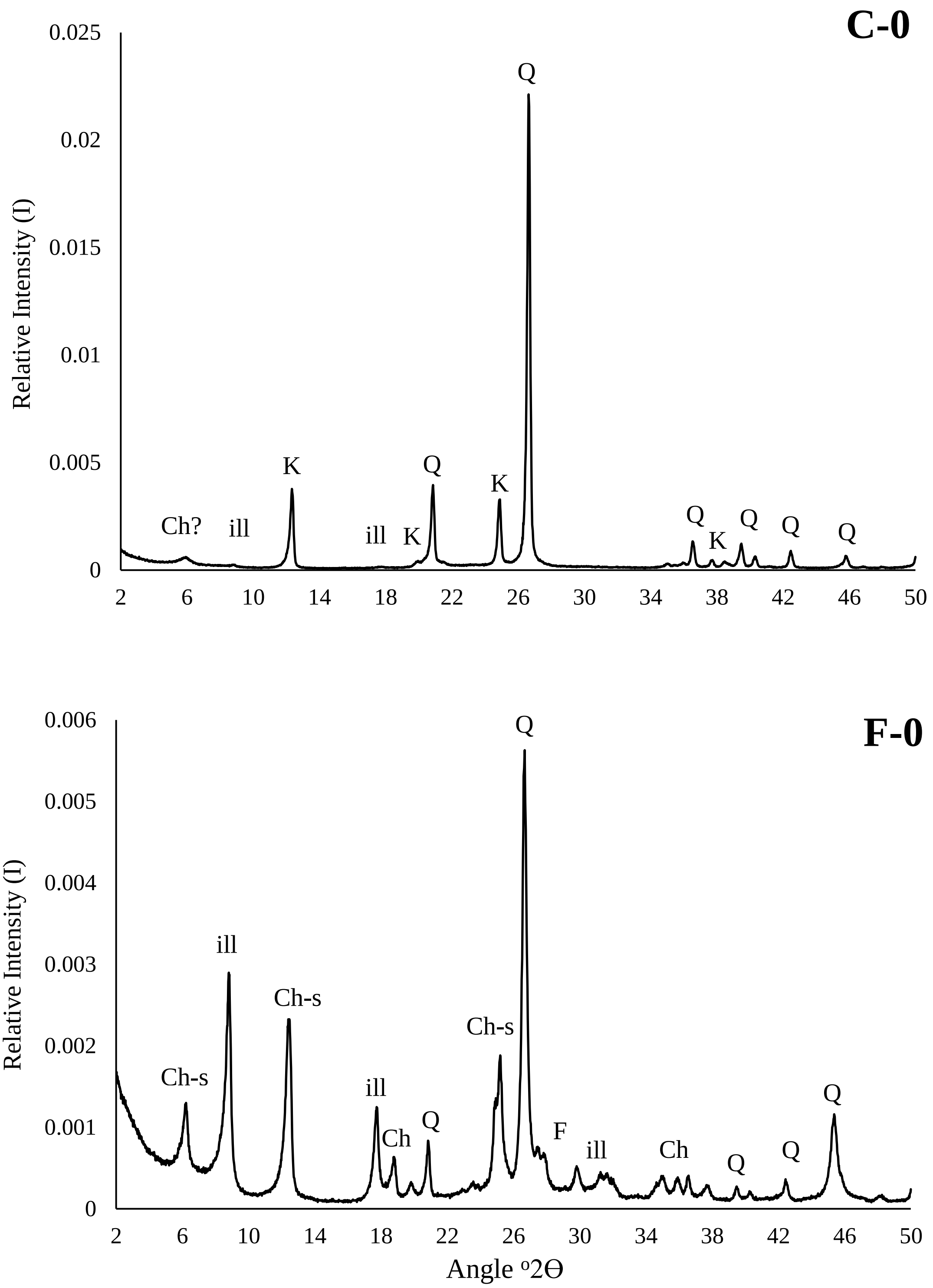

Figure 2.6: Diffractograms of clay minerals extracted from crushed bulk sandstones C-0 and F-0. Contamination of clays by other minerals such as quartz and feldspars is common. Q = quartz; K = kaolnite; ill = illite; Ch-s = chlorite-serpentinite; and F = feldspar.

2.4.3.2 EG and heat treatment of clay minerals

Figure 2.7 illustrates the typical behaviour of a smectite-bearing sandstone when treated with EG and exposed to elevated temperature. C-10 and F-10 are used as examples in Figure 2.7 as the changes in diffractograms induced by different treatments (EG, 400°C, and 550°C) were very similar for each sandstone regardless of saponite content (Figure 2.7). As stated previously, the main purpose of EG treatment is to determine the presence/absence of expansive clay minerals. The subsequent heat treatment is used to further refine the types of expansive clay minerals present. The following interpretations are based on the 'Clay Mineral Identification Flow Diagram' published on the the U.S Geological Survey (USGC) website which offers a systematic approach towards the identification of common clay minerals. Note that saponite is not included in this flow chart.

F-10 and C-10 shows a primary saponite clay peak at ~6° 2Θ as well as several other clay-related peaks at ~ 9° 2Θ, ~12° 2Θ, and ~25° 2Θ. With regards to F-10, after treatment with EG there is a lateral peak shift (from ~6° 2Θ to ~5.2° 2Θ) of the primary clay peak indicating the presence of expansive smectite, most likely the added saponite. This shift represents the expansion of clay minerals along the 001 plane. The shift also reveals an overlapping peak at 6° 2Θ of non-expansive chlorite in F-10 which remains unaffected by further treatments. Upon heating to 400°C the expansive clay peak is destroyed. Interstratified illite-chlorite is also present in F-10 with a peak at 9° 2Θ which is unaffected by EG treatment. The illite-chlorite peak becomes more intense upon heating. Chlorite and kaolinite commonly share a peak at 12° 2Θ which remains unaltered with EG treatment and treatment with 400°C before the peak is partially destroyed at 550°C. The main way to tell the difference between kaolinite and chlorite is by morphology based on SEM imaging. Kaolinite has a characteristic hexagonal morphology while chlorite is more variable but often platy. Based on XRD and SEM imaging the peak in F-10 is likely a combination of the two clays as both morphologies were observed by SEM (Figure 2.8).

C-10 also shows a characteristic lateral peak shift (from ~6° 2Θ to ~5.2° 2Θ) with EG treatment before being destroyed with treatment at higher temperatures. Other than the added saponite, the only other detected clay is kaolinite with peak position 12° 2Θ and 25° 2Θ, which are almost destroyed with heat treatment at 550°C. The minor traces of chlorite and illite detected in the analysis of C-0 (Figure 2.6) were probably masked by the prominent expansive saponite peak after doping. All samples in this study doped with saponite X show the characteristic shift of the primary clay peak at 6° 2Θ. The extent of this lateral peak shift is consistent across all samples regardless of the relative amount of saponite present in the doped bulk sandstone prior to extraction.

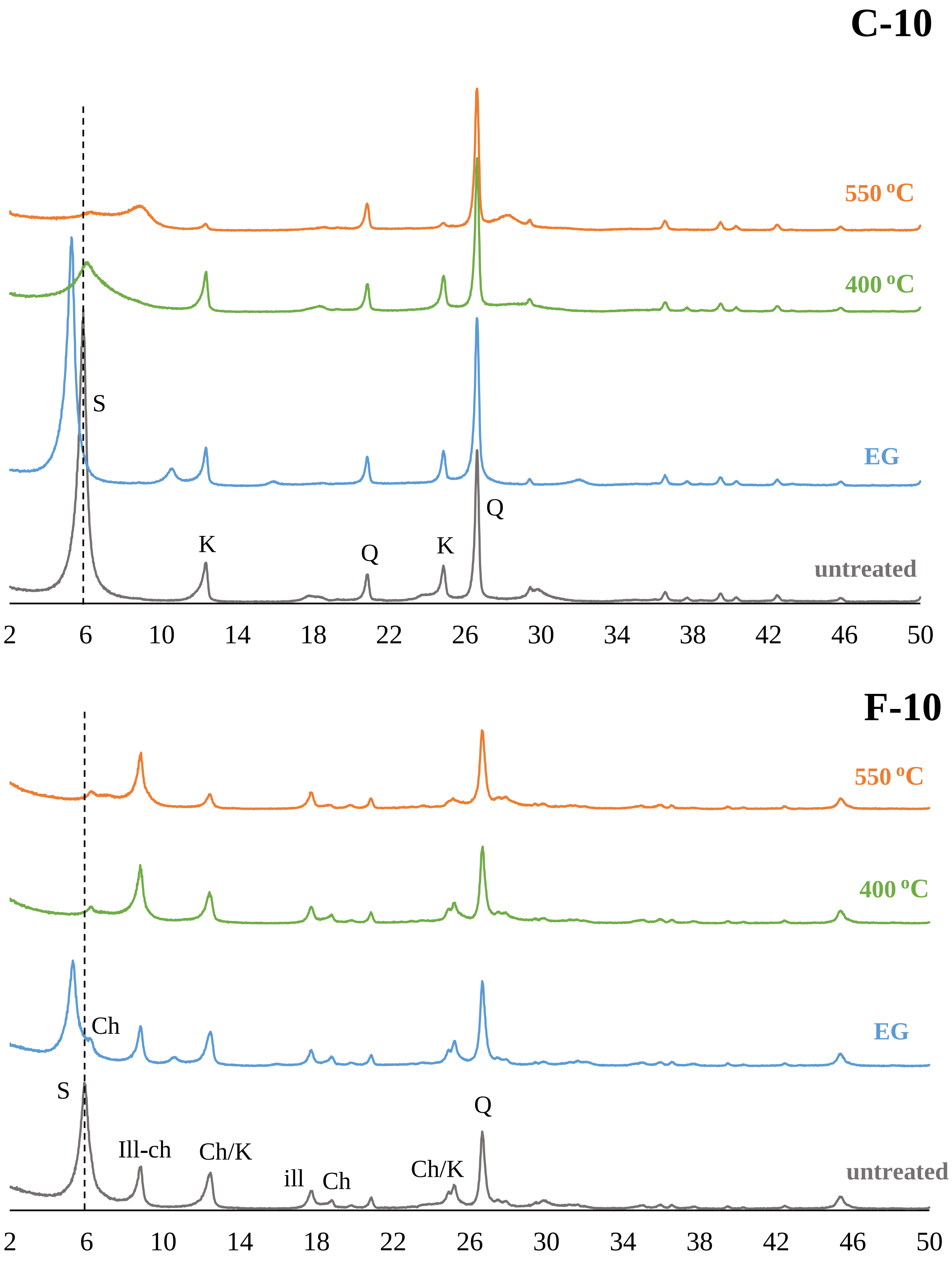

Figure 2.7: Diffractograms showing the effects of different treatment on C and F sandstones doped with 10 wt % saponite. The dashed vertical line highlights the lateral shift of the saponite clay peak after treatment with EG. Notice the progressive disintegration of the expansive clay peak with exposure to high temperatures. S = saponite; ill-ch = interstratified illite-chlorite; Ch/K = overlapping peaks of chlorite and kaolinite; Q = quartz.

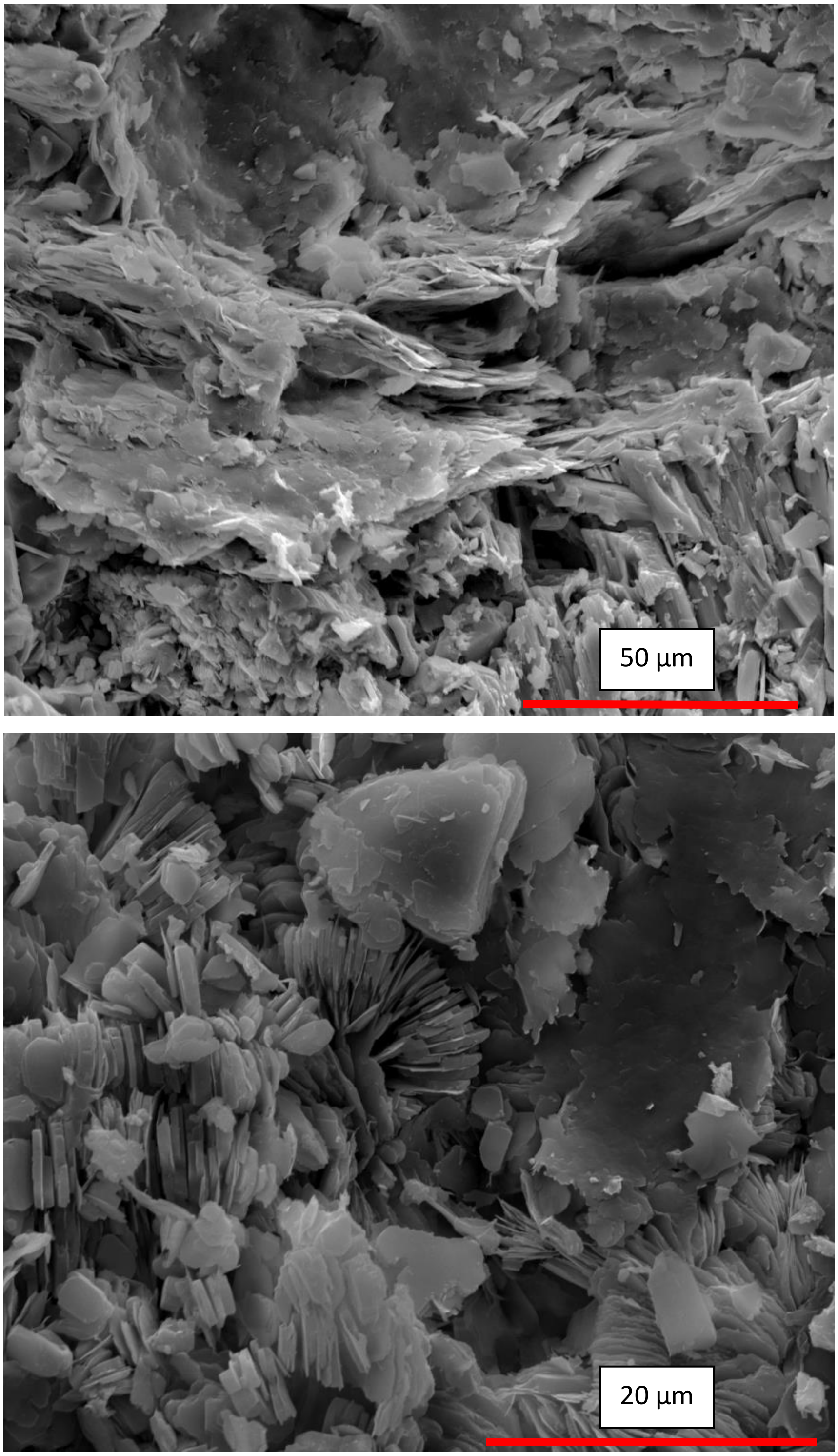

Figure 2.8: Morphology of clay minerals in Forest of Dean sandstone using secondary electron (SE) imaging with SEM. The top image is an example of the leafy structure of chlorite, and the bottom image is an example of the hexagonal structure of kaolinite which is often present in ‘stacks’.

2.4.3.3 Clay minerals extracted from doped bulk samples

Table 2.1 shows a similar trend in relative intensity of the primary clay and quartz peaks when analysing the extracted clay fractions. Similar to the bulk samples, the relative intensity of the primary clay peak of the extracted clay samples increases as saponite content increases (Figure 2.9). The relative intensity of the primary clay peak reaches a higher maximum due to the relatively lower abundances of minerals including quartz and feldspars (Table 2.1). The relative intensity of the primary quartz peak decreases with increasing saponite content due to the relatively greater amounts of clay present and lower crystallinity of the sample.

The C/Q ratios of the extracted clay fractions of both sandstone types are more similar to one another in comparison to the bulk ratios (Figure 2.5). This may be partly due to the clay extraction process which has filtered out some of the quartz, feldspars, etc, and as a result, making the two sandstone more mineralogically similar. Again the ratios of both sandstone types become increasingly different with higher clay content perhaps reflecting the differences in mineralogy and overall crystallinity.

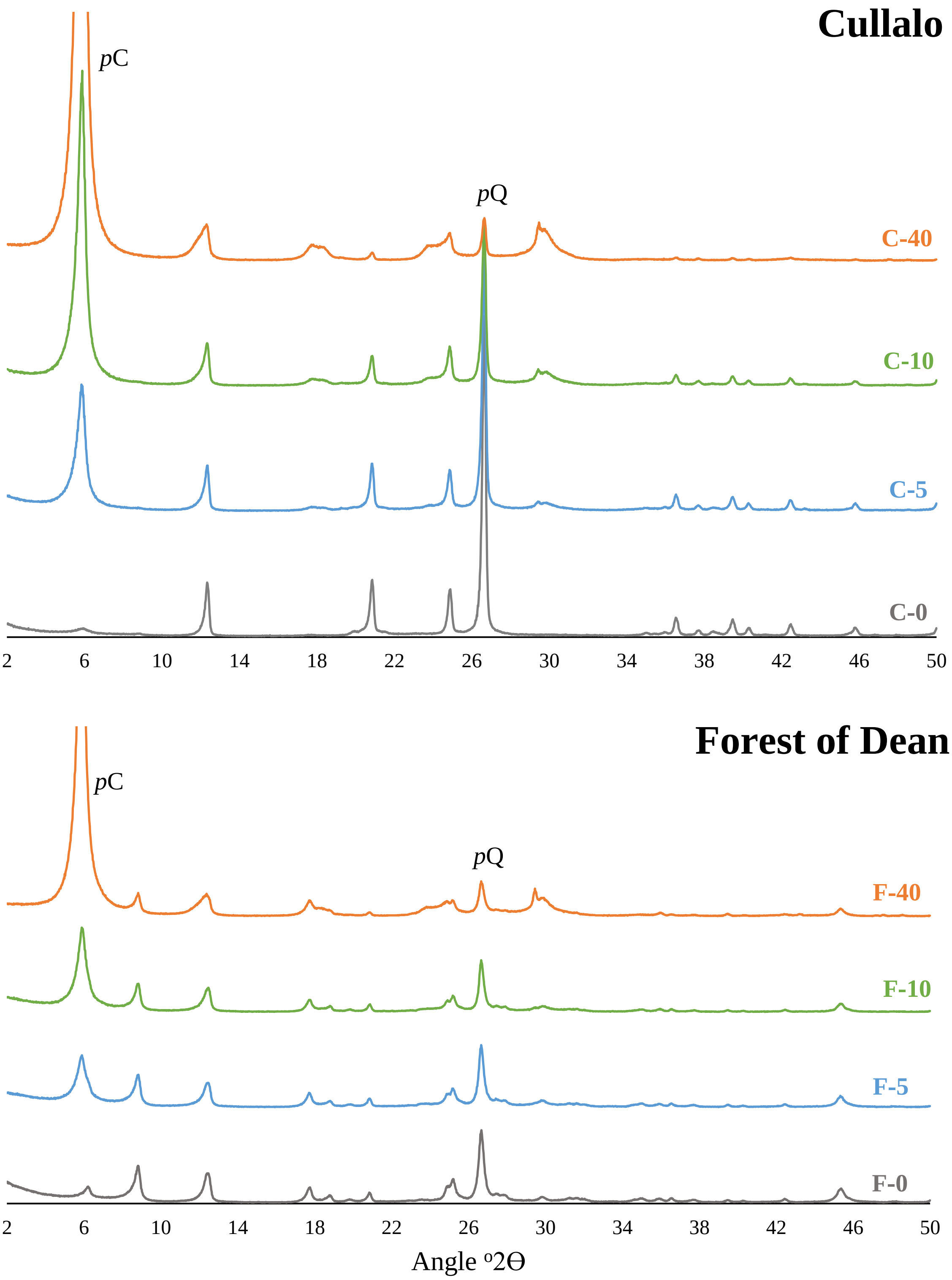

Figure 2.9: Diffractograms of clay fractions extracted from doped (0, 5, 10, and 40 wt. %) bulk sandstones. *p*C = primary clay peak; pQ = quartz.

2.4.4 Doping experiment: efficiency of clay extraction method

As a known amount of saponite has been added to each sample, the efficiency of the method used for extracting clay from crushed sandstone can be assessed. Overall, the calculated clay content (%) of the sandstone, based on the weight of the original bulk material (i.e., sandstone plus added saponite) and weight of subsequently separated clay minerals, grossly underestimates the true clay content value as seen from Table 2.2. The calculated clay content never surpasses 5 wt % for any samples across both sandstone types. The total amount of saponite extracted for each sample varies from ~ 70 % of total saponite extracted (F-5) to ~ 10 % of total saponite extracted (F-40). There is a similar trend across sandstones, where the higher the clay content, the more difficult it is to subsequently extract all of the clays. Previous research has noted that the physical properties of clay minerals, in particular their very fine grain size and large surface area, makes separation of clay minerals difficult – a difficulty which sandstones with higher clay content may be more prone to. Moreover, it is unlikely that all clay minerals are being crushed to within the 2-μm ‘clay fraction’. Many clay minerals may remain coarser and so not be extracted. Some clay minerals may be more susceptible to the above problems making their analysis in cases where sample amount is very limited (often case in study of heritage objects) more difficult.

Finally, during clay mineral extraction, the amount of crushed material placed inside a centrifuge tube was also reviewed. Using C-40, centrifuge tubes were filled with either 2.5 g [C-40(2)] or 5 g [C-40(1)] of crushed sandstone. Table 2.2 shows the results of the comparison, where less material inside the centrifuge tube yields around x5 more extracted clay. This provides at least one example where the extraction method can be adjusted slightly to allow for more efficient extraction of clay minerals. Less clay within the centrifuge tube may provide more physical space and reduce the occurrence of clay minerals becoming electrostatically ‘stuck together’ – thus allowing for extraction of more clay. Further trials could compare the amount of clay extracted from tubes containing 2.5 g and 2 g, or 1.5 g, etc.

Table 2.2: The measured clay content based on the amount of clay extracted from bulk sandstone mixtures compared to the true clay content of sandstones. The total proportion of saponite extracted, expressed as a percentage, is also highlighted. *This excludes clay minerals which were present prior to doping. This is most relevant to Forest of Dean, which contains kaolinite, illite and chlorite. -0 samples give an indication of the occurrence of clay minerals before doping.

	True clay content (wt. %)*	Measured clay content (wt. %)	Total proportion of saponite extracted (wt. %)
F-0	0	2.6	-
F-5	5	3.6	72.3
F-10	10	3.7	36.9
F-40	40	3.9	9.7
C-0	0	1.3	-
C-5	5	1.8	36.9
C-10	10	2.6	26.2
C-40	40	4.9	12.3
C-40(1)-5g	40	0.01	0.03
C-40(2)-2.5g	40	5.0	12.7

2.4.5 Mounting techniques: filter peel vs acetone slurry

2.4.5.1 SEM of saponites

As mentioned in section 3.2, saponites A-D were prepared for pXRD using two different mounting techniques. Prior to analysis, small chips of saponites were imaged by SEM. Figure 2.10 shows the variation in mineral morphology of the saponites despite their similar chemical composition and crystallographic structure. Saponite A, a white powdery clay from the Isle of Skye, was mostly comprised of ‘rosette’ clay structures which were sometimes covered in fibrous clay minerals that resemble illite (Figure 2.10). Saponite B, a dark brown and very hard clay, had the finest grain size of the saponite samples. Saponite C, an amorphous grey-green clay, was comprised of clay platelets which were often organised in a radial structure, with a ‘centre’ comprising relatively finer amorphous clay. Finally, saponite D had a bladed morphology in SEM which is consistent with macroscopic descriptions. The clay fraction present in weathered Dcath was mostly made up of individual platelets which were mostly located between grain and inside pores.

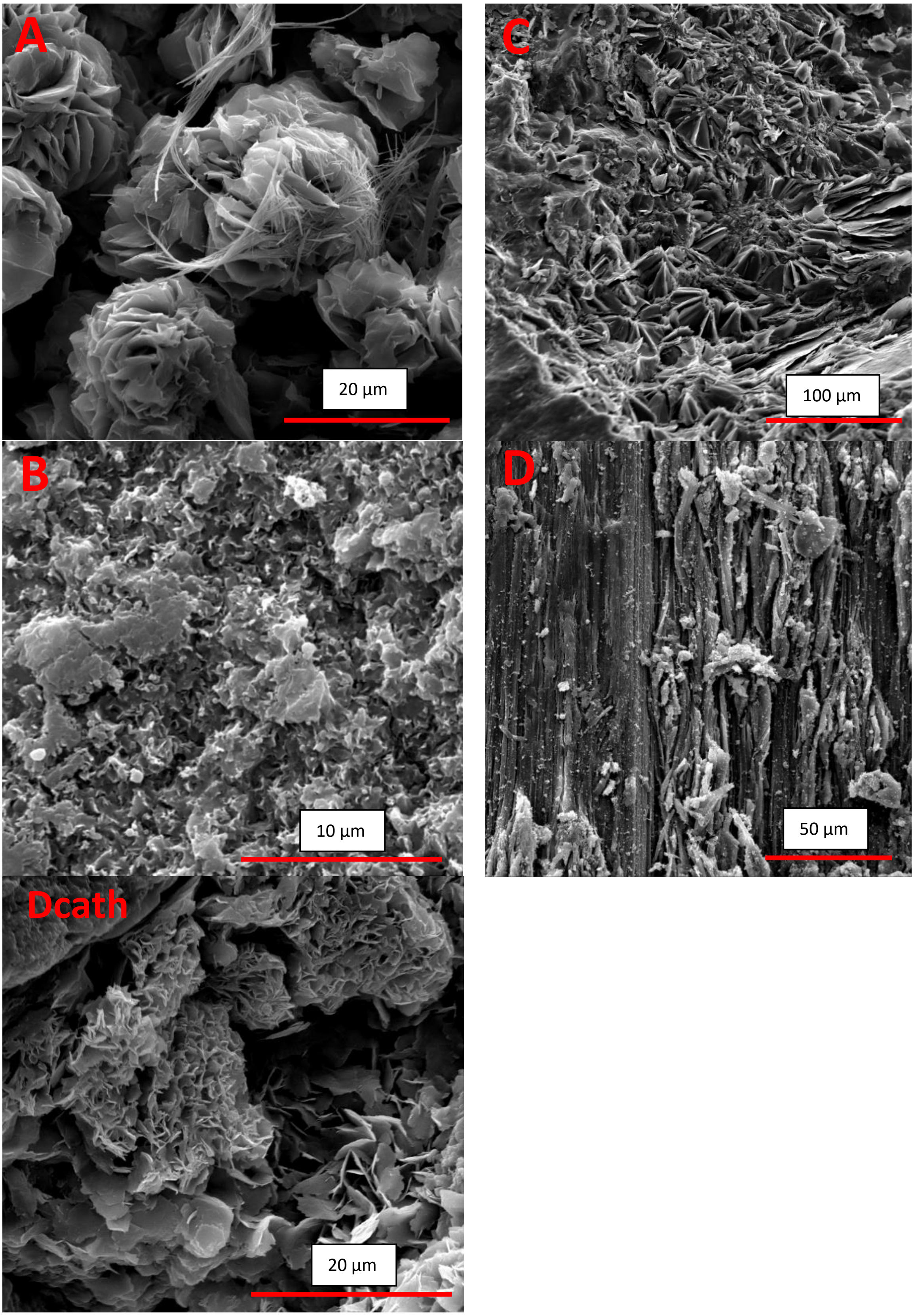

Figure 2.10: Secondary electron (SE) images of saponite A-D and weathered sandstone from Dunkeld Cathedral (Dcath).

2.4.5.2 Comparison of mounting techniques

Figure 2.11 compares the diffractograms of EG-treated and untreated clay samples mounted using the acetone and filter methods. All saponite samples show similar diffractograms with a major peak around 6° 2ϴ, and several other prominent peaks at 12° 2ϴ, 18° 2ϴ and 25° 2ϴ. The saponite diffractograms show a lateral peak shift of the primary clay peak associated with the EG-treated samples reflecting the expansion of smectite. The most notable difference between mounting techniques is the greater relative intensity of peaks associated with the samples prepared using the filter peel method. This is particularly true for the primary clay peak where CPS are up to x7 higher than the primary clay peak of samples prepared using the acetone method. This difference highlights the sensitivity of the primary clay peak to mineral alignment. This phenomenon has implications with regards to the quantification of clay content using the primary clay peak, as mineral alignment is evidently another factor which influences the properties of this peak. As discussed previously, there are a number of factors, including clay content, clay mineral alignment, crystallinity etc that impact the properties of this primary clay peak and so using this peak as a method of clay mineral quantification can be unreliable (Kahle et al., 2002; Środoń., 2002; Zhou et al., 2018). When comparing the two mounting techniques, there is little to no difference in overall peak positions. Furthermore, the lateral peak shift associated with the EG-treatment is consistent across both techniques, within an error of 0.02-0.12° 2ϴ.

The clay fraction extracted from the weathered Dunkeld building sandstone (Dcath) shows a more diverse mineralogical composition in comparison to the pure saponite clay samples. As well as extracted clays Dcath also contains: quartz, feldspar, kaolinite, chlorite, and calcite. The difference in diffractogram characteristics (e.g. peak heights) between mounting techniques is less apparent, perhaps due to the diverse and complex mineral assemblage relative to other samples. Moreover, the minerals, matrix, and cements, of Dunkeld sample are also very weathered. The process of weathering leads to physical and chemical disintegration of minerals and can therefore contribute to mineral lattice damage (Vdović et al., 2010; Zhao et al., 2018). The weathered condition of many minerals may explain why the relative intensity of peaks in the diffractogram are much lower. However, the primary clay peak of Dcath prepared using the acetone method has lower relative intensity relative to the sample prepared using the filter peel method, which is consistent with the rest of the results in this study. Finally, unlike the saponite samples, there is no change in the diffractogram after glycol treatment indicating an absence of expansive smectite.

There were some practical difficulties worth noting when preparing samples. When mounted using the filter peel method, saponite samples occasionally peeled from the glass slide after EG-treatment (in which case the sample was reprepared from a new batch of clay and analysed again). The issue of sample peeling from the slide after EG-treatment was observed only when using the filter suction method, and can be problematic for analysis (Rich., 1975). Peeling lifts the aligned clays from the slide, changing the overall topography and height of the sample. This can affect the presence and extent of peak shift which may be incorrectly interpreted as expansion of clay minerals. However, peeling seems to happen randomly and so by preparing multiple samples (2-3) it is unlikely to affect all of them.

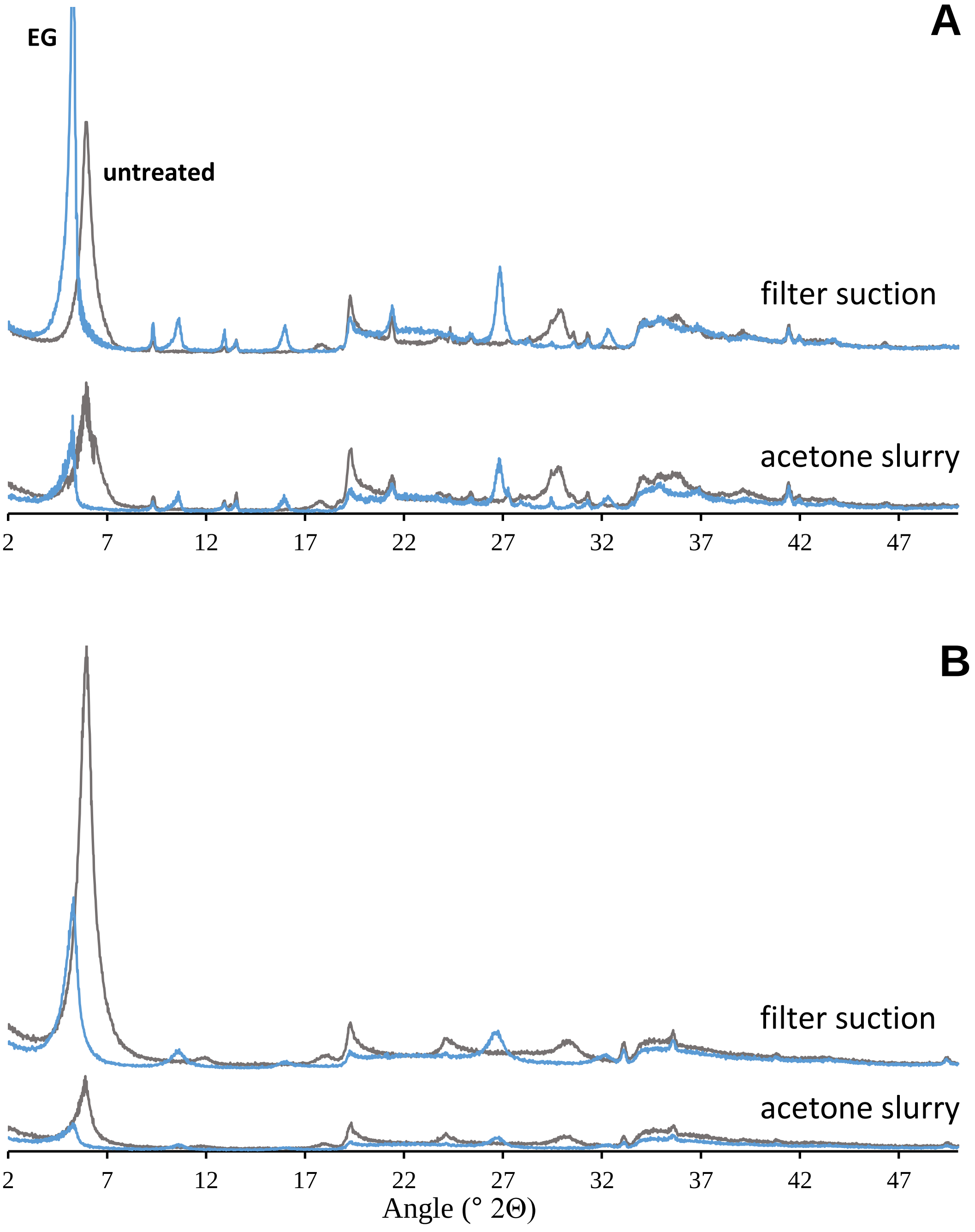

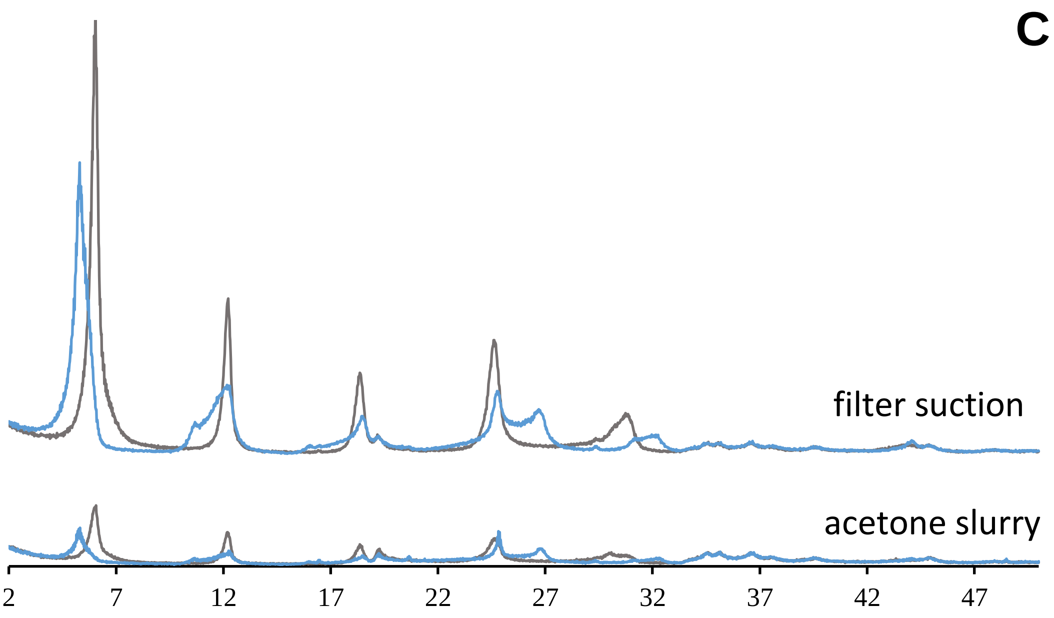
C
filter suction
acetone slurry
2
7
12
17
22
27
32
37
42
47

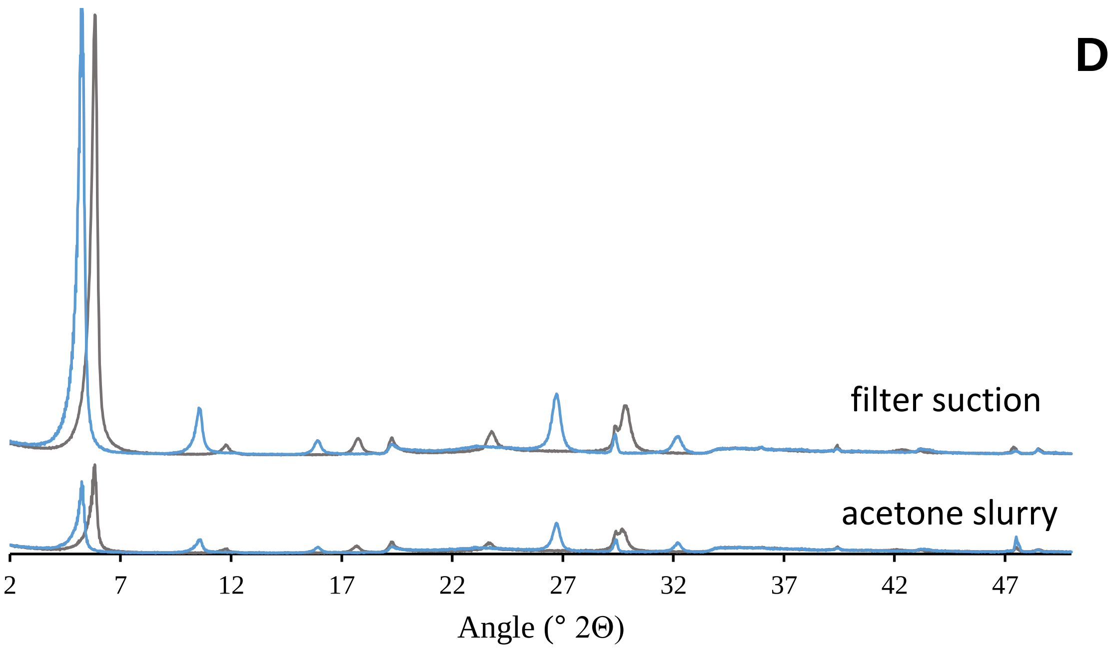
D
filter suction
acetone slurry
2
7
12
17
22
27
32
37
42
47
Angle (° 2Θ)

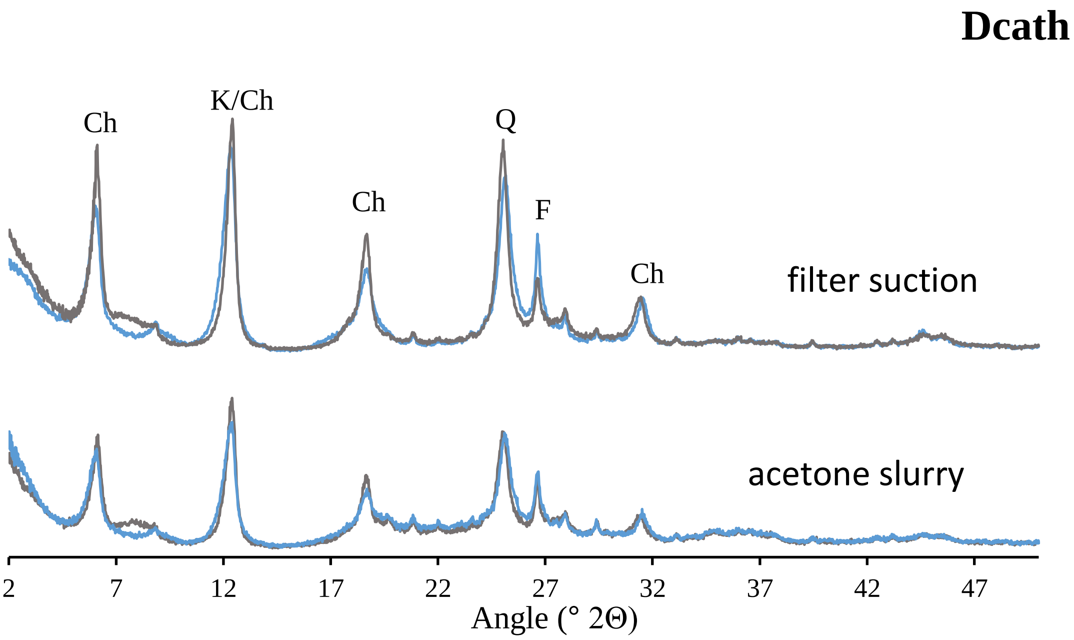

Figure 2.11: Diffractogram characteristics of the same sample prepared using two different methods. The figure includes the four studied saponites (A-D) and the weathered building stone from Dunkeld (Dcath). The grey diffractogram is prior to any treatment and the blue diffractogram is after EG treatment. Ch = chlorite; K = kaolinite; Q = quartz; and F = feldspar.

2.5 Final Discussion

All added saponite amounts (5, 10, and 40 wt%) were easily detected using pXRD in both bulk sandstone and extracted clay fractions. Further analysis could attempt to understand detection limits better by replicating this study using < 5% clay content. Clay content is mainly reflected in the diffractogram by 001 primary clay peak height at ~ 6° 2Θ. The differences in relative intensity of the primary clay observed in both bulk and extracted clay fraction correlates to the amount of clay present relative to other mineral quantities present in the sample. Relative peak heights also indicate the overall crystallinity of the sample, where increasing clay content leads to a decrease in relative intensity of the primary quartz peak relative to other mineral peaks, reflecting a decrease in overall crystallinity due to the poor crystallographic properties of clay minerals.

Despite the primary clay peak being partly controlled by the amount of clay present, and also to an extent the primary quartz peak, caution must be exercised when attempting to quantify the amount of clay present based on XRD diffractograms. Other factors can influence the properties of the primary clay peak including but not limited to, chemical composition of clay, mineral alignment, and mineral crystallinity (Kahle et al., 2002; Środoń., 2002; Zhou et al., 2018). The impact of mineral alignment on aspect ratio was shown in the mounting techniques study, where samples prepared using the filter method produced more well-defined peaks. Accurate quantification of clay content using XRD requires careful sample preparation and statistical analysis of diffractogram results (Zhou et al., 2018). Zhou et al (2018) provide a thorough critical review assessing different methods of quantitative analysis of clay minerals using XRD.

The amount of clay extracted from the sample does not reflect the amount of clay present in the sample, and therefore shouldn't be used as an indicator of clay content. Currently, a conversion factor based on the results is not possible as the amount of total saponite extracted from each sample is inconsistent. A conversion factor could be possible with more analysis. Improvements at the centrifuge stage, including placing less material into the centrifuge tube, could help maximise the amount of clay extracted from bulk mixture. Future work assessing ways in which clay extraction methods can be made more efficient would greatly benefit those studying heritage objects, when samples are mostly available in very small amounts due to the cultural significance and value associated with studied materials.

In general, the filter peel method produced diffractogram results with more well-defined peaks relative to samples prepared using the acetone method, particularly in reference to the primary clay peak (*p*C) in the case of the saponites. A well-defined primary clay peak is important in the analysis of expansive clays, as it is this peak which reflects expansion along the 001 which takes place after EG treatment (Sebastián et al., 2008; Ruedrich et al., 2010). Smaller peaks are also more defined with a higher with higher relative intensity using the filter peel technique, again aiding in mineral identification. Finally, the acetone technique was more useful when sample amount was extremely limited. This can often be the case after clay extraction from a bulk sandstone, where clay is only present in small quantities or when working with stone of great cultural and historic value.

2.6 Conclusions

- pXRD is a powerful tool which can be used to characterise the mineralogy of building stones.

- This study has shown that pXRD can detect clay mineral content in bulk mixtures from as little as 5 wt %.

- Increasing clay content leads to an increase in the relative intensity of the primary clay peak (001 peak), reflecting the increase in clay content, and decrease in the relative intensity of the primary quartz peak, reflecting the relatively lower amount of quartz and lower crystallinity of sample.

- Properties such as relative intensity and the ratio of the primary clay and quartz peaks (*p*C/*p*Q) can be used to accurately describe and understand diffractogram results.

- However, determining the amount of clay present in a bulk mixture using these properties is not a reliable method. This is mostly due to the fact that a number of other properties influence the primary clay peak outwith clay content including but not limited to mineral crystallinity (i.e. low crystallinity due to damages to mineral disintegration and damage to mineral crystal lattice) and clay mineral alignment.

- Quantification of clay mineral content in sandstone requires careful sample preparation for pXRD and application of statistical analysis.

- Despite these findings, this study has provided useful information on how XRD diffractograms of clay-rich sandstones change with changing clay content, while confirming that clay content as low as 5 wt % can be detected in bulk mixtures.

- Follow on studies should consider how well sandstones with clay content ranging between 1-5 wt% can be detected.

- This study has also provided detailed information on two preparation methods and provided advice on the appropriateness of each method in the context of studying stone decay in the built heritage.

2.7 References

Benavente, D., Cultrone, G., & Gómez-Heras, M. (2008). The combined influence of mineralogical, hygric and thermal properties on the durability of porous building stones. *European Journal Of Mineralogy*, *20*(4), 673-685. doi: 10.1127/0935-1221/2008/0020-1850

Christidis, G., & Koutsopoulou, E. (2013). A simple approach to the identification of trioctahedral smectites by X-ray diffraction. *Clay Minerals*, *48*(5), 687-696. doi: 10.1180/claymin.2013.048.5.22

Dassow, J., Li, X., Lee, M., Young, M., & Harkness, P. (2020). Ultrasonic drilling for the characterisation of building stones and salt induced decay. *Ultrasonics*, *101*, 106018. doi: 10.1016/j.ultras.2019.106018

Delago-Rodrigues, J. (2001) Swelling behaviour of stones and its interest in conservation. An appraisal. *Materiales De Construcción*, *51*(263-264), 183–195. https://doi.org/10.3989/mc.2001.v51.i263-264.363

Drever, J. I. (1973). The preparation of oriented clay mineral specimens for X-ray diffraction analysis by a filter-membrane peel technique. American Mineralogist: Journal of Earth and Planetary Materials, 58(5-6), 553-554.

Gibbs, R.J. (1965). Error due to segregation in quantitative clay mineral x-ray diffraction mounting techniques, American Mineralogist, 50 (5-6), pp. 741-751

Jiménez-González, I., Rodríguez-Navarro, C., & Scherer, G. (2008). Role of clay minerals in the physicomechanical deterioration of sandstone. *Journal Of Geophysical Research*, *113*(F2). doi: 10.1029/2007jf000845

Kahle, M., Kleber, R., Jahn, R. (2002) Review of XRD-based quantitative analyses of clay minerals in soils: the suitability of mineral intensity factors, *Geoderma*, 109, 191-205.

Pötzl, C., Dohrmann, R. & Siegesmund, S. Clay swelling mechanism in tuff stones: an example of the Hilbersdorf Tuff from Chemnitz, Germany. Environ Earth Sci 77, 188 (2018). https://doi.org/10.1007/s12665-018-7345-2

Reyes-Zamudio, V., Angeles-Chávez, C., & Cervantes, J. (2010). Clay minerals in historic buildings. *Journal Of Thermal Analysis And Calorimetry*, *104*(2), 405-413. doi: 10.1007/s10973-010-1041-0

Rich, C. (1975). Curling Inhibition of Clays Mounted on Slides for X-Ray Diffraction Analysis1. *Soil Science Society Of America Journal*, *39*(1), 155. doi: 10.2136/sssaj1975.03615995003900010041x

Ruedrich, J., Bartelsen, T., Dohrmann, R., & Siegesmund, S. (2010). Moisture expansion as a deterioration factor for sandstone used in buildings. *Environmental Earth Sciences*, *63*(7-8), 1545-1564. doi: 10.1007/s12665-010-0767-0

Scrivano, S., Gaggero, L., Aguilar, J., de Kock, T., Derluyn, H., & Cnudde, V. (2017). Texture and mineralogy influence on durability: the Macigno sandstone. *Quarterly Journal Of Engineering Geology And Hydrogeology*, *50*(4), 393-401. doi: 10.1144/qjegh2016-107

Sebastián, E., Cultrone, G., Benavente, D., Linares-Fernandez, L., Elert, K., & Rodriguez-Navarro, C. (2008) Swelling damage in clay-rich sandstones used in the church of San Mateo in Tarifa (Spain). Journal of Cultural Heritage, 9(1), 66-76, doi: 10.1016/j.culher.2007.09.002

Shekofteh, A., Molina, E., Arizzi, A., Cultrone, G., Ahmadi, H., & Yazdi, M. (2019) Characterization and damage assessment of stones used in the Pasargadae World Heritage Site, Achaemenian period, International Journal of Architectural Heritage, 13:4, 521-536, DOI: 10.1080/15583058.2018.1436728

Środoń, J. (2002) Quantitative mineralogy of sedimentary rocks with emphasis on clays and with applications to K-Ar dating, *Mineral. Mag*, 66, 677-687

Tiennot, M., Mertz, JD. & Bourgès, A. Influence of Clay Minerals Nature on the Hydromechanical and Fracture Behaviour of Stones. Rock Mech Rock Eng 52, 1599–1611 (2019). https://doi.org/10.1007/s00603-018-1672-1

U.S Geological Survey (USGS). Clay mineral identification flow diagram, Open-file report 01-041, available at https://pubs.usgs.gov/of/2001/of01-041/htmldocs/flow/index.htm

Vdović, N., Jurina, I., Škapin, S. D., & Sondi, I. (2010). The surface properties of clay minerals modified by intensive dry milling—revisited. Applied Clay Science, 48(4), 575-580.

Wangler, T., & Sherer, G. (2008). Clay swelling mechanism in clay-bearing sandstones. Environmental Geology, 56(3-4), 529-534. DOI: 10.1007/s00254-008-1380-3

Zhou, X., Liu, D., Bu, H., Deng, L., Liu, H., Yuan, P., Du, P., Song, H. (2018) XRD-based quantitative analysis of clay minerals using reference intensity ratios, mineral intensity factors, Rietveld, and full pattern summation methods: a critical review, 3(1), 16-29. DOI: 10.1016/j.sesci.2017.12.002

Zhao, J., Lu, C., Deng, L., & Liu, G. (2018). Impacts of simulated acid solution on the disintegration and cation release of purple rock (mudstone) in Southwest China. Geomorphology, 316, 35-43.

3.0 Mineralogical and petrophysical characterisation of sandstones used in the built heritage of Scotland.

3.1 Introduction

The durability of stone is determined by its resistance to weathering. This resistance is controlled by the mineralogical and petrophysical properties of stone which can be characterised using a variety of analytical techniques. Understanding the decay and durability of stone is essential in decision making relating to conservation approaches made by bodies such as Historic Environment Scotland (HES). Many common sandstones found in Scotland’s built heritage lack an extensive characterisation of both mineralogical and petrophysical properties. Moreover, the sometimes heterogenous and/or clay-rich nature of sandstones found in Scotland’s historic buildings can make understanding decay and durability more challenging due to the variability in stone properties and complex decay pathways. The presence of clay minerals in particular can adversely impact the durability of building sandstone and drive weathering processes (Warke and Smith., 2000; Sebastián et al., 2008; Jiménez-González., 2008; Wangler & Scherer., 2008). Clay minerals can reduce the overall durability of stone through processes relating to intracrystalline and intercrystalline swelling, disjoining pressure, and clay softening upon wetting (Madsen & Müller-Vonmoos., 1989; Azhar et al., 2020). However, there is no previous research which address the presence and influence of clay minerals on the durability of building sandstones in Scotland.

This chapter characterises, in detail, the mineralogy and petrophysical properties of six quarried sandstones commonly used in restoration projects around Scotland. Importantly, these quarried sandstones are similar to the original sandstone found in some of Scotland’s 12th century onwards Abbeys and Cathedrals, and so may provide insight into the decay and durability of sandstone at these sites. In addition to quarried sandstones, the mineralogy and petrography of original weathered sandstone from several historic buildings is assessed to a) confirm the similar petrography to quarried sandstones, and b) to provide insight into the dominant decay patterns and processes operating at the sites.

3.2 Samples

It is important to note that as some of the buildings researched in this project date back to the 11th century, sourcing the original quarry for sampling is rarely possible. This is mostly due to lack of documentation making stone provenance surveys difficult and/or the present state of the historic quarry (commonly infilled or flooded) making it inaccessible for sampling. For this project, fresh sandstone samples were obtained from either operational or disused quarries around the UK. Moreover, sampling at historic buildings is extremely challenging due to the high value associated with many buildings and consequent sampling restrictions imposed on them. As a result, very small pieces, often crustal samples, are commonly used in stone decay studies. Due to the small size and often weathered state of these samples, identifying a cause of stone decay can be difficult and in some cases impossible. Sampling restrictions and the adverse impact they can have on representativeness of data is well recognised in the field of heritage science (Kennedy., 2015; Strlic., 2015; Michette et al., 2020; Mitsos et al., 2022). Due to sampling issues, the development of non-destructive and/or in-situ tests has become a rapidly developing area in the field of heritage science (Avdelidis & Moropoulou., 2004; Chastre &Ludovico-Marques., 2018; Salvatici et al., 2020; Benavente et al., 2022).

All sandstones researched in this chapter are considered either modern analogues of the original sandstone used in the construction of historic buildings in Scotland, or common replacement sandstone used in their restoration. Fresh samples are required for petrophysical tests including strength testing, as they offer a more accurate representation of the original stone properties prior to weathering. In addition to fresh quarry samples, the mineralogy and petrography of several weathered sandstones obtained from historic buildings in Scotland are analysed. Weathered samples provide information on the type of weathering processes affecting the stone. Weathered samples are small in size (5 cm length) and so only their petrography and mineralogy is characterised. Weathered samples were provided by HES for research purposes. Below is a description of the fresh and weathered sandstone samples characterised.

3.2.1 Quarried sandstones

Forest of Dean, Fd, is a popular building stone known for its durability and distinctive grey-green colour (Figure 3.1). This sandstone is currently quarried in the county of

Gloucestershire, England, and forms part of the Pennant Formation deposited during the mid-late Carboniferous. Fd is extensively used as a replacement stone at Dunkeld Cathedral; a rapidly decaying building in the Scottish county of Perthshire, originally constructed using a heterogenous clay-rich sandstone. Fd is extremely similar in both mineralogy and petrophysical properties to the original stone used at the cathedral. The sandstone is fine-medium grain size (0.25-0.5 mm) (Figure 3.1). There are large, empty pores (~ 1mm in diameter) on the surface of the prepared samples. There are no obvious bedding or sedimentary structures present in the sandstone.

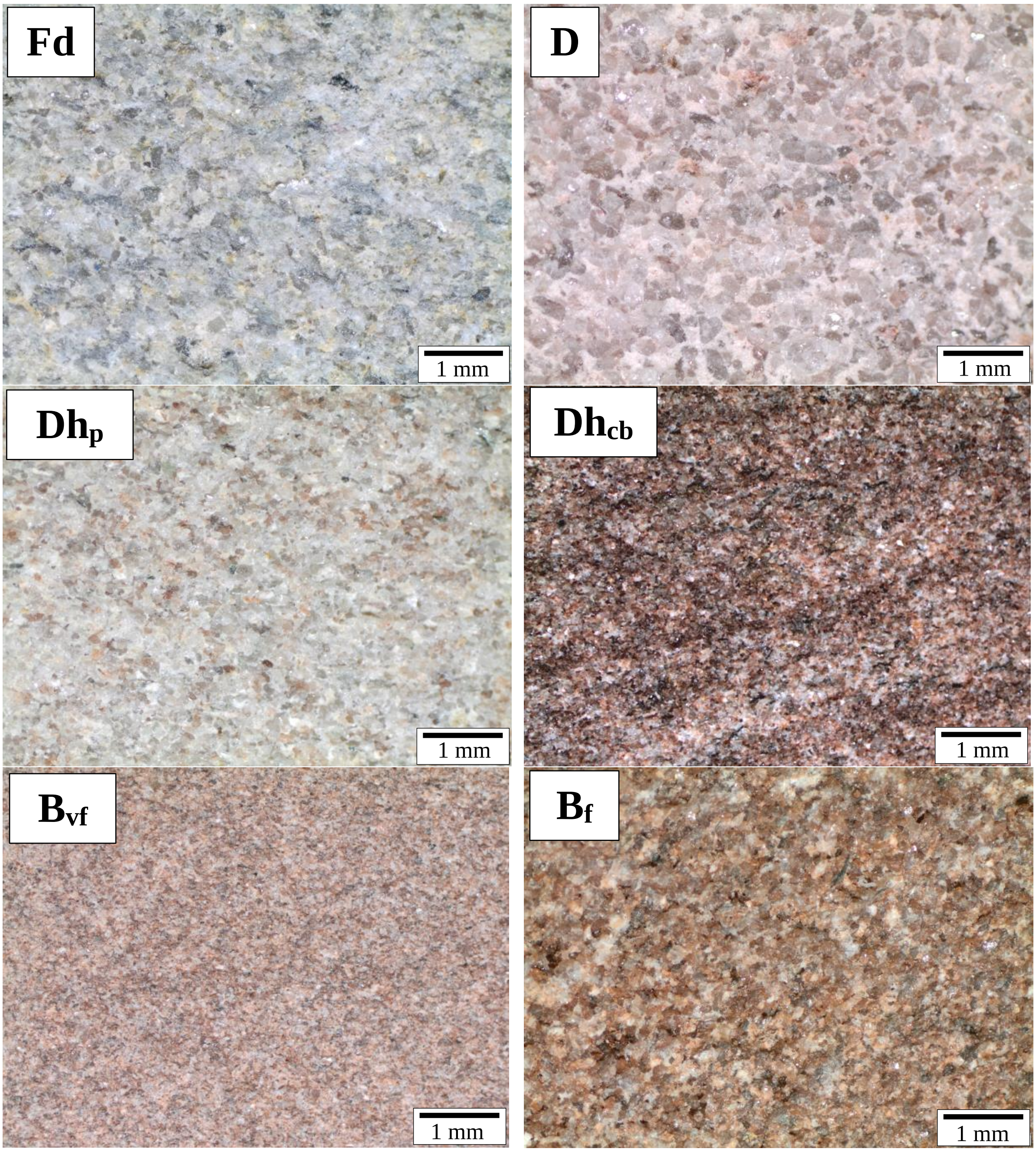

Figure 3.1: Macroscopic appearance of fresh sandstones used in historic building across Scotland. Fd = Forest of Dean sandstone; D = Doddington sandstone; Dh_p = Denholmhill Red sandstone; Dh_{cb} = Denholmhill Red (cross bedded) sandstone; B_{vf} = St Bees (very fine grained variety); and B_f = St. Bees (fine grained variety).

Doddington sandstone, D, is currently quarried at Doddington, near Wooler in the county of Northumberland, England. The sandstone is commonly used in construction and restoration works in Scotland, including the restoration of Jedburgh Abbey. D comprises part of the Fell sandstone group with a stratigraphic age of early-mid Carboniferous. The sandstone is light pink-cream in colour with dark brown specs of lithic fragments and biotite (Figure 3.1). The grain size of the sandstone is medium-coarse (0.5-1 mm) and is composed mostly of quartz with very little cementing material, resulting in poor cohesivity and a very grainy texture. There are no textural features such as bedding present in the D.

Another two sandstones used in this study were quarried at Dunholmhill; a 19th century quarry located approximately 5 miles SW of Jedburgh Abbey in the Borders region of Scotland. The sandstone is late Devonian – early Carboniferous in age, belonging to both the Stratheden and Inverclyde group. It has similar mineralogical and textural properties to the original building stone used at Jedburgh Abbey. There are two varieties of Denholmhill Red sandstone: planar bedded (de-p) and cross bedded (de-cb). De-cb is dark red-brown-purplish in colour with a very fine-fine grain size (0.125-0.25 mm) while de-p is light cream-brown in colour with a fine-medium grain size (0.25-0.5 mm) (Figure 3.1). Both sandstones are visibly micaceous and exhibit bedding and/or cross bedding on a scale of 2-5 mm.

St. Bees is an attractive red sandstone used as a replacement stone in many buildings across Scotland and is currently quarried at St. Bees Quarry Bigrigg,Cumbria, England. St Bees was deposited during the early Triassic period, forming part of the Chester Formation. St Bees is used in restoration projects at Arbroath Abbey. Two varieties of St Bees were studied: a fine-grained variety (Bf), and a very fine-grained variety (Bvf) (Figure 3.1). Both samples have a similar dark red-brown colour and both exhibit fine-scale (2-3 mm) planar bedding.

3.2.2 Weathered building sandstones

Jedburgh Abbey is one of four Border Abbeys in Scotland. It was founded in early 12th century and is classified as a ruin. The historic building has seen multiple phases of destruction and restoration. The weathered sandstone, J_w (Figure 3.2), studied in this project is from the lower storey part of the Abbey where sandstone has been weathering rapidly since its excavation in 1984 (Figure 3.3). J_w is pink-brown in colour and appears to be cross bedded (on a scale of 2-3 mm) where bedding planes have been preferentially weathered over time leading to orientated fractures throughout the stone. The original stone for the Abbey is thought to have been sourced from the Stratheden and Inverclyde sandstone groups (local bedrock sandstone) and quarried at multiple local sites including Ferniehirst quarry, located near Jedburgh in the Scottish Borders. Current replacement stones being used at the Abbey include Doddington, D, and Locharbriggs sandstone. Decay patterns at Jedburgh Abbey are highly variable as many different sandstone types have been introduced during different phases of construction. Decay patterns in the lower storey region of the Abbey (where sample for this project is from) consists mostly of fissuring (mostly splitting along planes of weakness including clay-rich bedding planes), and delamination of sandstone layers parallel to bedding planes. Inside the nave of the Abbey aveolization and sanding of pillars is also visible.

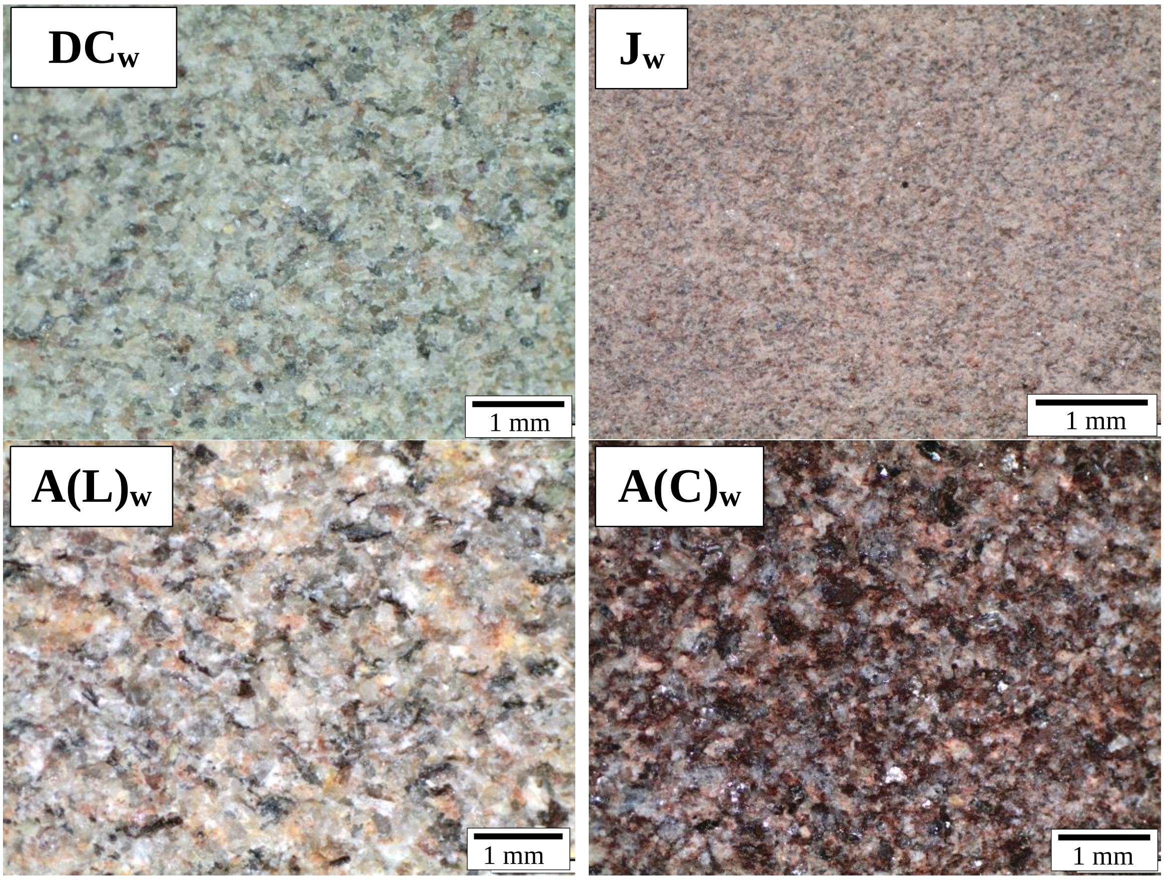

Figure 3.2: Macroscopic appearance of weathered sandstones found in historic buildings across Scotland: DC_w = weathered sandstone from Dunkeld Cathedral; J_w = weathered sandstone from Jedburgh Abbey; $A(L)_w$ and $A(C)_w$ = two varieties of weathered sandstone from Arbroath Abbey.

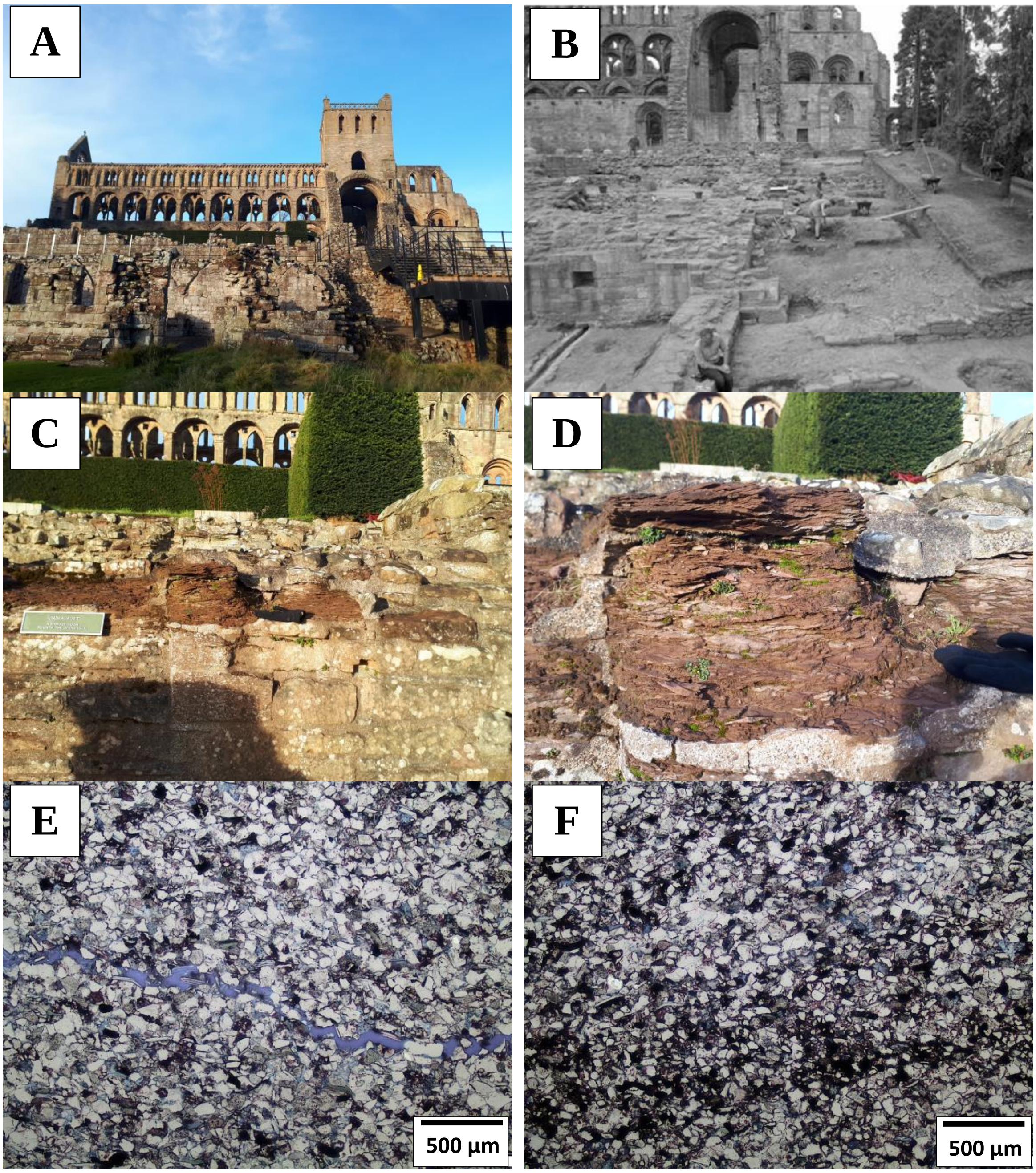

Figure 3.3: A) Jedburgh Abbey, Scottish Borders, Scotland; B) Archaeological excavation in 1984 uncovering previously buried masonry; C and D) rapidly decaying sandstone of the lower storeys; E and F) optical microscopy images of polished thin sections (impregnated with blue resin) showing fractures caused by weathering (E), and bands of oxides present in weathered sandstone (F).

Construction of Dunkeld Cathedral took place from the mid-1200s until the late 1400s. The Cathedral is located in the county and Perth and Kinross, and the central Nave of the Cathedral is still in use for religious services (Figure 3.4). The weathered sandstone, DC_W, studied in this project is grey-green in colour and contains clasts of clay (~ 5 – 10 mm length) (Figure 3.2). The original stone for the Cathedral is thought to have been sourced locally from the Teith Formation using multiple quarries. The current replacement stone used at the

Cathedral is Fd which is quarried in Gloucestershire, England. Decay patterns at Dunkeld Cathedral consist mainly of granular disintegration of individual stone blocks, spalling, flaking and preferential erosion of clay clasts (Figure 3.4).

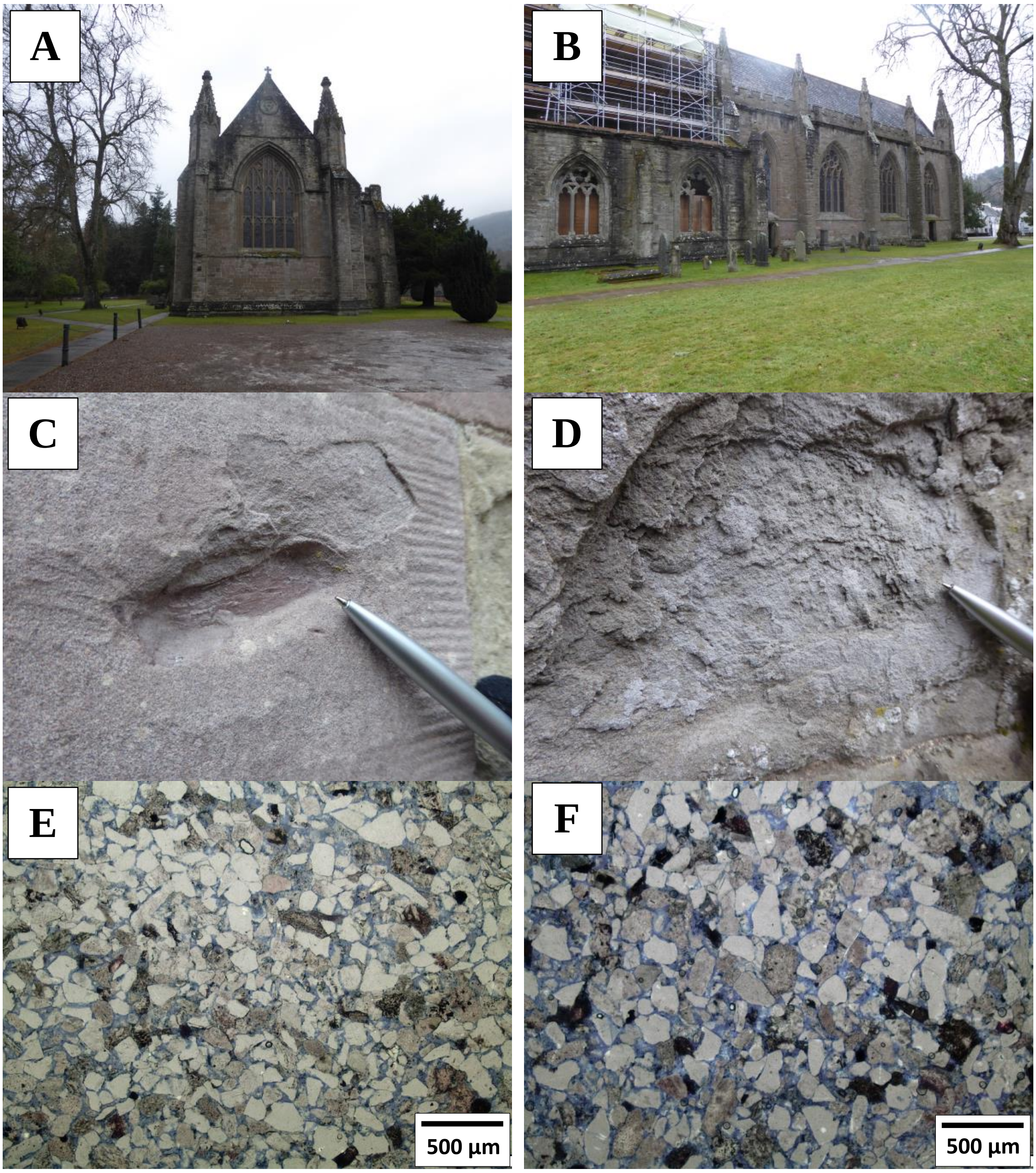

Figure 3.4: Dunkeld Cathedral, Perth and Kinross, Scotland; B) The main Nave still used for religious services today; C) clasts of clay preferentially eroding; D) spalling and granular disintegration of sandstone common; E and F) optical microscopy images of polished thin sections (impregnated with blue resin) showing an abundance of lithics and oxides.

Arbroath Abbey was founded during the late 12th century and is classified as a ruin (Figure 3.5). The Abbey is located in the town of Arbroath on the East coast of Scotland. The Abbey is famously associated with the Declaration of Arbroath – a written letter from Scottish nobles to Pope John XXII in 1320 defending Scotland as an independent nation separate from the sovereign kingdom. The weathered stone from Arbroath consists of a corbel, $A(C)_w$, and lintel block, $A(L)_w$ (Figure 3.2). $A(L)_w$ is light pink-brown in colour and contains clasts of clay (~ 1mm length). The stone is visibly micaceous (biotite and muscovite) where micas are orientated along bedding planes. $A(C)_w$ is dark red in colour and has a relatively finer grain size in comparison to the lintel block. The sandstone exhibits planar bedding on a scale of ~ 1mm. The current replacement stone used at the Abbey is St. Bees, although other types have been used previously including Wilderness Red quarried in Gloucestershire from the same geological unit as Forest of Dean sandstone. Decay patterns at Arbroath Abbey are diverse and include: alveolization (coving), sanding, powdering, flaking, spalling, blistering and granular disintegration (Figure 3.5). Table 3.1 provides a summary of all replacement and weathered stones characterised in this chapter.

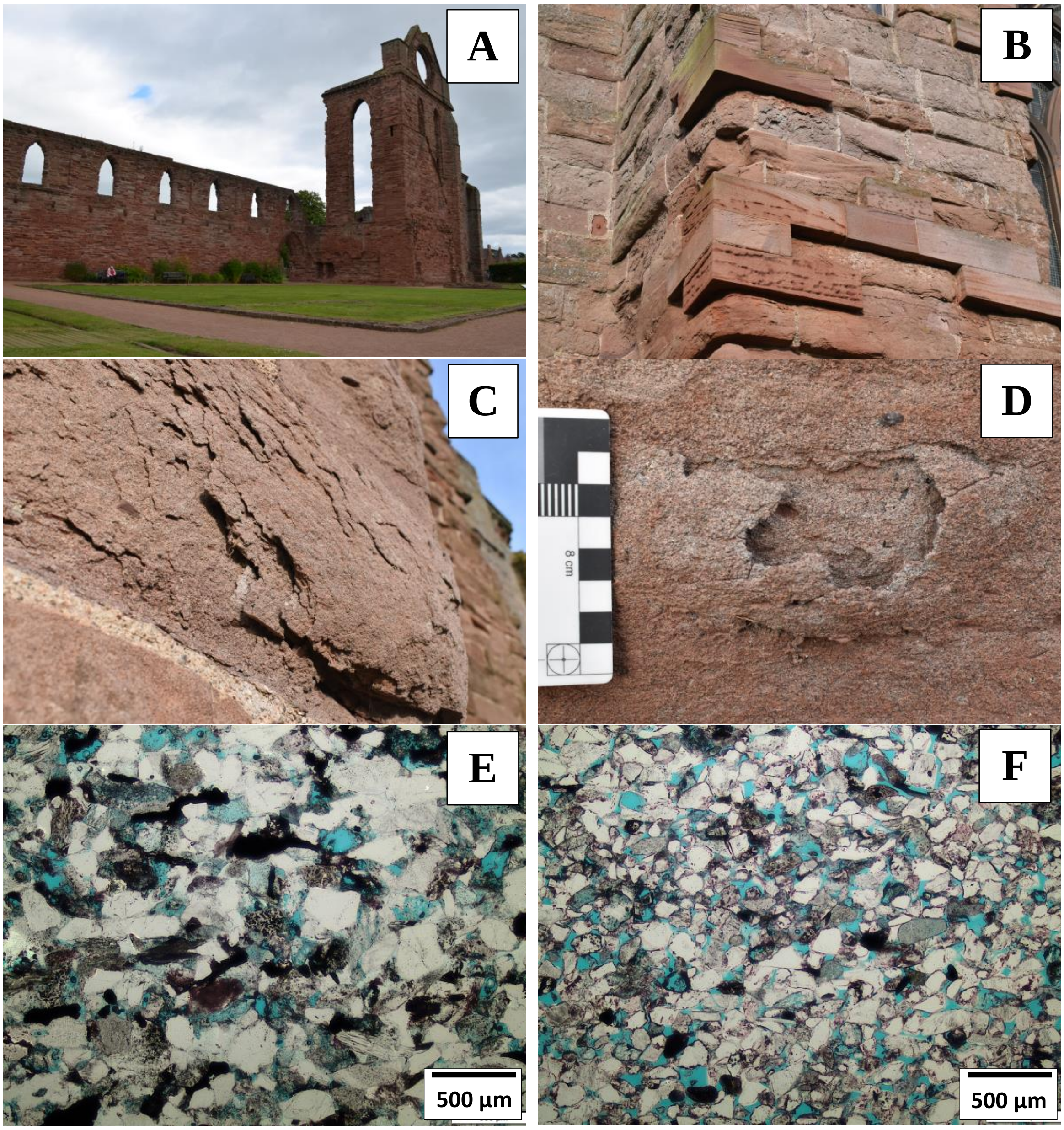

Figure 3.5: A) Arbroath Abbey, Arbroath, Scotland; B) stone replacement showing extent of weathering of original stone. Alveolization related to salt weathering is common; C) Scaling and spalling features; D) blistering of sandstone crust; E) optical microscopy image of $A(L)_w$; and F) optical microscopy image of $A(C)_w$.

Table 3.1: Summary of sandstones studied in this chapter.

Replacement stone

Sample name	Abbreviation	Source	Relevant historic building(s)	State of weathering
Forest of Dean	**Fd**	Forest of Dean quarry, Gloucestershire, England	Dunkeld Cathedral	Fresh
St. Bees (fine grained)	$\mathbf{B_{f}}$	St. Bees quarry, Cumbria, England	Arbroath Abbey	Fresh
St. Bees (very-fine grained)	$\mathbf{B_{vf}}$	St. Bees quarry, Cumbria, England	Arbroath Abbey	Fresh
Denholmhill Red (cross bedded)	$\mathbf{Dr_{cb}}$	Denholmhill quarry, Denholm, Scottish Borders	Jedburgh Abbey	Fresh
Denholmhill Red (planar bedded)	$\mathbf{Dr_{p}}$	Denholmhill quarry, Denholm, Scottish Borders	Jedburgh Abbey	Fresh
Doddington	**D**	Doddington, Northumberland	Jedburgh Abbey	Fresh

Original stone

Jedburgh Abbey	$\mathbf{J_{w}}$	Various quarries around Jedburgh Abbey and Scottish Borders area	Jedburgh Abbey	weathered
Arbroath Abbey corbel	$\mathbf{A(C)_{w}}$	Likely sourced from nearby coast in Arbroath area	Arbroath Abbey	weathered
Arbroath Abbey lintel	$\mathbf{A(L)_{w}}$	Likely sourced from nearby coast in Arbroath area	Arbroath Abbey	weathered
Dunkeld Cathedral	$\mathbf{DC_{w}}$	Various quarries around Dunkeld and Perth and Kinross area	Dunkeld Cathedral	weathered

3.3 Methods

3.3.1 Mineralogy and petrography

X-ray Diffraction (XRD) analyses was carried out using a Thermo Electron ARL X'TRA XRD at the Engine Shed (HES) in Stirling. The settings were as follows: CuKα radiation, running at 45mA and 44kV, step size of 0.02 degrees, and a scan rate of 1^o per minute. Bulk mineralogy was assessed on randomly orientated powder samples. Subsequently, a clay fraction was separated, and orientated samples were prepared for clay analysis. Clay samples were analysed prior to any treatment, after glycol treatment, and after heat treatment at 450^oC and 550^oC. Glycol and heat treatment are used to identify the presence and type of expansive clay present, if any, following protocols established by U.S. Geological Survey (USGS).

Scanning Electron Microscopy (SEM) was carried out using a FEI Quanta 200F Environmental SEM with EDAX Microanalysis. SEM was used to evaluate textural rock properties and distribution of clay minerals. Thin sections were prepared, and sputter coated in carbon for analysis. The samples were analysed in high vacuum, at 20 kV using backscattered and secondary electron imaging. In addition to thin section analysis, small gold-coated chips of samples were also analysed under the same conditions.

The average grain size was determined through point counting of 300 grains per sandstone, where grain size was measured along the longest grain axis. Furthermore, grains were recorded as quartz, feldspar, or lithic, so sandstone classification could be determined using the classification scheme of Folk (1974). Mineralogical and petrographic analysis was applied to both fresh quarry and weathered building stones.

3.3.2 Pore structure

The following methods used to characterise the pore structure of sandstones were carried out at the University of Alicante. Mercury Intrusion Porosity (MIP) was used to characterise the pore structure of sandstones. The technique involves the injection of mercury under pressure into the open porous network of a degassed sample. By increasing pressure, mercury is forced into the open pore space. The choice of mercury as a substance is driven by its 'non-wetting' behaviour, allowing for more control during experiments (Webb., 2001). Information obtained from this technique include connected porosity, pore size, pore volume,

v_p, mean pore radius, r_m, and pore size distribution, which can be calculated by comparing the volume of mercury injected into the sample and the associated applied pressure as seen from the Young-Laplace equation, also known as the Washburn equation (Van Brakel., 1981):

$$P = \frac{2\sigma cos\theta}{R}$$

where: P = pressure applied to mercury, R = radius of pore, σ = mercury surface tension, θ = contact angle of mercury and solid. There is an inverse relationship between pressure applied to mercury and radius of pore with increasing pressure relating to lower pore radius and vice versa.

The following analyses were performed using a PoreMaster 60 GT (Quantachrome Instruments) mercury porosimeter. A contact angle of 130° and surface tension of 480 mN m^{-1} were selected. The pore diameter interval detectable using MIP is 0.002-200 μm, corresponding to the highest (410 MPa) and lowest head (1 kPa) pressures.

Although MIP provides quantitative analyses of pore size and distribution, it fails to account for the total microporosity (micropore being defined here as pore with r 0-0.1 μm). Therefore, the nitrogen absorption technique (Autosorb-6 Quantachrome apparatus) was used to calculate pore volume and specific surface area (SSA) of samples. Pore volume is calculated as the liquid volume at relative pressure $P/P_0 = 0.95$ using type IV sorption isotherm. The BET method was used to determine the SSA in the relative pressure interval $P/P_0 = 0.05$–0.2. Initially the sample is degassed by heating before being transferred to a sorption chamber. The sample is then exposed to regular doses of gas at selected pressure intervals. The choice of gas depends on the pore-size range of the sample. In the study of stone decay, nitrogen is a commonly selected gas due to its small molecular size, making it ideal for micropore analysis. The pore size interval characterised using nitrogen absorption is 0.0009-0.015 μm.

The Open Porosity was also calculated using the water vacuum saturation test in accordance with BS EN 1936:2006. Cubic samples (50x50x50 mm) were used to characterise open porosity. Prior to this work, dry bulk density was calculated using the ratio of mass and sample volume. A vacuum system was used to calculate the open porosity of sandstone samples. Samples were placed in a desiccator under vacuum conditions and then saturated in water. Air is then introduced into the system and samples are left overnight before weighing the following morning. Hydrostatic and saturated weight are then measured before placing the samples in an oven to dry at 105^{o}C. Dry samples are then weighed again. Using dry, saturated, and hydrostatic weight, open porosity can be calculated using one of the following equations:

$$P\_open(\%) = \frac{Saturated\ wt - dry\ wt.}{saturated\ wt. - hydrostatic\ wt.}\ \ x\ 100$$

Alternatively,

$$P\_open(\%) = \frac{Saturated\ wt. - dry\ wt.}{volume\ (cm^3)}\ \ x\ 100$$

3.3.3 Hydric behaviour

Experiments carried out to understand the hydric behaviour of sandstones were undertaken in the University of Alicante. Two methods were used to quantify capillary water absorption rates: the continuous method, and non-continuous method. Cubic samples (40 x 40 x 40 mm) were used for analysis. The two methods are outlined below.

The non-continuous method was consistent with the procedure in BS EN ISO 15148:2002. Using the non-continuous method, samples were placed in a plastic container filled with water (depth ~ 3 mm). After samples were in the container the weight change was monitored and recorded regularly throughout the experiment until the samples were completely saturated. Weight change was recorded every 2 minutes for the first 15 minutes, after which point the time interval became progressively longer.

The non-continuous method does not provide an accurate calculation of capillary water absorption coefficients, C, for C (10 kg/m^{2}h$^{0.5}$) (Benavente et al., 2007). The continuous method uses a data-recording device and was used for very porous sandstone with high absorption rates. Using the continuous method, cubic samples are secured within a metal holder which is suspended from a balance which in turn records the weight of the sample. A container filled with water is directly underneath the sample. When the sample comes in contact with water, the balance continuously records the weight change. Using this method measurements can be logged as frequently as every 5 seconds and with better accuracy.

Using either of the above methods, the capillary absorption rate can be calculated using the following equation by relating the amount of water absorbed, over a given surface area:

$$C(kg\,m-2) = \frac{weight - dry\,weight}{surface\,area\,(m^2)}$$

Capillary absorption is then plotted against the square root of time. Over time the amount of absorbed water increases linearly. The capillary absorption rate slows as the samples reach complete saturation. The slope of the curve represents the capillary absorption coefficient, C ($kg/m^2h^{0.5}$).

Hydric expansion was measured by quantifying vertical deformation of sandstone samples when absorbing water using a Sensorex Linear Variable Displacement Transducer (LVDT)-SX8 displacement sensor, recording displacement every 5 seconds. LVDT systems quantify the amount of displacement by converting the change in position (linear displacement) relative to a reference, 0, into an electrical signal. Hydric swelling was measured at room temperature using cylindrical samples with dimensions 30x10x10 mm. The samples are partially submerged in water allowing for degasification before being completely submerged. Expansion is calculated as the maximum value of vertical deformation over the initial length prior to any deformation.

3.3.4 Thermal properties

Thermal expansion of samples were determined at the University of Alicante using a thermomechanical analyser (TA instruments). Small cubic samples (10x10x10 mm) are confined and placed under controlled force. The sample then equilibrates at 35°C and is then subject to a heating phase at a rate of 1°C/minute until 90°C. This is then followed by a cooling phase where temperature is reduced to 35°C before a second heating phase. In between each heating and cooling phase the sample is held under isothermal conditions for 10 minute periods. Throughout this entire process material deformation (physical expansion and contraction) is recorded.

Using the thermal expansion curve, the thermal expansion coefficient (10^{-6} K^{-1}) can then be calculated using the following equation:

$$\alpha = \frac{\Delta l / l_0}{\Delta T}$$

Where α = thermal expansion coefficient, Δl = change in length of sample, l_0 = original sample length, and ΔT = temperature interval.

3.3.5 Stone strength

The characterisation of Uniaxial Compressive Strength (UCS) and ultrasonic wave velocities was carried out at the University of Alicante. Prior to UCS testing, ultrasonic wave velocities were measured to fully characterise stone strength. Compressive (p) and shear (s) waves were measured using a Tektronix TDS 3012B 2 channel colour digital oscilloscope. Two visco-elastic couplants were used to ensure efficient coupling of the transducer and sandstone sample: an eco-gel for P-wave transducer, and shear wave couplant (SWC, GE Panametrics) for S-wave transducer. Samples with bedding were measured in two directions to assess degree of anisotropy present in samples. By measuring p and s waves, compressional wave velocities (vp) and shear wave velocities (vs) were calculated.

UCS was measured using cubic sandstone samples (50x50x50 mm) using a load rate of 150kg/s. UCS was defined as the maximum amount of force (MPa) applied before sample failure occurred. After measuring compressive strength and ultrasonic wave velocities, the Poisson ration and Young’s modulus can be calculated using the following equations:

Poisson ratio = $\frac{(v_p/v_s)^2-2}{2[(v_p/v_s)^2-1]}$

Young’s modulus = $\rho_{bulk}{v^2}_p\frac{(1-2v)(1+v)}{(1-v)}$

Where v_p= p wave velocity (m/s), v_s= s wave velocity (m/s), ρ_{bulk}= bulk density, and v = Poisson ratio.

3.3.6 Salt weathering experiment (Na_2SO_4)

Salt weathering experiments were carried out to evaluate the durability of sandstone samples in accordance with BS EN 12370:2020. The experiment used cubic sandstone samples (40x40x40 mm) being fully submerged in a saline solution (Na_2SO_4, conc. 14%) for 2 hours before being transferred to an oven at 105^oC to dry out overnight for approximately 16 hours. The samples are then removed from the oven and left to cool at room temperature (20^oC ± 1) for 3 hours. In instances where the temperature of the room is not suitable, a climatic chamber can be used to maintain 20^oC. This cycle continued for 15 days, testing the samples resistance to weathering related to the cyclic crystallisation and dissolution of salts. In the results and discussion section, sandstone samples which have been subject to artificial salt weathering are referred to as weathered sandstone.

vp was measured before and after weathering to assess any internal damage after weathering, and after salts were fully extracted. Further to this, some samples were selected for UCS testing after weathering.

3.3.7 Anisotropy

Sandstone samples with visible textural properties such as bedding were measured in two directions referred to as ‘parallel’ and ‘perpendicular’ for the following analysis: capillary water absorption, hydric swelling, stone strength (compressive strength and ultrasonic wave velocities), and thermal expansion. ‘Parallel’ and ‘perpendicular’ refers to the orientation of bedding relative to the orientation of a studied property such as water absorption, and compressive stress. Sandstone samples exhibiting textural properties are: De-p, De-cb. Bc and Bf. This analysis helps to determine whether or not textural properties result in different mechanical properties of the stone when tested in different directions.

Degree of anisotropy is determined using the ratio of the maximum and minimum value. The value of anisotropy can range from 0-1. A value of 1 indicates an isotropic sample, where the mechanical behaviour does not vary when the sample is measured in two directions. A value closer to 0 indicates an anisotropic sample, where the mechanical behaviour is contrasting when the sample is measured in different directions.

3.3.8 Summary of methods

Table 3.2 summarises the physical and mineralogical properties characterised in this chapter and the associated techniques used.

Table 3.2: Summary of analytical techniques and standard references (where appropriate) used in this research chapter.

Property		Methods	Standard used
Petrography		Optical microscopy; Scanning Electron Microscopy (SEM): Back scattered (BSE) and Secondary Electron (SE) imaging.	-
Chemistry and Mineralogy		X-Ray Diffraction (XRD)	U.S. Geological Survey (treatment and identification of clay minerals using XRD)
Pore structure	Pores in the range of 0.002 – 200 µm	Mercury Intrusion Porosimetry (MIP)	
	Open Porosity	Water vacuum saturation test	BS EN 1936:2006
	Microporosity (< 0.002 µm)	Nitrogen absorption	
Hydric properties	Water absorption coefficient (C, $kg/m^2h^{0.5}$)	Water absorption coefficient determined by partial immersion.	BS EN ISO 15148:2002
	Hydric expansion (mm/m)	Linear Variable Displacement Transducer (LVDT)-SX8 displacement sensor.	
Thermal properties	Thermal expansion coefficient (10^{-6} K^{-1})	Thermomechanical analyser (TA instruments)	
Durability	Resistance to weathering, decay (g)	Accelerated salt weathering experiment	BS EN 12370:2020

3.4 Results and Discussion

3.4.1 Mineralogy

XRD results for sandstone mineralogy are displayed in Figures 3.6-3.9. Sandstone D contains mostly quartz with relatively minor amounts of feldspar, kaolinite, and illite. Fd contains quartz, feldspars (albite and orthoclase), igneous-derived lithic fragments, chlorite, kaolinite, mica (muscovite and phlogopite) illite, and chlorite-serpentine, and interstratified illite-chlorite (Figure 3.6; Figure 3.7)..

Dh_p contains quartz, feldspars (albite and orthoclase), dolomite, kaolinite, and illite. Dh_{cb} contains quartz, feldspars (albite and orthoclase), dolomite, micas (muscovite, biotite, and phlogopite), dolomite, chlorite, interstratified illite-chlorite, and kaolinite (Figure 3.6; Figure 3.7).

B_{vf} contains quartz, feldspars (orthoclase and albite), calcite, and illite. B_f contains quartz, feldspars (orthoclase and albite), trioctahedral smectite (nontronite, montmorillonite or vermiculite), illite, and kaolinite (Figure 3.6; Figure 3.7).

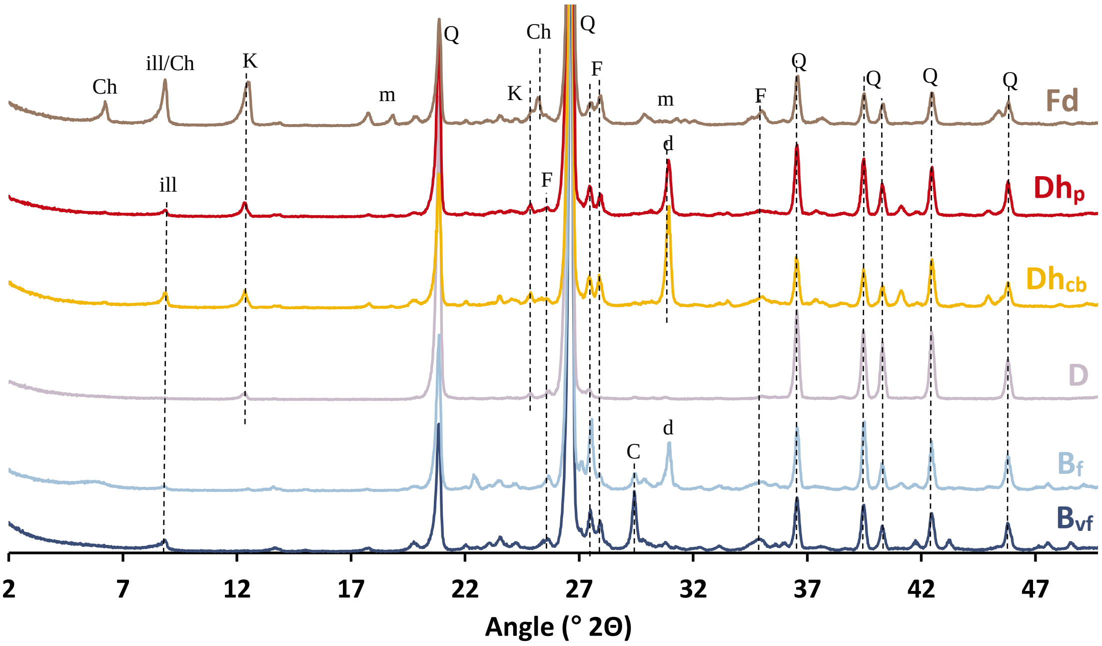

Figure 3.6: Bulk mineralogy of studied quarried sandstones. Overall the mineralogy of the sandstones is similar with quartz being the primary mineral in all. Some clay mineral peaks can be identified which were analysed in more detail by extracting a clay fraction from the sample (Figure 7, below). The primary feldspars identified in sandstones are albite and orthoclase. Q = quartz; F = feldspars; m = mica; C = calcite; d = dolomite; ill* = illite; K = kaolinite; and Ch = chlorite.

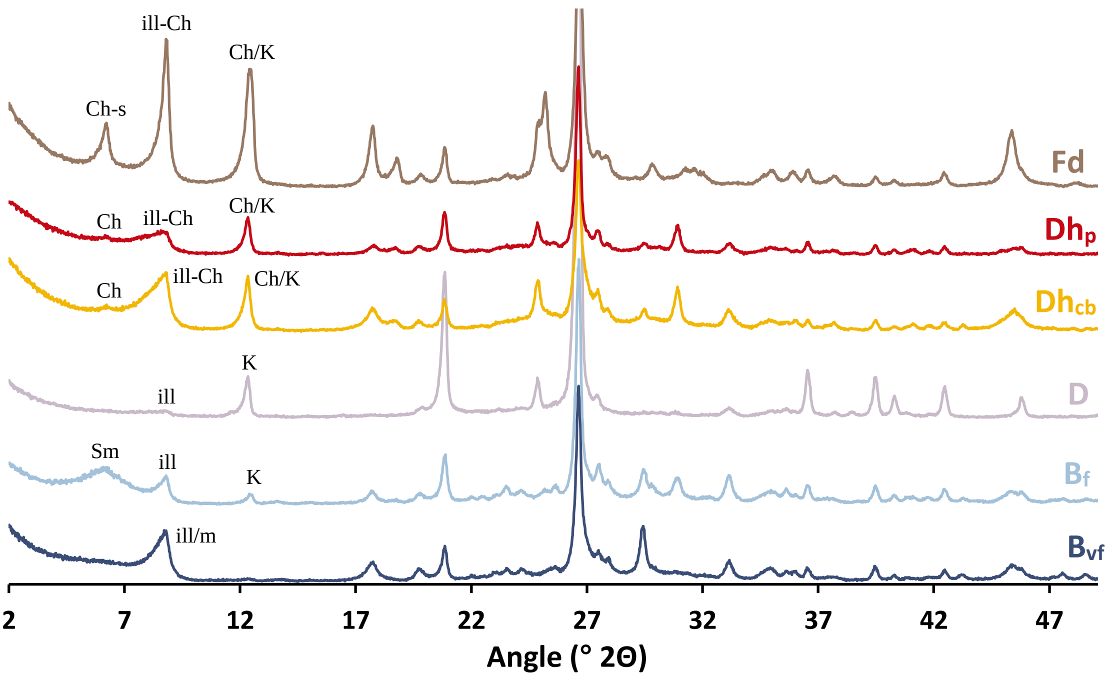

Figure 3.7: Clay mineralogy of studied quarried sandstones. Clay minerals were identified after treatment of the extracted clay fraction using EG, and heat treatment (400, 550). Ill/m = illite and mica; Sm = expansive smectite (montmorillonite, nontronite, or vermiculite); ill = illite; K = kaolinite; Ch = chlorite; ill-Ch = interstratified illite-chlorite; Ch/K = chlorite and kaolinite; Ch-s = chlorite serpentine.

J_w contains quartz, feldspars (albite and orthoclase), calcite, dolomite, micas (muscovite and phlogopite), chlorite, illite-chlorite, and kaolinite. DC_w contains quartz, feldspars (mostly albite and some orthoclase), calcite, kaolinite, and chlorite-serpentine (Figure 3.8; Figure 3.9).

$A(L)_w$ contains quartz, feldspars (orthoclase), dolomite, kaolinite, and illite. $A(C)_w$ contains quartz, feldspars (orthoclase and albite), calcite, kaolinite, illite, and a trioctahedral smectite (either montmorillonite, nontronite, or vermiculite) (Figure 3.8; Figure 3.9).

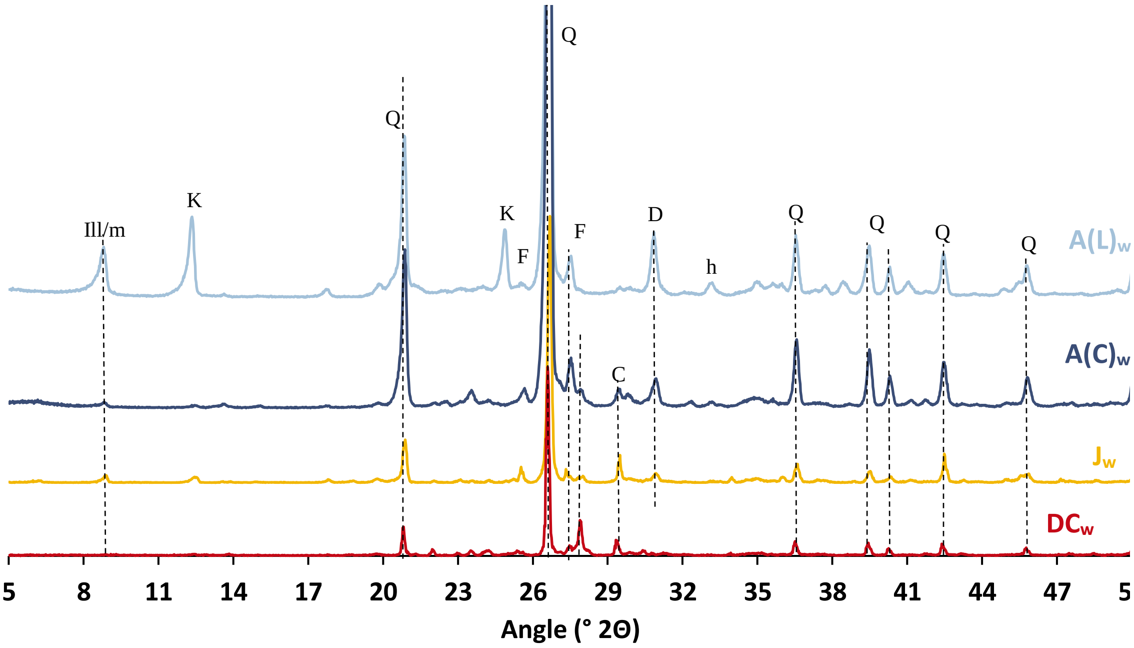

Figure 3.8: Bulk mineralogy of weathered building sandstones. Q = quartz; F = feldspars; K = kaolinite; Ill/m = illite and mica; D = dolomite; C = calcite; and, h = haematite.

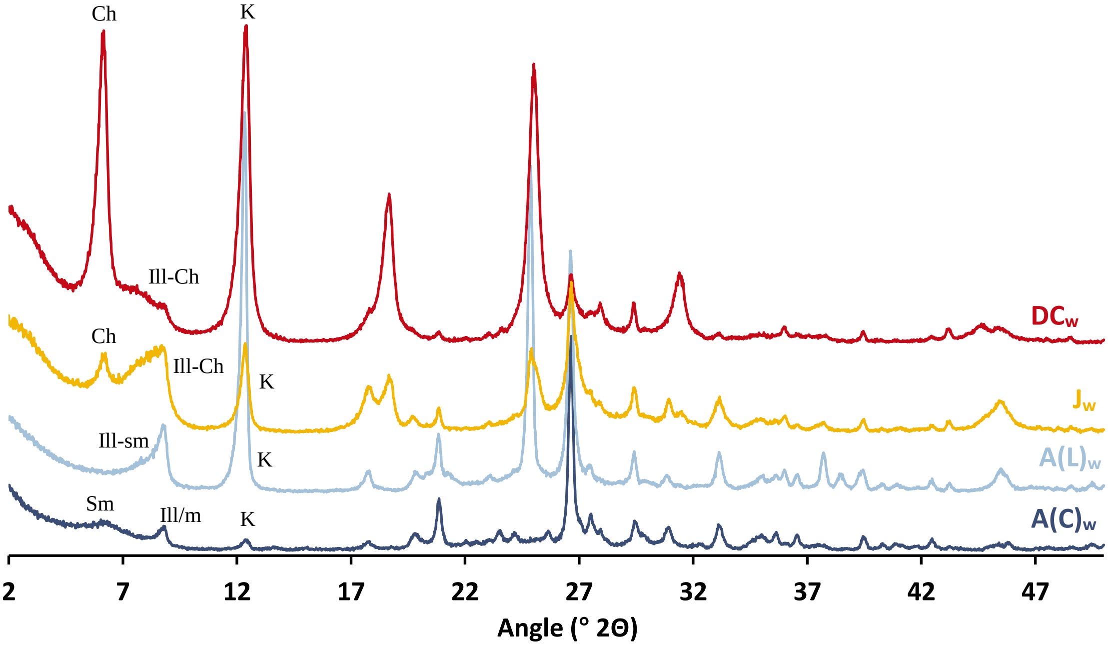

Figure 3.9: Clay mineralogy of weathered building sandstones. Clay minerals were identified after treatment of the extracted clay fraction using EG, and heat treatment (400, 550). Ill/m = illite and mica; Sm = expansive smectite (montmorillonite, nontronite, or vermiculite); ill-sm = interstratified illite-smectite (non-expansive); K = kaolinite; Ch = chlorite; and ill-Ch = interstratified illite-chlorite.

3.4.2 Petrography

Table 3.3 summarises the petrography of studied quarried and weathered sandstones. The texture and fabric of the sandstones was analysed using BSE and SE imaging. The average grain size of D is 0.23 mm. Grain shape is mainly sub-rounded to rounded, and grain boundaries show concavo-convex and long contacts (Figure 3.10A). There is little matrix material in D which consists of sporadic patches of kaolinite clay filling pores (Figure 3.10C-D). Other than these patches of kaolinite, the pores are devoid of any matrix and cements (Figure 11A). Overall D, is a mineralogically mature sandstone and is classified as a quartz arenite (Figure 3.20).

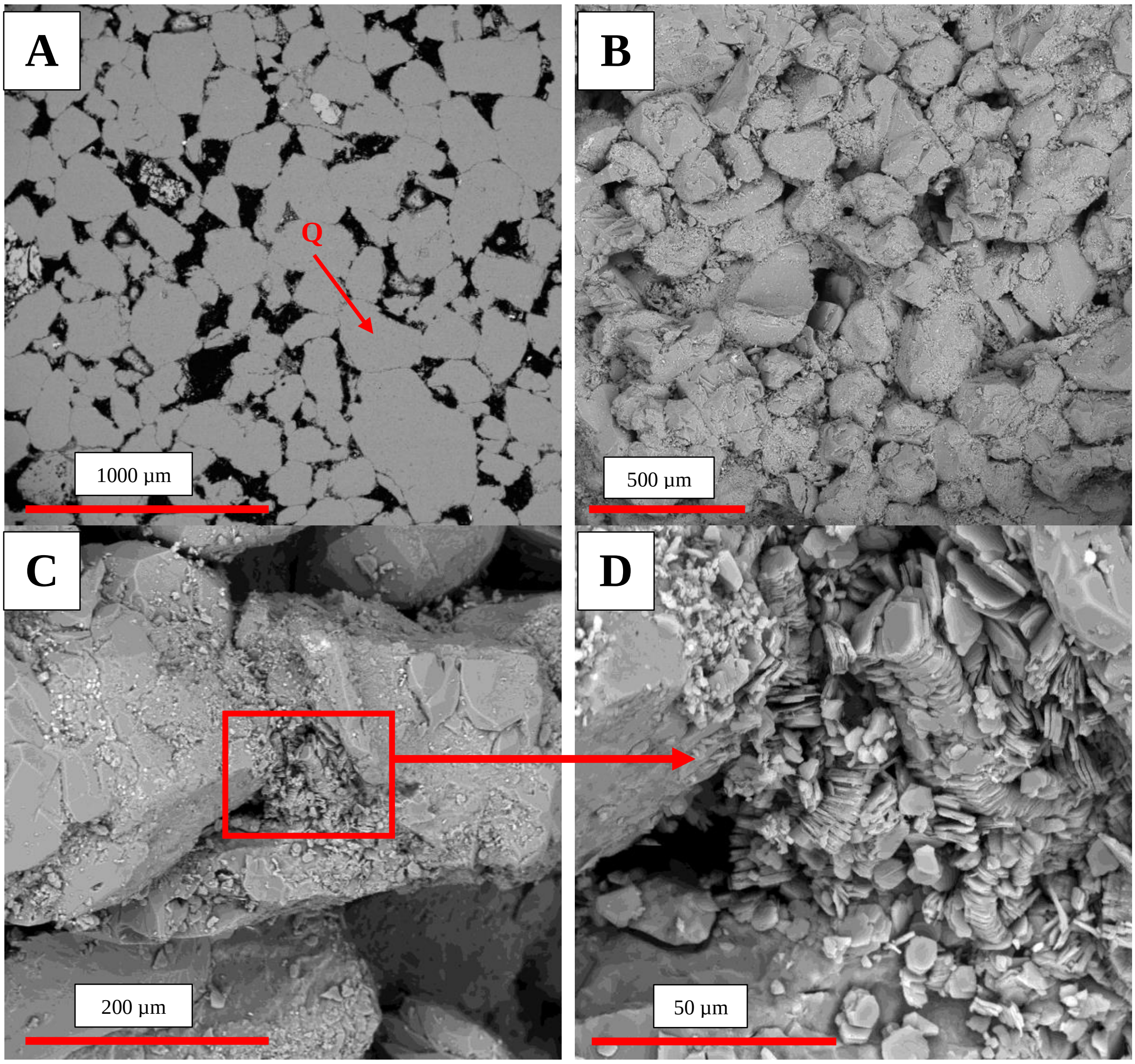

Figure 3.10: Backscattered Electron (BSE) images of polished thin section (A), and sandstone chips (B-D) of Doddington, D. A) Image showing mineralogically maturity of D where most grains are quartz (Q); B) BSE image of chip showing size and shape of quartz and feldspar grains, and thin film of clay minerals coating quartz grains; C-D) Images highlighting grain coating and pore filling clays which consist mainly of diagenetic kaolinite.

The average grain size of Fd is 0.2 mm where grain shape is angular to sub-rounded and grain boundaries show point and long contacts. Fd has a clay-rich matrix which is primarily composed of chlorite and illite as detected by XRD (Figure 3.11). Furthermore, clay minerals can also be found in pore throats and as cementing material, reducing the overall porosity and permeability of the sandstone. Fd also contains igneous-derived lithic fragments and micaceous minerals which are heavily altered. Overall, Fd is mineralogically and texturally immature, and is classified as a litharenite (Figure 3.20).

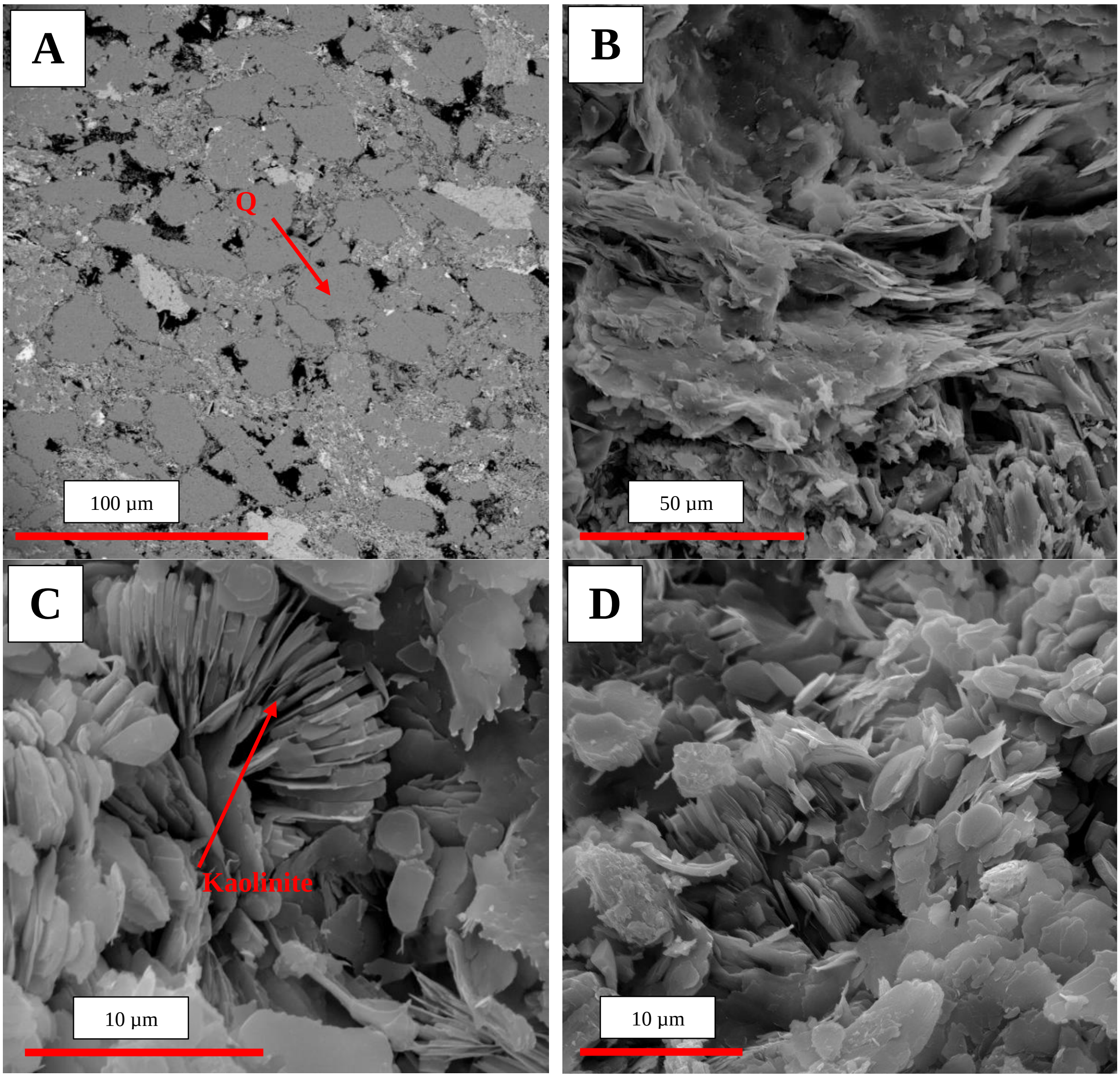

Figure 3.11: BSE and Secondary Electron (SE) images of polished thin section (A), and sandstone chips (B-D), of Forest of Dean, Fd: A) BSE image showing clay-rich matrix; B) Image of chip showing alignment of clay minerals; C-D) Images highlighting the clay minerals (mostly kaolinite and chlorite) found coating grains and filling pores.

The average grain size of Dh_p is 0.09 mm where grain shape is sub-rounded to sub-angular and grain boundaries show concavo-convex contacts (Figure 3.12A). Dh_p has a clay-rich matrix consisting mainly of fibrous illite and kaolinite (Figure 3.12C-D). There is also evidence of grain dissolution and crystallisation of diagenetic clay minerals (Figure 3.12B). Dh_p exhibits planar bedding on a scale of 2-3 mm. Overall, Dh_p is mineralogically sub-mature and texturally immature, and classified as a subarkose (Figure 3.20).

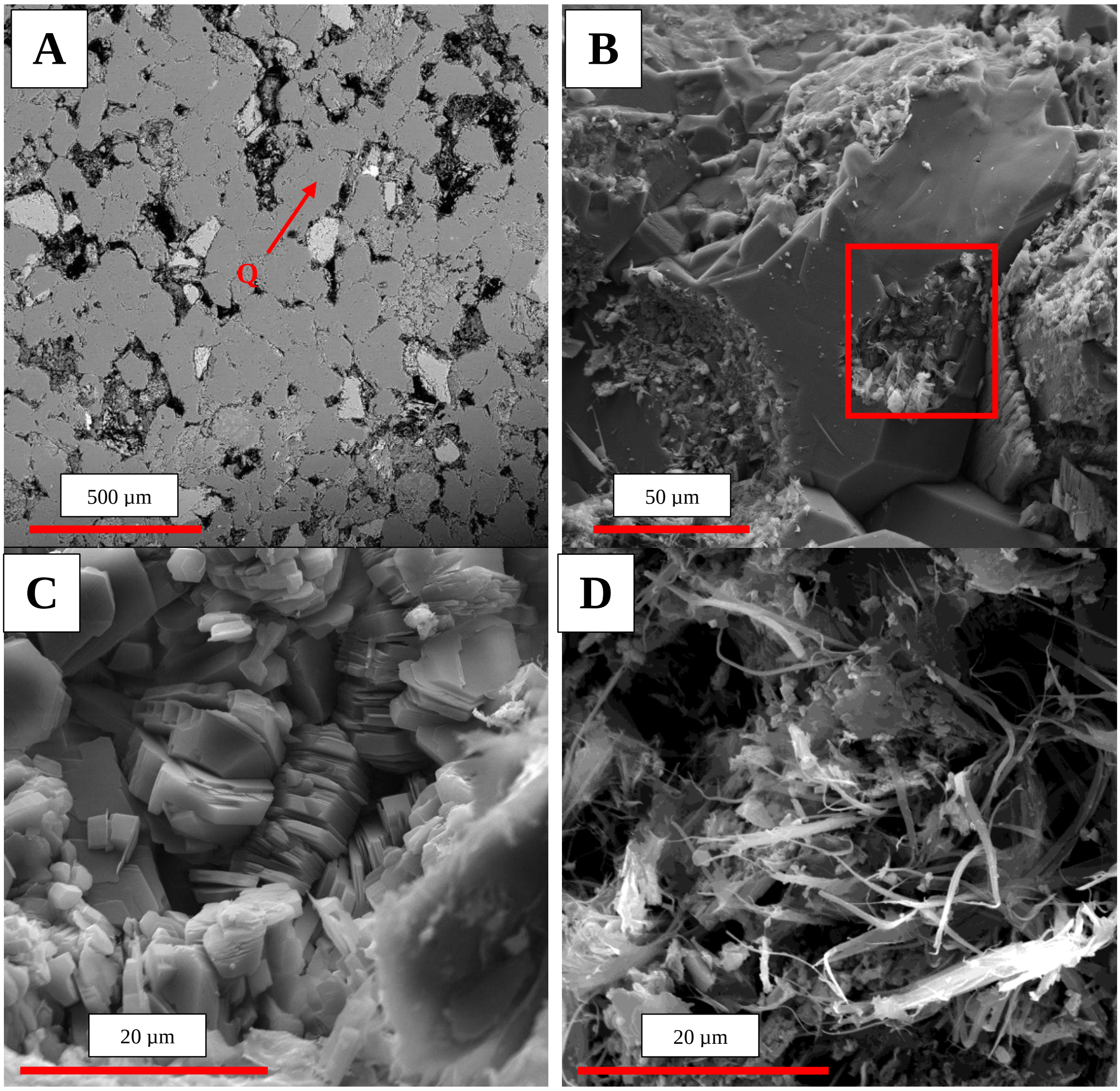

Figure 3.12: BSE and SE images of polished thin section (A) and sandstone chips (B-D) of Denholmhill, Dh_p: A) BSE image showing mineralogy and 2D porosity; B-C) Image highlighting dissolution of feldspar grain and crystallisation of diagenetic kaolinite; D) Image showing fibrous illite crystals found filling pores, and pore throats.

The average grain size of Dh_{cb} is 0.07 mm where grain size is sub-rounded and grain boundaries how concavo-convex and sutured contacts. Micas (mainly muscovite, biotite, and phlogopite) are abundant in Dh_{cb} and orientated parallel to cross beds (Figure 3.13). Weathered micas appear to be a common site for crystallisation of clay minerals in between micaceous layers. The matrix of Dh_{cb} is a combination of clay minerals and crystalline calcite. Overall, Dh_{cb} is mineralogically immature and texturally sub-mature, and classified as a micaceous subarkose (Figure 3.20).

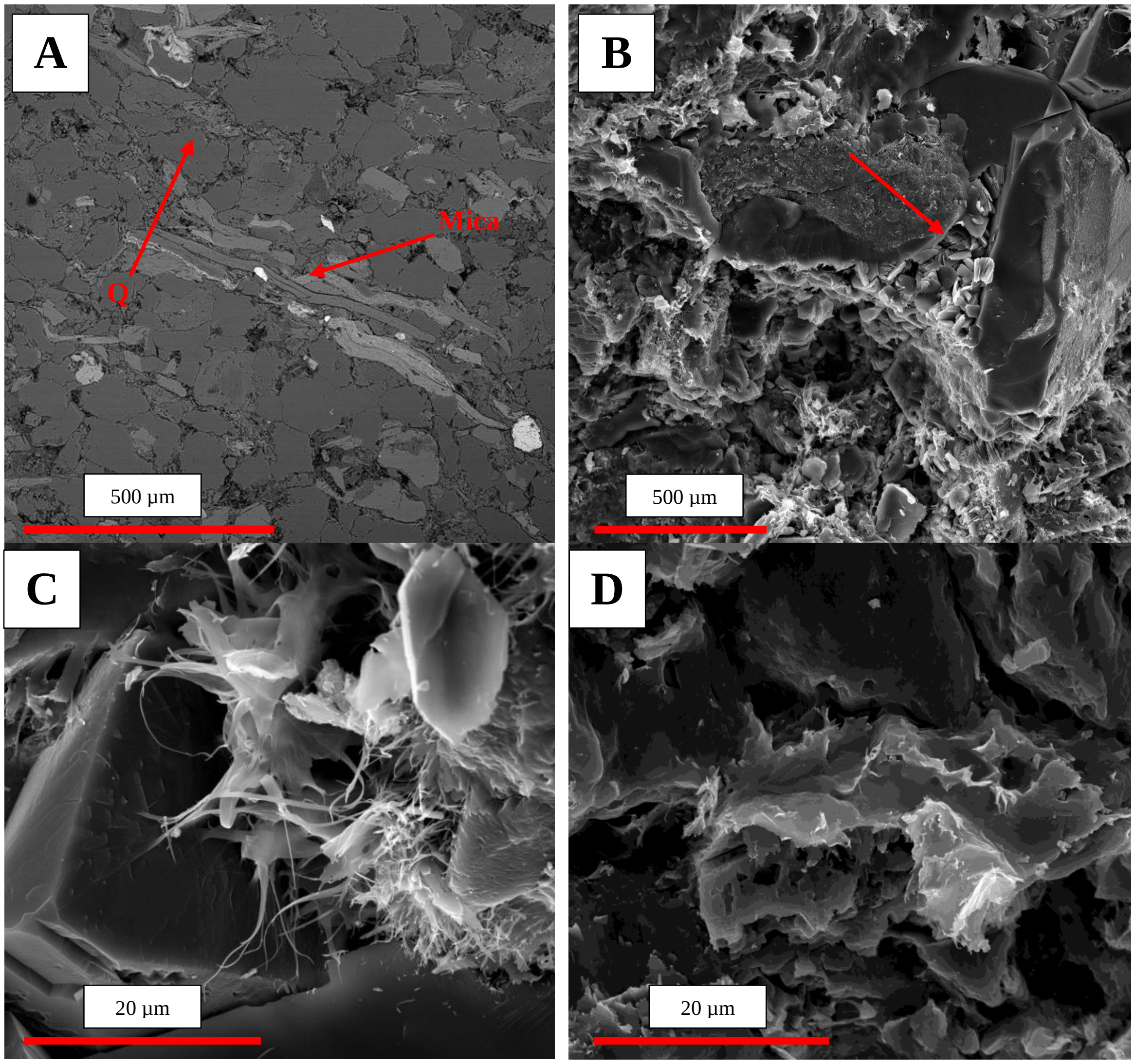

Figure 3.13: BSE and SE images of polished thin section (A) and sandstone chips (B-D) of Denholmhill, Dh_{cb}: A) BSE image showing mineralogy and 2D porosity of sandstone and alignment of micas along cross beds; B) Image showing clays in between grains filling pores; C) Image showing fibrous clay minerals attached to quartz grain; D) Image showing alignment of leafy clay minerals.

The average grain size of B_f is 0.14mm where grain shape is sub-angular to angular and grain boundaries show long and concavo-convex contacts. B_f has very little matrix material and the pores are mostly devoid of any minerals (Figure 3.14A). Clay minerals form thin films of cement coating detrital grains of quartz and feldspar (Figure 3.14B, C). Dissolution textures are also common in B_f where feldspars readily weather and crystallisation of clay minerals takes place (Figure 3.14D). B_f exhibits planar bedding on a scale of 1-2 mm.

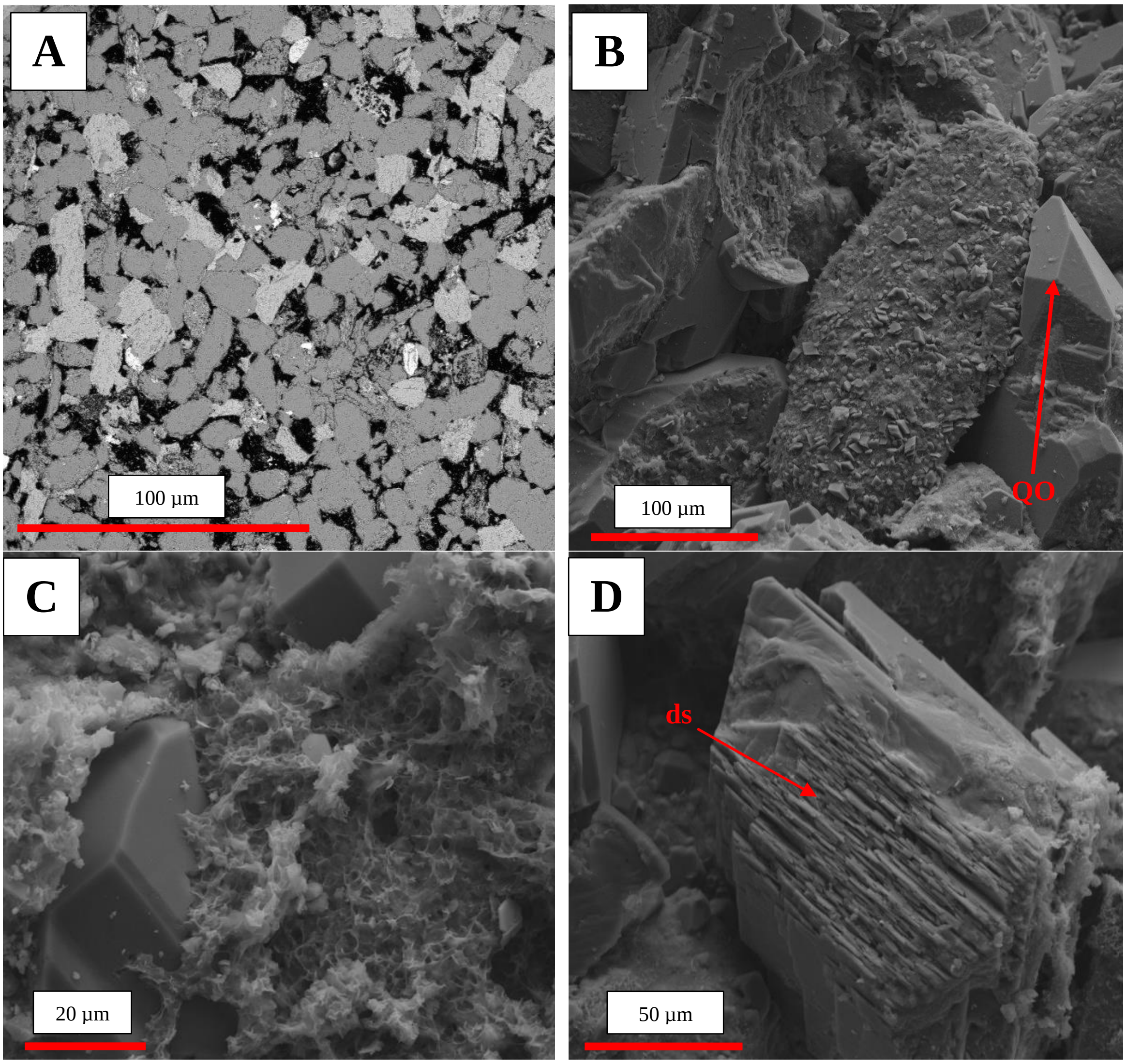

Figure 3.14: BSE and SE images of polished thin section (A) and sandstone chips (B-D) of St. Bees, B_f: A) BSE image showing mineralogy and 2D porosity of sandstone; B) Image showing detrital grains coated with clay minerals, and euhedral quartz overgrowth (QO); C) Image highlighting smectite-like clay minerals infilling pore space between quartz grains and coating grains; D) Image of dissolution of feldspar (ds) and nearby crystallisation of clay minerals.

The average grain size of B_{vf} is 0.08 mm where grain shape is sub-angular to sub-rounded and grain boundaries show concavo-convex contacts (Figure 3.15A). B_{vf} matrix and cementing material consists of mostly illite which coats grains and pore throats (Figure 3.15C-D). and B_{vf} exhibits bedding on a scale of 1-2 mm, along which are concentrated bands of Ti oxides.

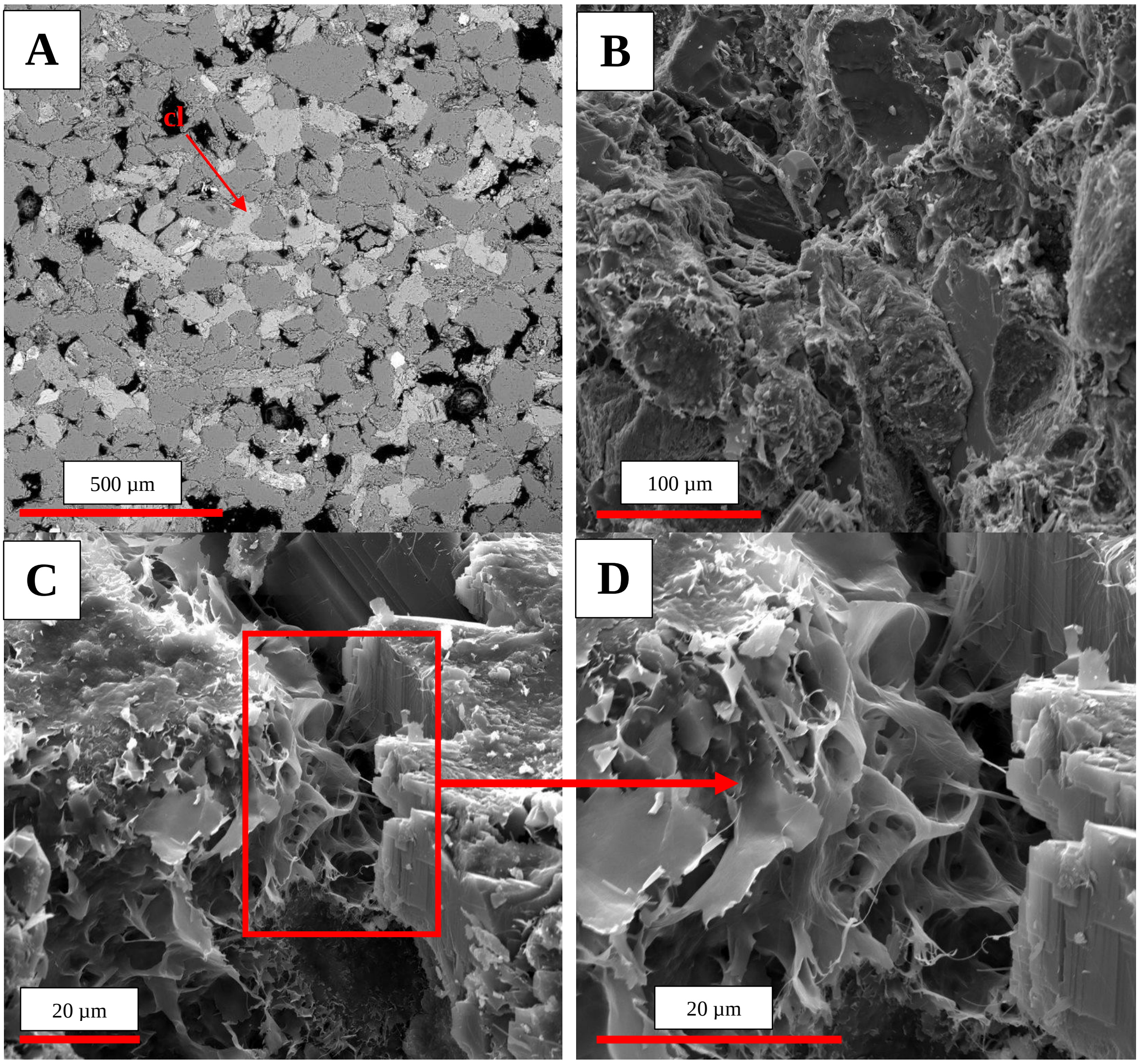

Figure 3.15: BSE and SE images of polished thin section (A) and sandstone chips (B-D) of St. Bees, B_{vf}: A) BSE image showing mineralogy and 2D porosity of sandstone, highlighting calcite-rich cements (cl); B) Image showing quartz and feldspar grains coated with clay and calcite; C-D) Images highlighting diagenetic fibrous clay minerals reducing pore throat space between feldspar grains.

The average grain size of J_w is 0.07 mm. Grain shape is mainly sub-angular to sub-rounded and grain boundaries show point and long contacts. The matrix is a mixture of clay minerals and dolomite, and clay mineral cements are also common (Figure 3.16C-D). Micas (mostly muscovite and phlogopite) are abundant, and often aligned and concentrated on cross beds (Figure 3.16A). Micas and clay minerals are heavily weathered near open fractures (Figure 3.16B). J_w is a poorly sorted immature sandstone and classified as a sublitharenite (Figure 3.20).

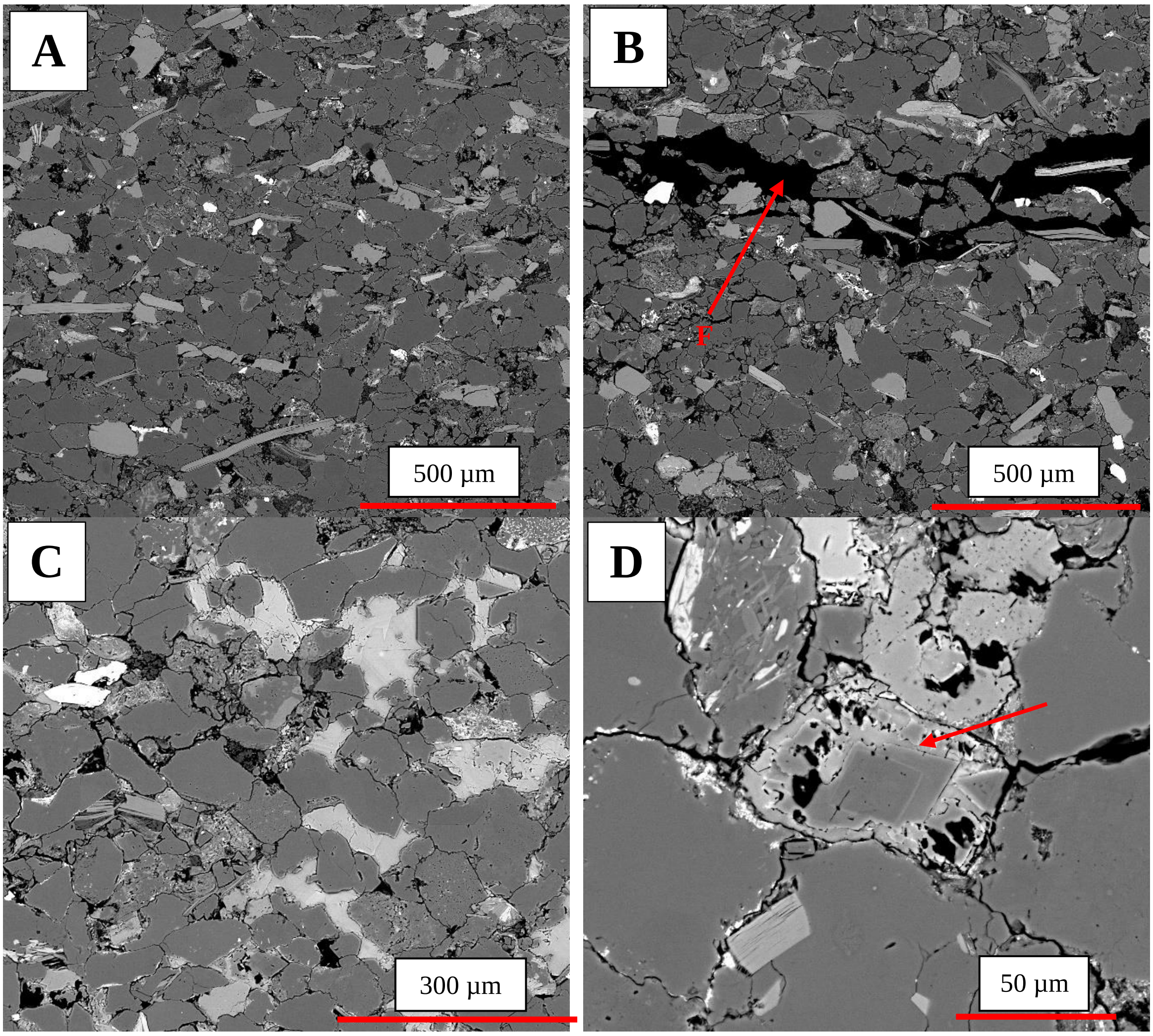

Figure 3.16: BSE images of polished thin sections from Jedburgh Abbey weathered sandstone, J_w: A) Mineralogy and 2D porosity and texture of sandstone; B) open fractures (F) which are a common type of decay in Jedburgh Abbey stone; C) dolomite cements; D) zoned dolomite crystal in matrix.

The average grain size of DC_w is 0.11 mm. Grain shape is sub-angular to sub-rounded and grain boundaries show point and long contacts (Figure 3.17A-B). The matrix is clay-rich consisting mostly of chlorite and kaolinite as shown by XRD. Clay mineral cements often coat individual grains (Figure 3.17C-D). DC_w is a clay-rich immature sandstone and is classified as a feldspathic litharenite (Figure 3.20).

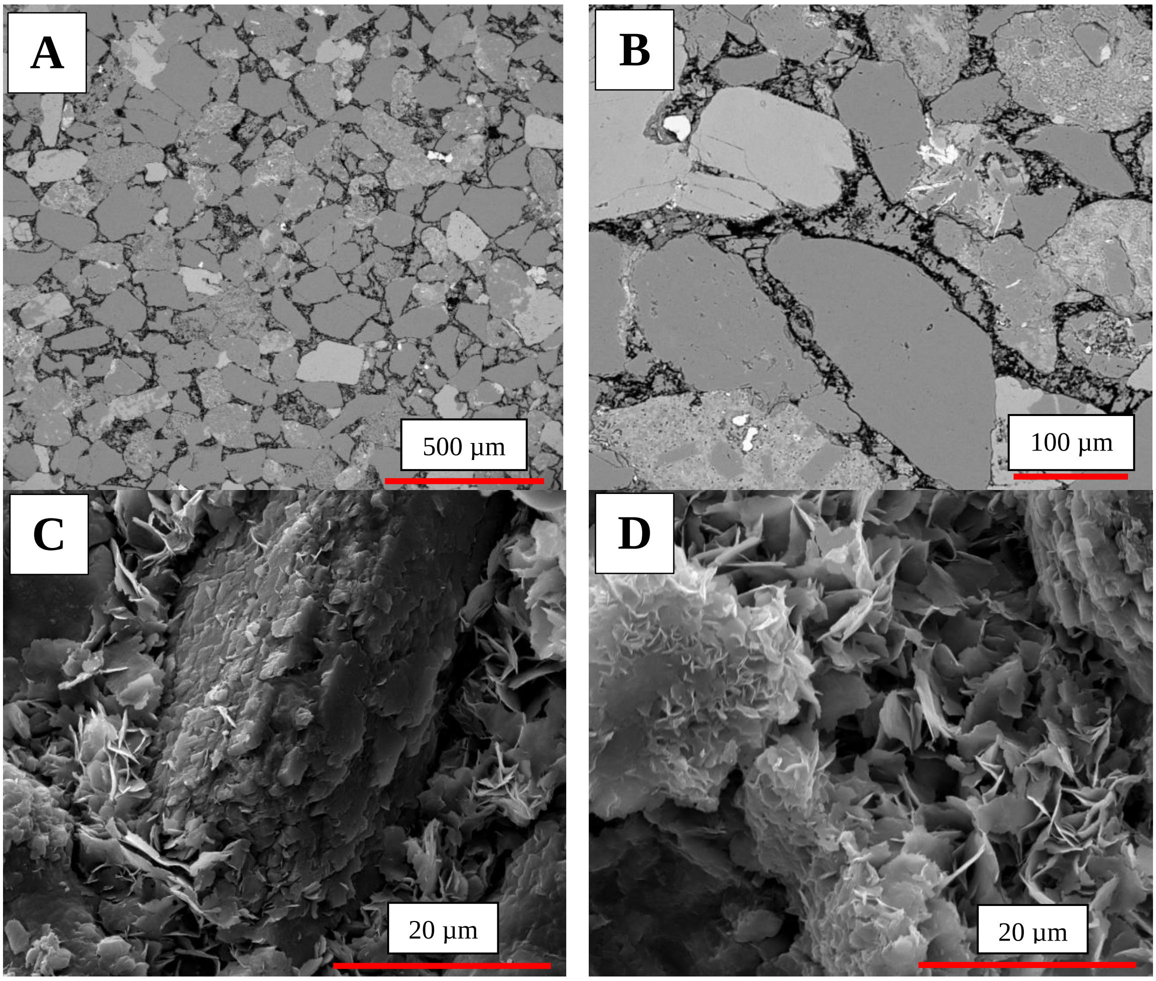

Figure 3.17: BSE and SE images of polished thin section (A-B) and sandstone chips (C-D) of Dunkeld Cathedral weathered sandstone, DC_w: A) BSE image showing mineralogy and 2D porosity; B) Image showing clay minerals infilling pores and coating grains; C) Image of chip highlighting clay minerals coating detrital feldspar grain; D) Image showing coating clay minerals which typically have 'leafy' smectite-like texture.

The average grain size of A(C)$_w$ is 0.11 mm. Grain shape is subrounded where grain boundaries show long and concavo-convex contacts (Figure 3.18A). The matrix is sparse however calcite is present both in the matrix and as a cementing material. There is a higher proportion of lithic grains relative to A(L)$_w$ (Figure 3.18B). Lithic grains have weathered extensively, leading to the formation of clay minerals with smectitic morphology (Figure 3.18C-D). As a result the distribution of clay minerals is restricted to isolated weathered clasts. A(C)$_w$ is poorly sorted and classified as a lithic arkose (Figure 3.20). The average grain size of A(L)$_w$ is 0.15 mm. Grain shape is angular to sub-rounded and grain boundaries show point and long contacts (Figure 3.19A-B). The matrix and cements consist primarily of clay minerals; mostly kaolinite (Figure 3.19C-D). The extent of weathering is greater in A(L)$_w$ relative to A(C)$_w$ as shown by the extent of mineral alteration. Feldspars and lithic grains weathering to mostly kaolinite. A(L)$_w$ is poorly sorted and classified as a lithic arkose (Figure 3.20).

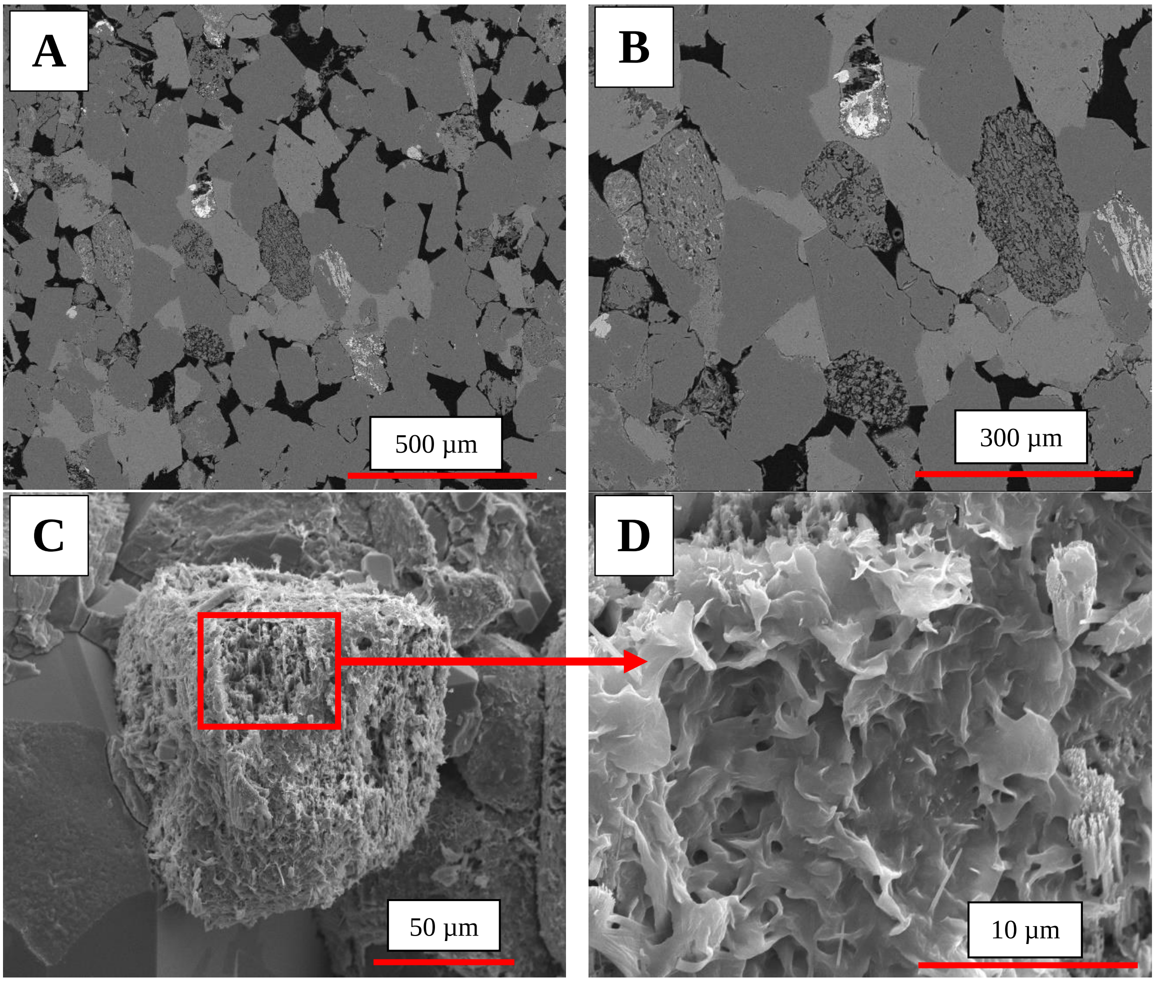

Figure 3.18: BSE and SE images polished thin sections (A-B) and sandstone chips (C-D) of Arbroath Abbey weathered sandstone, A(C)$_w$: A) BSE image showing mineralogy and 2D porosity of sandstone; B) Image highlighting presence of weathered lithic grains; C) Image of weathered lithic grains providing a source of clay mineral formation; D) Image showing texture of common, lithic coating clay mineral in A(C)$_w$ sandstone. Such texture commonly associated with smectite clay minerals.

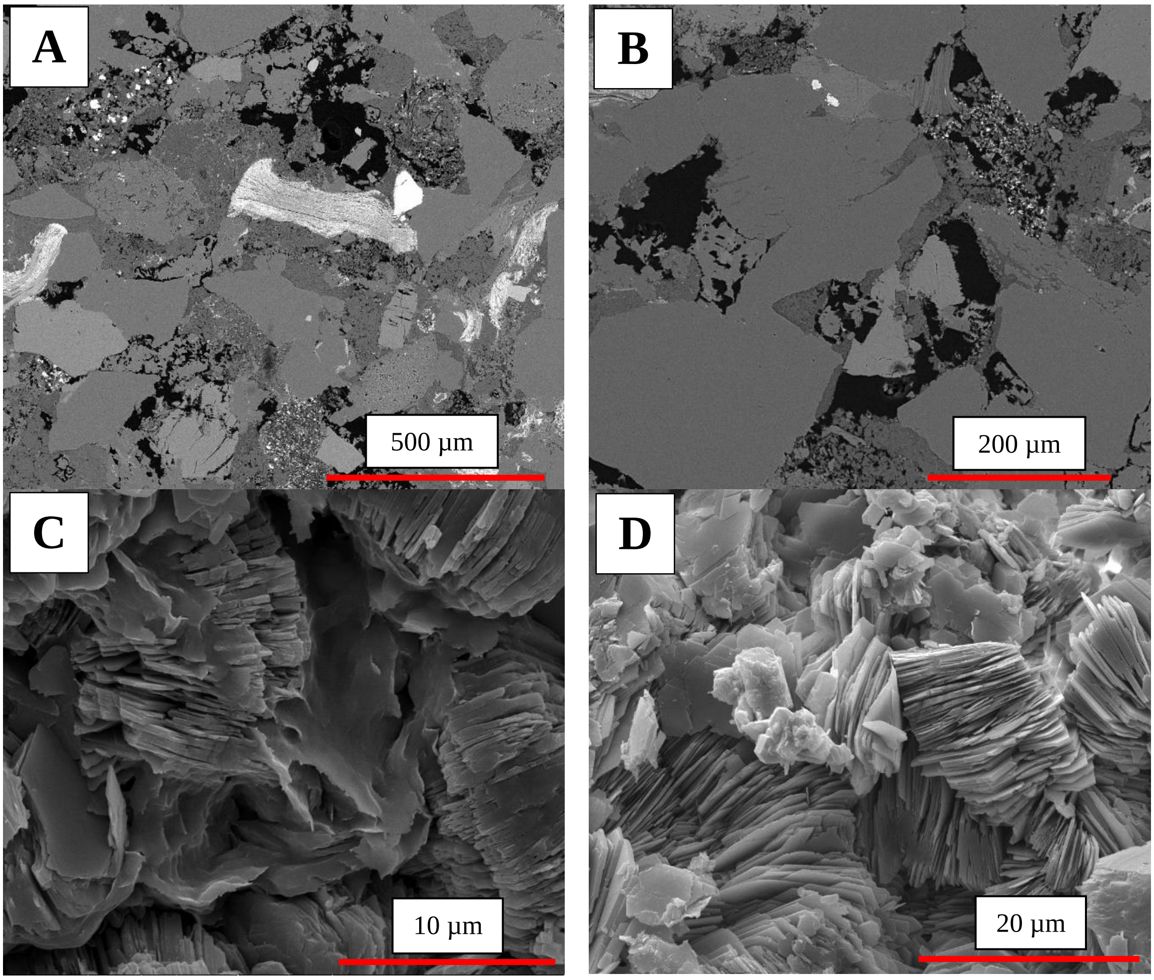

Figure 3.19: BSE and SE images of polished thin section (A-B) and sandstone chips (C-D) of Arbroath Abbey weathered sandstone, A(L)$_W$: A) BSE image showing mineralogy and 2D porosity; B) Image highlighting distribution of clay minerals which are usually coating grains and pores and reducing overall pore space; C) Image of chip showing transformation of clay minerals (smectite texture to typical kaolinite 'stacks'); D) Image of chip showing stacks of hexagonal kaolinite crystals.

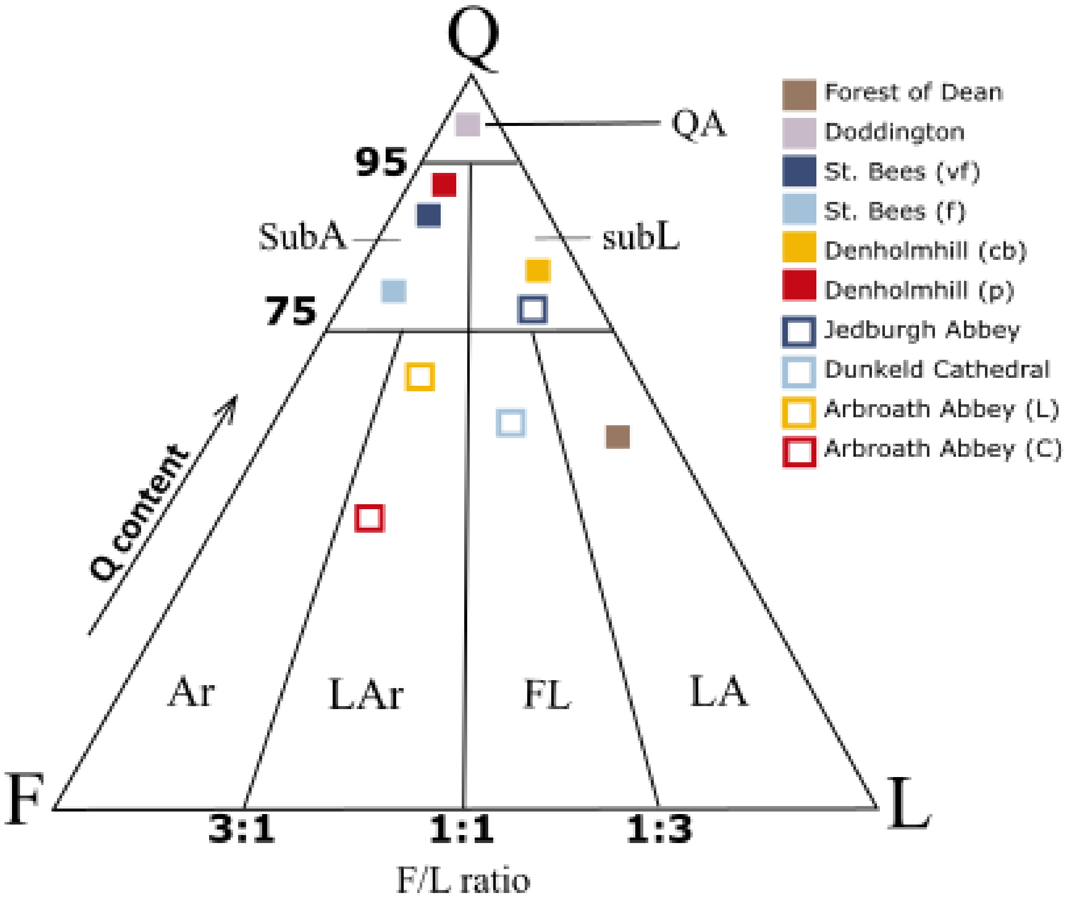

Figure 3.20: Sandstone types according to the Folk classification scheme (1974). Ar = Arkose; Lar = lithic arkose; FL = feldspathic litharenite; LA = litharenite; subL = sublitharenite; subA = subarkose; QA = quartz arenite.

Table 3.3: Summary of the mineralogy, petrography and classification of all studied sandstones.

Sample	Average grain size (mm)	QFL (%)			Sandstone classification	Clay mineralogy
Building stones						
D	0.26 (medium)	96	2	2	Quartz arenite	Kaolinite; illite
Fd	0.20 (fine)	68	7	25	Litharenite	Chlorite; kaolinite; illite; chlorite-serpentine; interstratified illite-chlorite
Dh$_{p}$	0.09 (very fine)	89	6	5	Subarkose	Kaolinite; illite
Dh$_{cb}$	0.07 (very fine)	77	10	13	Sublitharenite	Chlorite; interstratified illite-chlorite; kaolinite
B$_{f}$	0.14 (fine)	77	14	9	Subarkose	Trioctahedral smectite; illite; kaolinite
B$_{vf}$	0.08 (very fine)	81	12	7	Subarkose	illite
Weathered building stones						
J$_{w}$	0.07 (very fine)	75	12	13	Sublitharenite	Chlorite; illite-chlorite; kaolinite
DC$_{w}$	0.11 (v. fine-fine)	69	11	20	Feldspathic litharenite	Chlorite; chlorite-serpentine; kaolinite
A(C)$_{w}$	0.11 (v. fine-fine)	59	30	11	Lithic arkose	Trioctehedral smectite; kaolinite
A(L)$_{w}$	0.15 (fine)	73	18	8	Lithic arkose	Kaolinite; illite

3.4.3 Pore structure

Table 3.4 summarises the pore structure of the sandstones determined using the water vacuum saturation test, MIP and nitrogen absorption. The relationship between open porosity, calculated using the water vacuum saturation method, and density of samples is shown in Figure 3.21. Two distinct groups of sandstone can be identified: higher porosity sandstones (~ 20%) B_{f} and D, and lower porosity sandstones (~10-12 %) B_{vf}, Dh_{p}, Dh_{cb} and Fd. Sample D and B_{f} show the highest porosity values of 20.82% and 20.43%, respectively, while sample B_{vf} and Dh_{cb} show the comparatively lowest porosity measured at 10.85% and 10.61%, respectively.

Table 3.4: Pore structure properties of studied sandstones. ρ_{bulk} determined using ratio of dry weight (g) and sample volume. ϕP calculated using the water vacuum saturation test; ϕ(Hg), V_p(Hg) and r_M calculated using MIP; and V_p(N) and SSA calculated using the nitrogen absorption technique. *no data due to sampling restrictions. Average values are followed by standard deviation values and sample size.

	Water Vacuum Saturation Test		Mercury Intrusion Porosimetry (MIP)			Nitrogen absorption	
Sample	**Average Bulk density [ρ_{bulk}, g m^{-3}]**	**Average Open porosity [ϕP, %]**	**Connected porosity [ϕ(Hg), %]**	**Total pore volume [V_p(Hg)], cc/g]**	**Mean pore radius [r_M,]**	**Pore volume [V_p(N), cc/g]**	**Specific Surface Area [SSA, m^{2}g^{-1}]**
D	2.17 SD = 0.06 (6)	20.44 SD = 0.16 (6)	20.53	9.71 x10^{-1}	8.37 x10^{-1}	9.59 x10^{-4}	0.506
Fd	2.47 SD = 0.02 (12)	12.26 SD = 0.3 (12)	9.98	4.2 x10^{-2}	1.7 x10^{-1}	4.71 x10^{-3}	2.531
Dh$_p$	2.43 SD = 0.05 (10)	11.71 SD = 0.34 (10)	*	*	*	*	*
Dh$_{cb}$	2.47 SD = 0.03 (5)	10.29 SD = 0.25 (5)	6.62	2.7 x10^{-2}	4.4 x10^{-2}	6.39 x10^{-3}	5.213
B$_{vf}$	2.51 SD = 0.03 (6)	10.34 SD = 0.20 (6)	9.21	3.9 x10^{-2}	1 x10^{-2}	7.09 x10^{-3}	4.412
B$_f$	2.15 SD = 0.02 (6)	20.18 SD = 0.42 (6)	17.78	8.3 x10^{-2}	8.70 x10^{-1}	4.38 x10^{-3}	2.825

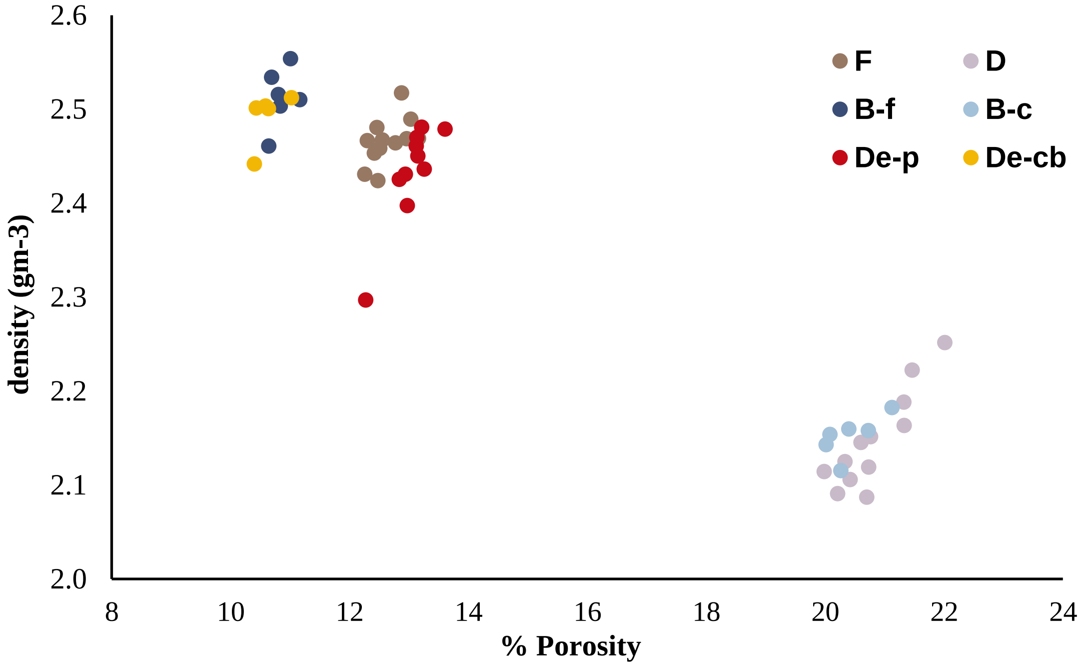

Figure 3.21: Density and open porosity of studied fresh sandstones. There are two notable groups: a low porosity (10-12%) group including Fd, Dh$_p$, Dh$_{cb}$, and B$_{vf}$, and; a relatively higher porosity sandstone group including B$_f$ and D.

Pore size distribution determined by MIP is illustrated in Figure 3.22. Sample D is the most porous sandstone with a mean pore radius of 8.4 x10^{-1} µm and connected porosity [ϕ(Hg)] of 20.53%. Sample D has the highest total pore volume [Vp(Hg)] of 9.71 x10^{-1} cc/g with the majority of total pore volume made up of pores ranging between 10 – 30 µm (radius) (Figure 3.22). Having a higher porosity makes D more susceptible to moisture ingress and potentially more vulnerable to processes such as salt weathering. Dh$_{cb}$ has the lowest total pore volume [Vp(Hg)] of 2.7 x10^{-2} cc/g and lowest connected porosity [ϕ(Hg)] of 6.62%, with the majority of total pore volume made up of pores ranging between 0.02 – 0.04 µm (radius) (Figure 3.22). As seen from nitrogen absorption results, sample B$_{vf}$ has the highest micropore total volume of 7 x10^{-3} cc/g and a relatively high SSA of 4.41 m^{2}g^{-1} (Table 3.4).

Along with B$_{vf}$, Dh$_{cb}$ and Fd, also have relatively higher micropore volume and SSA. Dh$_{cb}$ and Fd have a clay-rich matrix (Figure 3.13A; Figure 3.11A), where clay minerals reduce the overall pore space and connectivity, highlighting the influence clay mineralogy can have on the structure of the pore network. B$_{vf}$ and Dh$_{cb}$ also both have a very fine grain size, 0.08 and 0.07, respectively, which will also contribute to the increased prevalence of micropores. In contrast, D, which h as the lowest micropore volume and SSA, has the largest grain size of any studied sample and pore space which is devoid of any matrix/cementing material (3.10A).

A porosity value was also calculated using the saturated weight after capillary absorption tests (Figure 3.23). Figure 3.23 compares the porosity of each sample using the different techniques. Porosity values calculated using the saturated weight of samples after capillary absorption experiments are consistently lower than porosity values calculated using the water vacuum saturation test. The water vacuum saturation test involves the initial extraction of air and other particulate matter, creating more space for moisture ingress, which may explain the higher porosity value.

The difference in porosity values measured using MIP and water vacuum saturation test is small (1-2 %). However, this difference is greater in sample Dh$_{cb}$, where porosity calculated using the water vacuum saturation test is almost double that of porosity calculated using MIP. A potential cause of this discrepancy may be a larger average pore size (>200 µm) of Dh$_{cb}$ which is not detectable using MIP. Alternatively, the lower porosity value of Dh$_{cb}$ detected using MIP could reflect the porosity of a clay-rich cross bed rather than overall porosity due to the size (1 cm^3) of samples used in MIP.

In summary, obtaining and comparing porosity values calculated using a range of techniques provides a better understanding of porosity and how it varies through a sandstone. This is particularly important in the analysis of heterogenous sandstones where porosity of the same sandstone may vary widely due to mineralogy and/or textural properties such as bedding. Noticing such differences in porosity values may highlight areas for further investigation into pore size distribution.

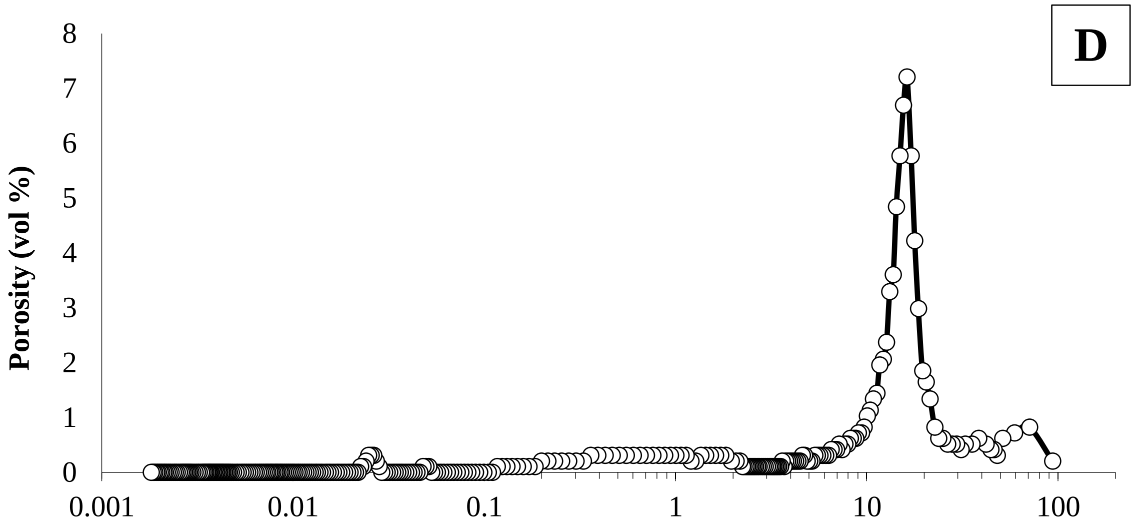

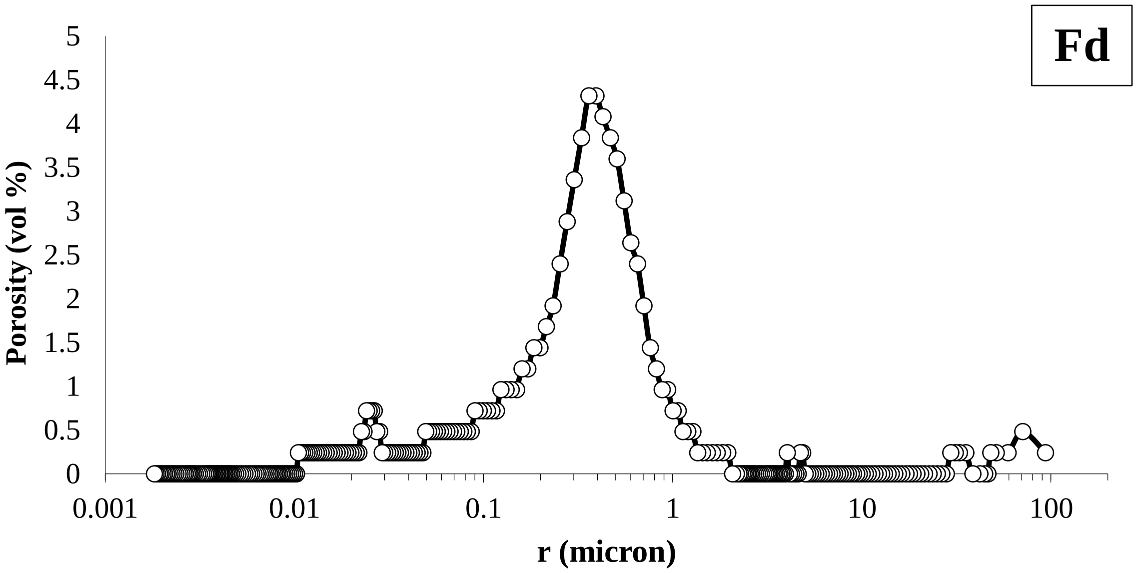

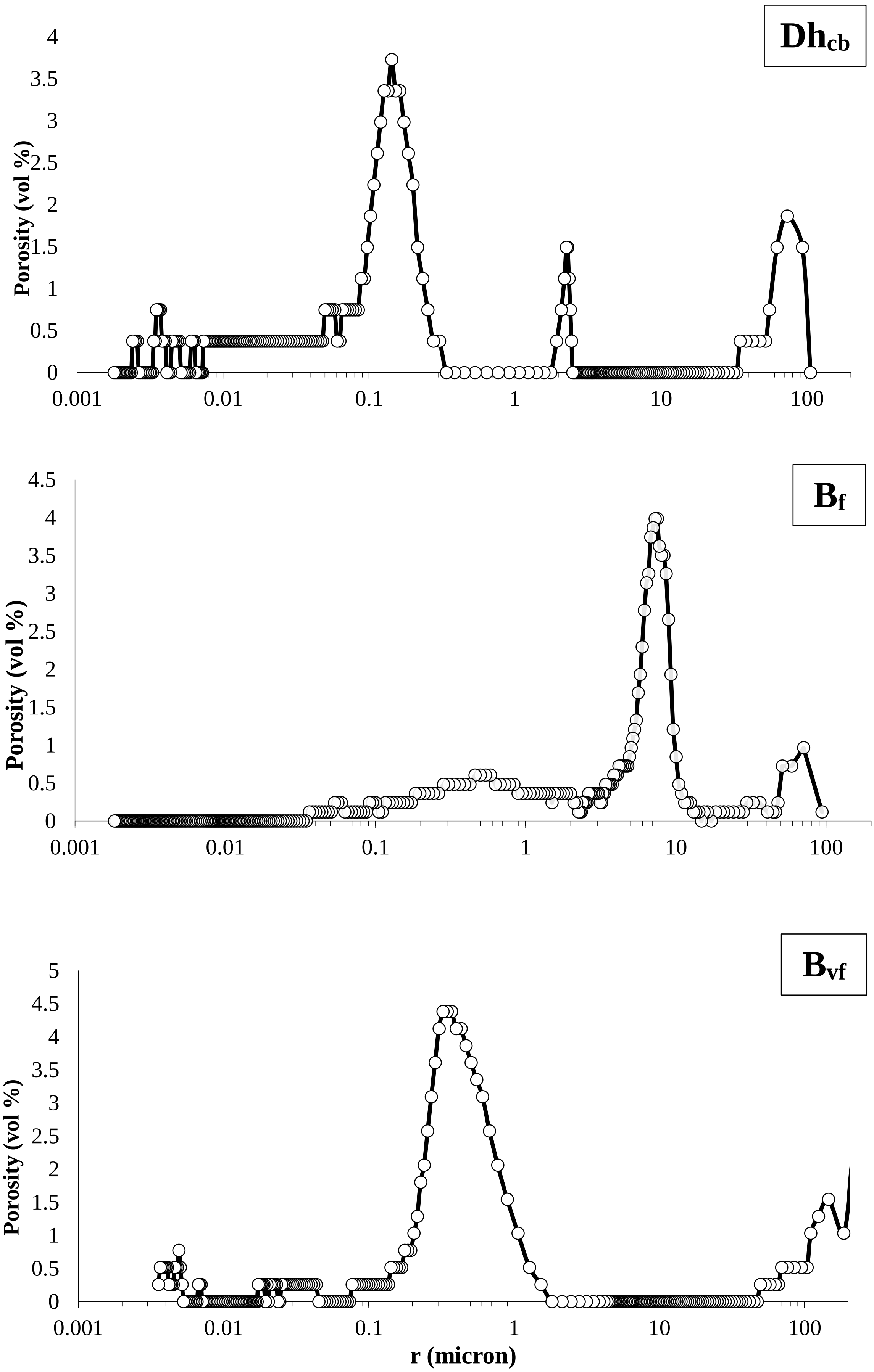

Figure 3.22: MIP results for studied fresh sandstones. Peaks represent the dominant pore groups accounting for the total intruded volume of mercury.

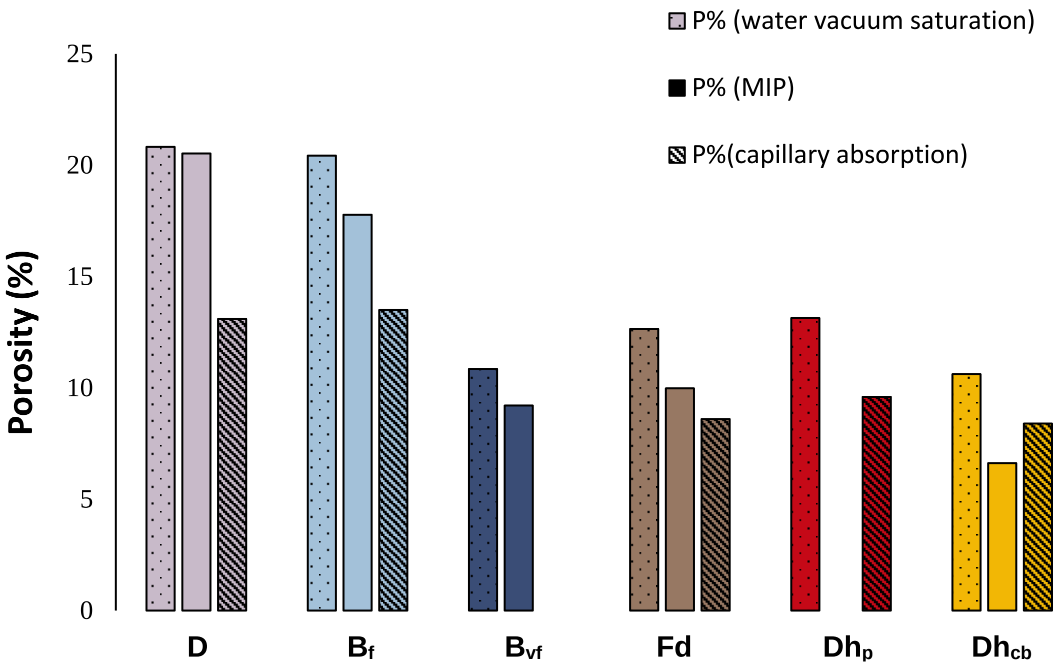

Figure 3.23: Porosity (%) of sandstones calculated using three different techniques: water saturation vacuum test, MIP, and saturation by capillary absorption.

3.4.4 Hydric properties

Table 3.5 summarises results of studied hydric properties, including capillary water absorption. Figure 3.24 compares the capillary absorption rates of the sandstone samples. There is a general trend where samples with higher porosity have higher rates of capillary absorption. As seen from Table 3.5, samples B_f and D have the highest porosity and correspondingly highest capillary absorption coefficients, 87.7-131.2 g/m^2 and 292.5 g/m^2, respectively, while B_{vf} has a relatively low capillary absorption coefficient of 5.43-7.44 g/m^2.

Rates of capillary absorption are also heavily dependent on pore size distribution (Ruedrich et al., 2011), and absorption by capillarity is dominant in the pore range of 1 – 1000 µm (Pötzl & Siegesmund., 2018). Referring to the MIP data, D and B_f have dominant pore groups ~ 10-20 µm and ~ 4-10 µm, respectively. The large SD (58.04) associated with D may be reflecting the heterogeneity of D in regards to capillary absorption which may be influenced by variations in the pore size distribution across different samples.

Table 3.5: Hydric and thermal properties of studied sandstones. Bedded samples (Dh$_{p}$, Dh$_{cb}$, B$_{vf}$, and B$_{f}$) were measured in two directions: parallel (-), and perpendicular (+) to bedding. Average values are followed by standard deviation values and sample size.

Sample	Average Capillary absorption coefficient (g/m-2 h$^{0.5}$)		Average Hydric swelling (mm/m)		Thermal expansion coefficient (10^{-6}K^{-1})	
D	292.5 SD = 58.02 (4)		0.27 SD = 0.12 (2)		11.99	
Fd	15.8 SD = 2.72 (5)		0.74 SD = 0.07 (3)		9.92	
Dh$_{p}$	- 19.59 SD = 1.09 (2)	+ 14.63 SD = 2.38 (2)	- 0.20	+ 0.54	*	*
Dh$_{cb}$	- 15.14 SD = 2.02 (5)	+ 14.49 SD = 2.02 (5)	- 0.50	+ 0.74	- 10.04	+ 9.85
B$_{vf}$	- 7.44 SD = 1.45 (4)	+ 5.43 SD = 0.73 (4)	- 0.40	+ 0.64	- 9.39	+ 9.66
B$_{f}$	- 131.16 SD = 1.16 (2)	+ 87.70 SD = 15.09 (2)	- 0.07	+ 0.20	- 10.14	+ 10.31

Hydric expansion results are summarised in Table 3.5. All samples show a degree of hydric swelling. The highest value of 0.74 mm/m was observed in samples Fd and Dh$_{cb}$. For context 1.5 mm/m is considered an important threshold at which swelling strain is likely to contribute to mechanical damage (Jiménez-González., 2008). Sample D had the lowest value of 0.07 mm/m when swelling was measured parallel to bedding. Fd and Dh$_{cb}$ are clay-rich however the clays are non-expansive as shown with XRD, ruling out intracrystalline swelling as a mechanism responsible for the observed hydric expansion. Two other potential causes of swelling in Fd are intercrystalline (osmotic) swelling, or through the high proportion of micropores leading to disjoining pressure within small pores (Ruedrich et al., 2011). Nitrogen absorption results did not suggest that Fd was particularly microporous. However, intercrystalline swelling in sandstones typically produces little expansion, and is therefore unlikely to be the main mechanism for expansion (Madsen & Müller-Vonmoos., 1989; Ruedrich et al., 2011). It is possible that the pore size distribution (PSD) of Fd, and Dh$_{cb}$ varies, for example near bedding planes, and that due to small sample size nitrogen absorption did not provide a true representation of PSD throughout the sample. In conclusion, it is likely that expansion due to disjoining pressure, as well as intercrystalline swelling, contribute to the observed swelling in samples Fd and Dh$_{cb}$.

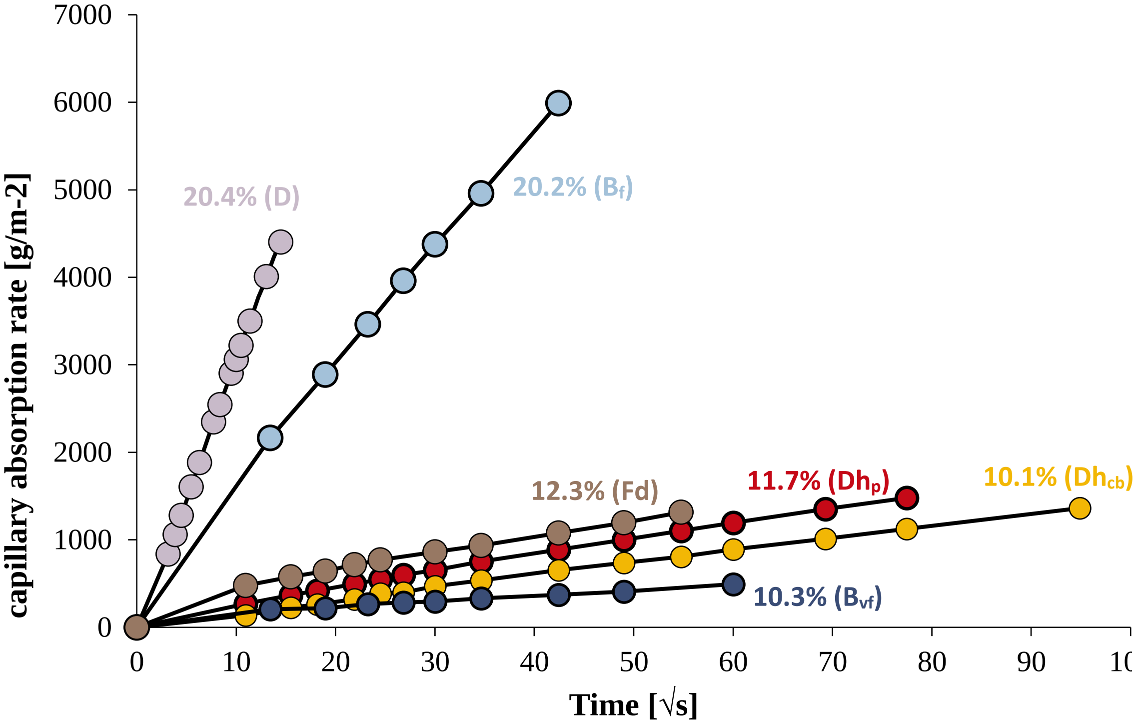

Figure 3.24: Comparison of capillary absorption rate for fresh sandstones. The percentage values reflect open porosity for each sandstone.

3.4.5 Thermal properties

As discussed in the introduction, there is a link between thermal expansion, mineralogy and stone texture. As seen from Table 3.5, D has the highest thermal expansion coefficient of 11.99 $10^{-6}K^{-1}$. This may be attributed to both the higher quartz content of D (quartz arenite) and also its relatively coarser grain size. The thermal expansion of all samples as seen from Table 3.5 is isotropic, meaning there is very little variation in thermal expansion when measured in two directions. The slightly greater thermal expansion observed perpendicular to bedding is influenced by the texture of stone such as the alignment of minerals. For example, common minerals in sandstone such as quartz, micas, and clays show a relatively higher thermal expansion coefficient perpendicular to their c-axis (Steiger & Charola., 2011). Finally, all samples show a degree residual strain (permanent deformation) after cooling (Figure 3.25). This can often be attributed to a dehydration reaction (water present in the sample) and/or the presence of hydrated clay minerals (Steiger & Charola., 2011). The largest residual strain is sample Dh_{cb}, which also acts as an example of a dehydration reaction (negative value upon drying) (Figure 3.25). Dh_{cb} has clay-rich cements and matrix which may contribute to the overall residual strain. Residual strain accumulates over time and so can indicate which stone types are more susceptible to weathering via thermal cycling (Steiger & Charola., 2011).

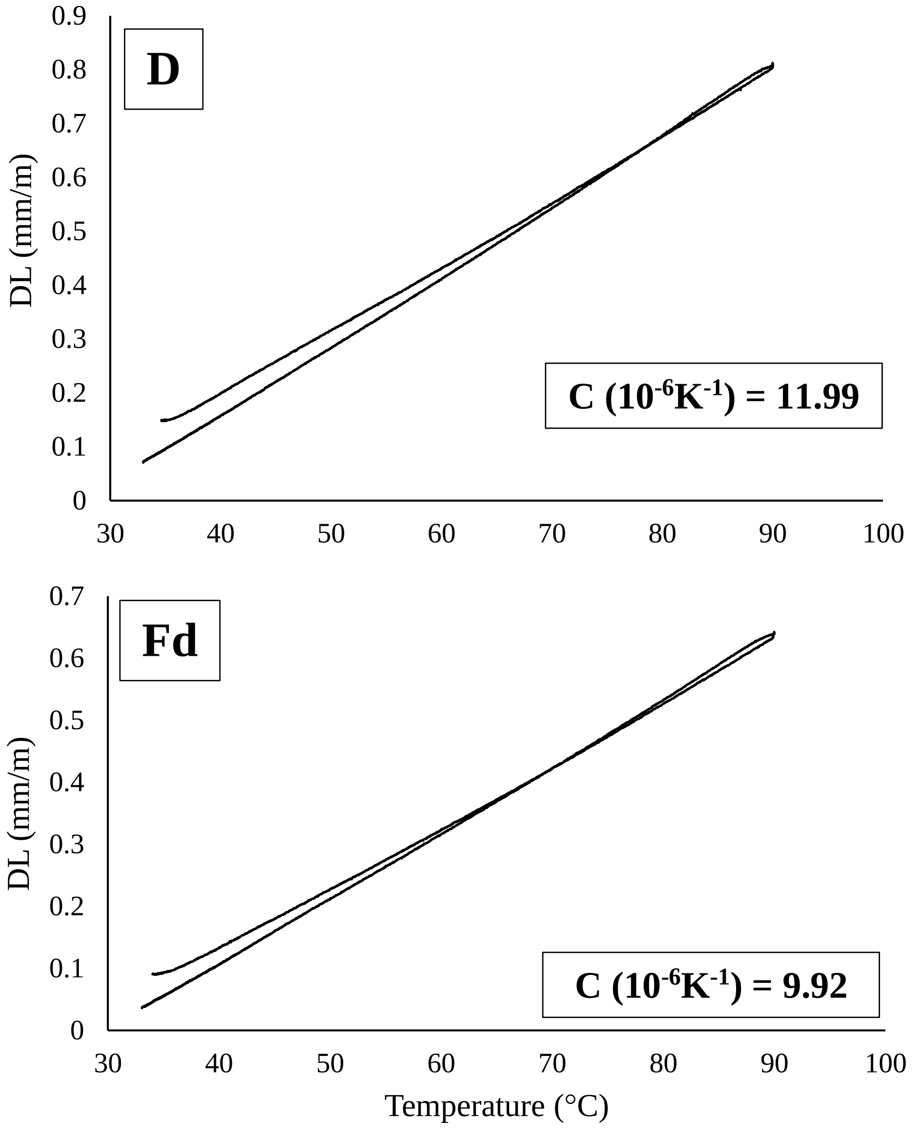

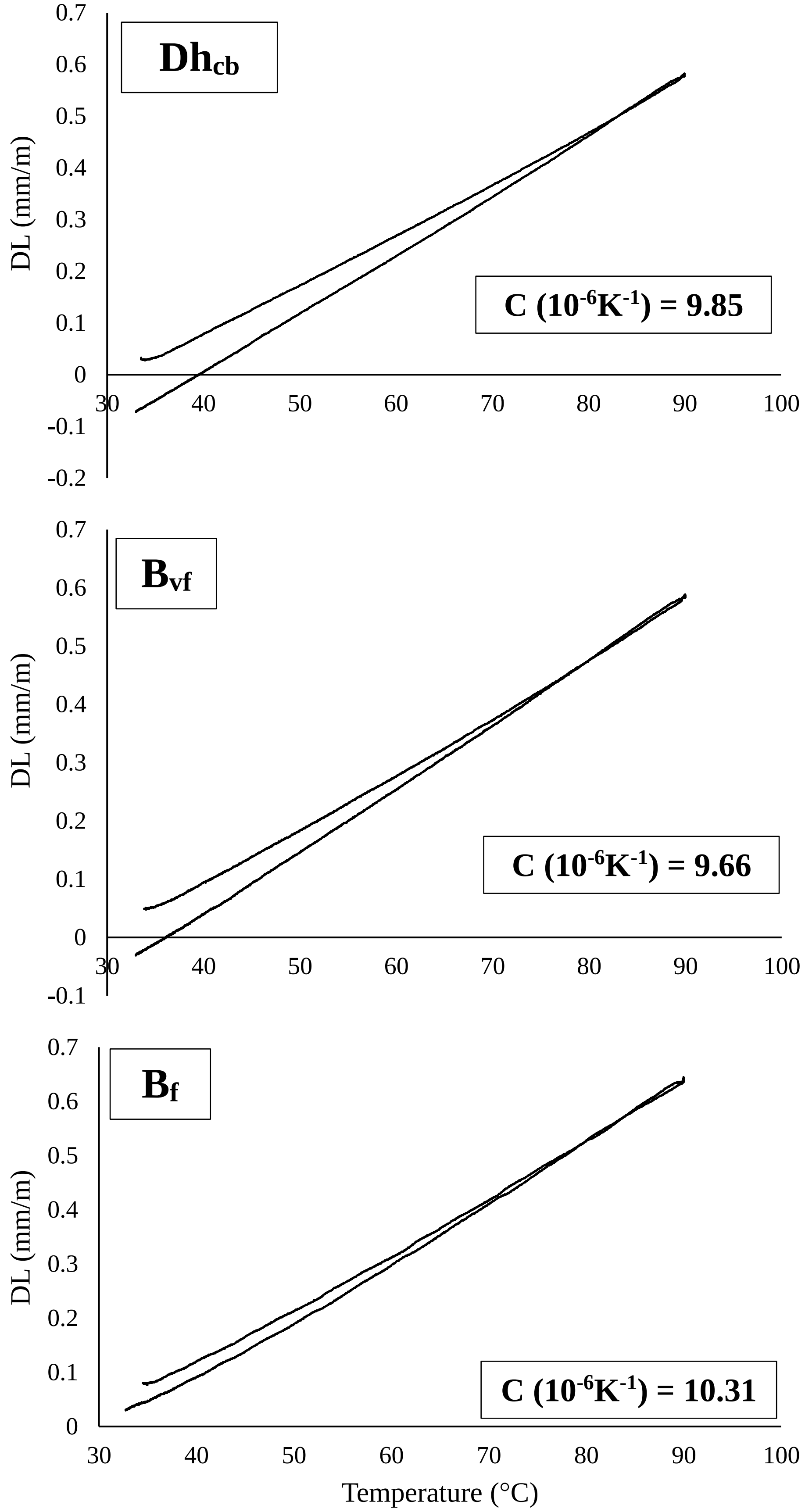

Figure 3.25: Thermal expansion coefficients for quarried sandstones. The figures represent a heating and a cooling phase, as well as the average thermal expansion coefficient, C. DL = Deformation Length.

3.4.6 Stone strength

As seen from Figure 3.26 there is a relationship between porosity and UCS. Dh_p has the highest average value of UCS-dry at 96.7 MPa (Table 3.6). Values of ~ 100 MPa are typical compressive strength values for low porosity (<13.4%) sandstones (Siegesmund & Dürrast., 2011). The UCS-dry of Dh_p is over twice that of sample D, which has the lowest UCS-dry of samples at 41.84 MPa (Table 3.6). Sandstones with high porosity (~ 20 %) exhibit lower UCS when dry in comparison to sandstones with low porosity (10-12 %). The samples with lower porosity are also the samples with higher clay mineral content and UCS. The clay minerals in these sandstones act primarily as matrix material reducing the overall porosity of the sandstone. In contrast the pore space of B_f and D is mostly empty. Outwith porosity and mineralogy, the UCS is also influenced by petrographic factors including grain size, compaction, and cements (Ruedrich et al., 2011). For example, despite the mineralogical maturity of D, it has the lowest compressive strength when dry likely influenced by a) high porosity where pores are mostly empty, and b) lack of mineral cement. In contrast samples Dh_p and De_{cb} have a very fine grain size where pores are filled with clay, and grains are binded together by quartz and carbonate cements.

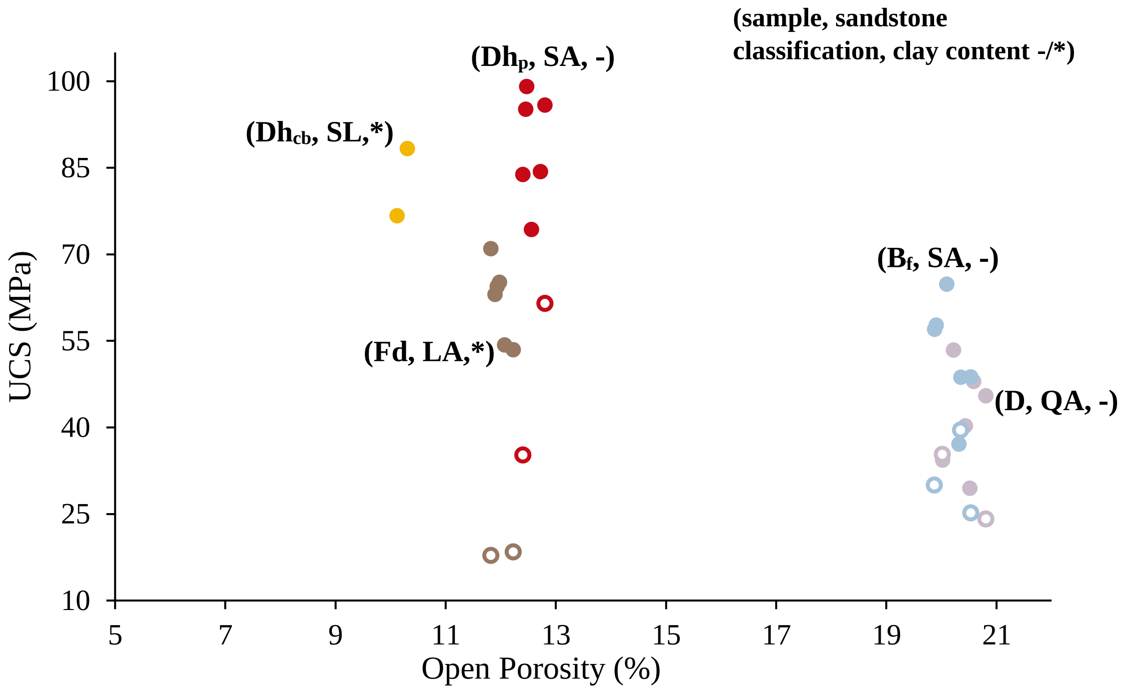

Figure 3.26: Open porosity and UCS of dry and saturated, fresh sandstones. LA = litharenite; SA = subarkose; SL = sublitharenite; and QA = quartz arenite. Empty circles represent UCS under saturated conditions and filled circles represent UCS under dry conditions.

The strength of selected replacement stones was also determined under saturated conditions. Overall, the UCS of sandstone is lower when saturated (Table 3.6). This is particularly true for sandstones which have a very fine grain size, low porosity and clay mineral content ($\mathrm{Dh_p}$, Fd) (Figure 3.26). The UCS of Fd reduces by up to 70.8 % when saturated. Fd is a sub-litharenite with a considerable clay fraction made up of non-expansive minerals (illite, kaolinite and chlorite). Along with sample $\mathrm{Dh_p}$, Fd also exhibited the highest rate of hydric expansion of any sample. The UCS of D seems less impacted by saturation perhaps due to its more mature mineralogy and differences in petrography relative to Fd. Hawkins & McConnell (1992) studied samples from the same location and geological unit as Fd, concluding that the significant strength loss after wetting was probably related to the softening of clay minerals, and that in general sandstones which were most sensitive to decrease in UCS with increasing moisture content, also had highest values of hydric expansion. According to the Hawkins & McConnell (1992) moisture content sensitivity scheme, the UCS of sample Fd is classed as being ‘extremely sensitive’ to increasing moisture content. Table 3.7 shows the sensitivity class of all studied sandstones based on the Hawkins & McConnell (1992) moisture sensitivity scheme, where samples with the highest rates of hydric expansion are the most sensitive.

Table 3.6: Uniaxial compressive strength (UCS) of dry and saturated fresh sandstone samples. Samples are measured in two directions: parallel (-) and perpendicular (+) to bedding. *no data due to sample restrictions.

Sample	Average Open Porosity	Average Young’s modulus (GPa)		Average Uniaxial Compressive Strength of dry samples (UCS-dry, MPa)		Average Uniaxial compressive strength of saturated samples (UCS-sat, MPa)
D	20.43 SD = 0.28 (6)	13.83 SD = 1.60 (6)		41.84 SD = 8.90 (6)		29.74 SD = 7.92 (2)
Fd	11.99 SD = 0.14 (6)	30.22 SD = 5.15 (6)		61.90 SD = 6.79 (6)		18.10 SD = 0.41 (2)
$\mathrm{Dh_p}$	12.57 SD = 0.16 (6)	- 26.44 SD = 0.92 (3)	+ 19.8 SD = 1.01 (3)	- 80.8 SD = 5.06 (3)	+ 96.7 SD = 2.10 (3)	- 48.34 SD = 18.58 (2)
$\mathrm{Dh_{cb}}$	10.21 SD = 0.13 (2)	- 24.32	+ 18.1	- 76.7	+ 88.4	*
$\mathrm{B_f}$	20.18 SD = 0.26 (6)	- 19.2 SD = 1.12 (5)	+ 18.5 SD = 0.16 (5)	- 44.3 SD = 5.97 (5)	+ 62.1 SD = 4.53 (5)	- 11.08 SD = 6.76 (2)

Table 3.7: Classification of sandstones sensitivity to reduction in UCS with increase in moisture content. Classification from Hawkins & McConnell (1992).

Reduction in UCS, %	Sensitivity class	Sample (reduction in UCS, %)	Lithology	Open porosity [ϕP, %]	Hydric expansion (mm/m)
0-10	Very low				
10-25	Low	B_f (21.6 %)	subarkose	20.18	0.07 (-) 0.20 (+)
25-40	Moderate	D (28.9 %)	Quartz arenite	20.43	0.27
40-55	High	Dh_p (50.0 %)	subarkose	12.57	0.20 (-) 0.54 (+)
55-70	Very high				
>70	Extremely high	Fd (71.0 %)	Clay-rich litharenite	11.99	0.74

3.4.7 Durability

Overall, all sandstone samples showed a degree of decay after being subjected to 15 cycles of salt weathering. Although most samples appeared to decay through granular disintegration and erosion, B_{vf} decayed through detachment of surface layers (1-2 mm thickness) which were parallel to stone faces. Figure 3.27 shows the relationship between bulk density and p-wave velocities (vp) which were measured before and after durability tests. Vp acts as an indicator of any internal weathering. Firstly, there is a relationship between bulk density and vp where samples with higher density (lower porosity) have higher vp values. This relationship indicates that there is less open pore space within the samples and so the p-waves travel through the sample faster. After weathering the vp and bulk density of samples generally becomes lower indicating an increase in porosity of samples after weathering (Figure 3.27). For some samples the vp remains similar which may suggest either a) limited decay, or b) the presence of leftover salts within pores, or a combination of the two. As discussed in the methods section, decay is quantified as the amount of material loss (g), relative to the original weight of the sample, expressed as a percentage. D and B_f experiences the most decay expressed as a percentage of material loss. Despite the obvious decay experienced by B_{vf} (detachment of surface layers) the sandstone experienced the least amount of decay of all samples (Table 3.8). This may suggest that weathering was limited to the surface of the stone (perhaps few mm) and that the rest of the stone was mostly unaffected.

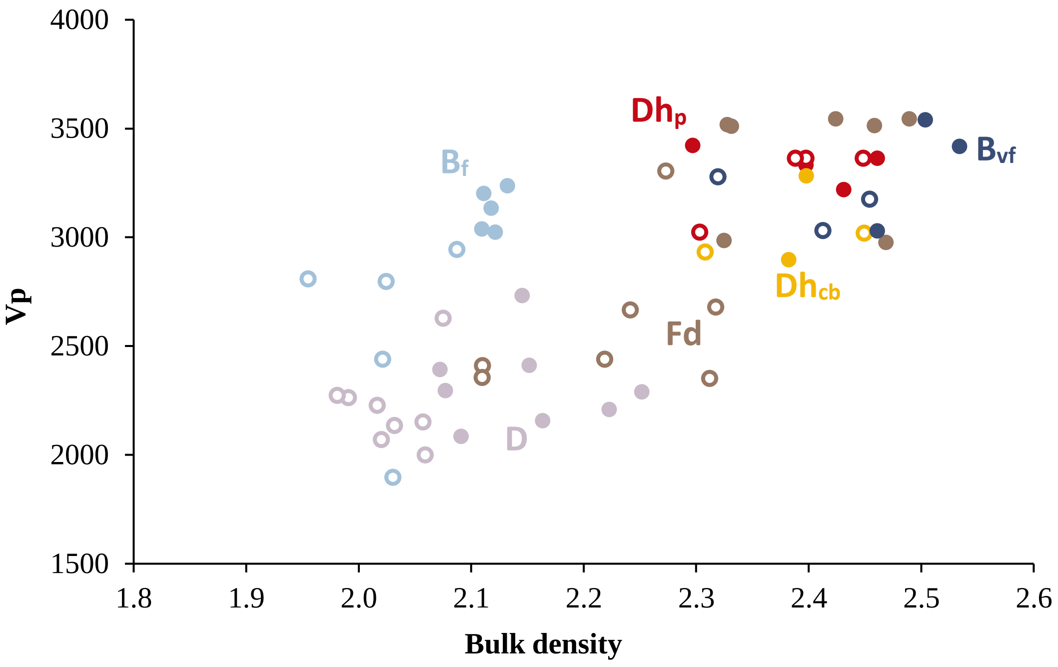

Figure 3.27: Relationship between bulk density and Vp, before and after salt weathering. B_f and D experienced the highest amount of decay. Empty circles represent vp and density after weathering.

Table 3.8: Durability of samples described by bulk density and Vp prior to and after salt weathering experiments, and decay (material loss, %). Compressive strength of weathered samples (UCS-w) was also measures when possible. *testing not possible due to integrity of sample after weathering.

	Prior to weathering			*After weathering*					
Sample	**Bulk density [ρ_{bulk}, g m^{-2}]**	**Compressional wave velocities (Vp, m/s)**		**Bulk density [ρ_{bulk}, g m^{-2}]**	**Compressional wave velocities (Vp, m/s)**		**Compressive strength of weathered samples (CS-w, MPa)**		**Decay (material loss, %)**
D	2.07 SD = 0.003 (2)	2345.0 SD = 68.4 (2)		1.99 SD = 0.007 (2)	2268.4 SD = 7.32 (2)		18.6 SD = 4.21 (2)		4.85 SD = 0.37 (2)
Fd	2.33 SD = 0.003 (3)	3338.5 SD = 305.6 (3)		2.30 SD = 0.02 (3)	2778.6 SD = 484.6 (3)		45.8 SD = 4.92 (3)		2.92 SD = 0.13 (3)
$\mathrm{Dh_p}$	2.40 SD = 0.07 (4)	- 3335.2 SD = 85.2 (4)		2.38 SD = 0.06 (4)	- 3278.1 SD = 169.9 (4)		- 76.7 SD = 4.55 (4)		0.98 SD = 0.34 (4)
$\mathrm{Dh_{cb}}$	2.39 SD = 0.01 (2)	- 2897.9	+ 3283.7	2.38 SD = 0.10 (2)	- 2932.2	+ 3019.3	- 38.6	+ 62.8	1.07 SD = 0.25 (2)
$\mathrm{B_{vf}}$	2.50 SD = 0.04 (3)	- 3479.3 SD = 85.6 (2)	+ 3030	2.40	- 3154.5 SD = 175.6 (2)	+ 3174.6 SD = 0 (1)	*		0.05 SD = 0.17 (3)
$\mathrm{B_f}$	2.12 SD = 0.009 (6)	- 3191.1 SD = 52.4 (3)	+ 3012.7 SD = 10.1 (3)	2.02	- 2849.6 SD = 82.1 (3)	+ 2168.0 SD = 383.4 (3)	- 31 SD = 3.36 (3)	+ 25 SD = 2.57 (3)	11.08 SD = 4.5 (6)

3.4.8 Anisotropy

Table 3.9 summarises the degree of anisotropy found in studied sandstone properties. As explained in section 3.3.7, a value of 1 indicates the sample is isotropic, where there is little to no difference in mechanical properties when measuring parallel or perpendicular to bedding. A value close to 0 means the sample is anisotropic, where there are significant differences in mechanical properties of sandstone when measuring parallel or perpendicular to bedding.

All bedded samples ($\mathrm{Dh_p}$, $\mathrm{Dh_{cb}}$, $\mathrm{B_f}$, $\mathrm{B_{vf}}$) show a degree of anisotropy (< 1) in tests relating to hydric behaviour and stone strength. When measured parallel to bedding, bedding planes are in direct contact with water allowing for preferentially capillary uptake. Capillary absorption rates were fastest when measured parallel to bedding for planar bedded samples Dh_p, B_f and B_{vf}, with varying degrees of anisotropy.

Similarly, for hydric expansion, all sandstone samples show a degree of anisotropy when measured in two directions. However, only two sandstones have values < 0.5 and closer to 0, sandstones Dh_p and B_f. Both samples display planar bedding on a scale of 2-5 mm and have a similar mineralogy.

There is a degree anisotropy in the UCS-dry of all samples. Anisotropy in UCS of sandstone is commonly reported in literature, attributed to a localised differences in petrophysical properties (PSD, alignment of minerals, clay content) on bedding planes relative to the bulk rock, leading to internal stress when a load is applied (Mezenes & Lempp., 2018). UCS-dry of B_f has a lower compressive strength when sigma 1 is parallel to bedding. However, UCS-dry of Dh_p and Dh_{cb} have a higher compressive strength when sigma 1 is parallel to bedding. After weathering, the anisotropy of Dh_{cb} is greater, where the UCS-w is ~ 55% less than UCS-dry parallel to bedding, and only ~ 30% less than UCS-dry perpendicular to bedding.

Table 3.9: Anisotropy calculated using the average values for parallel and perpendicular for each studied property. *No data available.

Sample	Capillary absorption	Hydric absorption	Vp	UCS-dry	Thermal expansion
Dh_p	0.75	0.38	0.87	0.83	*
Dh_{cb}	0.96	0.68	0.99	0.87	0.98
B_{vf}	0.73	0.62	0.86	*	0.97
B_f	0.67	0.34	0.97	0.71	0.98

3.5 Final Discussion

3.5.1 Implications of findings for historic sandstone buildings

Weathered stone from Jedburgh Abbey, J_w, and quarried sandstone from Denholmhill, Dh_{cb}, have a very similar petrography. Both sandstones are classified as sublitharenites which are micaceous where micas are orientated along cross beds. Furthermore, both sandstones have the same grain size and a matrix comprising mostly non-expansive clay minerals and dolomite. Denholmhill quarry is still accessible and may provide a source of replacement material for sandstone in the lower storey area of Jedburgh Abbey.

Decay patterns at the Abbey consists mostly of fissuring and delamination in the lower storey area. Fracturing occurs primarily along bedding planes which uptake water faster relative to the rest of the stone as seen from capillary absorption experiments of Dh_{cb}. The preferential uptake of water may lead to accelerated physical and chemical weathering of less stable minerals which are concentrated on bedding planes (micas and clay minerals) leading to fracturing orientated parallel to bedding. Finally, Dh_{cb} was one of the most sensitive samples to hydric expansion which may also accelerate physical weathering along bedding planes. Although not similar to J_w, Dh_p is appears to be more similar to stone used in the main nave of the Abbey. Both Dh_{cb} and Dh_p and from the Stratheden and Inverclyde group – thought to be the unit where the original sandstone for Jedburgh Abbey was quarried.

When comparing weathered stone from Arbroath Abbey, $A(C)_w$ and $A(L)_w$, there are notable differences in mineralogy and petrography. These differences include the presence of smectite in $A(C)_w$, and differences in grain size. The stones are otherwise broadly similar, and both classified as lithic arkose. Both weathered stones have a similar petrography to common replacement stones at the Abbey, B_f and B_{vf}. The key differences are the occurrence of more lithic fragments, and the occurrence of clay lithoclasts in the weathered original stones.

Decay patterns at the Abbey consist mostly of alveolization related to salt weathering, sanding, powdering, flaking, spalling, blistering, and granular disintegration. The results of the salt weathering experiments confirmed that of all studied stone types, B_f was the most sensitive to decay (material loss) after weathering highlighting the stone’s relatively lower durability related to salt weathering. This sensitivity to salt weathering may be partly influenced by a) stones high porosity, ~ 20%, and b) poorly cemented grains. Despite the presence of smectite in B_f, the sandstone showed little capacity for hydric expansion. The low hydric expansion may be explained by the higher porosity and large average pore size of B_f, allowing for adequate space for clay mineral expansion. This highlights that the presence of smectite is not necessarily having a direct impact on sandstone durability.

Weathered sandstone from Dunkeld Cathedral, DC_w, has a very similar mineralogy and petrography to quarried Forest of Dean sandstone, Fd. DC_w appears to have slightly higher proportion of feldspars and is therefore classified as a feldspathic litharenite. Both DC_w and Fd have a clay-rich matrix made up of non-expansive clay minerals.

Decay patterns at the Cathedral consist mostly of granular disintegration, spalling, flaking, and preferential erosion of clay clasts. Fd showed an extreme sensitivity to a reduction in

UCS with increasing moisture content. Previous literature has related this behaviour to the softening of clay minerals (Hawkins & McConnell, 1992; Ruedrich et al., 2011). Moreover, clay minerals typically coat individual grains in Fd perhaps leading to an accumulation of strain when clay minerals soften around rigid quartz grains contributing to decay patterns such as granular disintegration and spalling. Moreover, Fd also had a relatively higher value for hydric expansion again perhaps contributing to the weakening of stone when saturated described above.

3.5.2 Impact of clay mineralogy on durability

Although all sandstones contain clay minerals, only B_f and $A(C)_w$ contain expansive smectite. Both of these samples are relevant to Arbroath Abbey where $A(C)_w$ is weathered stone thought to be from the original construction of the Abbey, and B_f is the current replacement stone. Despite the presence of smectite in B_f, the hydric expansion was relatively low, indicating that expansion-contraction of smectite is unlikely to be a major influence of decay. This may be due to the relatively small amount of clay present in B_f which primarily exists only as very thin (micron thickness) coatings on individual grains. This may highlight that the mere presence of smectite does not necessarily equate to a poor-quality stone.

Non-expansive clay minerals on the other hand, have been shown in this chapter to influence the petrophysical properties of studied sandstones and make them more susceptible to weathering under certain circumstances. As seen from this research, clay minerals can alter the fabric of sandstone influencing pore size distribution (e.g. creation of microporosity) and porosity. Sample Fd exhibits some common behaviours associated with clay-rich sandstones, including higher rates of hydric expansion, and large decrease in UCS after saturation despite the absence of smectite. Clay minerals in Fd are ‘non-expansive’ types, however are plentiful where clay not only coats grains, but also infills pores and by doing so creates a microporous texture. The effect of a clay-rich mineralogy is also clearly seen when measuring UCS of sandstone under saturated conditions. The UCS of Fd for example, reduced by ~ 70 % when saturated, attributed in previous literature to the softening of clay minerals around rigid quartz grains (Hawkins & McConnell, 1992; Ruedrich et al., 2011).

Findings of this chapter emphasise that when trying to understand the role that clay minerals play in sandstone durability and decay, the occurrence of smectite is not the only factor that should be considered when characterising and understanding the clay fraction. A more thorough investigation identifying types of clay minerals present, relative abundance, distribution in sandstone, and their influence on petrophysical properties is required to better the understanding of clay-rich sandstone durability. It is difficult to conclusively prove or disprove the role clay minerals play in individual cases, but they no doubt influence durability substantially.

3.5.3 Climate change and decay of clay-rich sandstone

Scotland's climate projections forecast increases in precipitation, especially in winter, where rain events are longer in duration (UKCP 18). This may lead to longer periods of wetness for sandstone buildings with limited drying time. This wetter climate may negatively impact the durability of sandstone as seen from UCS testing of samples under saturated conditions. Table 3.10 attempts to categorise the sensitivity of studied sandstones to accelerated weathering brought on by increases in precipitation associated with climate change. Sensitivity to precipitation increase driven by climate change is determined here by several stone properties (open porosity, compressive strength when dry and saturated, rate of hydric expansion, and resistance to weathering described as decay). Values shown in Table 3.10 are average values of analyses discussed earlier in this chapter. Colours are based on values relative to one another. Red is allocated to the top 1-2 'worst performing' stones relative to a given property. In the case of porosity (P%) for example, the highest values are associated with the colour red, as high porosity contributes to more moisture ingress which increases likelihood of weathering. Green is allocated to the top 1-2 'best performing' stones relative to a given property. In the case of compressive strength (UCS-dry), the highest values are associated with the colour green as high compressive strength is associated with a more resilient stone with a greater resistance to weathering. Finally, the colour orange is attributed to stones which have values between red and green categories.

Overall, Fd seems particularly vulnerable to increases in precipitation relative to other samples, due mainly to the stone's sensitivity to hydric expansion and reductions in UCS when wet (Table 3.10). Moreover, studies have shown that the rapid reduction in UCS associated with saturation of clay-rich sandstone occurs at as little as 1% saturation (Hawkins & McConnell., 1992), suggesting historic sandstone buildings, and in particular historic clay-rich sandstones buildings, may be very vulnerable in the future climate of Scotland.

Table 3.10: Vulnerability of characterised sandstones to the impacts of precipitation increase driven by climate change in Scotland. Data used are average values of properties based on results discussed throughout this chapter. Green is associated with low level vulnerability to climate change, while yellow and orange are associated with relatively higher risk, and red is associated with high risk. P% = Open porosity, UCS-dry = Uniaxial Compressive Strength under dry conditions, UCS-sat = Uniaxial Compressive Strength under saturated conditions, hydric expansion, Decay (%) = material loss after weathering experiment expressed as a percentage. Fd = Forest of Dean, B_f = St. Bees (fine grained), B_{vf} = St. Bees (very fine grained), Dh_p = Denholmhill Red (planar bedded), Dh_{cb} = Denholmhill Red (cross bedded), D = Doddington. * No data available.

	Fd	Bf	Bvf	Dhp	Dhcb	D
P%	12.26	20.18	10.34	11.71	10.29	20.44
UCS-dry	61.9	62.1	*	88.4	88.4	41.84
UCS-sat	71%	22%	*	50%	*	30%
Hydric expansion	0.74	0.2	0.64	0.54	0.74	0.27
Decay (%)	2.92	11.08	0.05	0.98	1.07	4.85

3.6 HES recommendations

The following recommendations for HES were based on the research carried out in this chapter, with a specific focus on understanding and mitigating the decay of clay-rich sandstone buildings:

- **Database of vulnerable sandstone heritage.** Such a database could store any mineralogical and physical data regarding the building stone at a specific site and highlight the most vulnerable sites. Furthermore, a database could highlight, based on specific factors, which sites are to be most impacted by climate change so that potential case study sites for future research can be easily selected. Such sites may be prioritised for projects relating to long-term stone and climate monitoring (see below point for more detail) and research projects focussed on sandstone preservation (e.g., trialling of water repellents).

- **Long term stone and climate monitoring.** Such monitoring to be prioritised at sites deemed most vulnerable to decay allowing for a better understanding of the interactions between stone properties and climate. Properties which may be assessed regularly include mapping of visual surface changes, stone properties including density, porosity, and water absorption rates using in-situ and non-destructive tests monitoring, and relative humidity and temperature using ibuttons. Furthermore, lab-based accelerated weathering experiments (either using weathered samples or similar stone from quarry) using a climate chamber may be used as a means of provided information faster on the extent of weathering associated with different climate scenarios and sandstone types.

- **Regular petrophysical and mineralogical characterisation of sandstones.** Regular (perhaps annual) characterisation is especially important for sandstones as they can often be heterogenous within a quarry – meaning their properties can vary due to changes in environment during deposition. This has been shown to be the case with St. Bees in this research chapter which showed two varieties with different physical and mineralogical properties which have important controls on durability. Practically this may be challenging however, will further reduce the risk of selecting a stone which is not compatible with stone at a given site.

- **Development of a methodical approach to the characterisation of clay minerals using both XRD and SEM.** SEM and XRD provides data crucial information in regard to the role clay minerals play in sandstone decay and durability. Many studies identify clay minerals using pXRD without providing additional context. As shown from this research chapter the role played by clay minerals in the decay of sandstones extends further than the occurrence of smectite. Other important factors to characterise include clay mineral morphology, distribution of clay minerals and their impact on pore size distribution, and amount; properties which can be characterised using SEM and XRD. Quantitative XRD is a powerful tool not explored in this project, which could provide valuable information on the exact quantities of clay minerals present in stone. The ability to measure clay mineral quantities in crushed bulk samples would allow for research project assessing the impact of different clay mineral quantities on sandstone decay and durability.

3.7 Future research

There are several areas where research can be focussed with the aim of understanding the role that clay minerals play in the decay of sandstone buildings. Below are suggestions for research studies following on from the recommendations from the previous section:

- **Investigate relationship between clay mineral content and sandstone durability under different climate scenarios**. There is limited literature which reports quantitative values for clay mineral content in sandstone. Consequently, there is even less literature on how different quantities of clay minerals impact the durability of sandstone. Such research questions could be answered through quantitative pXRD analysis to determine clay mineral content, followed by accelerated weathering experiments using a climatic chamber. In addition to such as study, different UKCP scenarios could be used in the accelerated weathering experiment to determine which climates have the most adverse impact on durability of clay-rich sandstone.

- **The impact of water saturation degree on the strength of clay-rich sandstone**. As shown in this research chapter, the strength of clay-rich sandstone (Forest of Dean) is extremely sensitive to changes in degree of water saturation. These findings may have important implications for sandstone durability with regards to the future climate of Scotland, which predicts more rainfall and more intense rain events. The future climate of Scotland may lead to periods of prolonged stone wetness reducing the overall strength of stone which also changing the dominant weathering processes controlling decay (e.g. shift from predominantly physical weathering to chemical weathering). Such as study characterise the mineral content of selected stones and determine how different degrees of saturation impact stone strength (compressive, tensile, etc).

- **Durability of Scottish building stones under different UKCP scenarios.** Changes in climate will ultimately impact how stone weathers and decays. Accelerated weathering experiments can be used to assess how different UKCP scenarios impact different stone types, including weathered stone from sites (if sampling possible) and stone from quarries.

Such findings could then be used to help inform future decision making with regards to conservation approaches at specific sites.

3.8 References

Avdelidis, N. P., & Moropoulou, A. (2004). Applications of infrared thermography for the investigation of historic structures. Journal of Cultural Heritage, 5(1), 119-127.

Benavente, D., Cueto, N., Martínez-Martínez, J., Del Cura, M. G., & Cañaveras, J. C. (2007). The influence of petrophysical properties on the salt weathering of porous building rocks. Environmental Geology, 52(2), 215-224.

Benavente, D., Cultrone, G., & Gómez-Heras, M. (2008). The combined influence of mineralogical, hygric and thermal properties on the durability of porous building stones. European Journal Of Mineralogy, 20(4), 673-685. doi: 10.1127/0935-1221/2008/0020-1850

Benavente, D., Martinez-Martinez, J., Galiana-Merino, J. J., Pla, C., de Jongh, M., & Garcia-Martinez, N. (2022). Estimation of uniaxial compressive strength and intrinsic permeability from ultrasounds in sedimentary stones used as heritage building materials. Journal of Cultural Heritage, 55, 346-355.

British Standards (2006) *Natural stone test methods. Determination of real density and apparent density, and of total and open porosity* (BS EN:1936:2006), BSOL. www.bsol.bsigroup.com

British Standards (2016) *Hygrothermal performance of building materials and products. Determination of water absorption coefficient by partial immersion* (BS EN ISO 15148:2002+A1:2016), BSOL. www.bsol.bsigroup.com

British Standards (2020) *Natural stone test methods. Determination of resistance to salt crystallisation* (BS EN 12370:2020). BSOL. www.bsol.bsigroup.com

Chastre, C., & Ludovico-Marques, M. (2018). Nondestructive testing methodology to assess the conservation of historic stone buildings and monuments. In Handbook of Materials Failure Analysis (pp. 255-294).

Delago-Rodrigues, J. (2001) Swelling behaviour of stones and its interest in conservation. An appraisal. Materiales De Construcción, 51(263-264), 183–195. https://doi.org/10.3989/mc.2001.v51.i263-264.363

Hawkins, A. B., & McConnell, B. J. (1992). Sensitivity of sandstone strength and deformability to changes in moisture content. Quarterly Journal of Engineering Geology and Hydrogeology, 25(2), 115-130.

Jiménez-González, I., Rodríguez-Navarro, C., & Scherer, G. (2008). Role of clay minerals in the physicomechanical deterioration of sandstone. Journal Of Geophysical Research, 113(F2). doi: 10.1029/2007jf000845

Madsen, F.T., & Müller-Vonmoos, M. (1989). The swelling behaviour of clays, Applied Clay Science, 4(2), 143-156, doi.org/10.1016/0169-1317(89)90005-7.

Matija Strlic, 'A brief theory of heritage science' (London, National Heritage Science Forum, 2015) [online] https://nationalheritagescienceforum.wordpress.com/2015/04/16/a-brief-theory-of-heritage-science-by-professor-matija-strlic-ucl-institute-for-sustainable-heritage/

Menezes, F. F., & Lempp, C. (2018). On the structural anisotropy of physical and mechanical properties of a Bunter Sandstone. Journal of Structural Geology, 114, 196-205.

Met Office Hadley Centre (2018): UKCP18 Probabilistic Climate Projections. Centre for Environmental Data Analysis.

Michette, M., Viles, H., Vlachou, C., & Angus, I. (2020). The many faces of Reigate Stone: an assessment of variability in historic masonry based on Medieval London's principal freestone. Heritage Science, 8(1), 1-24.

Mitsos, D., Kantarelou, V., Palamara, E., Karydas, A. G., Zacharias, N., & Gerasopoulos, E. (2022). Characterization of black crust on archaeological marble from the Library of Hadrian in Athens and inferences about contributing pollution sources. Journal of Cultural Heritage, 53, 236-243.

Pötzl, C., Dohrmann, R., & Siegesmund, S. (2018). Clay swelling mechanism in tuff stones: an example of the Hilbersdorf Tuff from Chemnitz, Germany. *Environmental earth sciences*, *77*(5), 1-19.

Ruedrich, J., Bartelsen, T., Dohrmann, R., & Siegesmund, S. (2010). Moisture expansion as a deterioration factor for sandstone used in buildings. Environmental Earth Sciences, 63(7-8), 1545-1564. doi: 10.1007/s12665-010-0767-0

Salvatici, T., Calandra, S., Centauro, I., Pecchioni, E., Intrieri, E., & Garzonio, C. A. (2020). Monitoring and evaluation of sandstone decay adopting non-destructive techniques: On-site application on building stones. Heritage, 3(4), 1287-1301.

Scrivano, S., Gaggero, L., Aguilar, J., de Kock, T., Derluyn, H., & Cnudde, V. (2017). Texture and mineralogy influence on durability: the Macigno sandstone. Quarterly Journal Of Engineering Geology And Hydrogeology, 50(4), 393-401. doi: 10.1144/qjegh2016-107

Sebastián, E., Cultrone, G., Benavente, D., Linares-Fernandez, L., Elert, K., & Rodriguez-Navarro, C. (2008) Swelling damage in clay-rich sandstones used in the church of San Mateo in Tarifa (Spain). Journal of Cultural Heritage, 9(1), 66-76, doi: 10.1016/j.culher.2007.09.002

Siegesmund, S., & Dürrast, H. (2011). Physical and mechanical properties of rocks. In *Stone in architecture* (pp. 97-225). Springer, Berlin, Heidelberg.

Siegesmund, S. & Török, Á. (2011). Building stones (Chapter 3). *Stone in Architecture*. Heidelberg: Springer, 4th ed., pp. 11-97, doi: 10.1007/978-3-642-14475-2

Steiger, M. & Charola, E. (2011). Weathering and Deterioration. In *Stone in architecture* (pp. 227-317). Springer, Berlin, Heidelberg.

U.S Geological Survey (USGS). Clay mineral identification flow diagram, Open-file report 01-041, available at https://pubs.usgs.gov/of/2001/of01-041/htmldocs/flow/index.htm

Wangler, T., & Sherer, G. (2008). Clay swelling mechanism in clay-bearing sandstones. Environmental Geology, 56(3-4), 529-534. Doi: 10.1007/s00254-008-1380-3

Warke, P., & Smith, B. (2000). Salt distribution in clay-rich weathered sandstone. Earth Surface Processes And Landforms, 25(12), 1333-1342. doi: 10.1002/1096-9837(200011)25:12<1333::aid-esp141>3.0.co;2-6

4.0 Preservation of sandstone at Arbroath Abbey.

4.1 Introduction

This chapter is an investigation into the use of hydrophobic treatments as a means of protecting decaying sandstone at Arbroath Abbey (Figure 4.1). Arbroath Abbey, situated on the east coast of Scotland, was founded in 1178, and constructed using local sandstone from the nearby coast. The Abbey has undergone frequent episodes of restoration and the original Abbey stone has been replaced extensively.

In 1976 Brethane, a commercial hydrophobic treatment, was applied to several areas of Arbroath Abbey: the base of two columns located in the west arcade, and a S/SE facing façade. The treatment was applied using a brush. There has been two official observations since the application, which describe the treated stone as appearing sound with no optical changes or obvious detrimental impact to its integrity. The composition of the treatment is a mixture of methyltriethoxysilane, meths mixed with water, and a solution of Pb 36 in white spirit. Upon initial inspection the treated areas still retain a degree of hydrophobicity, preventing moisture ingress 46 years after initial application. Furthermore, the treatment does not appear to have accelerated weathering of surrounding untreated stone. Arbroath Abbey provides a unique opportunity to assess the long-term efficiency of water repellents in protecting sandstone and their suitability as a conservation method at the Abbey moving forward.

Protective treatments for the preservation of sandstone have been studied extensively (Pascua et al., 1996; Cnudde & Jacobs., 2004; Jiménez González & Scherer, 2004; de Ferri et al., 2011; Pinna et al., 2012; Akoğlu & Caner-Saltık., 2015; Wen et al., 2021). The two primary subdivisions of treatment are: protective coatings and consolidants (Elert & Rodriguez-Navarro., 2022). Coatings are typically hydrophobic and aim to prevent moisture ingress and therefore, reduce weathering and subsequent decay. Consolidants on the other hand aim to strengthen stone by increasing cohesion by cementing the material together (Elert & Rodriguez-Navarro., 2022). Consolidants can also have a hydrophobic element (Young et al., 2003). There are several specific concerns noted in research with regards to the compatibility of protective treatments with porous sandstone types. Application of treatments can lead to the modification of physical stone properties such as changes in vapour diffusion properties, hygric/hydric dilatation, and flexural strength of the surface

(Charola., 2003; Moropoulou et al., 2003). Changes in petrophysical stone properties may affect how moisture and salts (important in the case of Arbroath given its coastal location) move through the stone. Previous research has found that in some instances crystallised salts can accumulate and become trapped behind the hydrophobic surface, leading to the accumulation of strain and accelerated physical weathering through decay patterns such as spalling (Jia et al., 2019; Ershad-Langroudi et al., 2019; Gherardi., 2022).

More broadly speaking, the impact of climate change on the durability of sandstone in Scotland's historic buildings is not well understood. Increases in precipitation in Scotland associated with climate change may affect the dominant weathering processes which control decay at a specific site and may also accelerate weathering. It is therefore imperative to consider and investigate the suitability of preservation methods, such as hydrophobic treatments, in protecting the historic sandstone buildings of Scotland from future increases in precipitation.

The aim of the study is to determine the suitability of a hydrophobic cream as a means of protecting sandstone at Arbroath abbey. The compatibility of the treatment and stone will be assessed through on-site moisture mapping of the previously treated area, and lab-based experiments analysing properties of treated and untreated stones such as: capillary absorption, vapour diffusion resistance, and durability (by means of accelerated salt weathering). This study uses two blocks, a lintel and corbel, obtained during restoration work at the Abbey in 2019. The mineralogy and petrography of both blocks is studied in detail to not only assess the suitability of hydrophobic treatment, but also understand mineralogical and textural variations in the stone at different depths and the implications of this with regards to sampling methods at historic buildings. Sampling at sites of high heritage value is often heavily restricted where sampling is limited to the outer weathered crust. Unfortunately, lack of sampling commonly hinders scientific progress in the field of heritage science and limits our understanding of best conservation practices at a given site (Kennedy., 2015). Obtaining two blocks is very uncommon and offers a unique opportunity to appreciate any differences throughout the stone profile.

Figure 4.1: Arbroath Abbey located on the East Coast of Scotland.

4.2 Materials

4.2.1 Rock samples

Two weathered sandstones from Arbroath Abbey are used in this study. The weathered sandstone consists of a lintel block, A-L, and corbel block, A-C, which were removed from the Abbey during 2019 restoration work and are thought to have been part of the original construction which began in 1178. Sandstone used in the original construction of the Abbey is thought to have been sourced from the nearby coast. Sandstone here forms part of the Scone Formation deposited during the Devonian in an arid climate and fluvial depositional environment. Upon initial inspection, the blocks differ slightly in colour and mineralogy. The A-C sandstone has a deep red-brown colour, while A-L is comparatively lighter with a cream-pink colour (Figure 4.2). There is strong mineral alignment (of mostly mica) in A-L, while A-C exhibits planar bedding on a scale of ~ 1 mm.

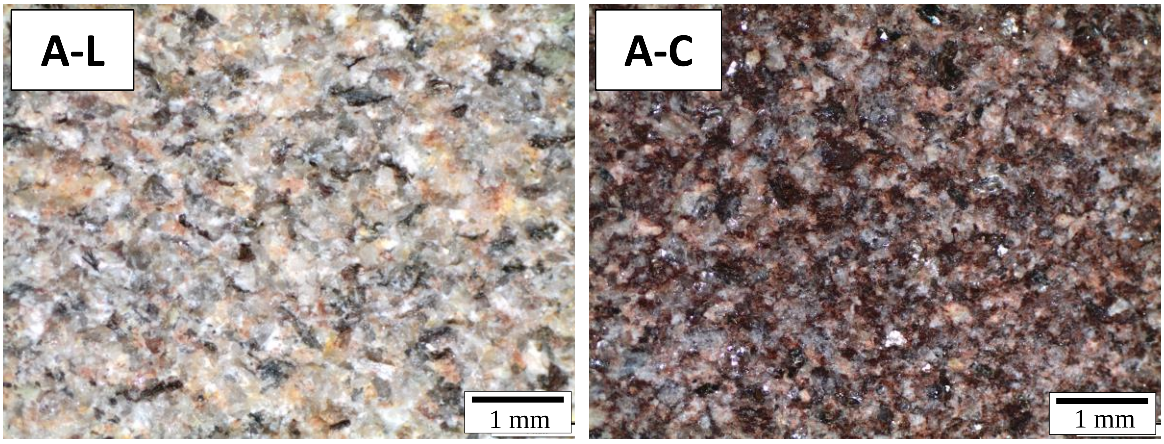

Figure 4.2: Macroscopic images of sandstones A-L and A-C. A-L contains lithoclasts of clay which are an average ~ 10 mm in length. Both sandstones are thought to date back to original construction which started in 1178.

4.2.2 Water repelling treatment

The commercial water repellent Brethane could not be used in this study as it is no longer manufactured. The selection of treatment was based on several factors. Firstly, the capillary absorption coefficient (w-value) was used to identify a recommended penetration depth of the water repellent of 7 mm (minimum) (WTA 2010; Snethlage., 2011). Based on the minimum desired penetration depth, open porosity, and estimated application time, a hydrophobic cream was selected (Snethlage., 2011). The choice of cream over a liquid agent is primarily due to the relatively low capillary absorption rates of sandstone samples thus requiring a longer application time for sufficient penetration of treatment. Cream takes longer to completely dry, allowing the treatment to penetrate the sample surface to a sufficient depth before fully curing. Table 4.1 summarises some of the properties of the cream including the composition and curing time.

Table 4.1: Characteristics of selected commercial hydrophobic masonry cream.

Hydrophobic cream property	Description
Composition	Silane/siloxane masonry cream containing: hydrocarbons (C11-C14); isoalkanes; cyclics; <2% aromatics; and triethoxyoctylsilane
Density	0.86 g/cm^3
Coverage	5 m^2 per litre (single coat recommended)
Curing time (time between application and post-application experiments)	28 days

4.3 Methods

4.3.1 Field observations

Decay patterns at the Abbey were described according to the ICOMOS-ISCS illustrated stone glossary. The glossary acts as a universal guide which aids in the identification of decay patterns using consistent, non-ambiguous terminology. According to the glossary, decay patterns can be divided into five main categories: cracks and deformation, detachment, features induced by material loss, discolouration and deposit, and biological colonisation.

4.3.2 Moisture analysis

A microwave moisture meter was used to evaluate the relative differences in moisture content on a façade (~7.5 m length) at Arbroath Abbey which were partially treated with a brethane repellent in 1976 (Figure 4.3). Two measurements were obtained per block making up an eighteen-point vertical transect, where each transect was 15 cm apart. Using three different probe heads penetrating to different depths (15 cm, 30 cm, and 80 cm), the stone façade was mapped under relatively dry conditions. After mapping under relatively dry conditions, the treated façade and adjacent untreated area was wetted using a pressurised hose system. The data was analysed using MoistTools software which interpolates data between measured data points.

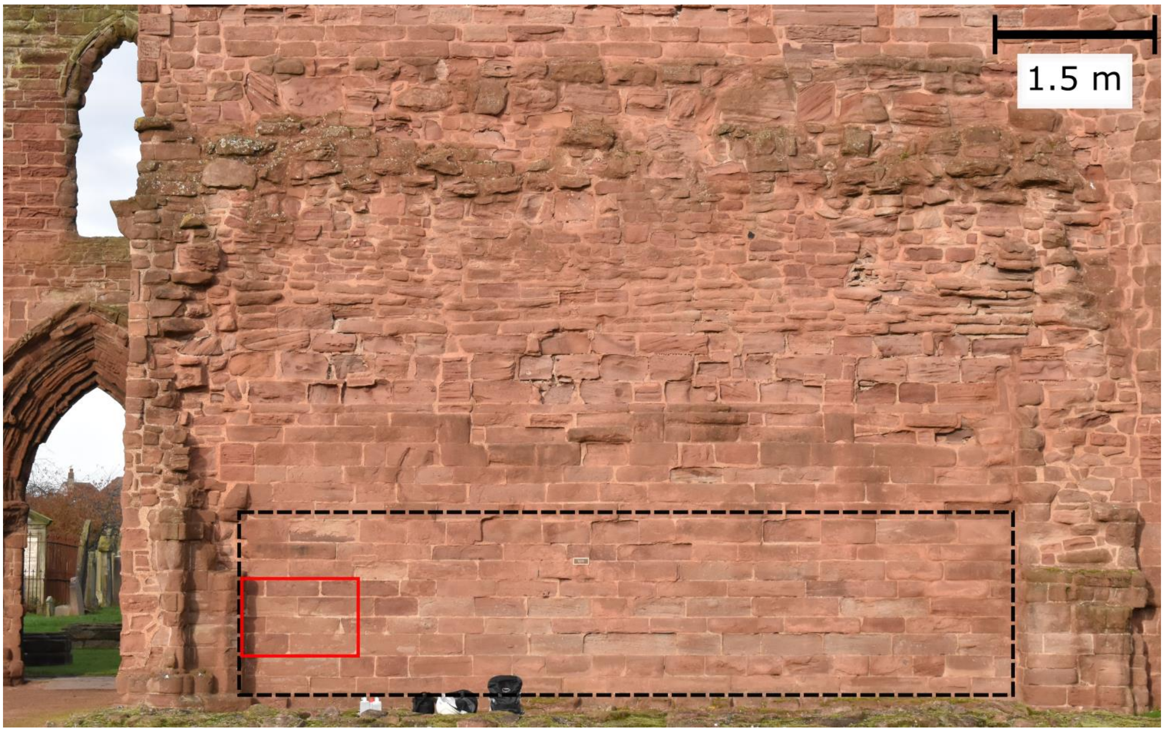

Figure 4.3: Studied façade at Arbroath Abbey. Black box outlines the boundaries of the tested area, and the red box outlines the boundaries of the area previously treated with Brethane.

4.3.3 Application of hydrophobic cream

The cream was applied to cubic samples (length 50 mm) which were dried to a constant mass using an oven at 105°C. Any loose debris was removed from the surface gently using a small brush. A single coat of cream was applied using a small paint roller as recommended by the products manufacturer. Alternatively, the treatment can be applied using a brush or spray. The treatment was left to cure at conditions of 20°C ±1 and 50 ±5 RH, for at least 28 days prior to any post-application experiments. The number of faces of each sample coated with the cream depended on the analysis to be carried out. Samples for capillary absorption experiments and salt weathering were coated on every face, while samples for vapour diffusion analysis were coated on one face only.

4.3.4 Mineralogy

The mineralogical composition was characterised using pXRD. X-ray Diffraction (XRD) analyses was carried out using a Thermo Electron ARL X'TRA XRD at the Engine Shed

(HES) in Stirling. The settings were as follows: CuKα radiation, running at 45mA and 44kV, step size of 0.02 degrees, and a scan rate of 1^{o} per minute. Mineralogy of the bulk and extracted clay fraction was characterised for: the weathered surface of both A-L and A-C, and the interior stone of both A-C and A-L. Finally, salts were also extracted from both weathered stones and analysed using XRD.

4.3.5 Petrography

Scanning Electron Microscopy (SEM) was carried out using a FEI Quanta 200F Environmental SEM with EDAX Microanalysis. SEM was used to evaluate textural rock properties and distribution of clay minerals. Thin sections were prepared, and sputter coated in carbon for analysis. The samples were analysed in high vacuum, at 20 kV using backscattered and secondary electron imaging. In addition to thin section analysis, small gold-coated chips of samples were also analysed under the same conditions.

4.3.6 Open porosity and apparent density

Open porosity and apparent bulk density were determined by the vacuum saturation method, according to BS EN 1936:2006. Cut sandstone samples are placed in desiccator before the pressure inside the desiccator is reduced to 2 ± 0.7 kPa. Deionised water is then slowly introduced into the desiccator while maintaining the aforementioned pressure. Finally, once the samples are immersed in water the desiccator pressure is gradually brought back to atmospheric pressure. The sample are left immersed overnight before a saturated weight, m_s, is taken the following day. The open porosity can then be calculated and expressed as a percentage by comparing the saturated weight, dry weight, and volume of the sample using the following equation:

$$P_o = \frac{m_s - m_d}{vol\ (cm^3)} \quad x\ 100$$

Where P_o = open porosity (%), m_s = saturated weight, and m_d = dry weight.

4.3.7 Water vapour diffusion resistance

The water vapour diffusion experiment was carried out at the Molema building, University of Glasgow. As previously discussed in the Introduction, the diffusion of water vapour through stone is essential to allow the free movement of water (and salts) and allow stone to dry thoroughly. The water vapour diffusion of sandstone samples is characterised here using a wet-cup test. The set up for the experiment is shown in Figure 4.4A. The test consists of selected materials which are secured onto containers which contain either distilled water or saturated solution (Figure 4.4B). The constructed sample is then placed into a controlled environment with specific RH and temperature (Figure 4.4). The difference in RH between the inside of the cup and the external chamber, leads to the diffusion of water vapour through a specified surface area, the rate of which is measured over time through changes in specimen mass.

The set up and procedure for this experiment was carried out according to the BS EN 12752:2016 standard. Three samples of A-C and three samples of A-L were prepared for the test. Sandstone dimensions for the experiment were 60 x 60 x 20 mm. After partly filling borosilicate glasses with distilled water, sandstone samples are secured onto glasses using tape and melted wax (60% microcrystalline wax and 40% paraffin wax). Care must be taken to ensure the sample is sealed to the container properly. The mass of the constructed samples is then recorded before being placed into a desiccator which is then placed inside an incubator maintaining a temperature of $21^{o}C \pm 1$. The RH inside the cup is 100 while the RH outside the cup (desiccator) is maintained at 45±5% using a saturated solution of potassium carbonate (K_2CO_3). Finally, as the maintained difference in RH between cup and desiccator is the driving force of the experiment, hygrochron ibuttons are placed inside the desiccator to continually monitor the temperature and RH throughout the experiment. The mass of the samples is recorded, and the ibuttons are checked every two days for four weeks. The wet-cup test is performed twice in this study, once prior to application of water repellent and once after application of water repellent, using the same samples. The water vapour diffusion resistance factor, μ, is calculated through a series of expressions described in Table 4.2.

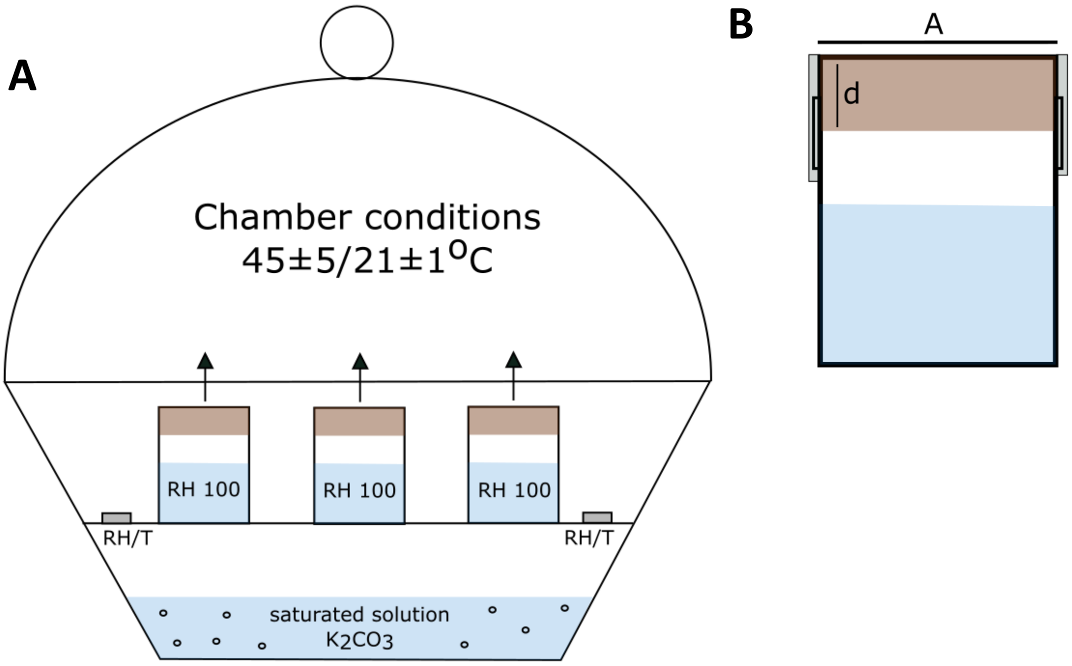

Figure 4.4: A) Experimental set up and conditions used for the wet-cup test. Each desiccator contained three samples in total; B) The sandstone samples, with measured thickness, d, are sealed to the cup using tape followed by melted wax. As well as securing the sample to the cup, the wax covers the exposed sides of the sandstone, therefore restricting the diffusion of vapour to the specified surface area, A.

Table 4.2: Summarising the series of equations used to determine the water vapour diffusion resistance factor, μ (Eq. 5).

Equation 1: mass rate change, $\triangle_m$	$\triangle_m = \frac{m_2 - m_1}{t_2 - t_1}$	$\triangle_m$ = change of mass per time for a single determination (kg/s); m_1 = mass of test assembly at time t_1 (s); m_2 = mass of test assembly at time t_2 (s). Water vapour flow rate, G, is then calculated as the mean of at least five successive determinations of $\triangle_m$.
Equation 2: Vapour pressure difference, $\triangle p$	$\triangle p = \Phi \cdot 610{,}5 \cdot e^{\frac{17{,}269\cdot\theta}{237{,}3+\theta}}$	Φ = RH, and θ = temperature (°C)
Equation 3: Water vapour permeance, W:	$W = \frac{G}{A \times \triangle p}$	Where G = water vapour flow rate through the specimen (kg/s), A = area of specimen (m^2), and $\triangle p$ = water vapour pressure difference.
Equation 4: Water vapour permeability, δ	$\delta = W \times d$	Where W = water vapour permeance [$kg/(m^2 \cdot s \cdot Pa)$] , and d = thickness of the sample (m).
Equation 5: Water vapour diffusion resistance factor, μ	$\mu = \frac{\delta air}{\delta}$	where δair = water vapour permeability of air at 23°C (for this experiment).

4.3.8 Capillary absorption

Cubic sandstone samples (length 50 mm) were used to characterise the capillary absorption a) before and after treatment with cream, and b) before and after salt weathering. The samples were placed in a shallow tray of water and the mass of the sample was measured regularly over the course of a day according to BS EN ISO 15148:2002. The rate of capillary absorption was measured in two directions, parallel and perpendicular with respect to bedding. During the experiment the difference between the mass per weighing over a given surface area is calculated using the expression:

$$\triangle\, m_t\ (kg/m^2) = \frac{m_t - m_i}{A\ (m^2)}$$

Where $\triangle m_t$ = rate of mass change, m_t = mass value at the time of the weighing, m_i = initial mass value, and A = specified surface area.

Then the capillary absorption coefficient, also known as the w-value, can then be calculated by dividing the capillary absorption rate by the square root of time ($\sqrt{t}$) as follows:

$$w - value\ (kg/m^2h^{0.5}) = \frac{\triangle\, m_t}{\sqrt{t}}$$

4.3.9 Ultrasonic wave velocities (V_p)

Compressive p-wave velocities (V_p) were measured on cubic samples using a Tektronix TDS 3012B 2 channel colour digital oscilloscope. An eco-gel visco-elastic couplant was used to allow for effective coupling of transducer and cubic sandstone sample. V_p was measured prior to, during, and at the end, of the salt weathering experiment (described below) to aid in determining the overall durability of untreated and treated samples.

4.3.10 Durability

The durability of untreated and treated samples was determined by conducting a salt weathering experiment. The experiment was carried out using a non-standard method according to Benavente et al (2001). The cubic samples (length 50 mm) were partially submerged in a Na_2SO_4 (conc. 14%) saline solution throughout the entire experiment, with the exception of a drying period which took place in an oven at 50°C between cycles. The samples were placed in the solution so that capillary uptake was parallel to bedding. The samples were subject to 20 temperature/RH cycles (10°C/90% and 20°C/50%) inside a climatic chamber. For each sandstone type, 12 samples were used where six were untreated and six were treated with the hydrophobic cream. Vp, described above was measured at the beginning of the experiment (prior to weathering), the middle of the experiment (samples containing salts), and the end of the experiment (samples containing salts, and salts extracted) to assess the extent of weathering. Finally, the porosity and capillary absorption coefficient was measured before and after weathering to evaluate the effectiveness and durability of the treatment.

4.4 Results and Discussion

4.4.1 Decay patterns at Arbroath Abbey

There are several prominent decay patterns present at Arbroath Abbey, as illustrated in Figure 4.5. Alveolization is probably the most common decay pattern on site, linked to the abundance of local sea salts (Figure 4.5A). Associated with alveolization are salt deposits and efflorescence (Figure 4.5B). Detachment patterns are also common, primarily blistering and delamination (Figure 4.5C-D). Delamination is associated with the weathering and detachment of stone layers along bedding planes. In these instances, the stones appear to have been placed where bedding is orientated parallel to the load of the building (Figure 4.5D). Finally, disintegration of stone via sanding and differential erosion is common (Figure 4.5E-F). Differential erosion occurs where stones weather much faster than the surrounding mortar material. Delamination and blistering are the most common decay patterns on the studied façade, including the treated test area.

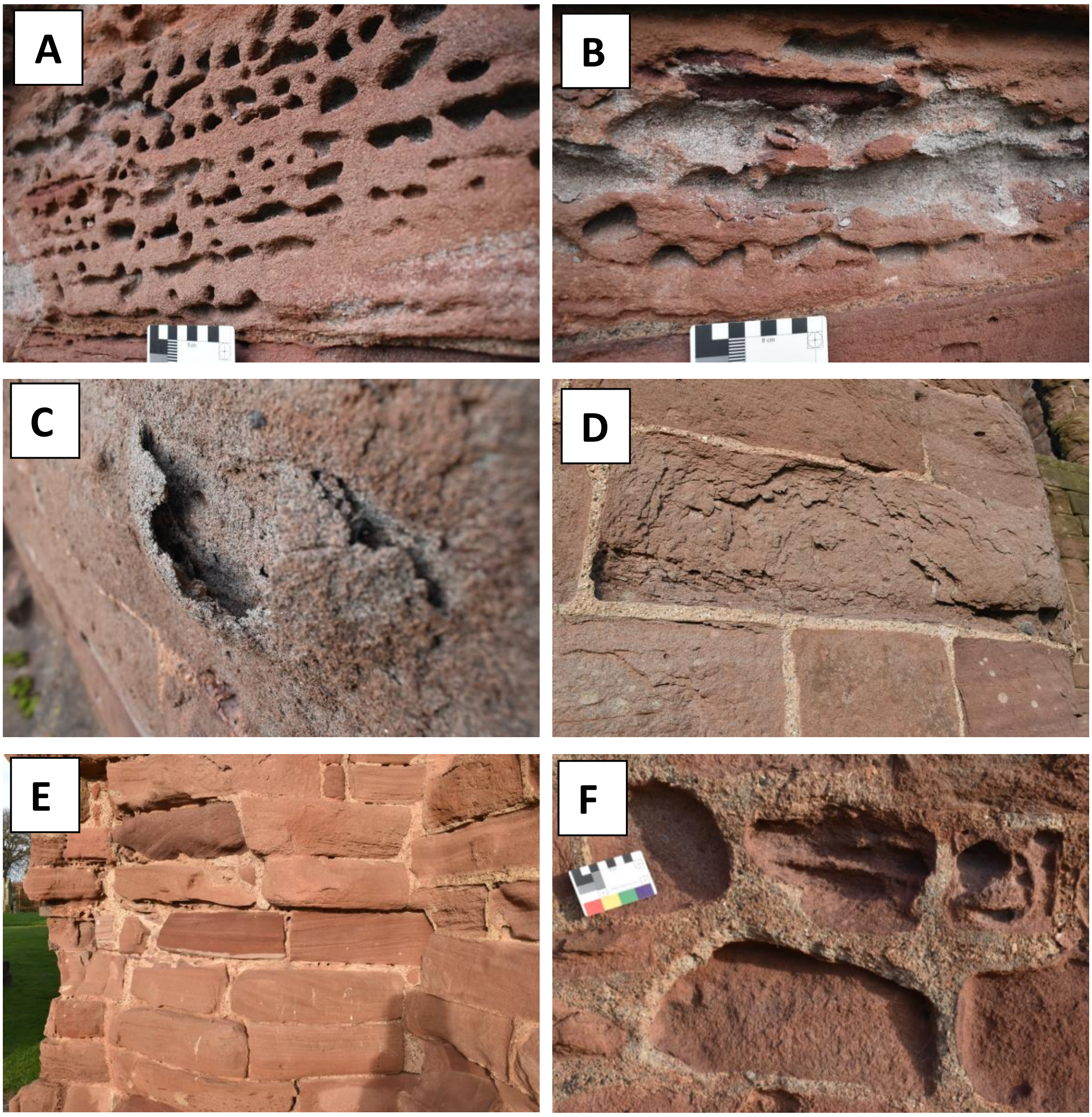

Figure 4.5: Prominent decay patterns identified at Arbroath Abbey. A = alveolisation; B = efflorescence and salt deposits; C = blistering*; D = lamination* (detachment of stone parallel to bedding); E = sanding; F = differential weathering. *Prominent patterns on studied façade, including treated test area.

4.4.2 Moisture mapping

Moisture analysis using a microwave moisture meter was carried out in a relatively dry and wet state. Figure 4.6 shows the entire façade in a dry state, including the treated area highlighted in the red box. As seen from the moisture map there are relative differences in moisture content across the façade. The lower stones of the façade appear to be relatively wetter perhaps indicating a degree of rising damp, which can often be associated with buildings which have a cemetery adjacent to them (Charola & Bläuer., 2015). This potential rising damp affects the treated area too as seen from Figure 4.6. In order to wet and reanalyse the area in a short time frame thus avoiding evaporation of water from wall (due to hot weather), a smaller area was wet and reanalysed as seen in Figure 4.7. Figure 4.7 shows the relatively dry and wet state of the treated and surrounding area. As seen from the red box there is a definite boundary where the stone is drier suggesting less moisture ingress upon wetting. This suggests that the treated area is still showing a degree of hydrophobicity around 45 years after its initial application.

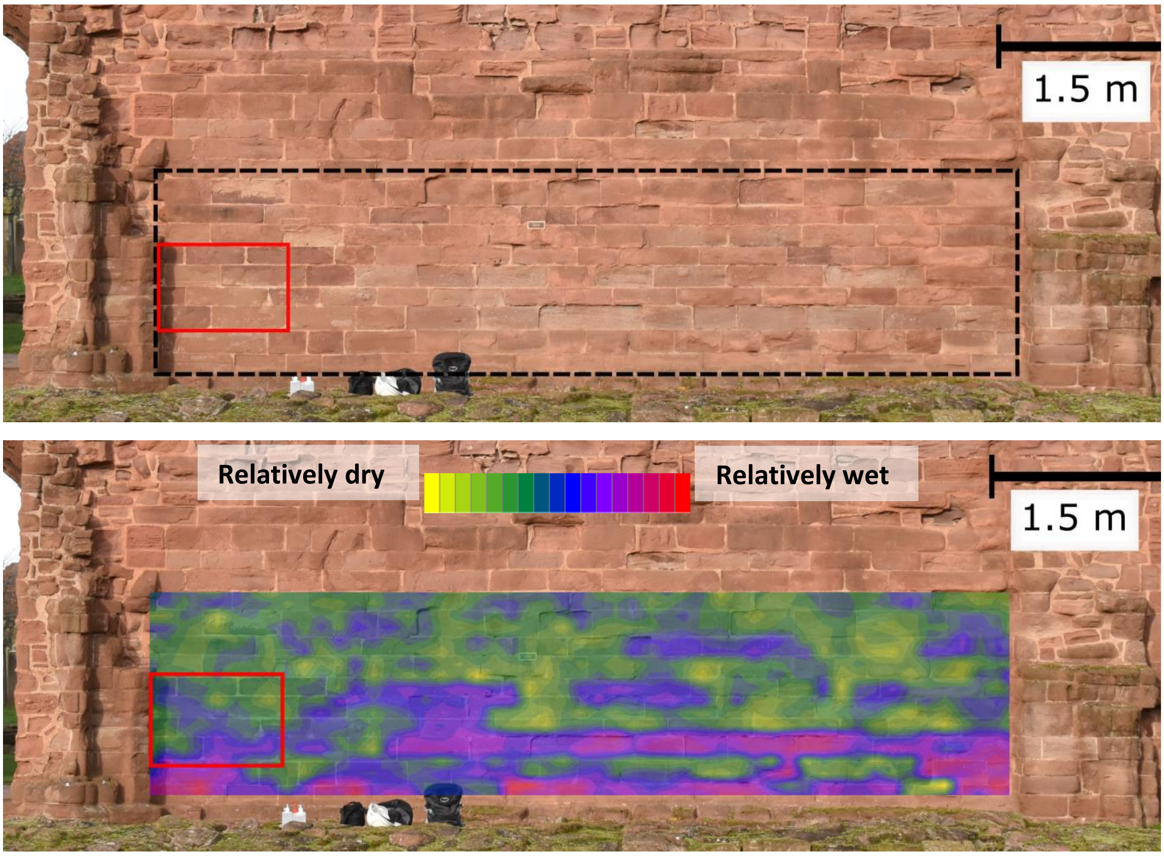

Figure 4.6: Relative dry state of the studied façade prior to any wetting. Yellow/green = relatively dry; pink/purple = relatively wet. Data in figure acquired using an 11 cm probe head.

Figure 4.7: Treated area before and after wetting of the façade. The box marks the boundary of the treated zone. Data in figure acquired an 11 cm probe head.

4.4.3 Mineralogy and Petrography

Overall both sandstones, A-C and A-L, have a similar bulk mineralogy compared to one another as seen from XRD results (Figure 4.8). The differences between the interior and the crust for each sandstone is also very small, however, the crust appears to have relatively more clay as seen from the higher, well defined clay peaks in the bulk analysis (Figure 4.8).

The primary difference between sandstones A-C and A-L is the occurrence of smectite in A-C which is absent in A-L as seen from the analysis of the extracted clay fraction (Figure 4.9). Due to overlapping peaks in the diffractograms, the type of expansive clay has been narrowed down to either: montmorillonite, nontronite, or vermiculite.

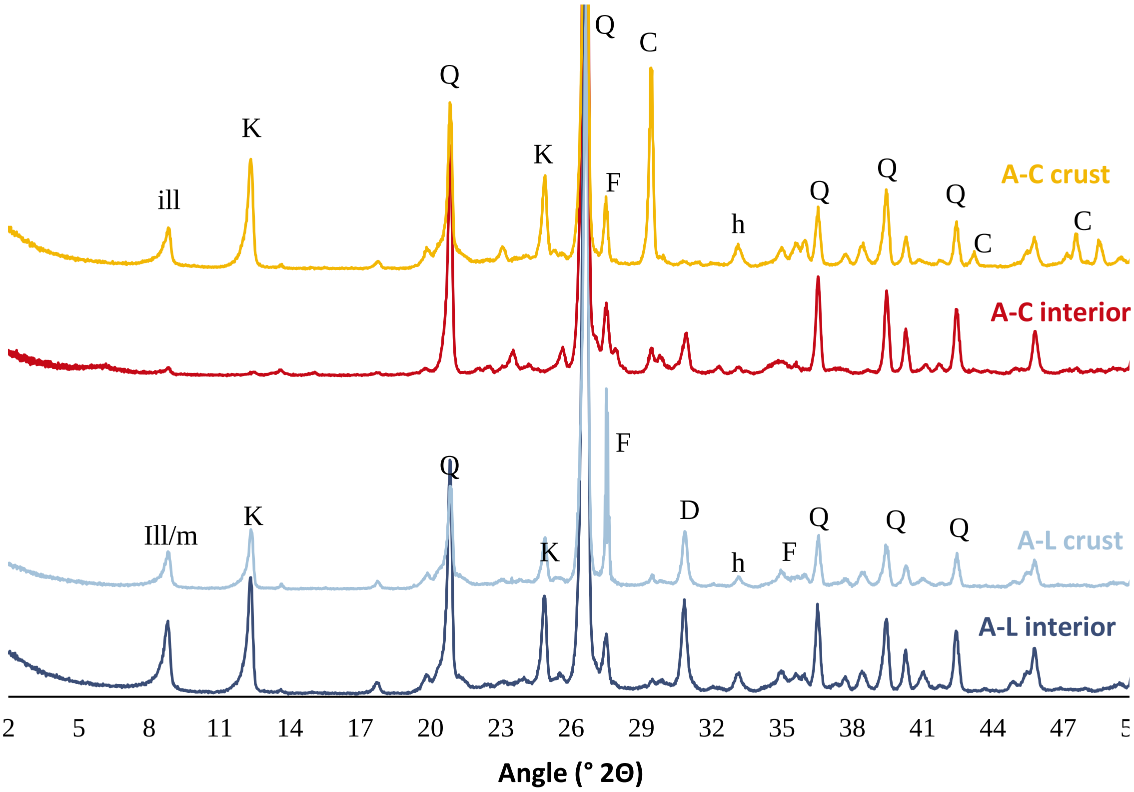

Figure 4.8: Bulk mineralogy of interior and crust samples of both A-C and A-L. Q = quart; F = feldspars; K = kaolinite; ill = illite; m = muscovite; C = calcite; h = haematite.

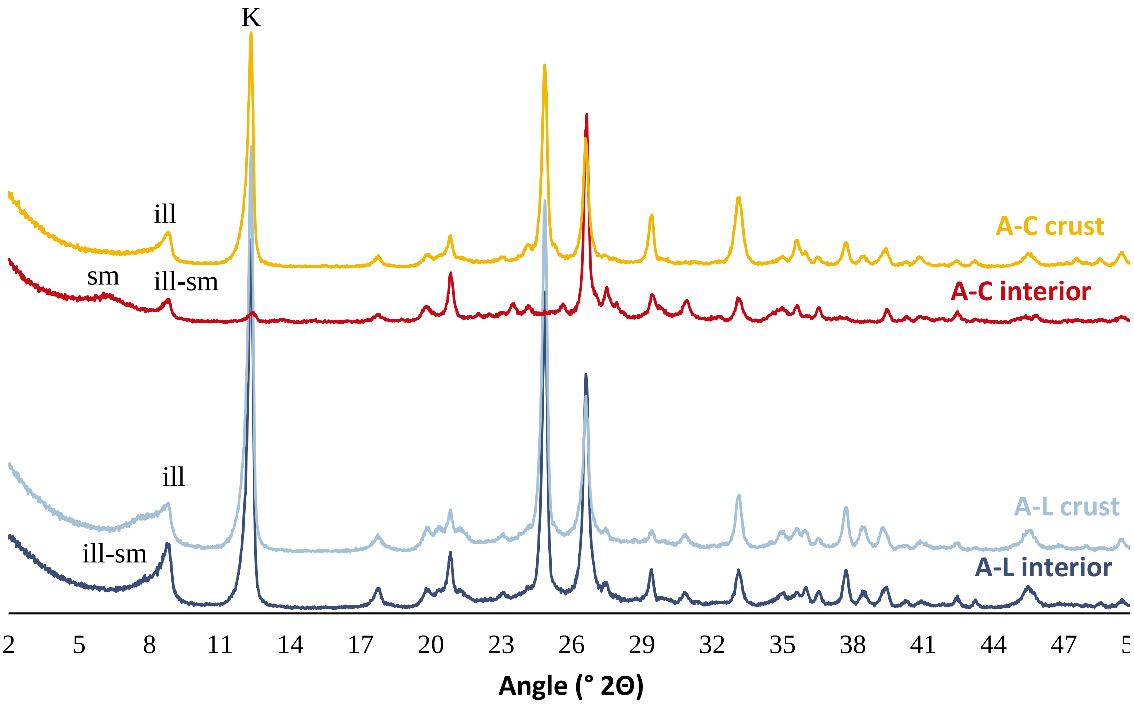

Figure 4.9: Clay mineralogy of interior and crust samples of both A-C and A-L. K = kaolinite; ill = illite; sm = smectite; illite-sm = interstratified illite=smectite.

Although present in the interior sandstone sample of A-C, smectite was consistently absent in the crust (first 5 mm of stone). The clay mineralogy of the crust is dominated by kaolinite. This spatial difference in clay mineralogy implies that the in-situ weathering of the building stone over time has altered the clay mineralogy at the stone surface, creating a clay-mineral profile through the stone. Smectite-kaolinite is a known weathering pathway in sediments and sandstones, primarily driven by the weathering of feldspars (Figure 4.10). Previous research has identified weathering profiles in building stone through analysis of total feldspar content, and cation exchange capacities (CEC) (Mausfeld & Grassegger., 1992; Schäfer & Steiger., 2002). Schäfer & Steiger (2002) attribute a lower CEC close to the surface to a reduction in mineral surface area associated with clay dissolution. The clay mineralogy of A-L is similar in both the interior and crust samples which both show the presence of mainly kaolinite. Salts extracted from weathered sandstone near the treated site are halite and gypsum (Figure 4.11); typical coastal salts which are not considered aggressive relative to other salts with regards to stone decay, but nonetheless will weathering stone over time.

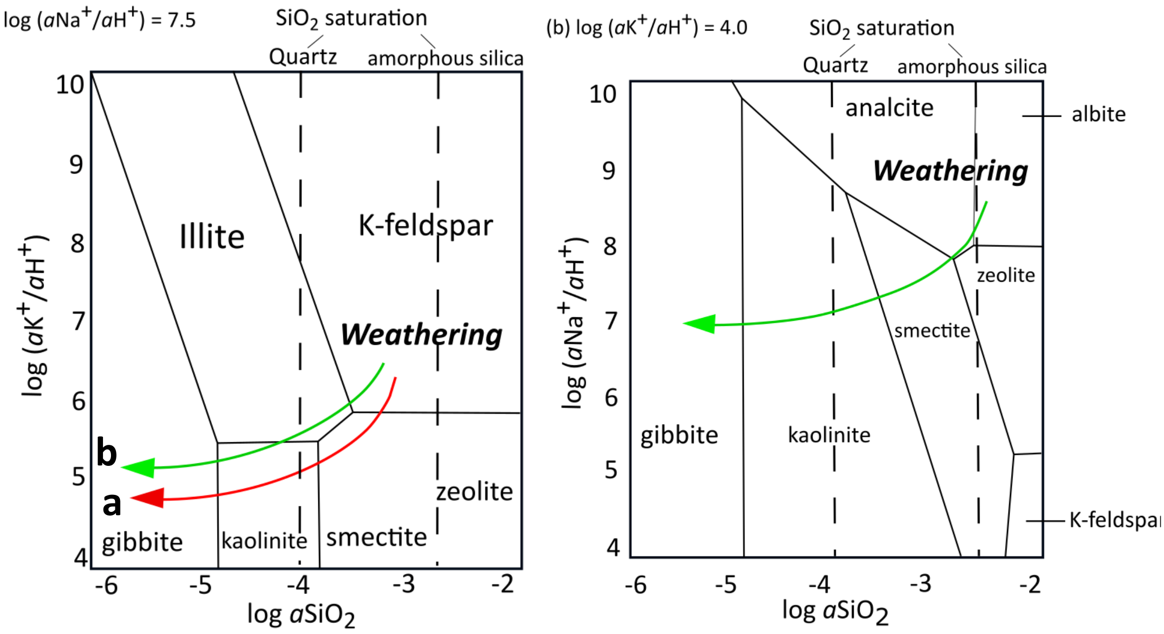

Figure 4.10: Common smectite-kaolinite weathering pathways. Figure adapted from McKinley et al (2003) (after Drever, 1982). (a) high pH or low potassium; (b) higher pH or high metal concentrations in fluid.

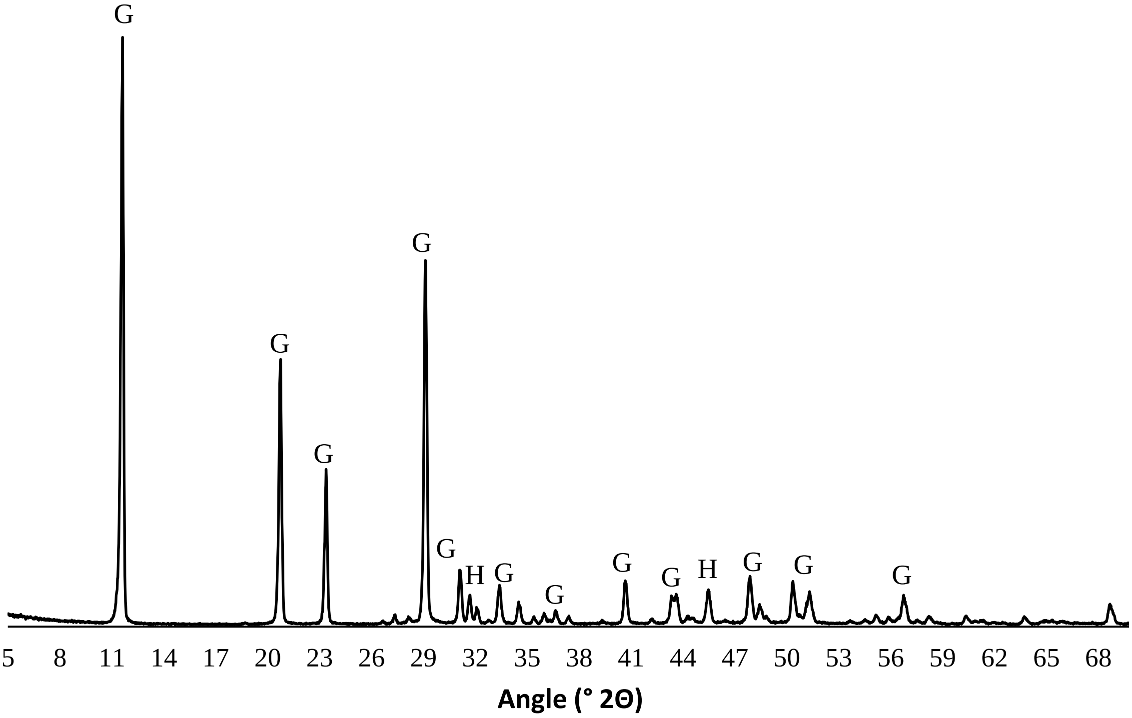

Figure 4.11: Salts extracted from weathered salt enriched crust located near the treated area. The dominant salt is gypsum with some halite also present. G = gypsum, H = halite.

The texture and fabric of the sandstones were analysed by Backscattered Electron (BSE) and Secondary Electron (SE) imaging using SEM. In addition to XRD, the mineralogy was characterised further using Energy Dispersive X-ray (EDX) mapping, and results are shown in Figure 4.12. EDS shows the composition of the feldspar grains, where A-L contains mostly orthoclase while A-C contains both orthoclase and albite. EDX mapping also shows the composition of the any material within the pore network. A-L pores are mostly filled with a Al-rich (clay) matrix, while calcite cements are more common in A-C pore network.

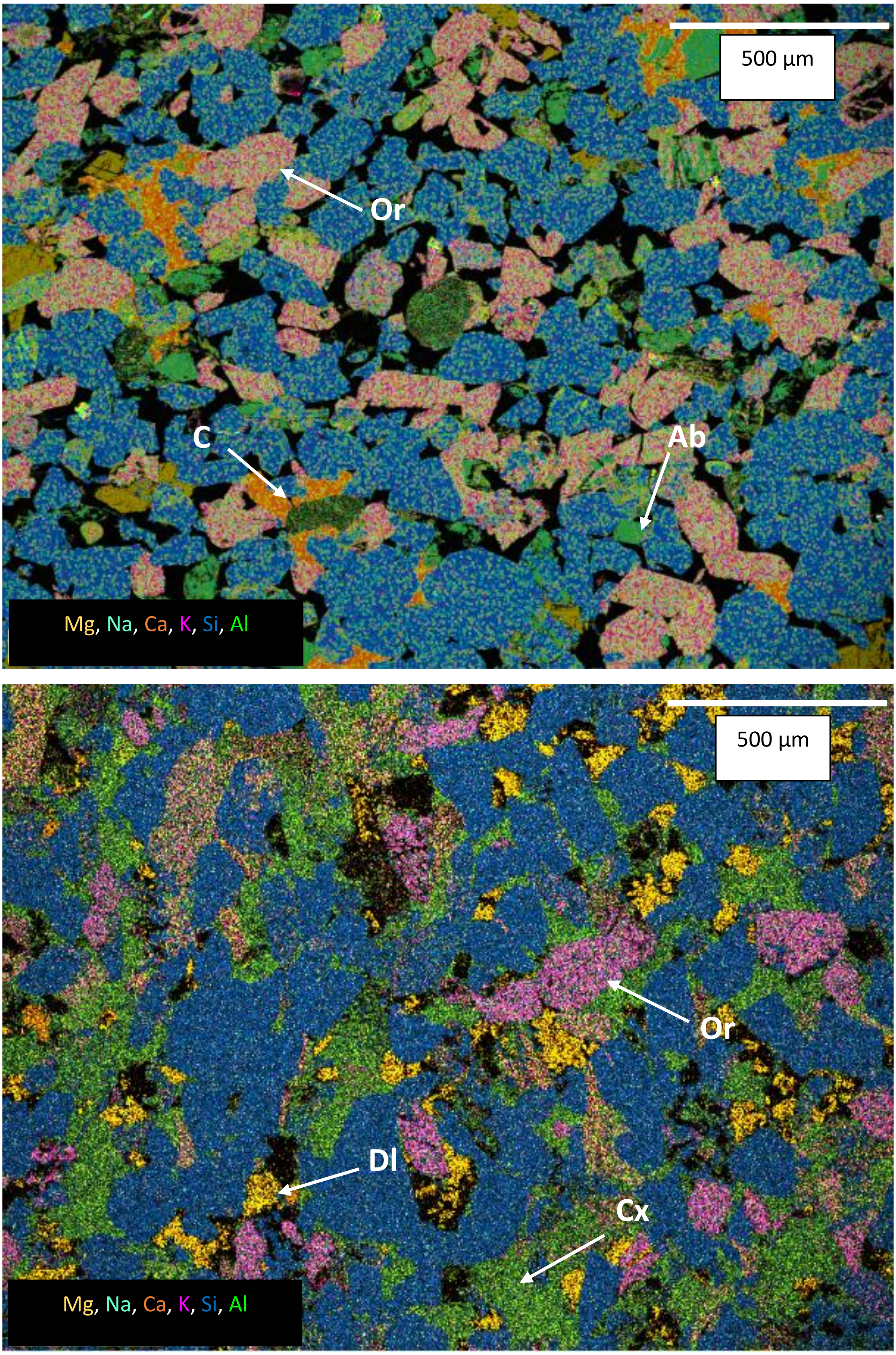

Figure 4.12: EDX mapping showing petrography of A-C (top) and A-L (bottom). A-L has much more clay-rich matrix material represented by the colour green (Al). The feldspar fraction of both sandstones is primarily orthoclase and albite, although A-L contains mostly orthoclase. Or = orthoclase; Ab = albite; C = calcite; Dl = dolomite; and Cx = clay matrix.

BSE and SEM analysis was carried out on thin sections and sandstone chips which reflect the interior of both stones. The average grain size of A-C is 0.11 mm. Grain shape is subrounded where grain boundaries show long and concavo-convex contacts (Figure 4.13D). The matrix is sparse however calcite is present both in the matrix and as a cementing material (Figure 4.13D). There is a higher proportion of lithic grains relative to A-L. Lithic grains have weathered extensively, leading to the formation of clay minerals with smectitic morphology (Figure 4.13A-B). The sandstone is poorly sorted and classified as a lithic arkose.

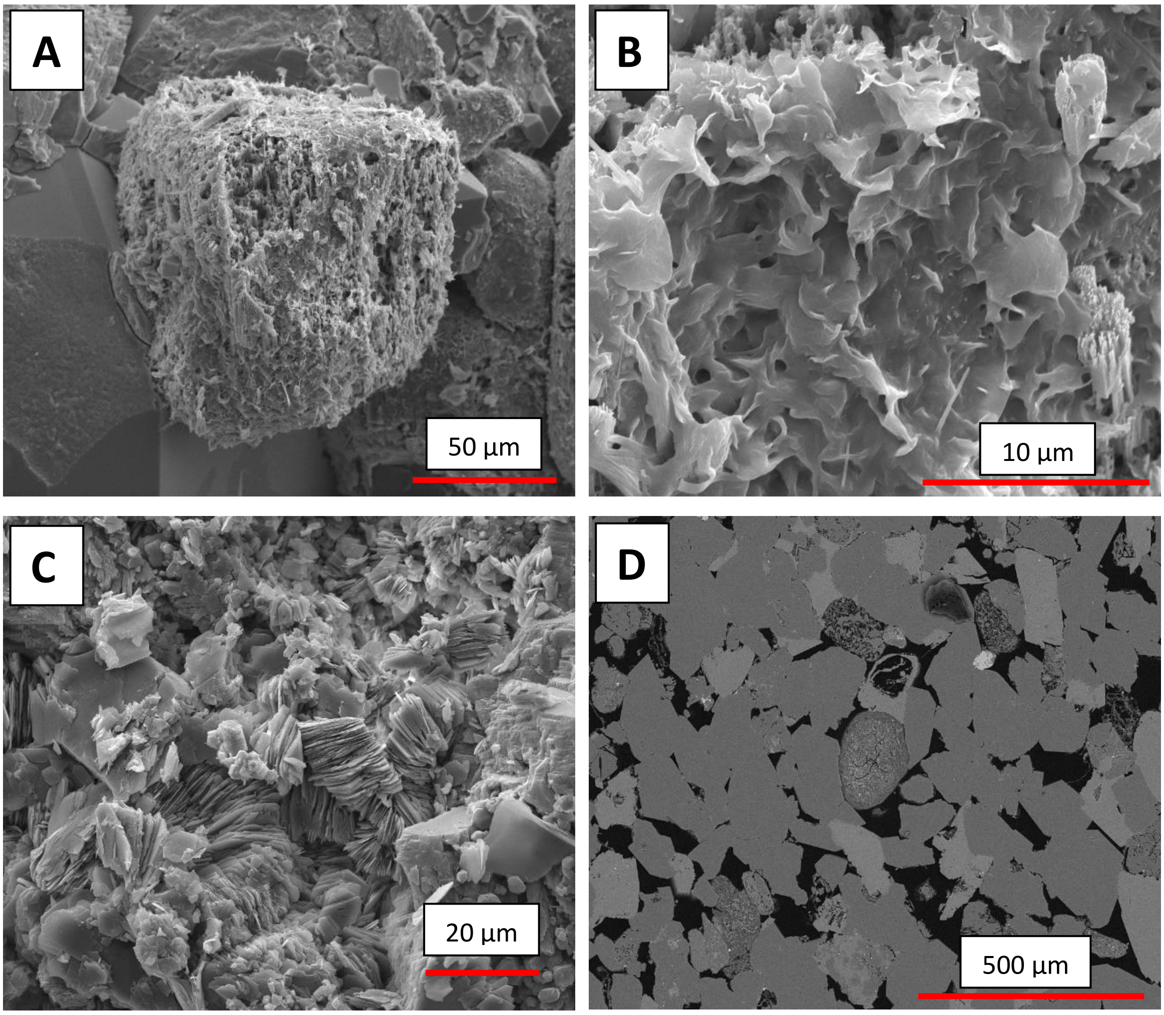

Figure 4.13: SEM images of A-C chips (A-C) and polished thin sections (D). A: Weathered lithic grain leading to formation of clay mineral with smectitic morphology; B: Smectitic morphology; C: Preservation of some kind of clay mineral transformation thought to be smectite-kaolinite; D: Thin section of A-C showing weathered lithics (centre) and mostly empty pore space (black).

The average grain size of A-L is 0.15 mm. Grain shape is angular to sub-rounded and grain boundaries show point and long contacts (Figure 4.14C). The matrix and cements consist primarily of clay minerals which are mostly kaolinite (Figure 4.14C-D). The extent of weathering is greater in A-L relative to A-C as shown by the extent of mineral alteration and open pore space. Feldspars and lithic grains weather mostly to kaolinite (Figure 4.14B). Analysis of A-L sandstone chips also showed textures which appear to have preserved clay mineral transformation of a more smectite-like clay to kaolinite (Figure 4.14A), an observation consistent with the idea that smectite-kaolinite is a common clay mineral transformation for Arbroath stones. The greater extent of weathering in A-L may explain the absence of smectite which has mostly weathered to kaolinite, as well as illite-smectite, and illite. A-L is poorly sorted and classified as a lithic arkose. The petrography of A-L and A-C is summarised in Table 4.3.

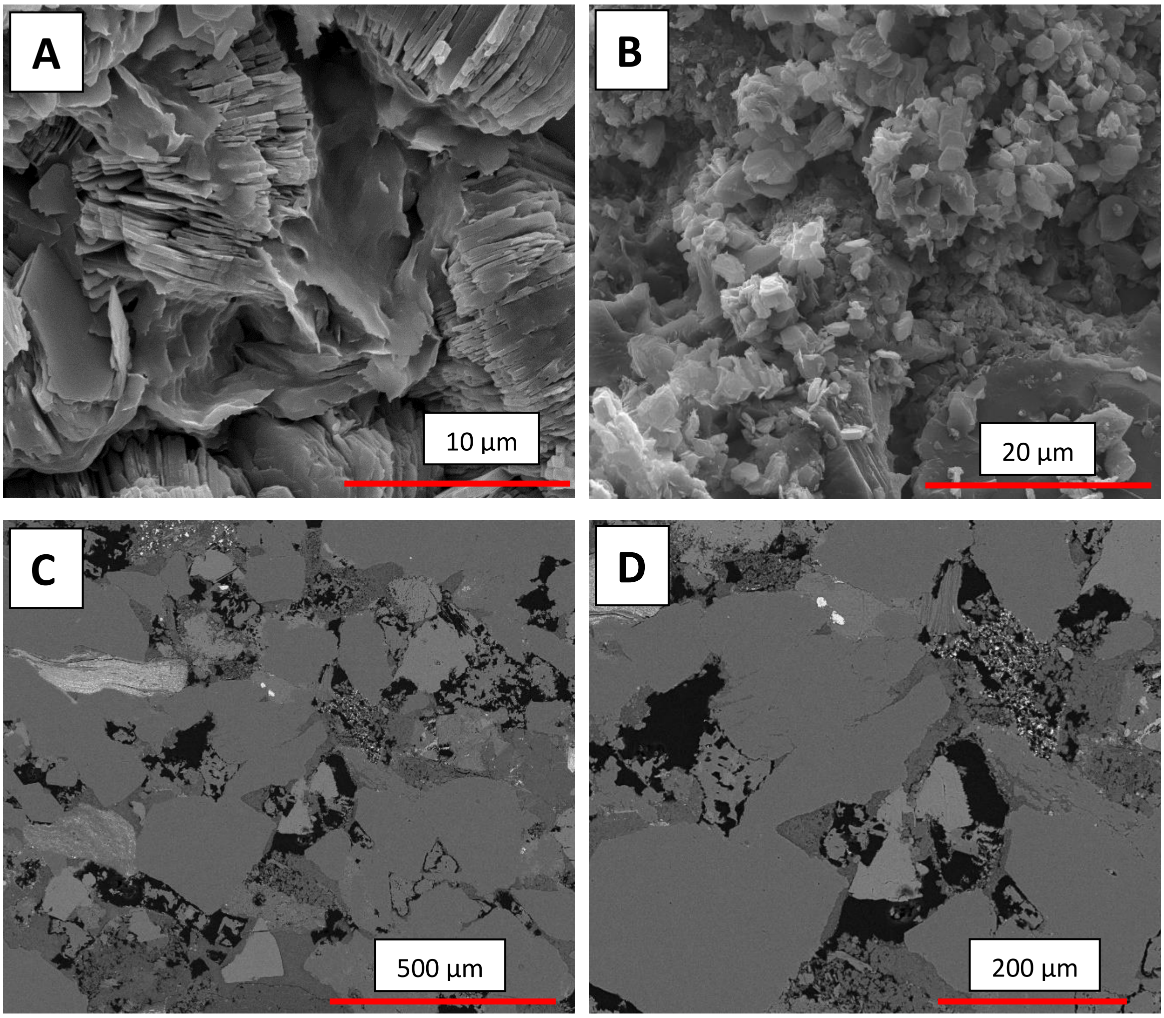

Figure 4.14: SEM images of A-L chips (A-B) and polished thin sections (C-D). A-B: Kaolinite stacks representing most common clay mineral found in A-L; C: Thin section image showing highly weathered state of A-L as well as very poor sorting; D: Thin section image highlighting distribution of clay minerals which is mainly coating grains, lining pores, and partially infilling pores and pore throats.

Table 4.3: Summary of the mineralogy and petrography of A-C and A-L based on XRD and SEM results.

	A-C		A-L	
	Interior	*crust*	*interior*	*crust*
Bulk mineralogy	Quartz; albite; orthoclase; calcite; dolomite	Quartz; albite; orthoclase; calcite; haematite; kaolinite; illite	Quartz; albite; orthoclase; dolomite; mica; kaolinite; illite; haematite	Quartz; albite; orthoclase; dolomite; mica; kaolinite; illite; haematite
Clay mineralogy	kaolinite; smectite (expansive); illite-smectite (non-expansive)	kaolinite; illite	illite-smectite (non-expansive); kaolinite	kaolinite; illite
Clay distribution	Weathered lithics; weathered feldspars; lining pores	Infilling pores; coating grains	Matrix; grain coatings; weathered feldspars	Matrix; infilling pores; coating grains
Average grain size (mm)	0.11		0.15	
Sandstone classification	Lithic arkose		Lithic arkose	

4.4.4 Open Porosity

The open porosity varies considerably from 11.5 % to 21.8 %, and 13.9 % and 23.2 %, for A-C and A-L, respectively (Table 4.4). The average porosity for A-C is 14.7% and the average porosity of A-L is higher at 19.3 %. As seen from Figure 4.15 there is a relationship between porosity and bulk density, with higher porosity samples having a lower bulk density. This lower density reflects the relative abundance of open pore space in comparison to low porosity samples.

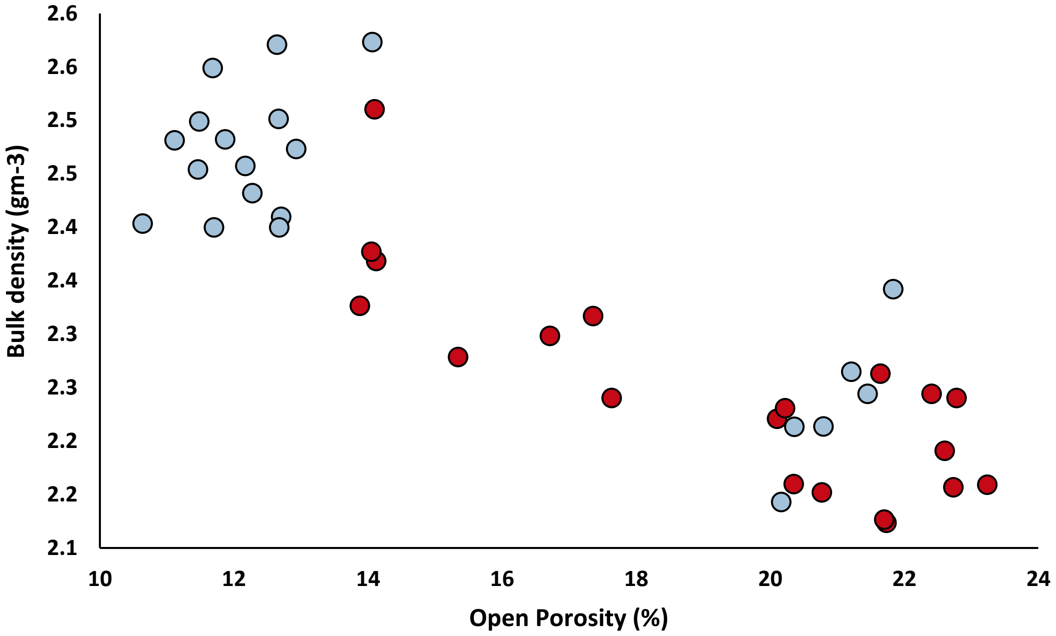

Figure 4.15: The relationship between bulk density and open porosity of A-C and A-L subsamples. Blue circles = A-C, red circles = A-L

Table 4.4: Average open porosity, bulk density, and capillary absorption coefficient before (C$_U$) and after treatment (C$_T$). Initially the samples were measured parallel (-) and perpendicular (+) to bedding, to understand the degree of sandstone anisotropy with regards to capillary absorption. After treatment, the samples are measured parallel to bedding only. This direction is selected as it reflects the orientation of bedding-water interactions in most buildings. Consequently, transport of water and efficiency of any treatments are best evaluated in this direction.

	Porosity, *P* (%)	**Bulk density (g/m^3)**	**Capillary absorption Coefficient, C_U (kg m^2 h$^{0.5}$)**		**Capillary absorption Coefficient, C_T (kg m^2 h$^{0.5}$)**
			-	+	-
A-C	14.7 SD = 4.16 (21)	2.39 SD = 0.12 (21)	0.95 SD = 1.69 (6)	0.17 SD = 0.23 (6)	0.37 SD = 0.22 (6)
			-	+	-
A-L	19.3 SD = 3.37 (21)	2.24 SD = 0.10 (21)	1.98 SD = 0.28 (6)	1.49 SD = 0.41 (6)	0.24 SD = 0.11 (6)

4.4.5 Capillary absorption

There was considerable variation in the capillary absorption rates between and within sandstones, A-C and A-L. This variation is likely linked to the porosity differences between individual samples of the same block. Overall, A-L has a faster average rate of capillary absorption, and so higher capillary absorption coefficient (Table 4.4). Both samples show a degree of anisotropy – variation in capillary absorption rates when measured in two different directions. Both sandstones show a faster rate of capillary absorption when measured parallel to bedding, where water can be absorbed along bedding planes. The anisotropic behaviour of bedded sandstones related to capillary absorption is well documented in literature (Ruedrich & Siegesmund., 2007; Sebastián et al., 2008; Benavente et al., 2008; Zhao & Plagge., 2015; Fořt., 2015). The degree of anisotropy is calculated using the maximum value divided by the minimum value for a given measured properties. Therefore, values close to 1 indicate a homogenous stone, where there is little to no variation, and values close to 0 indicate a heterogenous stone, where there is considerable variation for a given measured property. The anisotropy is stronger in A-C at 0.18 in comparison to A-L at 0.75.

Finally, the capillary absorption of A-C and A-L was measured after the samples were coated with the hydrophobic treatment. The capillary absorption after treatment was only measured in the direction parallel to bedding, as this is reflective of the direction moisture ingress would occur in reality at the Abbey. The overall aim of the treatment is to reduce the rate of capillary absorption of the treated sample to as low as possible. The capillary coefficient of A-C and A-L was reduced, on average, by 61 % and 88 %, respectively (Table 4.4). The efficiency of the treatment in reducing the capillary absorption of A-C and A-L was variable. Overall, the treatment was less effective in reducing the capillary absorption of A-C relative to A-L. (Table 4.4). The higher capillary absorption coefficients of treated A-C samples imply a lower penetration depth of the hydrophobic treatment. As the application process of the treatment was identical for all samples, the lower penetration depth associated with A-C is ultimately driven by the petrophysical properties of the stone including lower capillary absorption (prior to treatment) and lower porosity, relative to A-L. This trend was similar when comparing sandstone samples from the same block, where the treatment was less effective in reducing the capillary absorption of samples which had a lower porosity and lower capillary absorption rate prior to treatment (Figure 4.16). The variability in physical properties of individual stones and their response to the hydrophobic treatment highlights some potential issues with regards to large scale treatment of stone at Arbroath Abbey. Despite the uniform application of treatment, variations in physical properties between and within individual stones may lead to differences in the efficiency of a hydrophobic treatment. The potential variation in treatment efficiency may make certain stones more susceptible to weathering and exacerbate differential weathering.

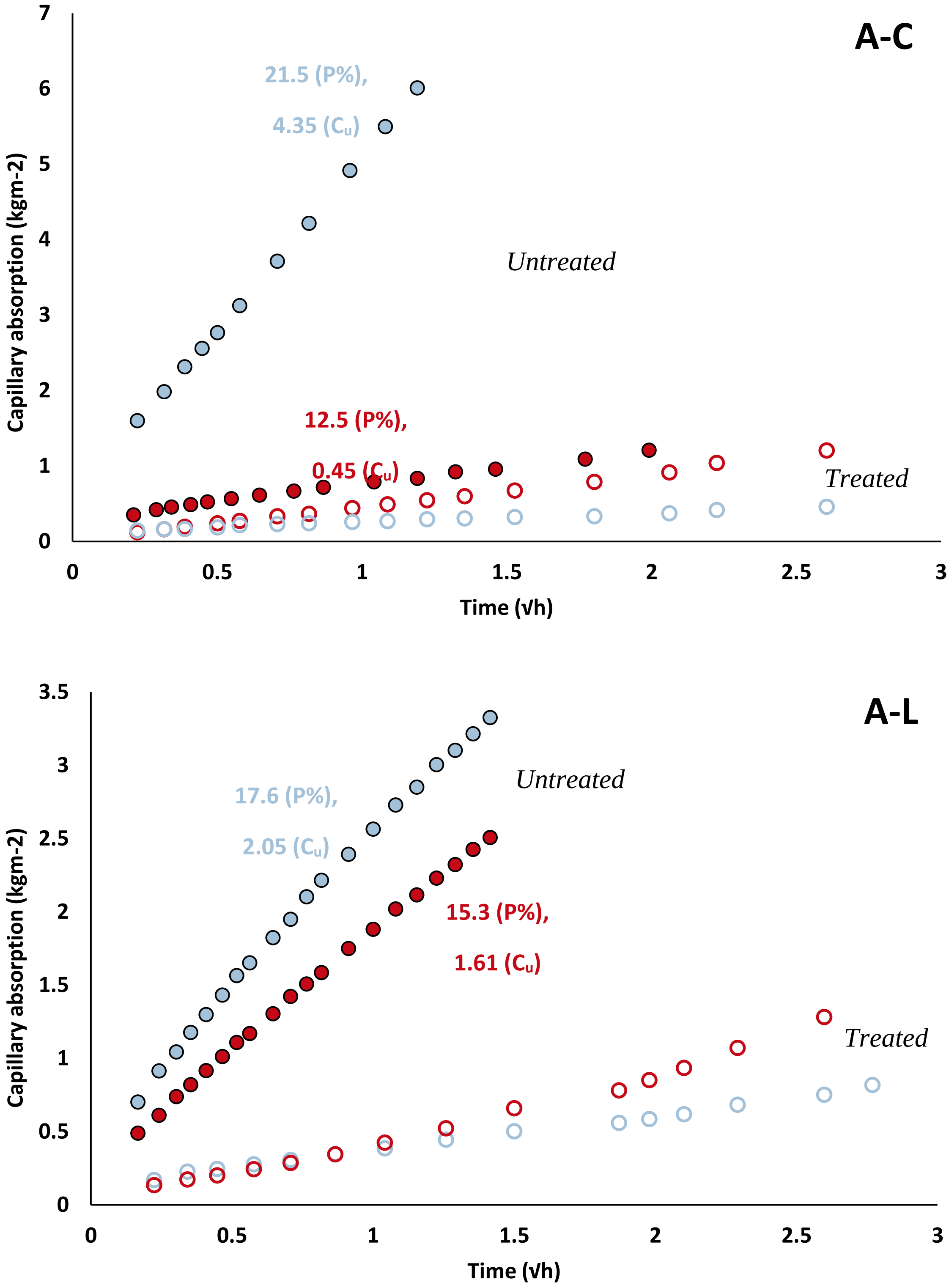

Figure 4.16: Capillary absorption of a) A-C (high and low porosity examples) before and after treatment, and; b) A-L (high and low porosity examples) before and after treatment.

4.4.6 Vapour diffusion resistance

The assessment of water vapour diffusion resistance is considered an essential method of understanding the compatibility of a given stone and hydrophobic treatment (Snethlage., 2011; Ludovico-Marques & Chastre., 2014). The water vapour diffusion resistance factor was calculated before and after treatment using the same samples. The resistance factor and associated porosity of each sample is shown in Table 4.5. An increase in the diffusion resistance up to ~ 20% is considered acceptable according to Snethlage (2011). As seen from Table 4.5, A-C3 is the only sample which surpasses a 20% increase in resistance after treatment. This compares to sample another sample from A-C, A-C1, where resistance increases by only 4%, again, highlighting the implications that variations in physical properties associated with heterogenous stone can have on the efficiency and compatibility of a hydrophobic treatment. Similarly, A-L shows variation in % change of resistance ranging between 4-15% increase.

Table 4.5: Vapour diffusion resistance factor before and after treatment with hydrophobic coating.

	Resistance factor, μ	**Resistance factor, μ_t**	**Change in resistance, %**	**Porosity**
A-C1	42.3	44.1	4.1	11.5
A-C2	50.1	58.3	14.1	11.7
A-C3	32.6	41.1	20.7	10.6
A-L1	27.1	28.1	3.6	22.8
A-L2	23.7	26.8	11.6	22.6
A-L3	31.2	36.7	15	17.4

4.4.7 Durability (salt weathering experiment)

Decay is quantified as the percentage of material lost at the end of the experiment. Figure 4.17 shows the typical relative changes in mass of a sample throughout the experiment. The mass during the experiment (7th cycle) and at the end prior to salt extraction (20th cycle) is higher than the original mass. This difference represents the presence of crystallised salts within the sample. After salt extraction at the end of the experiment the mass is (usually) lower than the original weight if weathering has occurred.

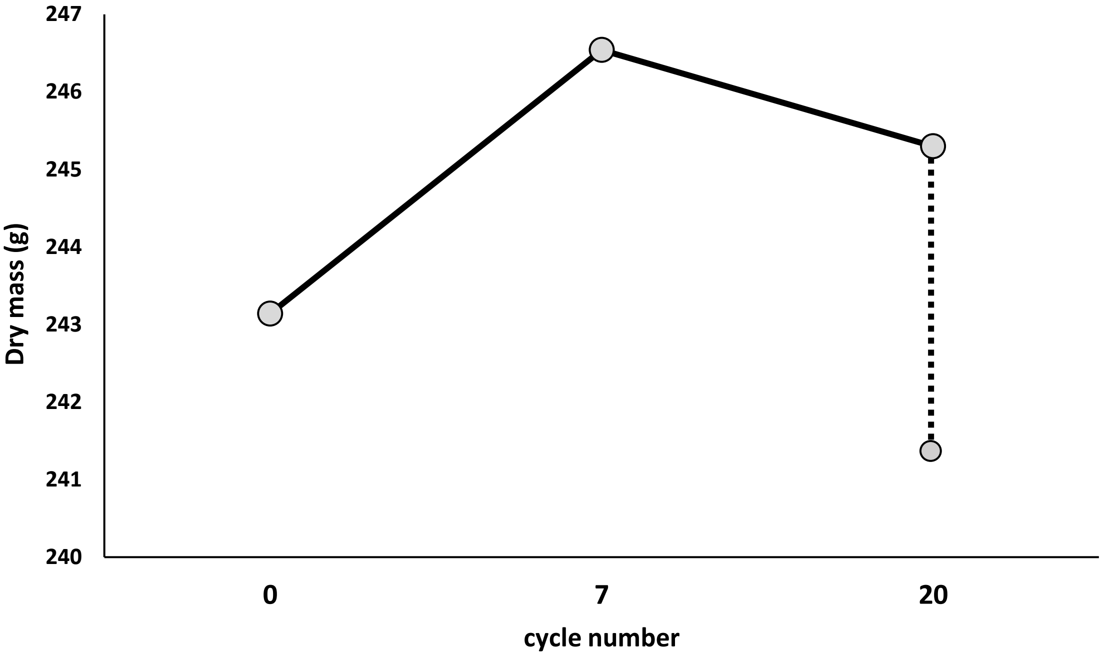

Figure 4.17: Example of one sandstone sample illustrating the relative changes in mass throughout the salt weathering experiment. The mass during the experiment (7th, 20th cycles) is higher than the original mass due to the presence of salts. The final mass obtained after cycle 20 is after removal of salts.

Overall, untreated samples were more susceptible to decay for both A-C and A-L as reflected by the higher values of percentage decay (Figure 4.18). The values for decay of the treated samples are all negative suggesting the presence of salts within pores after salt extraction (Table 4.6). However, sandstones commonly contain some salts even after salt extraction. Overall, it is likely that the treated samples also experienced less decay relative to the untreated samples due to the hydrophobic treatment. For both treated and untreated samples, visually the decay is very minor and unnoticeable, where decay usually manifests as granular disintegration. For most individual samples, Vp is less after weathering reflecting an increase in pore space associated with weathering (Table 4.6). In some individual cases the Vp is higher after the experiment which may reflect the presence of salts within samples. Generally there is not much difference in the behaviour of Vp between treated and untreated samples.

A-L was slightly more susceptible to decay in comparison to A-C as represented by the higher values of decay associated with A-L (Table 4.6). The higher susceptibility of A-L to weathering may be linked to the original porosity of the stone which is, on average, slightly higher than that of A-C (Figure 4.18). Porosity of untreated samples was slightly higher after weathering reflecting more open pore space due to decay. The porosity of treated sandstone samples was slightly lower after weathering, implying the presence of salts and/or that little weathering has taken place.

On average, and for most individual samples, the capillary absorption coefficient is higher after salt weathering suggesting an increase in porosity leading to an increase in capillary absorption (Table 4.6). A-L samples (both treated and untreated) experienced a higher percentage increase in capillary absorption on average compared to A-C. Again, this probably related back to the slightly higher open porosity of A-L. There is little difference in the capillary absorption increase after weathering when comparing treated and untreated samples.

Table 4.6: Summary of salt weathering results: Average values for, open porosity (P%); p-wave velocities (Vp); capillary absorption coefficient (C) before and after salt weathering, and decay as a result of weathering expressed as percentage weight loss (d %).

	A-C$_U$	**A-C$_T$**	**A-L$_U$**	**A-L$_T$**
P%	15.4	14.9	17.9	19.7
	SD = 4.38 (6)	SD = 4.40 (6)	SD = 4.31 (6)	SD = 3.52 (6)
P%$_w$	16.0	14.0	18.5	19.3
	SD = 4.22 (6)	SD = 4.55 (6)	SD = 4.96 (6)	SD = 3.62 (6)
Vp	3219.6	3546.0	3206.1	3284.6
	SD = 433.8 (6)	SD = 399.6 (6)	SD = 279.3 (3)	SD = 162.8 (6)
V*p*$_w$	3114.4	3359.0	3117.8	3133.4
	SD = 215.7 (6)	SD 287.2 (6)	SD = 104.5 (6)	SD 160.2 (6)
C	1.65	0.34	1.33	0.27
	SD = 1.86 (6)	SD = 0.22 (6)	SD = 0.55 (6)	SD = 0.07 (6)
C$_w$	2.30	0.42	1.57	0.34
	SD = 2.05 (6)	SD = 0.29 (6)	SD = 0.55 (6)	SD = 0.13 (6)
d (%)	0.32	-0.25	0.42	-0.16
	SD = 0.15 (6)	SD = 0.17 (6)	SD = 0.20 (6)	SD =0.10 (6)

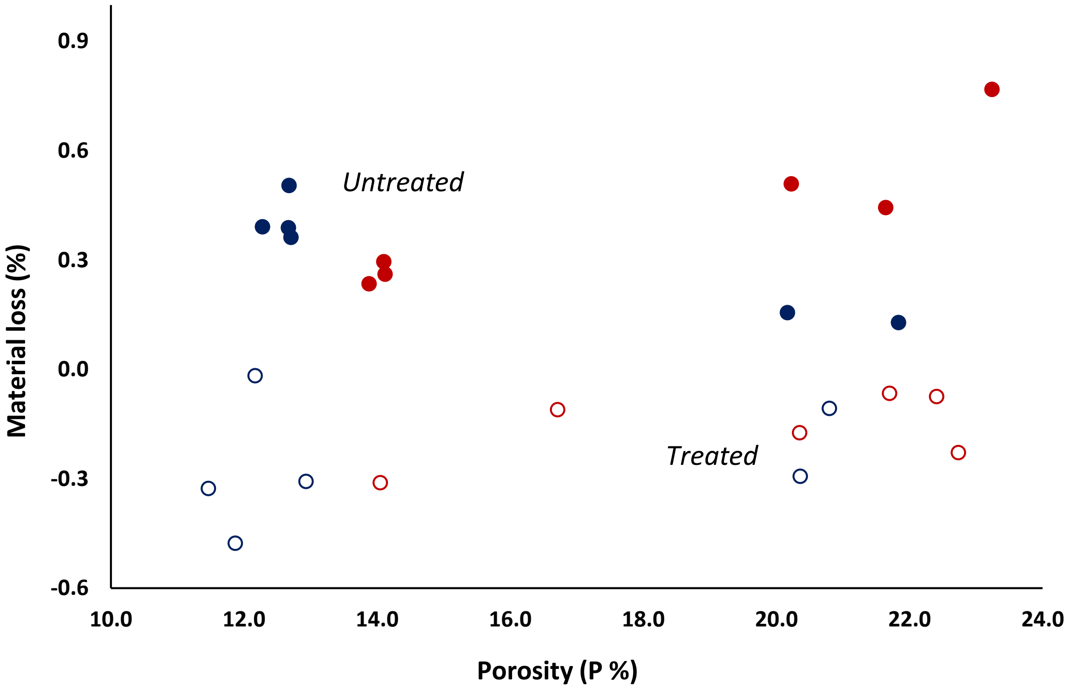

Figure 4.18: The relationship between open porosity and material loss (decay). Treated samples were less prone to decay overall while untreated samples experiences relatively higher amounts of decay. Note negative values imply presence of salts in addition to less decay.

4.5 Final Discussion and Conclusions

On average both stone types at Arbroath, A-C and A-L, experienced less weathering after being coated with a hydrophobic treatment. Moreover, moisture mapping also showed promising results suggesting that such protective coatings can perform over decades without any obvious detrimental impact to stone integrity. However, some of the results presented in this study suggest that such treatments can be unsuitable in the case of heterogenous sandstone, such as that found at Arbroath Abbey.

Firstly, the differences in intrinsic stone properties between A-C and A-L , mainly porosity and capillary absorption, affect the performance of the hydrophobic treatment. For example, due to the higher porosity and capillary absorption rates of A-L, the treatment is able to penetrate deeper into the sample during application, reducing the capillary absorption far more effectively than in the case of A-C. Furthermore, petrophysical properties and mineralogy vary within individual stone types. For example, the open porosity of A-C varied between ~ 11 and 21 %, and the vapour diffusion of the same stone varied between X. All of these difference between and within individual samples means that despite an identical application approach, individual blocks of stone can respond very differently when such a treatment is applied on site. Different responses to treatment could lead to differential weathering caused by some parts of the façade being better protected than other parts. Differential weathering is a concern commonly mentioned in literature regarding hydrophobic treatments, especially in the context of heterogenous stone types(Charola., 2001; Angeli et al., 2007; McKinley & Warke., 2007; McAllister et al., 2016; Zoghlami et al., 2017).

Mineralogical results from this study have interesting implications for sampling at heritage sites. As stone decay studies often deal with valuable materials, sampling can be heavily restricted. For this reason, small samples of crust or highly weathered samples are often used for XRD and SEM characterisation of mineralogy. However, as seen from this research these weathered samples may not be reflective of the overall mineralogy of the stone, especially in the case of less stable expansive clays which may have weathered at the surface but still be present in the interior of the stone. This sampling issue may mean that smectite is underrepresented in many previous stone characterisation studies.

Overall, sourcing a single hydrophobic product which is equally compatible with every stone at a given site is unrealistic, especially in cases such as Arbroath where sandstone is heterogenous. In the case of Arbroath Abbey, the efficiency of treatment varies between stones A-C and A-L and within individual stone types. Despite some of the obvious drawbacks of hydrophobic treatments associated with these stone types, such options may need to be considered more seriously in Scotland as a result of climate change. Increases in precipitation and intensity of precipitation may enhance moisture ingress and lead to prolonged stone wetness. It is therefore, imperative to continue to explore any options which potentially limit the amount of moisture penetrating the stone. This may be especially important for built sites of extreme cultural value and significance which are very close to ruin and where alternative suitable conservation methods have not been identified.

4.6 Recommendations for HES

- When carrying out sampling try to obtain samples from both the outer crust and interior of the stone. Sampling from only the crust (common in heritage science where samples are limited) may not provide a representative assessment of mineralogy, especially those minerals which are unstable and reactive, and may be absent in the crust but present deeper in the stone. When sampling crust samples, multiple samples should be taken from various parts of the building to try build a more accurate representation of stone mineralogy (Kennedy., 2015).

- Trial hydrophobic treatments outdoors at ruinous sites. Conduct these kinds of experiments over longer time scales (years) to understand better the interaction between, stone, climate and weathering. Such a project could involve the public through crowdsourcing. This would entail visitors being encouraged to take photos of the tests sites and send them to HES so that visual differences over time may be picked up.

- Appreciate the potential of treatments to alter the colour of stone and take this into consideration prior to application.

4.7 Future research

- **Mapping and understanding clay mineralogy profiles through weathered stone.** For example, does smectite disappear at the weathered surface? How far into the stone should samples be collected before clay mineralogy changes? Do these changes in mineralogy affect physical properties which may influence durability and decay? For example, if the interior bulk stone is expanding due to the presence of smectite and the surface doesn't, there may be a zone in between the two where strain is accumulating.

- **Long term study evaluating the efficiency of different treatments outdoors at different sites.** Conduct regular non-destructive techniques (e.g. microwave moisture meter and Karsten tube) to assess the long-term behaviour of treatment. Such a study should also include monitoring of local climate (perhaps using ibuttons) to gain a better understanding of all properties affecting stone durability and treatment efficiency.

- **Investigation into the hygroscopic properties of Arbroath sandstone.** A hygroscopic stone is a stone which absorbs and interacts with moisture present in the air. Upon interacting with moisture in the air, hygroscopic minerals including some salts and clays, can enhance weathering through cycles of dissolution-crystallisation, and expansion-contraction, respectively. As hydrophobic treatments do not prevent the movement of moisture in the form of vapour, it is important to evaluate the hygroscopic properties of a stone and how this might contribute to weathering, especially in the presence of a hydrophobic treatment. Characterisation of properties including hygric expansion, and sorption/desorption curves, would give detailed insight into how hygroscopic minerals, including smectite identified in A-C during this project, influence the mechanical behaviour of the stone and whether this has implications for sandstone durability and preservation (Tabasso & Simon., 2006; Liu & Charola., 2014).

4.8 References

Akoğlu, K. G., & Caner-Saltık, E. N. (2015). Hydric dilation of Mount Nemrut sandstones and its control by surfactants. *Journal of Cultural Heritage*, *16*(3), 276-283.

Angeli, M., Bigas, J. P., Benavente, D., Menéndez, B., Hébert, R., & David, C. (2007). Salt crystallization in pores: quantification and estimation of damage. *Environmental geology*, *52*(2), 205-213.

Benavente, D., Cultrone, G., & Gómez-Heras, M. (2008). The combined influence of mineralogical, hygric and thermal properties on the durability of porous building stones. *European Journal of Mineralogy*, *20*(4), 673-685.

Benavente, D., del Cura, M. G., Bernabéu, A., & Ordóñez, S. (2001). Quantification of salt weathering in porous stones using an experimental continuous partial immersion method. *Engineering geology*, *59*(3-4), 313-325.

Charola, A. E. (2003). Water Repellents and Other" Protective" Treatments: A Critical Review/Hydrophobieren und andere" schützende" Maßnahmen: Ein kritischer Überblick. *Restoration of Buildings and Monuments*, *9*(1), 3-22.

Charola, A. E., & Bläuer, C. (2015). Salts in masonry: an overview of the problem. *Restoration of Buildings and Monuments*, *21*(4-6), 119-135.

Cnudde, V., & Jacobs, P. J. S. (2004). Monitoring of weathering and conservation of building materials through non-destructive X-ray computed microtomography. *Environmental geology*, *46*(3), 477-485.

de Ferri, L., Lottici, P. P., Lorenzi, A., Montenero, A., & Salvioli-Mariani, E. (2011). Study of silica nanoparticles–polysiloxane hydrophobic treatments for stone-based monument protection. *Journal of Cultural Heritage*, *12*(4), 356-363.

Elert, K., & Rodriguez-Navarro, C. (2022). Degradation and conservation of clay-containing stone: A review. *Construction and Building Materials*, *330*, 127226.

Ershad-Langroudi, A., Fadaei, H., & Ahmadi, K. (2019). Application of polymer coatings and nanoparticles in consolidation and hydrophobic treatment of stone monuments. *Iranian Polymer Journal*, *28*(1), 1-19.

Fořt, J. (2015). Effect of Sandstone Anisotropy on its Heat and Moisture Transport Properties. *Materials Science, 21*(3), 455-459.

Garcia Pascua, N., Sánchez De Rojas, M. I., & Frias, M. (1996). The important role of colour measurement in restoration Works. Use of consolidants and water repellents in sandstone. In *8th International Congress on deterioration of stone* (pp. 1351-1361).

Gherardi, F. (2022). Current and Future Trends in Protective Treatments for Stone Heritage. In *Conserving Stone Heritage* (pp. 137-176). Springer, Cham.

Jia, M., Liang, J., He, L., Zhao, X., & Simon, S. (2019). Hydrophobic and hydrophilic SiO2-based hybrids in the protection of sandstone for anti-salt damage. *Journal of Cultural Heritage, 40*, 80-91.

Jiménez González, I., & Scherer, G. W. (2004). Effect of swelling inhibitors on the swelling and stress relaxation of clay bearing stones. *Environmental Geology*, *46*(3), 364-377.

Kennedy, C. J. (2015). The role of heritage science in conservation philosophy and practice. The Historic Environment: Policy & Practice, 6(3), 214-228.

Liu, Y., & Charola, A. E. (2014). Hygric behavior of Portland sandstone as a function of the applied water repellent formulation. *Hydrophope VII*.

Ludovico-Marques, M., & Chastre, C. (2014). Effect of consolidation treatments on mechanical behaviour of sandstone. *Construction and Building Materials*, *70*, 473-482.

Mausfeld, SA., & Grassegger, G. (1992). Abbauprozesse an Feldspaten und Tonmineralen unter den Bedingungen der Bauwerksverwitterung. Z dt geol Ges 143:23-39.

McAllister, D., Warke, P., McCabe, S., & Gomez-Heras, M. (2016). Evaporative moisture loss from heterogeneous stone: Material-environment interactions during drying. *Geomorphology*, *273,* 308-322.

McKinley, J. M., & Warke, P. A. (2007). Controls on permeability: implications for stone weathering. *Geological Society, London, Special Publications*, *271*(1), 225-236.

Moropoulou, A., Kouloumbi, N., Haralampopoulos, G., Konstanti, A., & Michailidis, P. (2003). Criteria and methodology for the evaluation of conservation interventions on treated porous stone susceptible to salt decay. *Progress in Organic Coatings*, *48*(2-4), 259-270.

Pinna, D., Salvadori, B., & Galeotti, M. (2012). Monitoring the performance of innovative and traditional biocides mixed with consolidants and water-repellents for the prevention of biological growth on stone. *Science of the Total Environment*, *423*, 132-141.

Ruedrich, J., & Siegesmund, S. (2007). Salt and ice crystallisation in porous sandstones. *Environmental Geology*, *52*(2), 225-249.

Schäfer, M., & Steiger, M. (2002). A rapid method for the determination of cation exchange capacities of sandstone: Preliminary data. In: Siegesmund S, Weiss T, Vollbrecht A (eds) Natural stone, weathering phenomena, conservation strategies and case studies. Geological Society London, Special Publications 205:431-439.

Sebastián, E., Cultrone, G., Benavente, D., Fernandez, L. L., Elert, K., & Rodriguez-Navarro, C. (2008). Swelling damage in clay-rich sandstones used in the church of San Mateo in Tarifa (Spain). *Journal of cultural heritage*, *9*(1), 66-76.

Siegesmund, S., & Dürrast, H. (2011). Physical and mechanical properties of rocks. In *Stone in architecture* (pp. 97-225). Springer, Berlin, Heidelberg.

Snethlage, R. (2011). Stone Conservation, In *Stone in architecture* (pp. 516-518) Springer, Berlin, Heidelberg

Tabasso, M. L., & Simon, S. (2006). Testing methods and criteria for the selection/evaluation of products for the conservation of porous building materials. *Studies in Conservation*, *51*(sup1), 67-82.

Wen, Y., Qing, H., Shu, H., & Liu, Q. (2021). Evaluating the Protective Effects of Calcium Carbonate Coating on Sandstone Cultural Heritage. *Coatings*, *11*(12), 1534.

WTA Merkblatt AG 3.17 (2010) Hydrophobierende Imprägnierung von mineralischen Baustoffen. WTA Publications 3–17. Ausgabe 06.2010

Zhao, J., & Plagge, R. (2015). Characterization of hygrothermal properties of sandstones—Impact of anisotropy on their thermal and moisture behaviors. *Energy and Buildings*, *107*, 479-494.

Zoghlami, K., López-Arce, P., & Zornoza-Indart, A. (2017). Differential stone decay of the Spanish tower façade in Bizerte, Tunisia. *Journal of Materials in Civil Engineering*, *29*(6), 05016005.

5.0 Final Discussion and conclusions

The overall aim of this research programme is to better understand the durability and decay of vulnerable sandstones used in the built heritage of Scotland, with a focus on the influence of clay mineralogy. Furthermore, this research explores the suitability of preservation treatments in protecting vulnerable sandstone. Below is a summary of the research aims as laid out in the Introduction:

I. *Critical evaluation of the preparatory and analytical procedures for clay minerals using pXRD (Chapter 2).*

II. *Improve understanding of the decay and durability of selected sandstones used in the built heritage of Scotland through detailed characterisation of their physical and mineralogical properties (Chapter 3).*

III. *Investigate the use of hydrophobic treatments as a means of protecting vulnerable sandstone from accelerated weathering and decay (Chapter 4).*

IV. *Provide a summary of recommendations for Historic Environment Scotland (HES) regarding topics including sandstone durability, preservation of vulnerable sandstone sites, and future research (Chapter 6).*

This research has refined the methodology associated with the preparation and analysis of clay minerals using pXRD. The pXRD technique is heavily relied upon for the characterisation of clay minerals in the study of stone decay and durability (Wangler & Scherer., 2008; Benavente et al., 2008; Pötzl & Siegesmund., 2018; Tiennot et al., 2019; Shekofteh et al., 2019). As shown in this research, amounts as low as 5 wt % expansive clay in bulk samples can be detected by pXRD and is it likely that <5 wt % can also be detected. Further research is required to assess the lower limit of clay mineral detection, which may vary with different models of XRD machine. This research has also shown that the amount of clay extracted from a bulk sandstone is not representative of the size of the clay fraction of the sandstone, and is often a gross underestimation. Therefore, care should be taken when attempting to quantifying the wt % of clay in a sandstone using this method as it has been shown here to be unreliable.

Of the total number of studied sandstones, smectite was found in only two, both from Arbroath Abbey: weathered original stone (A-C_w) and St. Bees replacement stone (B_f). The weathered stone was quarried locally and forms part of the Scone Formation. Theis geological unit consists of sandstones deposited during the Devonian in arid fluvial conditions, conditions which are considered to be one of the most suitable for preserving unstable and reactive clay minerals such as smectite. St. Bees is a Permo-Triassic sandstone quarried in Cumbria forming part of the Chester Formation. Similarly, these sandstones were deposited in arid climates, within fluvial environments with an aeolian input. Depositional environments of sandstones in Scotland can therefore provide a good indication of possible likelihood of the prevalence of smectite in sandstone. This information may be used by HES to identify which historic buildings are more likely to contain expansive clays based on the history of the underlying geology of a specific building as stone used in the original construction of historic buildings in Scotland was usually sourced locally.

Despite the presence of smectite in the sandstones described above, it is difficult to conclude whether this clay mineral has a substantial impact on durability of the sandstones studied in this project. For example, St. Bees replacement stone (B_f), which contains expansive smectite, had one of the lowest rates of hydric expansion among the sandstones measured. This apparent contradiction emphasises the role that other properties play in influencing the mechanical properties of sandstones. In the case of Bf, the low hydric expansion may be explained by the higher porosity and large average pore size, allowing for adequate space for clay mineral expansion. Nonetheless, this research has shown that clay minerals, including non-expansive types, can have indirect impacts on the texture of sandstone which may make the stone more susceptible to certain weathering processes.

For example, clay minerals can alter the pore size distribution of sandstones by reducing the average pore size, as is the case with weathered Jedburgh (J_w) and quarried Denholmhill (Dh_{cb}) sandstones. This alteration in pore size distribution can potentially make sandstones more susceptible to mechanical weathering processes such as salt weathering and freeze-thaw weathering. Clay minerals are also more prone to alteration and weathering and so sandstones with clay-rich cements and matrix may be more prone to loss of cement and overall weakening through chemical weathering. Finally, the concentration of clay in layers such as with both Denholmhill sandstones (Dh_p, Dh_{cb}), may make sandstones more prone to differential weathering where bedding planes are more susceptible to a variety of physical and chemical weathering processes.

Clay mineral profiles in building stone were also identified in weathered stone at Arbroath Abbey ($A\text{-}C_w$) where smectite was present in the interior, relatively less weathered portion of the stone, but had altered to kaolinite in the stone's outer crust. This observation is consisted with literature which emphasises the instability of smectite at the Earth's surface and tendency to alter to more stable clay minerals. Small samples taken from the outer surface of a stone are often used in stone decay studies to characterise mineralogy due to sampling restrictions. However, sampling from the surface may lead to an unrepresentative picture of mineralogy, especially of less stable minerals such as clays and micas. Therefore, it is possible that smectite has been underrepresented in previous stone decay studies.

The studied sandstones displayed varying degrees of heterogeneity in their mineralogical and/or physical properties. Heterogenous rocks pose a number of difficulties with regard to understanding stone decay and durability. The variation in physical and mineralogical properties makes identifying the types of weathering that are most prominent at a specific site a complex challenge. Moreover, heterogenous stones may be more susceptible to differential erosion and weathering. Sandstone from Arbroath is considered very heterogenous, which was reflected in the broad range of porosity values and differences in capillary absorption and mineralogy. These differences existed between blocks ($A\text{-}C_w$ and $A\text{-}L_w$) and within individual stones. In this specific case, due to sandstone heterogeneity, the efficiency of hydrophobic coating was extremely variable. Heterogeneity is a common characteristic of sandstone due to the nature of rock's formation (deposition of sand in evolving depositional environments). Therefore, care should be taken when sampling, and consideration for how representative a stone sample is of the entire site. If possible, samples from various stones, and parts of individual stones, should be taken to understand how mineralogical and physical properties vary.

Finally, climate change is perhaps one of the biggest threats to the future conservation of historic sandstone buildings. As sandstone is a porous material it is more sensitive to the presence and interaction of moisture. Increases in precipitation associated with climate change will undoubtedly affect how the sandstone-built heritage weathers. For example, it may mean that chemical weathering becomes the dominant process due to the increasing presence of water, increasing the duration of stone wetness and facilitated more chemical processes to take place. Aside from chemical weathering, the increase in moisture may have dramatic implications for the strength of sandstones, particularly those that are considered clay-rich. As seen from this research the compressive strength of Forest of Dean sandstone (Fd) fell by over 70 % when saturated, which is thought to be related to the softening of clay minerals. Other sandstones also displayed a significant loss of strength upon wetting. The weakening of a stone may make it more susceptible to weathering and disintegration over time.

Overall, this research has contributed to a greater understanding of the role the clay minerals play in the decay and durability of sandstone in Scotland. Clay minerals influence both the mineralogical and physical properties of sandstones, and both expansive and non-expansive clay minerals can influence sandstone decay and durability. Clay-rich sandstones such as Forest of Dean are very vulnerable to changes in climate, and in particular to increases in precipitation associated with Scotland's future climate. It is therefore imperative to identify and prioritised such stone types for future research and conservation work which will ultimately focus on minimising the impact of climate change on the integrity of Scotland's built heritage.

References

Benavente, D., Cultrone, G., & Gómez-Heras, M. (2008). The combined influence of mineralogical, hygric and thermal properties on the durability of porous building stones. *European Journal Of Mineralogy*, *20*(4), 673-685. doi: 10.1127/0935-1221/2008/0020-1850

Pötzl, C., Dohrmann, R. & Siegesmund, S. Clay swelling mechanism in tuff stones: an example of the Hilbersdorf Tuff from Chemnitz, Germany. Environ Earth Sci 77, 188 (2018). https://doi.org/10.1007/s12665-018-7345-2

Shekofteh, A., Molina, E., Arizzi, A., Cultrone, G., Ahmadi, H., & Yazdi, M. (2019) Characterization and damage assessment of stones used in the Pasargadae World Heritage Site, Achaemenian period, International Journal of Architectural Heritage, 13:4, 521-536, DOI: 10.1080/15583058.2018.1436728

Tiennot, M., Mertz, JD. & Bourgès, A. Influence of Clay Minerals Nature on the Hydromechanical and Fracture Behaviour of Stones. Rock Mech Rock Eng 52, 1599–1611 (2019). https://doi.org/10.1007/s00603-018-1672-1

Wangler, T., & Sherer, G. (2008). Clay swelling mechanism in clay-bearing sandstones. Environmental Geology, 56(3-4), 529-534. Doi: 10.1007/s00254-008-1380-3

6.0 Summary of recommendations to HES for research and conservation.

Each chapter of this thesis has included recommendations and suggestions to HES regarding future research and conservation work. This chapter is a summary of recommendations and suggestions provided throughout this thesis in the context of work currently being undertaken by HES regarding stone decay and durability. Below is a brief description of two recent large-scale project undertaken by HES which are relevant to some of the recommendations and suggestions made throughout this thesis.

HES have recently undertaken tactile surveys of properties. These surveys aim to assess the condition of stone at high elevations – often not assessable through traditional site visits, at over 200 properties. There are several aims to the project which include, assessing public safety regarding unstable masonry, assessing the impact of climate change on historic building stone, and assessing the extent of stone weathering and decay. The surveys resulted in access restrictions at ~ 70 sites (Jan, 2022) emphasising the value of tactile surveys in understanding high-elevation stone condition and ensuring public safety. The results of this work will also inform HES's repair strategies and future conservation plans.

One relatively new project led by HES aims to conduct a stone survey for each property in their care. The PiC (properties in care) stone survey project is supported by the British Geological Survey (BGS) who are offering up their knowledge and expertise of stone characterisation and provenance surveys. This large-scale project aims to characterise stone from 300 + properties, providing invaluable information on the provenance of stone at selected sites, and its sensitivity to weathering and decay. The study may also inform and influence the re-opening of historic quarries for the purpose of supplying stone for conservation projects at historic sites. With regards to stone provenance, the project will rely on the BSDS (Building Stone Database for Scotland) created by BGS which catalogues all confirmed historic and active stone quarries across the country. Moreover, the database also allows the user to view photos, lists of buildings, and geological history, associated with a specific quarry.

6.1 HES recommendations

6.1.1 Database of vulnerable sandstone heritage.

The suggestion of recording vulnerable historic buildings is perhaps something that could be incorporated into the already existing BSDS. Such classification could be based on mineralogical and physical properties of building stone at a specific site. The PiC stone survey can progress this recommendation as it characterises stone types across all properties allowing comparison between sites to determine which sites are most vulnerable. Furthermore, a database could highlight, based on specific factors, which sites are to be most impacted by climate change using a traffic light system so that potential case study sites for future conservation and research can be prioritised. Such sites may be prioritised for projects relating to long-term stone and climate monitoring (see below point for more detail) and research projects focussed on sandstone preservation (e.g., trialling of water repellents).

One factor which may be used to determine the potential vulnerability of stone to weathering and climate change is depositional environment associated with historic stone and/or local underlying geology. As discussed in the Introduction and Final Discussion, specific environmental conditions active during the deposition of sandstone (e.g., arid climate and fluvial environment) are more likely to preserve expansive smectites amongst other reactive and unstable minerals. Understanding and cataloguing the geological history of building stones and the surrounding areas, including depositional environment, may prove a useful tool in identifying which buildings are most at risk of weathering and climate change.

6.1.2 Long term stone and climate monitoring on site.

This recommendation builds on the tactile stone surveys conducted by HES which aim to understand condition of stone at high elevations. Such monitoring is being prioritised at sites deemed most vulnerable allowing for a better understanding of the interactions between stone properties and climate. As well as understanding the condition of stone at high elevations, other properties which may be assessed regularly include mapping of visual surface changes, stone properties including density, porosity, and water absorption rates using in-situ and non-destructive tests, and relative humidity and temperature using ibuttons. Furthermore, lab-based accelerated weathering experiments (either using weathered samples or similar stone from quarry) using a climate chamber may be used as a means of providing information faster on the extent and types of weathering associated with different climate scenarios and sandstone types.

6.1.3 Regular petrophysical and mineralogical characterisation of replacement sandstones.

Regular characterisation is especially important for sandstones as they can often be heterogenous within a quarry – meaning their properties can vary due to changes in environment during deposition. This has been shown to be the case with St. Bees in this research which showed two varieties with different physical and mineralogical properties which have important controls on durability. Practically this suggestion may be challenging however, will further reduce the risk of selecting a stone which is incompatible with stone at a given site.

6.1.4 Obtain samples from both the outer crust and interior of the stone.

Sampling from only the crust (common in heritage science where sampling is heavily restricted) may not provide a representative assessment of mineralogy, especially those minerals which are unstable and reactive, and may be absent in the crust but present deeper in the stone.

6.1.5 Trial hydrophobic treatments outdoors at ruinous sites.

Conduct long-term (multiple years) trials of hydrophobic to understand better the interaction between, stone, climate and weathering. Such a project could involve crowd sourcing techniques in order to collect more qualitative data of visual changes to test sites over time. This would entail visitors being encouraged to take photos of the tests sites and send them to HES so that visual differences may be monitored over time (Brigham et al., 2018).

6.2 Future research

6.2.1 Methodical approach to the characterisation of clay minerals using XRD and SEM.

SEM and XRD provides data crucial information in regard to the role clay minerals play in sandstone decay and durability. Many studies identify clay minerals using pXRD without providing additional context. As shown from this research chapter the role played by clay minerals in the decay of sandstones extends further than the occurrence of smectite. Other important factors to characterise include clay mineral morphology, distribution of clay minerals and their impact on pore size distribution, and amount; properties which can be characterised using SEM and XRD. Quantitative XRD is a powerful tool not explored in this project, which could provide valuable information on the exact quantities of clay minerals present in stone. The ability to measure clay mineral quantities in crushed bulk samples would allow for research project assessing the impact of different clay mineral quantities on sandstone decay and durability.

6.2.2 Relationship between clay mineral content and sandstone durability under different climate scenarios.

There is limited literature which reports quantitative values for clay mineral content in sandstone. Consequently, there is even less literature on how different quantities of clay minerals impact the durability of sandstone. Such research questions could be answered through quantitative pXRD analysis to determine clay mineral content, followed by accelerated weathering experiments using a climatic chamber. In addition to such as study, different UKCP scenarios could be used in the accelerated weathering experiment to determine which climates have the most adverse impact on durability of clay-rich sandstone.

6.2.3 The impact of water saturation degree on the strength of clay-rich sandstone.

As shown in this research chapter, the strength of clay-rich sandstone (Forest of Dean) is extremely sensitive to changes in water saturation degree. These findings may have important implications for sandstone durability with regards to the future climate of Scotland, which predicts more rainfall and more intense rain events. The future climate of Scotland may lead to periods of prolonged stone wetness reducing the overall strength of stone which also changing the dominant weathering processes controlling decay (e.g. shift from predominantly physical weathering to chemical weathering). Such as study characterise the mineral content of selected stones and determine how different degrees of saturation impact stone strength (compressive, tensile, etc).

6.2.4 Durability of Scottish building stones under different UKCP scenarios.

Changes in climate will ultimately impact how stone weathers and decays. Accelerated weathering experiments can be used to assess how different UKCP scenarios impact different stone types, including weathered stone from sites (if sampling possible) and stone from quarries. Such findings could then be used to help inform future decision making will regards to conservation approaches at specific sites.

6.2.5 Mapping and understanding clay mineralogy profiles through weathered stone.

For example, does smectite disappear at the weathered surface? How far into the stone should samples be collected before clay mineralogy changes? Do these changes in mineralogy affect physical properties which may influence durability and decay? For example, if the deeper bulk stone is expanding and the surface doesn’t, there may be a zone in between the two where strain is accumulating.

6.2.6 Long term study evaluating the efficiency of different treatments outdoors at different sites.

Conduct regular non-destructive techniques (e.g. microwave moisture meter and Karsten tube) to assess the long-term behaviour of treatment. Such a study should also include monitoring of local climate (perhaps using ibuttons) to gain a better understanding of all properties affecting stone durability and treatment efficiency.

6.2.7 Investigation into the hygroscopic properties of Arbroath sandstone.

A hygroscopic stone is a stone which absorbs and interacts with moisture present in the air. Upon interacting with moisture in the air, hygroscopic minerals including some salts and clays, can enhance weathering through cycles of dissolution-crystallisation, and expansion-contraction, respectively. As hydrophobic treatments do not prevent the movement of moisture in the form of vapour, it is important to evaluate the hygroscopic properties of a stone and how this might contribute to weathering, especially in the presence of a hydrophobic treatment. Characterisation of properties including hygric expansion, and sorption/desorption curves, would give detailed insight into how hygroscopic minerals, including smectite identified in A-C during this project, influence the mechanical behaviour of the stone and whether this has implications for sandstone durability and preservation (Tabasso & Simon., 2006; Liu & Charola., 2014). A methodical approach could be developed which assesses the sensitivity of a given stone to deterioration based on its hygroscopic properties.

6.3 References

Brigham, R., Grau-Bové, J., Rudnicka, A., Cassar, M., & Strlic, M. (2018). Crowdsourcing as an analytical method: Metrology of smartphone measurements in heritage science. Angewandte Chemie, 130(25), 7545-7549.

Liu, Y., & Charola, A. E. (2014). Hygric behavior of Portland sandstone as a function of the applied water repellent formulation. *Hydrophope VII*.

Tabasso, M. L., & Simon, S. (2006). Testing methods and criteria for the selection/evaluation of products for the conservation of porous building materials. *Studies in Conservation*, *51*(sup1), 67-82.